Zeolite-A as a Remediation Technique for Soil Contaminated with Lead

by

Rebecca Blake Tanney

Thesis

Submitted to the University of Kent

for the degree of

Doctor of Philosophy

School of Physical Sciences

September 2017

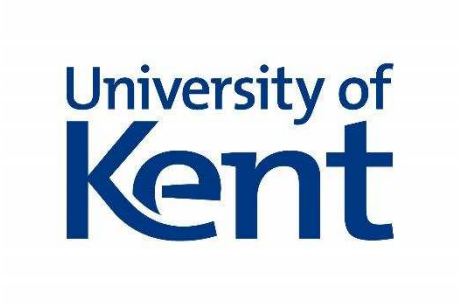

Table of Contents

Table of Contents ii
List of Figures vii
List of Tables xi
Acknowledgements xii
Dedication xiii
Declaration xiv
Abstract xv
Chapter 1 Introduction 16
1.1 Aims 16
1.2 Background 16
1.3 The Current Study 16
1.3.1 Experimental and Computational Analyses 17
1.4 Summary 18
Chapter 2 Literature Review 20
2.1 Aim 20
2.2 Introduction 20
2.3 Background 20
2.4 Toxic Effects 22
2.5 Sources and Spread of Contamination in Soil 25
2.6 Soil Classification 26
2.7 Detection of Heavy Metals 27
2.8 Acid Mine Drainage and Pyrite Ash 28
2.9 Acid Rain 31
2.10 Remediation Techniques 35
2.11 Zeolites for Remediation 38
2.11.1 Zeolite General Characteristics 39
2.11.2 Natural Zeolites for Remediation 44
2.11.3 Gismondine 46
2.11.4 Synthetic Zeolites for Remediation 48
2.11.5 Zeolite-A as a Remediation Technique 51
2.11.6 Computational Background 53
2.12 Conclusions 54
Chapter 3 Area of Study 55
3.1 Aim 55

3.2 Introduction 55
3.3 Site Background 55
3.4 Hydrology of the Site 58
3.5 Conclusions 60
Chapter 4 Experimental Techniques 61
4.1 Aims 61
4.2 Introduction 61
4.3 Atomic Absorption Spectroscopy 61
4.3.1 Flame AAS (FAAS) Theory 62
4.3.2 Furnace AAS Theory 67
4.3.3 AAS Specification 67
4.3.4 ICP-MS vs AAS 70
4.4 X-ray Diffraction 71
4.4.1 Introduction 71
4.4.2 Theory 71
4.4.3 XRD Sample Collection 74
4.5 X-ray Fluorescence 75
4.5.1 Introduction 75
4.5.2 Theory 75
4.5.3 XRF Sample Preparation 77
4.6 Scanning Electron Microscope (SEM)/ Energy Dispersive X-ray (EDX) 77
4.6.1 Introduction 77
4.6.2 Theory 77
4.6.3 SEM-EDX Sample Preparation 80
4.6.4 Limitations of SEM 82
4.7 pH Meter 82
4.8 Computational Method 82
4.8.1 Introduction 82
4.8.2 Hartree-Fock Theory 83
4.8.3 Density Functional Theory (DFT) 87
4.8.4 CRYSTAL09 89
4.9 Conclusions 89
Chapter 5 Materials and Methods 90
5.1 Aim 90
5.2 Introduction 90
5.3 Sample Collection 90

5.4 Quality Assurance and Statistical Testing 91
5.5 Sample Preparation 91
5.6 Lead Standards for AAS Calibration 92
5.7 Difficulties Using Flame Atomic Absorption Spectroscopy (FAAS) 92
5.8 Zeolite-A Synthesis 93
5.9 Digestion of Soil Samples 94
5.9.1 Analysis in 0.25M HNO_3 94
5.9.2 Analysis in Purified Water 95
5.9.3 Naming of Samples 95
5.10 Conclusions 96
Chapter 6 Results and Discussion 97
6.1 Aim 97
6.2 Introduction 97
6.3 Identification of Zeolite-A 98
6.3.1 Ball milling of Zeolite-A 99
6.3.2 Determining the solubility and pH dependence of Zeolite-A 99
6.4 Soil Classification 102
6.5 Mineral Characterisation of Soil 1 103
6.5.1 XRD of S1untreated, S1w and S1a 103
6.5.2 Microscopy of Soil 1 – Zooming 111
6.5.3 SEM-EDX of S1untreated – Soil 1 after drying and sifting 112
6.5.4 SEM-EDX of S1w – Soil 1 washed in deionised water 114
6.5.5 SEM-EDX of S1a – Soil 1 washed in 0.25M HNO_3 115
6.5.6 XRF Analysis of S1untreated with S1w and S1a 117
6.6 Mineral Characterisation of Soil 2 118
6.6.1 XRD of S2untreated, S2w and S2a 118
6.6.2 SEM-EDX of S2untreated – Soil 2 after drying and sifting 121
6.6.3 SEM-EDX of S2w – Soil 2 washed with deionised water 123
6.6.4 SEM-EDX of S2a – Soil 2 washed with 0.25M HNO_3 125
6.6.5 XRF Analysis of S2untreated with S2w and S2a 127
6.7 Comparison of Soil 1 and Soil 2 128
6.7.1 XRF Analysis Comparing S1untreated and S2untreated 129
6.8 Analysis of Treated Soils 131
6.8.1 XRD of Soil 1 in Water 131
6.8.2 SEM-EDX of S1wZA25 – Soil 1 in Water with 0.25 g of Zeolite-A 134
6.8.3 SEM-EDX of S1wZA50 – Soil 1 in Water with 0.50 g of Zeolite-A 136

6.8.4 XRF of Soil 1 in Water with Increasing Zeolite-A 139
6.8.5 XRD of Soil 1 in Acid 140
6.8.6 SEM-EDX of S1aZA25 – Soil 1 in Acid with 0.25 g of Zeolite-A 143
6.8.7 SEM-EDX of S1aZA50 – Soil 1 in Acid with 0.50 g of Zeolite-A 146
6.8.8 XRF of Soil 1 in Acid with Increasing Zeolite-A 148
6.8.9 XRD of Soil 2 in Water 150
6.8.10 SEM-EDX of S2wZA25 – Soil 2 in Water with 0.25g of Zeolite-A 152
6.8.11 SEM-EDX of S2wZA50 – Soil 2 in Water with 0.50g of Zeolite-A 154
6.8.12 XRF of Soil 2 in Water with Increasing Zeolite-A 156
6.8.13 XRD of Soil 2 in Acid 158
6.8.14 SEM-EDX of S2aZA25 – Soil 2 in Acid with 0.25g of Zeolite-A 160
6.8.15 SEM of S2aZA50 – Soil 2 in Acid with 0.50g of Zeolite-A 162
6.8.16 XRF of Soil 2 in Acid with Increasing Zeolite-A 165
6.9 XRF for Treated Soil 1 and 2 in Water 166
6.10 XRF for Treated Soil 1 and 2 in Acid 167
6.11 Conclusions 168
Chapter 7 Leaching Experiments 169
7.1 Aim 169
7.2 Introduction 169
7.3 pH of Soil Leachate 169
7.4 Analysis of the Leachates for S1w, S1a, S2w and S2a 171
7.4.1 FAAS of the Leachates of S1w and S1a 171
7.4.2 GFAAS of the Leachates of S1w and S1a 171
7.4.3 FAAS of the Leachate of S2w and S2a 172
7.4.4 GFAAS of the Leachate of S2w and S2a 173
7.5 Analysis of the Leachate from Treated Soil 1 in Water or Acid with Increasing Zeolite-A 174
7.5.1 FAAS of the Leachate of Soil 1 in Water with Increasing Zeolite-A 174
7.5.2 GFAAS of the Leachate of Soil 1 in Water with Increasing Zeolite-A 174
7.5.3 FAAS of Leachate of Soil 1 in Acid with Increasing Zeolite-A 175
7.5.4 GFAAS of Leachate of Soil 1 in Acid with Increasing Zeolite-A 176
7.6 Analysis of Leachate from Treated Soil 2 in Water with Increasing Zeolite-A 177
7.6.1 FAAS of Leachate of Soil 2 in Water with Increasing Zeolite-A 177
7.6.2 GFAAS of Leachate of Soil 2 in Water with Increasing Zeolite-A 178
7.6.3 FAAS of Leachate of Soil 2 in Acid with Increasing Zeolite-A 179
7.6.4 GFAAS of Leachate of Soil 2 in Acid with Increasing Zeolite-A 180
7.7 Zeolite-A as a Remediation Technique 180

7.7.1 Comparison of GFAAS Soil 1 and 2 in water 181
7.7.2 Comparison of GFAAS Soil 1 and 2 in acid 182
7.8 Conclusions 183
Chapter 8 Results and Discussion: Computational Analysis 184
8.1 Aim 184
8.2 Introduction 184
8.3 Method 185
8.4 Results 187
8.4.1 Energies 187
8.4.2 Structural Data 189
8.5 Conclusions 191
Chapter 9 Conclusions and Recommendations 193
9.1 Aims and Introduction 193
9.2 Summary and Discussion 194
9.3 Proposition of gismondine formation 195
9.4 Future Work and Recommendations 197
Chapter 10 References 199
Chapter 11 Appendices 220

List of Figures

Figure 2.1 - Heavy metals, such as Hg^{2+}, form a complex with alkaline proteins and precipitate 23
Figure 2.2 - Cycle of pyrite oxidation by microorganisms 29
Figure 2.3 - The oxidation of pyrite 30
Figure 2.4 - The Acid Rain Cycle 32
Figure 2.5 - Pourbaix Diagram for Iron 33
Figure 2.6 - Basic zeolite structure obeying Löwenstein's rule 40
Figure 2.7 - Structures of four zeolites and their pore sizes 41
Figure 2.8 - (a) A zeolite sodalite cage structure (b) Schematic model of α-cage (c) Schematic model of β-cage 41
Figure 2.9 - Results of Li et al. (2009). Addition of zeolite to the lead-contaminated soil causes an increase in pH 43
Figure 2.10 - Gismondine structure 47
Figure 2.11 - Zeolite-A Structure 52
Figure 2.12 - Crystallographic unit cell of anhydrous Zeolite-A containing 672 atoms ($NaSiAlO_{12}$), where red represents oxygen, purple is sodium, grey is silicon and cream is aluminium. 53
Figure 3.1– a) Map of Sweden and b) Overview of the industrial paper mill current site where samples S1untreated and S2untreated were collected at sites marked “1” and “2”, respectively 56
Figure 3.2 – a) Average Rainfall per Year in Sweden: 1961-1990, b) Number of Days with Heavy Rainfall in Sweden: 1961-1990, c) Percentage of Rain as Snow in Sweden: 1961-1990 59
Figure 3.3 - Zoomed in area showing the location of the site where samples were collected 60
Figure 4.1 - a) Diagram of X-ray electron shell model and b) Jablonski diagram 62
Figure 4.2 – Schematic design of an AAS Spectrometer where the numbers refer to the description in the text 63
Figure 4.3 – Flame temperature distribution in FAAS 65
Figure 4.4 - Absorption of Light by a Sample 66
Figure 4.5 - Linear Calibration Line 66
Figure 4.6 - FAAS calibration curve for lead samples with a set of soil results 68
Figure 4.7 - Powder X-ray Diffraction Set Up 72
Figure 4.8 - Bragg's Law Diagram 72
Figure 4.9 - X-Ray Shell Diagrams 76
Figure 4.10 – Principles for SEM analysis 79
Figure 4.11 - Plot showing 1s atomic orbital (Slater type orbital, STO) in comparison with Gaussian type orbitals (GTO) up to a 4th term linear combination 86
Figure 4.12 - Self Consistent Field Cycle (SCF) 87
Figure 6.1 - XRD pattern of Zeolite-A and red peaks corresponding to Zeolite-A in database 98
Figure 6.2 - a) SEM Image of Zeolite-A as synthesised, b) EDX Spectrum of the sample 99
Figure 6.3 - Zeolite-A – The Effect of pH on the Remediation of Lead 102
Figure 6.4 - XRD Pattern for S1untreated and corresponding minerals 105
Figure 6.5 - XRD Pattern for S1a and corresponding minerals 108
Figure 6.6 - XRD Pattern of S1a with gismondine peaks overlaid in red 109
Figure 6.7 – a) SEM image showing S1untreated, b) image of blue circle in (a) enlarged, and c) image of orange circle in (b) enlarged 111
Figure 6.8 - a) SEM image showing S1untreated and b) EDX spectrum corresponding to the point marked with a red arrow 112

Figure 6.9 – a) SEM map area image showing S1untreated, b) Corresponding EDX sum spectrum, and c) Corresponding EDX element map.....113
Figure 6.10 - a) SEM image showing S1w and b) EDX spectrum corresponding to the point marked with a red arrow.....114
Figure 6.11 – a) SEM map area image showing S1w, b) Corresponding EDX sum spectrum, and c) Corresponding EDX element map.....115
Figure 6.12 - a) SEM image showing S1a and b) EDX spectrum corresponding to the point marked with a red arrow.....116
Figure 6.13 – a) SEM map area image showing S1a, b) Corresponding EDX sum spectrum, and c) Corresponding EDX element map.....117
Figure 6.14 - XRD Pattern for S2untreated and corresponding minerals.....119
Figure 6.15 - XRD Pattern for S2a and corresponding minerals.....120
Figure 6.16 - XRD pattern for S2awith gismondine peaks overlaid in red.....121
Figure 6.17 - a) SEM image showing S2untreated and b) Corresponding EDX Spectrum.....122
Figure 6.18 – a) SEM map area image showing S2untreated, b) Corresponding EDX sum spectrum, and c) Corresponding EDX element map.....123
Figure 6.19 - a) SEM image showing S2w and b) EDX spectrum corresponding to the point marked with a red arrow.....124
Figure 6.20 – a) SEM map area image showing S2w, b) Corresponding EDX sum spectrum, and c) Corresponding EDX element map.....125
Figure 6.21 - a) SEM image showing S2w and b) Corresponding EDX spectrum.....126
Figure 6.22 – a) SEM map area image showing S2a, b) Corresponding EDX sum spectrum, and c) Corresponding EDX element map.....127
Figure 6.23 – Normalised XRF data of S1untreated and S2untreated.....131
Figure 6.24 - XRD Pattern for S1wZA25 and corresponding minerals.....133
Figure 6.25 - XRD pattern of S1wZA25with gismondine peaks overlaid in red.....134
Figure 6.26 - a) SEM image showing S1wZA25 and b) EDX spectrum corresponding to the point marked with a red arrow.....135
Figure 6.27 - a) SEM map area image S1wZA25, b) Corresponding EDX sum spectrum, and c) Corresponding EDX element map.....136
Figure 6.28 - SEM image showing S1wZA50: 200 µm.....137
Figure 6.29 - a) SEM image showing S1wZA50 and b) EDX spectrum corresponding to the point marked with a red arrow.....137
Figure 6.30 - a) SEM map area image showing S1wZA50, b) Corresponding EDX sum spectrum, and c) Corresponding EDX element map.....138
Figure 6.31 - XRF percentage composition of lead for Soil 1 (water).....139
Figure 6.32 - XRD Pattern for S1aZA25 and corresponding minerals.....142
Figure 6.33 - XRD pattern for S1aZA25with gismondine peaks overlaid in red.....143
Figure 6.34 - a) SEM image showing S1aZA25 and b) EDX spectrum corresponding to the point marked with a red arrow.....144
Figure 6.35 - a) SEM map area image showing S1aZA25, b) Corresponding EDX sum spectrum, and c) Corresponding EDX element map.....145
Figure 6.36 - a) SEM image showing S1aZA50, b) EDX spectrum corresponding to the point marked with a red arrow, and c) EDX spectrum corresponding to the point marked with an orange arrow.....146
Figure 6.37 - a) SEM map area image showing S1aZA50, b) Corresponding EDX sum spectrum, and c) Corresponding EDX element map.....148
Figure 6.38 - XRF percentage composition of lead for Soil 1 (acid).....149

Figure 6.39 - XRD Pattern for S2wZA25 and corresponding minerals 151
Figure 6.40 - XRD pattern of S2wZA25with gismondine peaks overlaid in red..... 152
Figure 6.41 - a) SEM map area image showing S2wZA25 and b) EDX spectrum corresponding to the point marked with a red arrow 152
Figure 6.42 - a) SEM map area image showing S2wZA25, b) Corresponding EDX sum spectrum, and c) Corresponding EDX element map 153
Figure 6.43 - a) SEM initial image showing S2wZA50, b) image of blue circle in (a) enlarged, c) image of green circle in (b) enlarged, and d) image of orange circle in (a) enlarged 154
Figure 6.44 - a) SEM image showing S2wZA50, b) EDX spectrum corresponding to the point marked with a red arrow, and c) EDX spectrum corresponding to the point marked with an orange arrow 155
Figure 6.45 - a) SEM map area image showing S2wZA50, b) Corresponding EDX sum spectrum, and c) Corresponding EDX element map 156
Figure 6.46 - XRF percentage composition of lead for Soil 2 (water) 157
Figure 6.47 - XRD Pattern for S1aZA25 and corresponding minerals 159
Figure 6.48 - XRD pattern of S2aZA25with gismondine peaks overlaid in red..... 160
Figure 6.49 - a) SEM image showing S2aZA25 and b) EDX spectrum corresponding to the point marked with a red arrow 160
Figure 6.50 - a) SEM map area image showing S2aZA25, b) Corresponding EDX sum spectrum, and c) Corresponding EDX element map 161
Figure 6.51 - a) SEM image showing S2aZA50 and b) EDX spectrum corresponding to the point marked with a red arrow 162
Figure 6.52 - a) SEM map area image showing S2aZA50, b) Corresponding EDX sum spectrum, and c) Corresponding EDX element map 163
Figure 6.53 - a) SEM map area image 2 showing S2aZA50, b) Corresponding EDX sum spectrum 2, and c) Corresponding EDX element map 2..... 164
Figure 6.54 - XRF percentage composition of lead for Soil 2 (acid) 165
Figure 6.55 - XRF of Soil 1 and Soil 2 in water, normalised to 100%..... 167
Figure 6.56 - XRF of Soil 1 and Soil 2 in dilute acid, normalised to 100% 167
Figure 7.1 - pH of soil samples with noted changes in pH with the increase of Zeolite-A 171
Figure 7.2 - FAAS results showing the concentration of lead in S1w and S1a leachates 171
Figure 7.3 - GFAAS results showing the concentration of lead in S1w and S1a leachates..... 172
Figure 7.4 - FAAS results showing the concentration of lead in S2w and S2a leachates 173
Figure 7.5 - GFAAS results showing the concentration of lead in S2w and S2a leachates..... 173
Figure 7.6- FAAS results showing the concentration of lead in S1w leachates with increasing Zeolite-A 174
Figure 7.7-GFAAS results showing the concentration of lead in S1w leachates with increasing Zeolite-A 175
Figure 7.8-FAAS results showing the concentration of lead in S1a leachates with increasing Zeolite-A 176
Figure 7.9- GFAAS results showing the concentration of lead in S1a leachates with increasing Zeolite-A 177
Figure 7.10- FAAS results showing the concentration of lead in S2w leachates with increasing Zeolite-A 178
Figure 7.11 - GFAAS results showing the concentration of lead in S2w leachates with increasing Zeolite-A 179
Figure 7.12 - FAAS results showing the concentration of lead in S2a leachates with increasing Zeolite-A 179

Figure 7.13 - GFAAS results showing the concentration of lead in S2a leachates with increasing Zeolite-A 180
Figure 7.14 - GFAAS of S1w and S2w with increasing Zeolite-A 182
Figure 7.15 - GFAAS of S1a and S2a with increasing Zeolite-A 183
Figure 8.1 - Crystal structure of Zeolite-A showing a) a simplified cell containing 160 atoms (Fm-3c) and b) 2x2x2 supercell with 672 atoms (P1). The α-cage represents the super-cage and β-cage the sodalite cage. S6R, S8R and D4R represents the positions for which the cation substitutions have been analysed. 186
Figure 8.2 - 25% loading of lead in Zeolite-A corresponding to distributions; a) PB_S6R_S8R, b) PB_S6R/S8R_S8R, and c) PB_S8R_S8R 187
Figure 8.3 - 50% loading of a) barium and b) lead in Zeolite-A. Bond distances for the geometry optimised structures are given in Angstroms. 190
Appendix Figure 1.1 - ICP-MS report for Soil 1 and Soil 2 (recorded as P1 and P6, respectively) 220
Appendix Figure 3.1 - XRF spectrum of S1untreated 223
Appendix Figure 3.2 - XRF spectrum of S2untreated 224
Appendix Figure 4.2 - XRD pattern of S1w 225
Appendix Figure 4.3 - XRD pattern of S2w 226
Appendix Figure 4.4 - XRD pattern of S1wZA50 227
Appendix Figure 4.5 - XRD Pattern of S1aZA50 228
Appendix Figure 4.6 - XRD pattern of S2wZA50 229
Appendix Figure 4.7 - XRD Pattern of S2aZA50 230
Appendix Figure 4.8 - XRD Pattern of S1w with gismondine peaks overlaid in red 231
Appendix Figure 4.9 - XRD Pattern of S2w with gismondine peaks overlaid in red 231
Appendix Figure 4.10 - XRD Pattern of S1wZA50 with gismondine peaks overlaid in red 232
Appendix Figure 4.11 - XRD Pattern of S1aZA50 with gismondine peaks overlaid in red 232
Appendix Figure 4.12 - XRD Pattern of S2wZA50 with gismondine peaks overlaid in red 233
Appendix Figure 4.13 - XRD Pattern of S2aZA50 with gismondine peaks overlaid in red 233
Appendix Figure 5.1 - Input file for Anhydrous Zeolite-A with basis sets for lead and barium both provided. Coordinates may be substituted as needed. This input file is for a 25% substitution of sodium. 239

List of Tables

Table 2.1 - Zeolite General Characteristics, where 's' denotes a synthetic zeolite and 'n' denotes a natural zeolite, 1 - (Baerlocher & McCusker, 2016), 2 - (First et al., 2011) 42
Table 3.1– Rain and temperature fluctuations as recorded in the village Oskarström and a nearby village, Simlangsdalen,in 1970..... 59
Table 4.1 - FAAS Spectrometer Settings..... 69
Table 4.2 - GFAAS Spectrometer Settings..... 69
Table 4.3- XRD parameter settings..... 74
Table 4.4 – Explanation of SEM parameters..... 81
Table 5.1 - FAAS calibration standards..... 92
Table 5.2 - FAAS of various nitric acid samples..... 93
Table 6.1 - Zeolite-A as a remediation technique at varying pH..... 101
Table 6.2 - Soil classification according to British soil classification 102
Table 6.3 - Mineral components of S1untreated, S1w, and S1a identified using the EVA database by Bruker..... 104
Table 6.4 - XRF elemental composition above 0.9% for S1untreated, S1w, and S1a 118
Table 6.5 - Mineral components of S2untreated, S2w, and S2a identified using the EVA database by Bruker..... 119
Table 6.6 - XRF elemental composition above 0.9% for S2untreated, S2w, and S2a 128
Table 6.7 – Mineral components of S1untreated and S2untreated identified using the EVA database by Bruker..... 129
Table 6.8 - XRF elemental composition above 0.9% for S1untreated and S2untreated..... 129
Table 6.9 - Mineral components of S1untreated, S1w, S1wZA25, and S1wZA50 identified using the EVA database by Bruker 132
Table 6.10 - XRF elemental composition above 0.9% for S1untreated, S1w, S1wZA25, and S1wZA50 140
Table 6.11 - Mineral components of S1untreated, S1a, S1aZA25, and S1aZA50 identified using the EVA database by Bruker 141
Table 6.12 - XRF elemental composition above 0.9% for S1untreated, S1a, S1aZA25, and S1aZA50 . 149
Table 6.13 - Mineral components of S2untreated, S2w, S2wZ25, and S2wZ50 identified using the EVA database by Bruker 150
Table 6.14 - XRF elemental composition above 0.9% for S2untreated, S2w, S2wZA25, and S2wZA50 157
Table 6.15 - Mineral components of S2untreated, S2a, S2aZA25, and S2aZA50 identified using the EVA database by Bruker 158
Table 6.16 - XRF elemental composition above 0.9% for S2untreated, S2a, S2aZA25, and S2aZA50 . 166
Table 7.1 - Remediation effects of Zeolite-A from GFAAS results 181
Table 8.1 - Energy differences of the distributions of Pb^{2+} ions or Ba^{2+} ions in 25% loaded Zeolite-A. The first part of the name refers to the cation, the second part is the cation substitution site, and the third part of the name is associated with the sodium ion vacancy position. 188
Table 8.2 - Geometry optimised lattice parameters for Zeolite-A within the cubic structure Fm-3c. The structures correspond to 100% sodium ions as well as 50% of these ions replaced by calcium, barium, or lead ions. 189
Appendix Table 2.2 - Table of GFAAS results including dilution factors and final concentration of lead in ppm..... 221
Appendix Table 3.1 - Complete XRF data for each soil sample as well as Zeolite-A 222

Acknowledgements

I would like to thank my supervisor, Dr. Maria Alfredsson, for her never-ending enthusiasm and constant positivity. Maria was never daunted and constantly found solutions. Maria was there for the laughs, for the tears, and she taught me skills that I will carry with me forever.

I would also like to thank the School of Physical Sciences Department at the University of Kent, specifically James Redmond, for helping me successfully jump all of the hurdles required for international students. Also, thanks to the many administrators and lecturers in the department who were friendly, positive, and similarly helped me remain. A special thank you to the other students in my group; Piero, John, Mikey, and Jimmel. They were my role models and my companions throughout this journey. Holly French was not only a great friend with a shoulder to lean on but also an AAS wizard.

Tim Kinnear deserves his own mention because without him, this thesis would not exist in its current form. He was my computer genius and I thank him from the bottom of my heart for being such an incredible friend and colleague.

My family in California was wonderful and supportive. The care packages and thoughtful letters helped remind me that I was missed and loved. My Grandmother, in particular, was a very positive influence.

Nick Featherstone was compassionate and understanding. His support was untiring and absolute whilst his patience was immeasurable. Nick taught me to trust, both in others and in myself and my own abilities.

Finally, I would like to thank my mother, for her unwavering love and support.

Dedication

To Tim –

For dubbing me ‘Tenacious’ and being a true friend.

To Nick –

For being patient, supportive and understanding. For being everything I needed.

And for waiting.

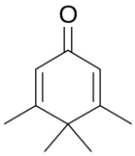

To my Mother –

The greatest cheerleader that anyone could ever hope for

This is for us.

RB

Declaration

I hereby declare that the work presented in this thesis is entirely that of the author, except where due acknowledgement has been made. This work has not been previously submitted, in whole or in part, for any other academic degree.

Candidate: Rebecca Blake Tanney

Abstract

The aim of the current project is to determine if Zeolite-A is suitable for lead remediation in pyrite ash contaminated soils. Pyrite ash is the waste product formed by roasting sulphide-bearing minerals for the production of sulphuric acid. The main sulphide mineral in the original material is pyrite, FeS_2. After roasting, the soils contain a large amount of iron oxide in the form of hematite (α-Fe_2O_3), as this is the main product in the roasting process of pyrite. It was found that concentrations of 23000 to 26000 ppm of lead were present in the pyrite ash layers.

Zeolite-A was chosen as a method of remediation because it is a synthetic zeolite that is easy to synthesise, has a small pore size, and has a high affinity towards lead as shown by other studies on wastewater treatment.

Zeolite-A was added to soil samples and washed with water and dilute nitric acid to simulate rain and acid rain conditions. It was found that the addition of Zeolite-A to all soil samples investigated resulted in a pH increase by over 2 pH units. In soils washed with acid, having a pH of around 0.30, the pH increased to about 3.00. In soils with a pH of around 4.50, the addition of Zeolite-A increased the pH to nearly 8.00.

It was demonstrated that the addition of Zeolite-A to the samples resulted in a reduction of lead ions in all the leachates, independent of initial pH. The effect of Zeolite-A varied as a function of pH, but was found to reduce lead concentration in the leachate by approximately 82% to 99%. It was concluded to be successful for lead remediation.

One explanation for the successful result of lead remediation by Zeolite-A was the formation of a natural zeolite, gismondine ($CaAl_2Si_2O_8 \cdot 4H_2O$). It was found that gismondine was formed both when the soils were washed with water or with acid. Hence, the gismondine formation was independent of pH. It is also proposed by this study that Zeolite-A stimulated the crystalline formation of gismondine.

Chapter 1 Introduction

1.1 Aims

The aims and objectives of this study were to analyse the suitability of Zeolite-A addition to soil as an effective remediation technique and to evaluate the zeolite's effect on lead present in pyrite ash waste material. For this purpose, soils were obtained from an industrial site in Oskarström, Sweden. The soils were known to present levels above the legal limits of lead and were collected and analysed prior and post the addition of Zeolite-A.

1.2 Background

The industrial site was the location of a paper mill that retired in the 1960's. As part of the paper pulp manufacturing, sulphuric acid was produced directly at the site. This process is known to generate pyrite ash – a waste product often associated with high concentrations of heavy metals, including lead. This originates from the sulphide minerals used in the sulphuric acid production (Turk, 2016). The pyrite ash waste was generally used as landfill material at the site and also employed as a pesticide around the local railways. One of the concerns at the site in Oskarström, is the proximity to a major river in the area and the possibility of lead leaching from the soil into the nearby river with catastrophic consequences to the flora and fauna. Concerns regarding the fish population in the river were raised, as it was a major spawning ground for salmon. The area of land affected is currently closed off to the public. A court case was brought against the paper mill by the Environment Protection Agency of Sweden. The court concluded that the paper mill was not to be held accountable for the contamination that occurred, resulting in the government needing to deal with the affected area. This called for an inexpensive and simple method to be found that could bring the concentration of lead in the soil to below legal limits, allowing the area to be reopened to the public.

1.3 The Current Study

The first step in this study was to establish the amount of lead in the pyrite ash. Soil samples from two different locations at the site were collected. The first location, with lower levels of lead, was identified as the area in which the roasting process had

taken place. It was where the initial sulphide minerals (and later pure sulphur) had been loaded into the roasting furnace. The procedure was where the oxidation process of sulphide to oxide material would occur, as the purpose was to extract sulphur to produce sulphuric acid. The second location showed high concentrations of lead, well above legal limits. This location had been used for dumping pyrite ash waste after the roasting procedure. This procedure is where the oxidation process of sulphide to oxide material would occur, as the purpose is to extract sulphur to produce sulphuric acid. The aim with the present study was to find a method that would remediate the contamination at its source, in this case, lead in the pyrite ash waste material. Zeolites are commonly used in remediation for their molecular microporous structures. Zeolite-A was selected as it is simple and inexpensive to synthesise in large quantities. It also has a pore size that would fit a lead ion.

Before the addition of Zeolite-A, the soils from the site were investigated to determine the main elements and mineral components present. It was also important to analyse the physical properties of the soils, particularly the pH, as it may influence the remediation ability of Zeolite-A to remediate. This involved characterising the mineral composition of untreated pyrite ash, using X-ray Diffraction. The structure and mobility of heavy metals in the ash was established by conducting acid digestion experiments of the collected soils followed by chemical analysis on the leachate as well as the residue.

Depending on the silicon to aluminium ratio in the zeolite structure, the sensitivity to pH fluctuations will control the solubility of the zeolite. As part of the study, it was, therefore, important to determine how the pH influences the dissolution process of Zeolite-A. An experiment was conducted that analysed the concentration of lead in the leachate when synthetic Zeolite-A was added to lead nitrate solutions. These solutions had a known concentration and were in a controlled range of pH values. It was found that synthetic Zeolite-A was stable at pH values higher than 4.00.

1.3.1 Experimental and Computational Analyses

To determine the success of Zeolite-A when applied to the contaminated pyrite ash waste, three different amounts of Zeolite-A were added to a constant mass of soil

sample in a constant volume of either purified water or dilute acid. As for the untreated soil samples. the mobility of lead was established from acid digestion experiments, analysing both the leachate as well as the soil residues.

The experimental work was complemented by computational analysis. Simulations were run varying the location of the lead ions. Energy data was generated regarding the adsorption of lead ions into the sodalite cage or absorption into the framework, both at 25% or 50% capacity.

The conclusions from the project were that the addition of Zeolite-A is successful in reducing the amount of lead in the leachate, suggesting that the contaminant is contained in the soil residue. XRD was used to identify the minerals in the different soil residues. It was proposed that, independent of the pH of the leachate and the addition of Zeolite-A, a new mineral component was detected, which had not been present in the original soil samples. One possibility in identifying this new structure is the formation of gismondine, a natural zeolite, which naturally forms under hydrothermal conditions in silicate poor soils. However, because increased additions of Zeolite-A resulted in a further decrease of lead, it is possible that Zeolite-A assisted in the formation of this mineral which resulted in a higher concentration of lead being trapped in the soil residue and not leaching.

Together with the mineral formation, it was noted that the diffraction peaks assigned to lead silicate were diminished, suggesting that the remediation of lead in the pyrite ash waste samples is a concerted mechanism in which lead silicates are transforming to gismondine, which is further encouraged in the presence of Zeolite-A. It can, therefore, be concluded that the addition of Zeolite-A to lead-rich pyrite ash waste is a suitable remediation technique, in which up to 99% of lead is confined in the soil samples.

1.4 Summary

- The current study investigates the effect of Zeolite-A as a remediation technique for soil contaminated with lead.
- The background and results of the current study will be presented as follows:

- Literature Review – Relevant studies discussing factors to consider in the current investigation.
- Area of Study – A review of the area chosen for analysis and background on the site, including the definition and formation of pyrite ash.
- Materials and Methods – Materials and methods used to collect samples, including statistical analysis used, as well as for the synthesis of the remediation and method of addition to soil.
- Experimental Techniques – Equipment and theories used to perform analysis of soil residues and liquid leachate.
- Results and Discussion – The experimental results are divided into two parts: i) characterisation of soil residues before treatment with Zeolite-A and ii) Leaching Experiments to understand the effect of using Zeolite-A for remediation of lead
- Computational Analysis – Set up and results provided by carrying out ab initio calculations on Zeolite-A with varying distributions and loading of lead ions.
- Conclusions and Recommendations – an overall summary and discussion of results along with future suggested work.
- References
- Appendices – additional results and information.

Chapter 2 Literature Review

2.1 Aim

The purpose of this section is to offer a review of relevant studies that have been presented in the literature with the aim to better understand the underlaying chemistry associated with pyrite ash. The discussion includes an understanding of the effects of heavy metals in soil, acid rain and acid mine drainage. Importantly, the different methods of soil remediation are explained and the choice of remediation for this study is given with reasoning.

2.2 Introduction

In the past few years, there has been an emphasis put on remediating areas of land contaminated by industry. This is defined as protecting and restoring the environment of the area and its surroundings, as well as making the land available for other desired purposes.

Many different forms of contamination have been recorded, requiring a range of remediation techniques to be available. The most effective and inexpensive treatment is still being determined through research and investigation.

2.3 Background

Pollution is a serious issue that is occurring worldwide in air, soil and water. Pollution is often so common that environmental disasters now receive minimal press and feedback. The fines and duties imposed are minimal and do not always cover full remediation costs. For example, in *Newcastle Port Corporation v MS Magdalene Schiffahrtsgesellschaft MBH,* the court imposed 20% fines based on the worst projected outcome and awarded significant discounts (Norton Rose Fulbright, 2014). In addition, these forms of accountability are only realised after an event has occurred.

In the last few decades, governments have finally acknowledged that pollution is damaging the environment and currently they focus on making long term goals to try to protect what remains. An example is the Paris Climate Change Conference, held in 2015. Its purpose was to cut greenhouse gas emissions, which specifically

contribute to depletion of the ozone layer whilst raising land and sea temperatures (BBC News, 2015; Ravishankara et al., 2009).

"Smaller" disasters affect single countries, cities and towns and are often overlooked and left to local governments to try and resolve. The result is that the contaminated site is often left to the elements, as smaller courts deal with cases to decide who is responsible for causing the contamination and, therefore, who is required to pay compensation. Because the area affected is not immediately undergoing treatment, rain causes the contamination to spread and, thereby, pollutes nearby areas causing more damage. Below are a few examples directly related to this thesis.

The Brazil mining disaster of November 2015 made worldwide headlines for a short period of time. The Fundão mine tailing dam in Bento Rodriguez collapsed and released 50 million tonnes of iron ore waste in the form of mud and sludge (Massarani, 2015). This contained silica and high concentrations of potentially toxic heavy metals (OHCHR, 2015) including mercury, arsenic, chromium and manganese (Massarani, 2015). It has taken months for the courts and governments to assign blame and require remediation to be funded by the company at fault. Meanwhile, the sludge continued to leach and move from the nearby river, Rio Doce, into the southern Atlantic Ocean (Douglas, 2015).

The Colorado Gold King Mine in Silverton, Colorado, was not in use and was being treated by the Environmental Protection Agency (EPA) when three million gallons of heavy metal waste spilled into a river in August 2015 (Berzon, 2015). Later in October 2015, another smaller spill occurred. This prompted a new bill to be offered for Federal Regulations to be formed regarding working at abandoned coal and hard rock mines. The bill would force requirements for safety and security of the toxic waste as remediation was being attempted (Henry, 2016).

The focus of the current study is on the remediation of lead from contaminated soil that originated from pyrite ash waste produced by pulp manufacturing. The elevated amounts of lead in the pyrite ash waste was determined in a previous study using Inductively Coupled Plasma (ICP) (Appendix 1). Lead is defined as a heavy metal,

with specific toxic effects. These as well as the definition of heavy metals are presented in Section 2.3.

2.4 Toxic Effects

Heavy metals refer to elements that have a density of over five times that of water, have a high atomic mass and are considered to be metals or metalloids (Tchounwou et al., 2012). Toxic heavy metals are known to have the ability to cause detrimental effects to the environment, and concerns are associated with their ability to bioaccumulate through the food chain.

There are naturally occurring heavy metals, which occur due to processes such as mineral erosion and leaching from ore deposits (Momodu & Anyakora, 2010). Small amounts of these metals are required to retain a body's normal metabolism as some enzymes require metals such as iron, zinc and copper for their catalytic activity (Adepoju-Bello et al., 2009). The problem with heavy metals is that only a small concentration is manageable by the human system. Any further exposure results in toxic effects.

Metal toxicity is relevant for all living systems, affecting plants, animals and humans. It has been shown that plants will take up metals with water and nutrients. Lead, specifically, does this by binding to the carboxylic groups of acids located on root surfaces (Morel et al., 1986; Sharma & Dubey, 2005). The majority of the lead contamination will stay stored in the roots (Blaylock & Huang, 2000) where it is exchanged with carbonates and phosphates in the cell walls via ion exchange (Blaylock & Huang, 2000; Sahi et al., 2002; Sharma & Dubey, 2005). The lead can now move freely through the channels of calcium and accumulate near the inner layer of cells within the roots and stems (Huang & Cunningham, 1996; Antosiewicz, 2005). From this ideal location, the lead can increase the concentration in other tissues of the plant. Any animals that ingest the contaminated plant will now store the metal in their system and may experience metal poisoning due to bioaccumulation (the gradual increase of a chemical in an organism that occurs over time). The reasons for the bioaccumulation are that either the chemical is not being broken down via metabolism, or it is being absorbed faster than it can be excreted (Mader, 1996; Cox,

1997). In animals, this usually ends in death. It has been found that garden snails can accumulate 43% of its lead from food, which is stored in its soft tissue. Similarly, a link has been found between lead contaminated grass and a detrimental effect on grasshoppers (Laskowski & Hopkin, 1996). With humans, there are multiple ways that heavy metals can affect the human body and its systems.

Metals can form complexes with proteins or enzymes found in the body (Figure 2.1, (Sundin, 2016)). Amine, carboxylic acid, and thiol groups are the usual interaction sites, of which metals prefer thiol bonding, causing the protein or enzyme to change structure and the cell to either malfunction or die. Metals can also cause free radical formation leading to the oxidation of biological molecules (Adepoju-Bello & Alabi, 2005).

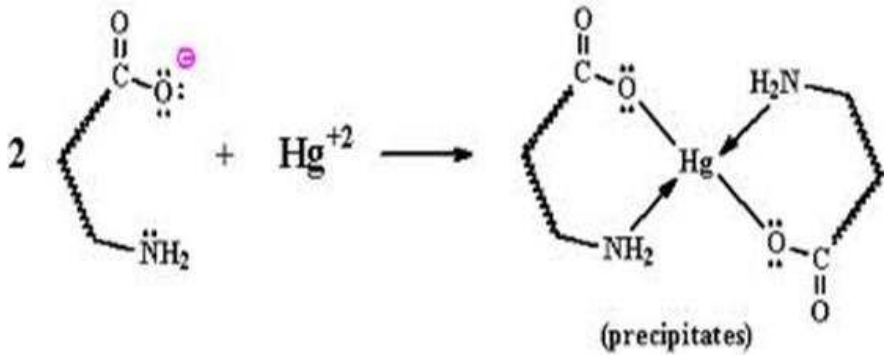

Figure 2.1 - Heavy metals, such as Hg^{2+}, form a complex with alkaline proteins and precipitate

Metals that are used daily can cause serious health issues if ingested in high concentrations. Ingestion of aluminium, a light metal, widely used in multiple sectors including transportation, packaging, and food and beverage containers, has been connected to neurological disorders (e.g. Parkinson's and Alzheimer's diseases (Momodu & Anyakora, 2010)). Arsenic, a metalloid, used in wood preservation, insecticides, and semiconductors (Royal Society of Chemistry, 2016), is well known to for its toxic effects as even a small amount can cause abdominal pain and skin lesions whilst increasing the risk of cancer (American Cancer Society, 2014). Cadmium, which is used extensively in batteries and electroplating, can cause kidney damage (Momodu & Anyakora, 2010). Mercury, especially its presence in fish, can cause numerous negative effects on the nervous, digestive and immune systems (World Health Organisation, 2015).

Lead is a particularly dangerous metal. It is measured by the level present in the blood, referred to as the blood lead level (BLL). It can affect every organ system by acting as though it is calcium. This allows it to interact with proteins. Once in the body, lead is distributed all over, including to the brain as well as being stored in teeth and bones. It is here that it accumulates and over time causes even more damage (World Health Organisation, 2015).

In adults, lead can have effects on the renal, endocrine, gastrointestinal, and cardiovascular systems, whilst it can cause developmental problems for the foetus when affecting a pregnant adult. The precise effects are being investigated. It is also known that lead has strong effects haematologically, causing the body to be unable to produce haemoglobin, resulting in two different types of anaemia. The most devastating effects are neurological, whilst lead encephalopathy is associated with high levels of lead in the blood, affecting the peripheral nerve function. Lead toxicity also leads to issues with bone development and general health (World Health Organisation, 2015).

Lead affects children differently than adults. This is because a child is still growing and its systems are not fully complete. Studies have shown that a child who grows up with lead toxicity is more likely to experience serious health issues as an adult. The lead works to undermine the body's natural processes and as the child grow up, the toxic effects increase (World Health Organisation, 2015).

The Environment Protection Agency (EPA) in the United States has classified lead as a 'probable human carcinogen'. The connection between lead poisoning and cancer is being investigated (Agency for Toxic Substances and Disease Registry, 2012). The World Health Organisation (WHO) has estimated that lead poisoning causes around 143,000 deaths per year. They have a list of ten chemicals of 'major public health concern' and lead is on this list. They note that lead contamination is entirely preventable. The most common methods of getting lead into a system is by inhalation and ingestion.

Lead contamination is often caused by mining, smelting, manufacturing and recycling processes, where one of the most common applications is lead-acid batteries in motor vehicles.

2.5 Sources and Spread of Contamination in Soil

Heavy metals are non-biodegradable (Esmaeili Bidhendi et al., 2010) and contamination can be spread through many different media. Air, soil, and water can all carry heavy metals and cause their spread. This project will focus on the contamination of soil, as the lead associated with the site under investigation was localised to the pyrite ash waste. In order to provide controls for analysis, samples were collected from the contaminated location in soil layers above and below the contaminated pyrite ash layer as well as at locations not containing the layer of pyrite ash. This was to determine the spread of the contamination and confirm the source.

Metals easily interact with soil via ion exchange or chemisorption by iron, aluminium, silicon, and manganese oxides. The organic matter present can also form metallo-complexes (Christensen et al., 1996) whilst the colloidal matter has a high affinity for heavy metals (Gounaris et al., 1993).

The mobility of the contamination can be caused by several factors. The heavy metal's specific properties need to be considered as well as those for the soil. The number of binding sites present, the pH, the concentration of complexing anions and competing cations, as well as the organic matter present capable of soluble transport of the heavy metals are all integral details (Tyler & McBride, 1982).

The concerns with mobile toxic heavy metals as opposed to localised contamination is the interaction they have with the environment and how they will affect animals, which then also leads to human exposure. Mobility of heavy metal species can lead to the accumulation of concentration in living organisms over time via bioaccumulation. Long term damage can occur quite quickly and does not require the level of heavy metal contamination in the soil to be particularly high as it is cumulative (Jeffrey, 2011). This can then be transferred to humans through ingestion (Laskowski & Hopkin, 1996).

2.6 Soil Classification

Soil classification allows for heavy metal mobility to be analysed, and addresses the soil pH, particle size, appearance, and organic content.

Soil is not homogenous in size but consists of a wide range of particle sizes due to the addition of minerals, fragments of rock, and organic matter. Water and air then fill the spaces in-between the particles. Weathering can change the appearance of the particles via temperature and abrasion. However, when chemical weathering occurs, involving oxidation and hydrolysis, a wide range of properties both chemical and physical can be affected (Radojevic & Bashkin, 2009).

Soils are classified into various types based on their particle size. The British Soil Classification System has compiled a list with subdivided groups defined by the texture of the soil. The size of the particles affects their binding ability with heavy metals (Jensen et al., 1999) as well as the leaching ability of the soil and, therefore, the mobility of the heavy metals. The sizes range from 200 mm and higher, classified as boulders, to less than 0.002 mm, classified as clays (Jeffrey, 2011).

Organic material and colloidal organic material can both affect the interaction of soil with heavy metals. These materials have a high affinity for heavy metals and as a result, metal-organic complexes are formed (Christensen et al., 1996; Gounaris et al., 1993). This interaction affects the overall concentration of toxic heavy metals in the soil. If the organic material is soluble, then it can facilitate the mobility of heavy metals. Conversely, insoluble organic material would cause the heavy metals to be retained in the soil.

The pH of the soil is arguably the most important characterisation needed to understand the interaction with heavy metals. The general principle is that in more acidic environments, a higher level of leaching will occur (Radojevic & Bashkin, 2009). pH also determines the formation of complexes between heavy metals and organic compounds. This occurs in ion exchange as well as chemisorption reactions, where functional groups in the organic molecule bind to metal ions. Chelation, the removal of heavy metals, can occur in this situation when there have been multiple bindings between organic compounds and a heavy metal. The chelation ring does not allow the

heavy metal to move from the soil to the leachate (Snoeyink & Jenkins, 1980). At a low pH, the solution is acidic meaning there are numerous protons available to be taken up by the organic functional groups and the metal ion must compete for a binding site. Consequently, fewer metal ions will successfully bind to the coordination sites, meaning that more of the metal ions will be available to leach. This is often discussed under Cation Exchange Capacity (CEC).

2.7 Detection of Heavy Metals

Analytical techniques used to detect heavy metal toxicity differ depending on the specific type of contamination suspected, as well as the personal preferences and availability of equipment to the researcher. There are also varying allowable limits of heavy metals in different countries. It is usually required for the concentration to have reached trace level, micrograms per litre (of water), before being considered in need of remediation. The WHO has published maximum permissible limits (MPLs) for different heavy metals in varying matrices.

To determine the level of contamination, 'traditional' analytical techniques were used. Flame Atomic Absorption Spectroscopy (FAAS) is commonly used for trace detection analysis (Ekpo & Ibok, 1999; Charlesworth & Lees, 1999) with Graphite Furnace AAS (GFAAS) being considered to be a more sensitive technique (Sarzanini, 1999; Tyler, 1991). Inductively Coupled Plasma (ICP), ICP-Mass Spectroscopy (ICP-MS), and ICP-Atomic Emission Spectroscopy (ICP-AES) are also used (Tyler, 1991; Hill et al., 1993; Tomlinson et al., 1994; Sutton et al., 1997; Divjak et al., 1998). The differences between AAS and ICP and ICP-MS are analysed in Section 4.3.4. High Performance Liquid Chromatography (HPLC) can be employed (Santoyo et al., 2000) as well as X-ray Diffraction (XRD) and X-ray Fluorescence (XRF) (Radojevic & Bashkin, 2009). With the exception of AAS and ICP, these techniques provide different information. Hence, to obtain a more complete understanding of the samples, a combination of these techniques were applied.

When the contamination in soil is being measured, it is also important to analyse the leachate and not just the solid soil residue. Leaching is characterised as the mobility of metals in groundwater, and it can be analysed to help determine the total

amount of metals in the contaminated soil. The purpose of conducting and analysing leaching experiments is to mimic the natural processes that occur, such as rain, and account for the affects that these have on the soil.

To obtain accurate leachate data, one approach employed in this study involve agitation experiments. This involves mixing soil with aqueous acidic solutions and then agitating the flask via rotating or shaking. Toxicity Characteristic Leaching Procedure (TCLP) is used to analyse the mobility of contaminants (Saether et al., 1997; Wang et al., 2001). One method involves a mixture of acetic acid and sodium hydroxide which is added to soil and agitated for 18 hours. This is to produce results comparable to long term leaching in nature (United States Environmental Protection Agency (USEPA), 1986). This produces a leachate which is contaminated. Other techniques exist which utilise nitric acid, sulphuric acid or phosphoric acid in place of acetic acid (Tokunaga & Hakuta, 2002).

2.8 Acid Mine Drainage and Pyrite Ash

Acid mine drainage (AMD) is an acidic water that contains high amounts of iron, sulphate, and other metals (Skousen, n.d.). Acid mine drainage is the waste produced when materials containing sulphur (e.g. sulphide minerals) are exposed to oxygen and water. This can occur naturally, although in much smaller amounts than when directly associated with mining sites (Peppas et al., 2000).

AMD causes a decrease in water quality by lowering the pH of groundwater and, thereby, increasing the dissolved metal content (Mills, 2012; Fraser Institute, 2012). This can negatively affect the aquatic life (Jennings et al., 2008; Fraser Institute, 2012). In fact, AMD is one of the main causes of pollution in the mid-Atlantic United States (U.S. Environmental Protection Agency, 2016).

AMD is formed in oxidising environments, commonly produced in coal mining, which involve sulphide-rich and carbonate-poor materials. The most common metal-sulphide mineral in rocks is iron pyrite, FeS_2, which often contains lead as an impurity as well as copper and zinc. The method of mining increases the rate of acid generation due to the increased surface area of the exposed sulphide ores (Baker & Banfield, 2003). Microorganisms also populate AMD. Their presence increases the rate of AMD

formation by causing the catalysis of iron and sulphur oxidation (Baker & Banfield, 2003). The ferric iron formed by the microorganisms are then able to react with further pyrite, in a spontaneous reaction, forming more ferrous irons, sulphate ions, or precipitate (Equation 2.1) (Taylor, 1996; Brock, 1994; Ohmura et al., 1993; Perry & Kleinmann, 1991; Schippers et al., 1995). Figure 2.2 shows the cycle of ferrous ions being biologically oxidised to ferric ions (Snoeyink & Jenkins, 1980; Taylor, 1996). As a result, the main solid waste product in AMD is an iron oxide precipitating as oxides and hydroxides in the soil or water sources.

$$FeS_2 + 14Fe^{3+} + 8H_2O \leftrightarrow 15Fe^{2+} + 2SO_4^{2-} + 16H^+ \quad (2.1)$$

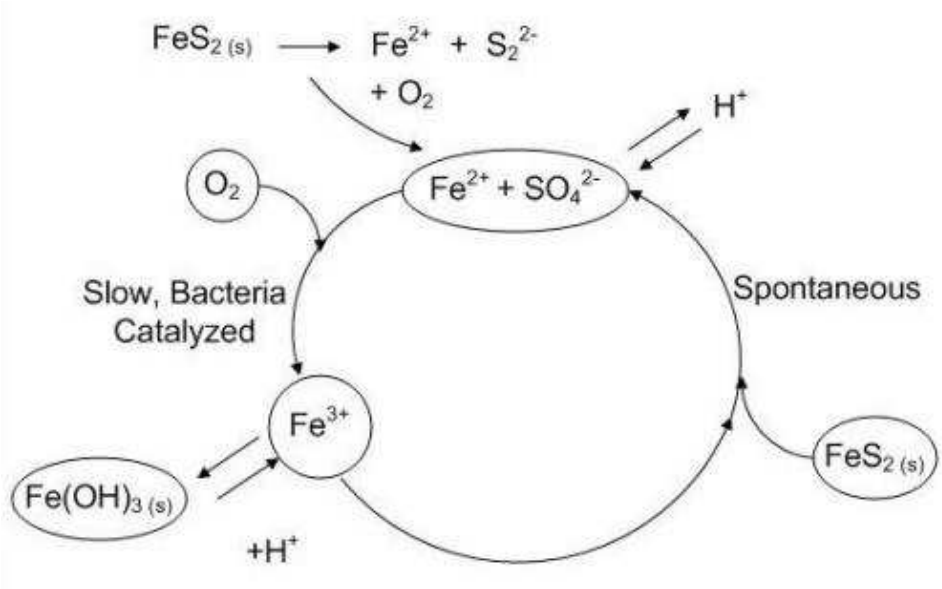

Figure 2.2 - Cycle of pyrite oxidation by microorganisms

Pyrite ash waste is produced as a result of the industrial production of sulphuric acid. In Figure 2.3, equation [1] refers to the oxidation of pyrite to sulphate. This reaction should be compared with the oxidation of sulphide minerals by bacteria. Equation [1a] shows the dissolving followed by oxidation of pyrite, whilst equation [2] represents the reaction for when aqueous ferric oxide acts as the oxidising reagent. In order to replenish this ferric oxide, equation [3] uses oxygen to oxidise ferrous iron whilst equation [4] is the formation of insoluble iron (III) hydroxide.

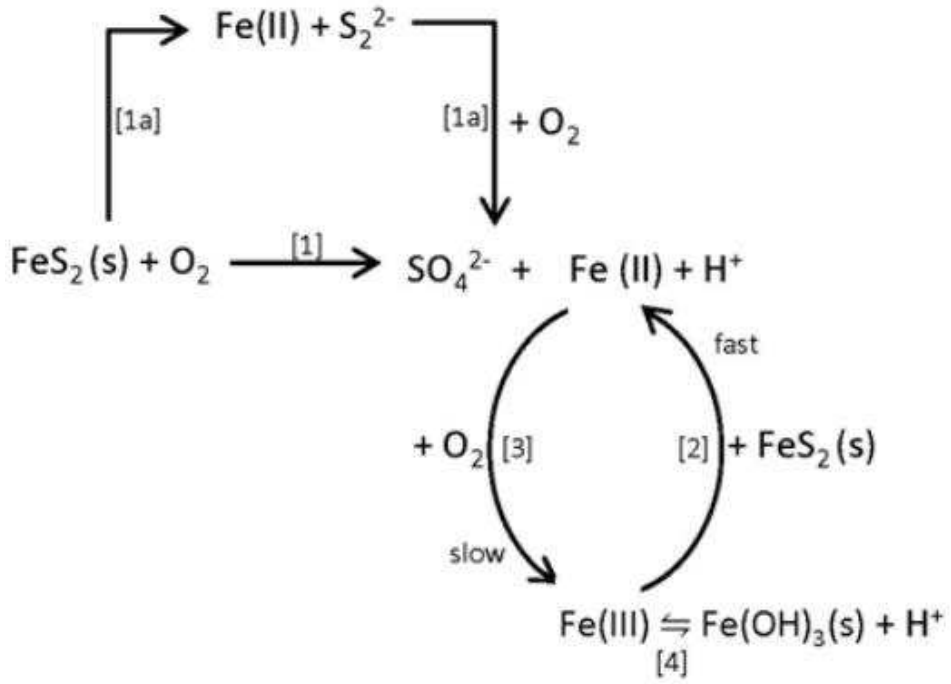

Figure 2.3 - The oxidation of pyrite

Pyrite ash has often been treated as waste and it is usually discarded into landfills or the sea. However, research suggests that the waste can be useful as a raw material for producing iron ore which involves treating the ashes to ensure they achieve strength, allowing them to survive handling, drying and firing (Tugrul et al., 2007). Pyrite ash made into pellets has been found to be the most useful. The changes to their structural behaviour have been analysed in a study that determined that Fe_3O_4 could be reduced to a metallic iron phase confirmed by XRD and XRF (Tugrul et al., 2009). The reactions identified in this process include Equation 2.2, which shows the formation of magnetite from iron hydroxides (Schikorr, 1933; Mohapatra et al., 2013). Equation 2.3 is the same process as that used in the steel industry to obtain metallic iron ore which is further reduced (Greenwood & Earnshaw, 1997).

$$3Fe(OH)_2 + 2H_2O \rightarrow Fe_3O_4 + H_2 + 4H_2O \quad (2.2)$$

$$Fe_3O_4 + 4CO \rightarrow 3Fe + 4CO_2 \quad (2.3)$$

Also, AMD has been studied for use in remediation. It has been found that AMD with hydraulic fracturing fluids was successfully used to remediate radium, barium and strontium. It was found that a blend of the two caused a precipitation of secondary minerals, including iron-bearing minerals, and that the toxic compounds were

sequestered. It was noted that the pH and concentration of sulphur in the solution were factors that controlled optimal conditions for removal of toxic compounds (Kondash et al., 2014).

AMD has also been used as an additive to reduce the concentration of radioactive material found in fracking waste. The method used was to mix the wastewater with AMD, enabling the fracking contaminants to bind into solids, which were removed prior to discharging the wastewater back into rivers (Duke University, 2014).

Sulphide-rich mine waste resembles pyrite ash waste, as it is formed in an oxidising reaction of pyrite generating iron oxides. The initial presence of SO_4^{2-} ions will form sulphates and second order minerals as opposed to forming SO_2 in gas form, as discussed in Section 3.3 for the "sulphite" process. An example of sulphide-rich minerals is the copper mine in Falun, Sweden. At this mine, a similar process was carried out as utilised by the site in the current study. Pyrite was roasted and the by-products, iron oxide-rich materials, were stored in large piles that burned to further oxidise the minerals to be used as a red pigment. These piles were exposed to light and weathering, causing the Fe^{3+} to form hematite. The 'pyrite ash' layers were formed deeper within the piles, protected from the weather and unable to be reached by sunlight. These layers leached into the soil causing heavy metal contamination and a decrease in pH. The effect of AMD on soil can be compared to the issues associated with acid rain.

2.9 Acid Rain

Acid rain has been known to affect the toxicity of metals in soil and water. By causing leaching of toxic elements into nearby rivers, the rain itself also affects the environment resulting in some major issues as shown in Figure 2.4 (Weller, 1982; EPA, 2016). Acid rain is mainly formed by sulphur oxides and nitrogen oxides producing that form sulphuric, sulphurous, and nitric acids. In addition, acid rain contains hydrochloric acid. These acids lower the pH of the rain to below 5.65, which is the value for distilled water in a state of equilibrium with carbon dioxide (Pyatt, 1987; EPA, 2016). The cause of acid rain in Sweden in the 1960s and 1970s was mostly due to

winds directed from the heavily industrialised UK and mainland Europe. The Swedish Ministry of Agriculture stated that “when water is acidified… a variety of other metal ions including zinc, lead, and cadmium become more readily soluble and consequently available to the fauna and flora of such affected ecosystems” (Pyatt, 1987; Rieuwerts et al., 1998).

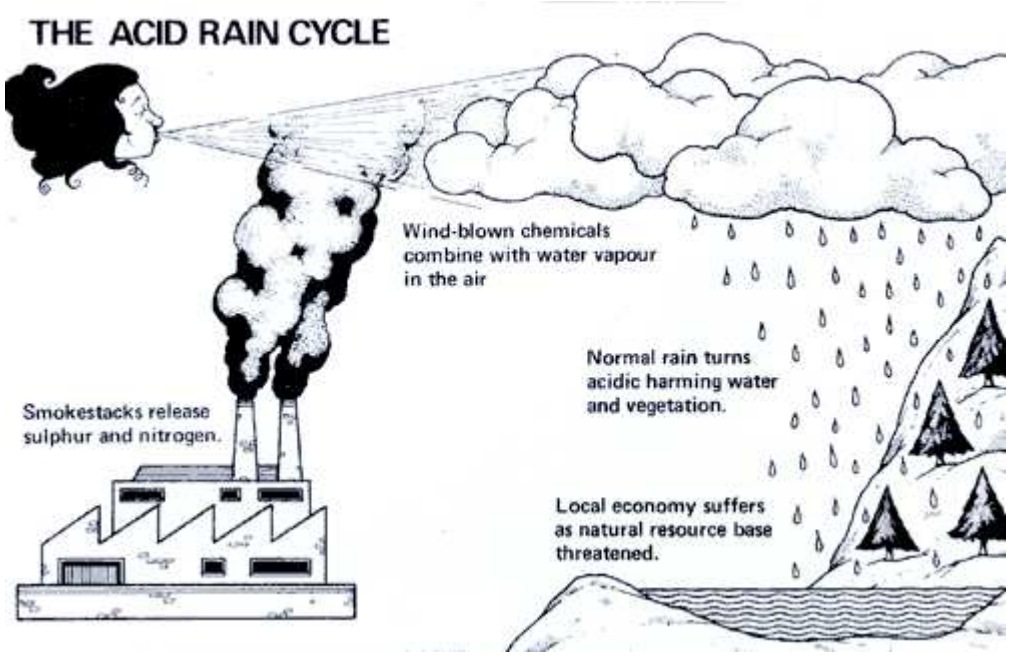

Figure 2.4 - The Acid Rain Cycle

Research has been conducted to attempt to determine the specific effects that acid precipitation has on toxic metals entering the human system, demonstrating that seemingly healthy people have adverse effects to medical treatments when they have been exposed to toxic metals due to acid rain (Nordberg et al., 1985).

The acid rainfall in Sweden in the 1970s led to a change in legislation. The 1972 United Nations Conference on the Human Environment in Stockholm, Sweden introduced an international corporation, which addressed air pollution and acid deposition. This then led to a legally binding international agreement to reduce air pollution regionally at the 1979 Geneva Convention on Long-range Transboundary Air Pollution.

The factors that affect the rate of acid generation are applicable for both acid mine drainage and acid rain. They are as follows:

pH, temperature, oxygen content, degree of saturation with water, chemical activity of iron (III), surface area of exposed metal sulphide, chemical activation energy required to initiate acid generation, and bacterial activity (Peppas et al., 2000).

The reaction mechanism of iron in various pH and oxidising environments can be summarised in a Pourbaix Diagram. These diagrams show the relationship between redox activity and Brönsted acidity. They allow the estimation of which oxidation state and which species/minerals are present under the conditions present in the soils.

Figure 2.5 shows a simplified Pourbaix diagram for iron, where low concentration species have been omitted (Russell & Hall, 2006). The diagram assumes that the iron species are in natural water. This is because this maintains a low iron concentration, whereas, at a high concentration, iron species can become complex multinuclear compounds.

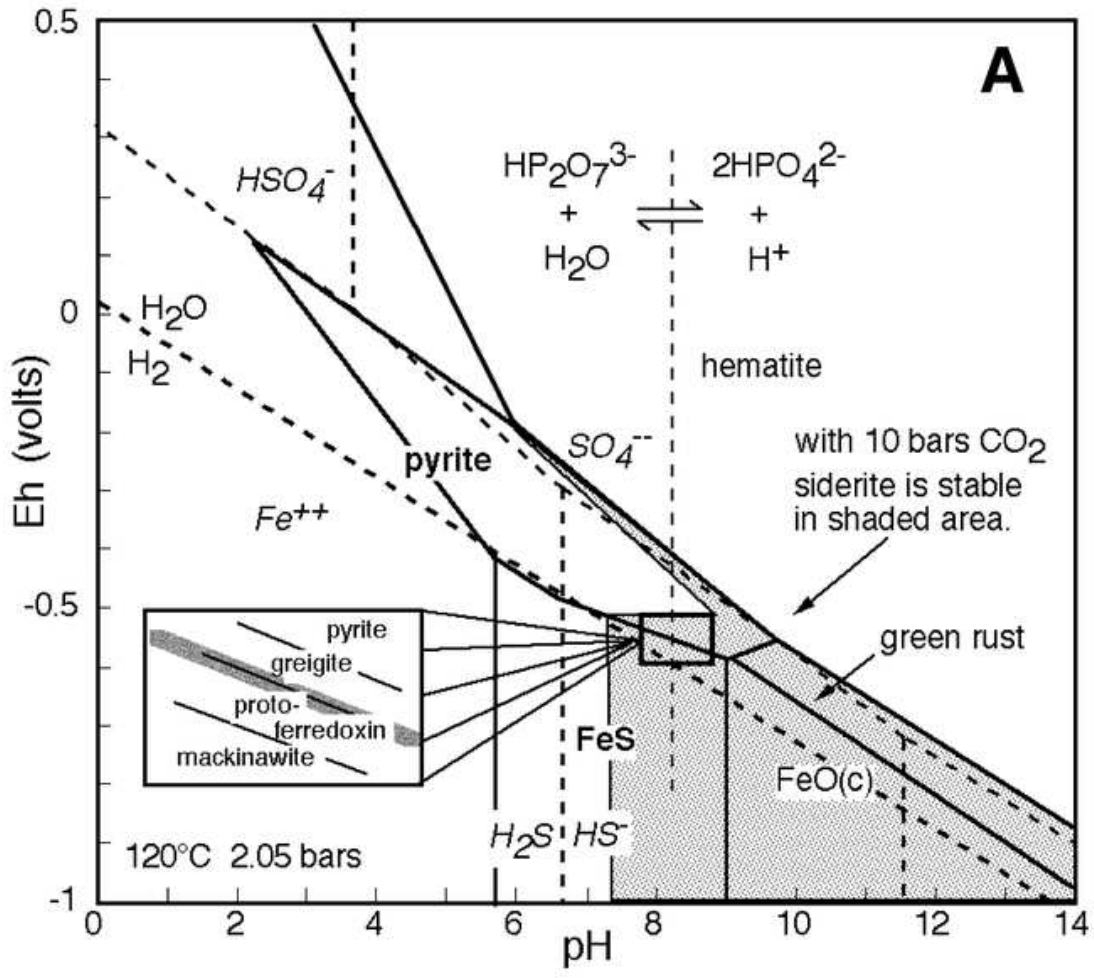

Figure 2.5 - Pourbaix Diagram for Iron

The origin of the different regions in the diagram lies in the half reactions for iron in an oxidising aqueous environment as shown in Equation 2.4.

$$Fe^{2+}(aq) \rightarrow Fe^{3+}(aq) + e^{-} \qquad E= -0.77V \tag{2.4}$$

This reaction does not involve any H^+ ions, which implies that the iron potential is independent of pH and causes a horizontal line to be formed (Atkins et al., 2006).

Fe^{3+} will be the major product when there is a couple[1] in the environment consisting of a more positive, oxidising, potential. Couples that are not thermodynamically stable in water have a redox agent that is too strong, as shown in Equation 2.5 (Atkins et al., 2006).

$$Fe^{3+}(aq) + 3H_2O(l) \leftrightarrow Fe(OH)_3(s) + 3H^+(aq) \tag{2.5}$$

This equation does not involve a change in oxidation number for any of the ions and, therefore, is not a redox equation. This means that the boundary between the regions of $Fe^{3+}(aq)$ and $Fe(OH)_3(s)$ is independent of electrochemical potential. The boundary is affected by pH. Fe^{3+} will be the major product at a low pH and iron hydroxide precipitate will be expected in a more basic environment (Atkins et al., 2006).

Another possible Fe-H_2O system reaction can also occur as shown in Equation 2.6.

$$Fe(OH)_3(s) + 3H^+(aq) + e^- \leftrightarrow Fe^{2+}(aq) + 3H_2O(l) \tag{2.6}$$

This occurs due to Fe^{2+} being oxidised and $Fe(OH)_3$ being reduced. Therefore, Fe^{2+} is favoured in an oxidising environment with a low pH. However, natural water is usually more neutral/basic. The increase in pH is not enough to cause the reduction. There must, therefore, also be strong reducing agents to cause this change. This is unlikely if the water contains plenty of oxygen. It is important to consider that soil and water surfaces are very rich in oxygen, which would likely cause $Fe(OH)_3(s)$. This is because oxygen in the air is able to interact with the surface. At depth, there is decreased oxygen content, favouring Fe^{2+} formation (Atkins et al., 2006).

[1] In electrochemistry, a couple is a term for an electrode consisting of an active metal (strong reducing agent) and a less active metal (Atkins et al., 2006).

More importantly, acid mine drainage is directly related to pyrite and pyrite ash. Pyrite, FeS_2, is a common sulphide mineral. Pyrite is further oxidised to hematite. This is due to pyrite containing iron in the +2 oxidation state rather than +3. The sulphide mineral is first oxidised into dissolved iron, sulphate and hydrogen as seen in Equation 2.7 (Atkins et al., 2006). This lowers the pH of the environment. A further reaction will take place if there is sufficient O_2 present.

$$FeS_2 + 3.5O_2 + H_2O \rightarrow Fe^{2+} + 2SO_4^{2-} + 2H^+ \quad (2.7)$$

In Equation 2.8, the ferrous iron is oxidised to ferric iron.

$$Fe^{2+} + 0.25O_2 + H^+ \rightarrow Fe^{3+} + 0.5H_2O \quad (2.8)$$

The Pourbaix diagram shows that, at a low pH, ferric iron will form solid $Fe(OH)_3$. This not only lowers the pH but also removes most of the Fe^{3+} from the solution. Equation 2.9 shows the schematic progress of the oxidation of iron into hematite.

$$Fe^{2+} \rightarrow Fe^{3+} \rightarrow Fe_2O_3 \quad (2.9)$$

Any Fe^{3+} that did not contribute to forming the solid can then act as an oxidising agent and oxidise further pyrite, according to Equation 2.10.

$$FeS_2 + 14Fe^{3+} + 8H_2O \rightarrow 15Fe^{2+} + 2SO_4^{2-} + 16H^+ \quad (2.10)$$

Combining equations (2.8) and (2.10) it is possible to see that pyrite forms solid Fe_2O_3.

$$2FeS_2 + 7.5O_2 + 4H_2O \rightarrow Fe_2O_3 + 4H_2SO_4 \quad (2.11)$$

2.10 Remediation Techniques

The purpose of remediation is to remove or neutralise contaminants so that their toxicity is reduced to the extent that they no longer affect the environment. There are multiple methods that can be undertaken to achieve this. The most practiced method is the excavation of the contaminated material. This involves physically removing the soil along with any other affected material, which is then placed in a landfill. The benefit of this is that it is a quick process and completely removes the contaminants from the contaminated (Wood, 1997). The disadvantage

is that it is costly and does not address the initial issue of contamination, which is only moved to another location instead of being neutralised.

One of the most environmentally friendly methods is the addition of plants as phytoremediators. This has a low set-up cost whilst being widely accepted. The process of phytostabilisation involves plants that are resistant to heavy metals, minimising certain factors, such as wind and water erosion that contribute to contamination spread. Phytoextraction involves plants that are able to remove heavy metals from soil and concentrate the toxic metals in their own tissues. For example, the Chinese Brake Fern is able to remove arsenic and the Indian Mustard plant removes lead. This method can be used for water contamination as well, where it is called rhizofiltration (United States Environmental Protection Agency (USEPA), 2000). Past studies have shown that vetiver grass was capable of up-taking cadmium, lead and zinc (Chen et al., 2000). The main disadvantage of this method is that the remediation is slow.

Electrochemical remediation is often used for soils. This involves applying an electrical signal causing organic components in soils to mineralise and contaminants to mobilise (Centre for Public Environmental Oversight (CPEO), 2010). This method works better in soils with smaller particle sizes. The benefit of this technique is that it can affect large surface areas of soils that have little movement of water. However, this method only works if the metal contaminants are made mobile, which is difficult in soils with a high pH, where the contaminants are immobilised (Yeung & Gu, 2011).

It is more common to add chemicals to stabilise the contaminants on site. Heavy metals can interact with the chemicals and thereby form less toxic compounds. This fixes the metal ions in place and stabilises the system so that the heavy metals are not biologically available or mobile. This is significantly less costly than the previously mentioned excavation method. Phosphate salt-containing fertilisers have been used with positive results (Jeffrey, 2011). A more standard method is adding calcium dihydrogen phosphate ($Ca(H_2PO_4)_2$) along with calcium carbonate, ($CaCO_3$), which results in the formation of hydroxyl pyromorphite ($Pb_5(PbO_4)_3OH$) (Wang et al., 2001). This mineral is insoluble and, therefore, will not leach or spread easily. Calcium

polysulphide (CaS_4) has also been proven to produce non-toxic compounds in the form of heavy metal sulphides (Jacobs et al., 2001). In addition, zerovalent iron (Fe^0) has been found to stabilise arsenic and chromium as the iron can change the soil pH due to its oxidising nature. This contributes to cation and anion sorption. The disadvantage of adding chemicals to the soil is that they can increase the problems faced by the environment, leaching into water systems, causing their own pollution. For example, phosphorus-containing chemicals can lead to the growth of algal blooms causing aquatic death (Hart et al., 2004). The soils are not improved in biological quality and the plants growing in the soil are not developmentally supported with this method.

The need for high quality soil facilitated the remediation of soils by adding composts that have been amended by minerals. This improves the biological quality of the soil and plants as well as increasing fertility. It simultaneously offers organic binding sites which will immobilise heavy metals. Compost is inexpensive and easy to obtain. Added to the compost are environmentally friendly alternatives to phosphates. Zeolites are commonly employed for this purpose (Van Herwijnen et al., 2006).

Lead is used in acid batteries. Studies have been conducted to attempt to solidify and stabilise lead in soil at an abandoned battery factory. The lead was found both in elemental as well as oxide form. The soil was at a high pH, 8.87. After attempting multiple methods, the researchers concluded that adding KH_2PO_4, KH_2PO_4 with sintered magnesia or H_3PO_4 with sintered magnesia, both in a 1:1 ratio, were all effective methods of stabilising lead in the soils and thereby reducing the amount of lead detected in the leachate considerably (Zhang et al., 2015).

Studies have also been conducted to attempt to use manganese and iron oxides to adsorb lead from contaminated soils. This was carried out by using both natural and synthetic oxides whilst maintaining a pH of 5.5. Manganese oxides have been proven to be extremely capable of adsorbing aqueous trace metals in soils even though they are less abundant than iron oxides (O'Reilly & Hochella Jr, 2003; Jenne, 1968; Burns, 1976; Chao & Theobald, 1976; Schwertmann & Taylor, 1989). Iron oxides are quite reactive and have high surface areas which make them very able sorbents of heavy

metal cations such as lead (McBride, 1994; McKenzie, 1980; Jenne, 1968; O'Reilly & Hochella Jr, 2003; Schwertmann & Taylor, 1989). Iron (III) oxides and hydroxide minerals found in soils have a strong affinity for lead which makes them very good at sequestering lead from the surroundings (Rickard & Nriago, 1978; Nriagu, 1978). The study of iron oxides used an iron oxyhydroxide, goethite (α-FeO(OH)), as well as hematite (α-Fe_2O_3). The analysis was conducted using XRD as well as AAS and Scanning Electron Microscopy (SEM). It was determined that Mn-oxides were more efficient at adsorbing lead than Fe-oxides (O'Reilly & Hochella Jr, 2003). A more recent publication agreed with these findings when testing natural surface coatings (Dong et al., 2007). Another specifically analysed natural manganese oxides. They noted that waste supplies of MnO_x are easily available and would otherwise be disposed of, so that they would be inexpensive to obtain as well. Importantly, the researchers determined that their method would only be applicable to remediate lead from contaminated water, and not soil, due to the large diversity of the soil pollutants (McCann et al., 2015).

2.11 Zeolites for Remediation

Zeolites are effective tools for remediation. They are well known to have ion exchange properties and modifications can provide properties for anion sorption (Colella, 1999; Misaelides, 2011). Metal cation uptake is determined by a number of factors including: temperature, pH of solution, complexing agents, competing cations, dimensions of hydrated dissolved compounds, channel diameters, external surface activity aqueous chemistry and hydrolysis reactions, (Barrer & Sand, 1978; Ming & Mumpton, 1989; Dyer, 1995; Colella, 2007; Yuan et al., 1999).

Zeolites became a popular method of remediation when scientists were searching for a remedy for nuclear waste management (Misaelides, 2011). A study used clinoptilolite to remediate radioactive caesium (Ames, January 16, 1962). Sites at both Three Mile Island (Collins, 1982) and Chernobyl (Chelishchev, 1993) experienced zeolite remediation to remove strontium and caesium. Zeolites have also been used in acid mine drainage, as discussed further in Section 2.7.

Zeolites can be regenerated (Li et al., 2007) and are able to remove and stabilise heavy metals (Li et al., 2009) and reduce the concentration of hazardous substances

(Leggo et al., 2006). They have also been found useful in the protection of plants by restoring friendly plant and animal life, assisting in fertilisation, and increasing the vitality of the plants (Buondonno et al., 2005).

They have also been used in the purification and treatment of waters and wastewaters (Colella, 2007; Armbruster, 2001; Misaelides, 2011). In addition, studies have researched using a combination of materials such as zeolite with lava and limestone (Baltrenas & Brannvall, 2006; Upmeier, 2006). Surfactant-modified zeolites combine the abilities of enhanced cation sorption, anionic species absorption, and the sorption of non-polar organic species, and pathogens from aqueous streams (Bowman, 2003).

Zeolites can also cause long-term effects that need to be investigated. Zeolites have been found to affect the pH of the soil and the essential metal availability. There are also possible affects due to long-term binding of polluting metals and release of sodium ions. The removal of nutrients in soil as well as quantitative precipitation and the recovery in slow-release fertiliser are all considered in further investigations (Liberti et al., 1999). This is beyond the scope of this investigation and therefore, is mentioned for background, only.

2.11.1 Zeolite General Characteristics

Zeolites are aluminosilicate compounds composed of sodium, aluminium, silicon and oxygen. They have large framework structures that involve silicon and aluminium tetrahedra connected together with Si-O-Al linkages (Figure 2.6), which are governed by Löwenstein's rule. This states that Al-O-Al linkages will not occur in structures where the ratio of silicon to aluminium is greater than 1 (Ribeiro, 1984). This implies that in simple zeolites, where the ratio is 1:1, silicon and aluminium atoms must alternate throughout the framework (Smart & Moore, 2005).

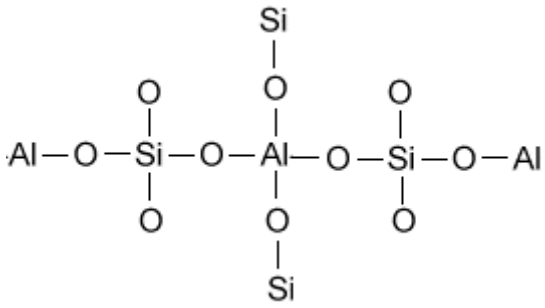

Figure 2.6 - Basic zeolite structure obeying Löwenstein's rule

Silicon oxide structures consist of $[SiO_4]^{4-}$ units, which are linked to form an electronically stable and charge neutral framework. When some of the tetrahedra are replaced with $[AlO_4]^{5-}$, this introduces a negative charge into the molecule, which needs to be neutralised. This is done with the addition of small cations, usually Na^+, K^+ or Ca^{2+}. The general formula of a zeolite is shown by Equation 2.12 where n represents the valency of M, the metal (Smart & Moore, 2005).

$$M_{x/n}[(AlO_2)_x(SiO_2)_y]\cdot mH_2O \qquad (2.12)$$

The benefits of using zeolites for remediation involve their ion exchange properties (van Velzen, 2015), which is why they are used as detergents (Schwuger & Smolka, 1978) and known as molecular sieves. Cations provide stabilisation by neutralisation, and allow zeolites to undergo cation exchange, where the cations in the zeolite structure will be diffused out of the structure and be replaced by external cations. Because zeolites have open frameworks, there is a large surface area for the absorption of cations into the cages. This can allow for multiple small ions or singular large ions. In terms of detergents, zeolites can exchange lighter ions, such as sodium, for calcium and magnesium ions, which are species responsible for causing water hardness (Schwuger & Smolka, 1978). The sizes of allowed cations depend on the particular framework measurements of the specific zeolite. Zeolites have particular channel sizes as well as α and β cage diameters (Figure 2.7, 2.8 and Table 2.1) (Moirou et al., 2000; Yoshida et al., 2013; Weitkamp, 2000).

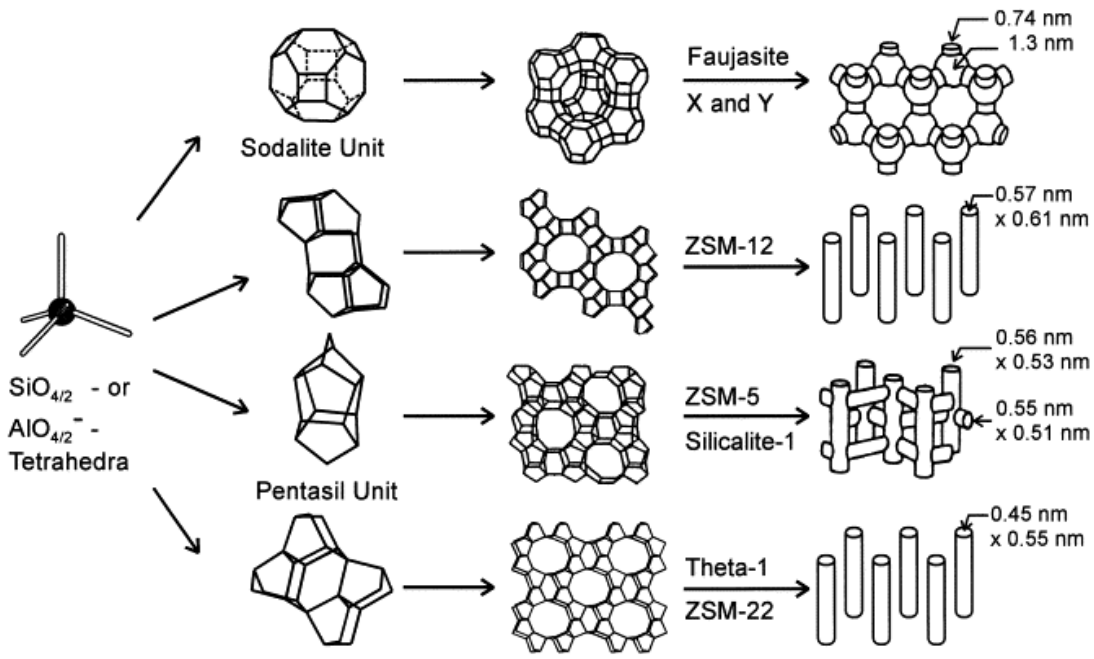

Figure 2.7 - Structures of four zeolites and their pore sizes

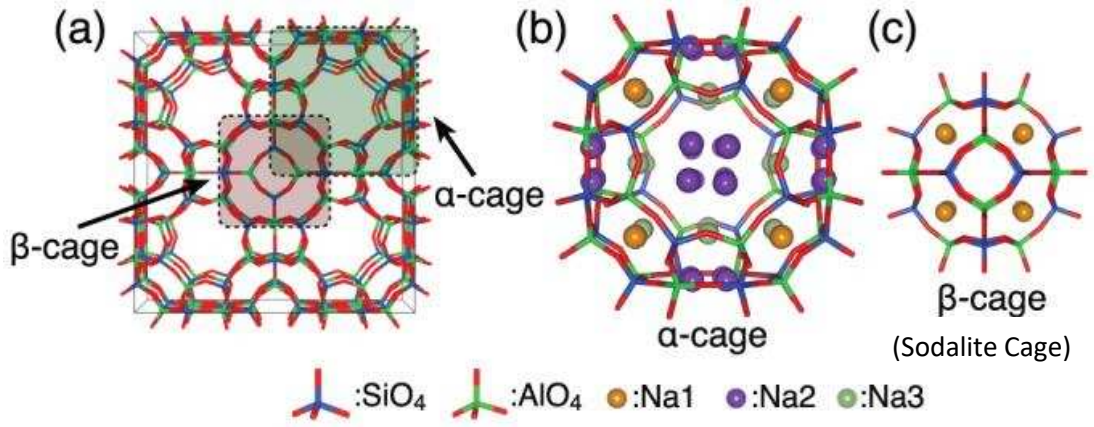

Figure 2.8 - (a) A zeolite sodalite cage structure (b) Schematic model of α-cage (c) Schematic model of β-cage

Table 2.1 - Zeolite General Characteristics, where 's' denotes a synthetic zeolite and 'n' denotes a natural zeolite, 1 - *(Baerlocher & McCusker, 2016)*, 2 - *(First et al., 2011)*

Zeolite Mineral Name	Formula	Largest Cavity Diameter (Å)	Pore Limiting Diameter	Si:Al Ratio
Zeolite-A (LTA, Na-A)[s1]	$[Na^{+}_{12}(H_2O)_{27}]_8[Al_{12}Si_{12}O_{48}]_8$	11.7	4.9	Si = Al
Clinoptilolite[n2]	$Ca_3(Si_{30}Al_6)O_{72}{\cdot}20H_2O$	17.96	7.4	Si > Al
Faujasite[n1] (Zeolite X and Zeolite Y)	$(Ca, Na_2, Mg)_{3.5}[Al_7Si_{17}O_{48}]{\cdot}32H_2O$	11.9	6.7	Si > Al
ZSM-5[s2]	$Na^{+}_{n}(H_2O)_{16}[Al_nSi_{96-n}O_{192}]$	7.0	5.0	Si > Al
Gismondine[n1]	$(Ca, Ba)Al_2Si_2O_8{\cdot}4H_2O$	5.6	3.9	Si = Al
Phillipsite[n2] (Na-P_1,K-M)	$(Na,K)_6(Si_{10}Al_6)O_{32}{\cdot}12H_2O$	6.0	4.3	Si > Al
Chabazite[n2]	$Ca_2(Al_4Si_8O_{24}){\cdot}13H_2O$	8.0	4.2	Si > Al
Linde F[s2]	$Na_{27.5}(H_2O)_{17.2}[Si_{108}O_{216}]$	8.1	8.1	n/a

Pore size is also relevant for other common uses of zeolites, including adsorption and separation, and is included in Table 2.1. It is possible to separate molecules based on size, shape and polarity. Zeolites containing cations are particularly useful as desiccants and gas separators, whilst hydrophobic silica zeolites are used to absorb organic solvents (Peskov, 2017; Guisnet & Gilson, 2002). Zeolites are also industrially used as catalysts. Their cation exchange properties allow for a variety of cations that have a range of different catalytic properties. The pore sizes also influence the reaction yield by affecting the access to reactants and products (Weitkamp & Puppe, 1999).

In addition, zeolites have been found to cause an increase in the pH of systems (Li et al., 2009). Li et al. (2009) conducted experiments on garden soil contaminated with lead. They analysed the effect of adding natural zeolite, a mixture of clinoptilolite and heulandite mixed with feldspar, quartz, hydrobiotite and apatite. It was found that the pH of the samples increased, regardless of the initial pH as shown in Figure 2.9. The increase of pH is related to the amount of zeolite added, however, the increase of pH is not consistent across the samples.

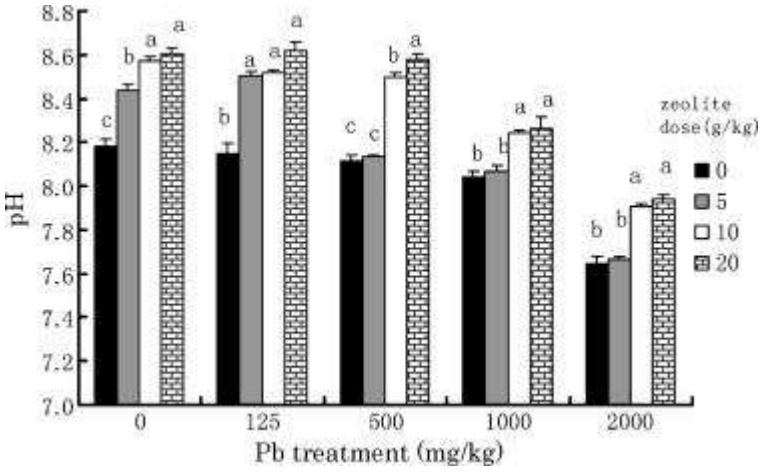

Figure 2.9 - Results of Li et al. (2009). Addition of zeolite to the lead-contaminated soil causes an increase in pH

Zeolites can have acidic or basic properties, depending on the Si/Al ratio. The framework oxygens are the basic sites and the density of basic sites decreases as the Si/Al ratio increases. The basic strength increases as the electropositivity of the counteraction in zeolites increases (Huang et al., 1995). It has been determined that the electronegativity of the framework atoms affects the basicity of a zeolite, as do the bond angles and lengths. Other relevant parameters that control the positivity of the framework includes, the location of aluminium in the framework, the ionicity of the structure, and the crystallographic locations of the oxygens (Barthomeuf, 1991). Barthomeuf et al. (1988) found that the basicity of zeolites increased by incorporating monovalent cations following the series Li < Na < K < Rb < Cs (Barthomeuf et al., 1988).

The Brønsted acid sites are the hydroxyl protons that are covalently bonded to the oxygen atoms that bridge the silicon and aluminium atoms in the framework. These act as proton donors. Changing the distribution of aluminium atoms in the

framework affects the acid strength of hydroxyl groups. The Lewis acid sites are electron acceptors and are formed by cation exchange.

2.11.2 Natural Zeolites for Remediation

Zeolites are one of the most common additives used in soil and water treatment, acting as a remediation tool. Natural zeolites are formed from the interaction between volcanic ash and water, where the water has a high pH and salt content (Gadepalle et al., 2007). They have been used for remediation due to their innocuous interaction with soils and plants.

Sewage contaminated with heavy metals has been treated with natural zeolite to allow the sorption of the toxic metals onto the zeolite. It was found that pre-treatment of the sewage with zeolites led to a significant decrease of 5-40% before further treatment was undertaken. (Wasag, 2007).

Clinoptilolite, $Ca_3(Si_{30}Al_6)O_{72}{\cdot}20H_2O$, is a very common natural zeolite. It has been used extensively in remediation and found to have a strong affinity, in particular, for lead (Yuan et al., 1999; Blanchard et al., 1984; Malliou et al., 1994; Curkovic et al., 1997; Semmens & Martin, 1988; Semmens & Seyfarth, 1978; Zamzow et al., 1990).

When analysing the effect of the addition of clinoptilolite to contaminated soil and the bioavailability upon adding it to compost mixed with iron oxides, it was found that plant growth increased when compared to untreated soil. This was possibly due mostly to the addition of compost. The other benefit was that bioavailability was reduced. This combination of materials successfully remediated arsenic from contaminated soil (Campbell & Davies, 1997).

Clinoptilolite has also been used to remediate radioactive caesium from soil. The exchange of sodium and potassium ions with caesium ions was found to not be the only cause for Na^+ and K^+ to be released into the soil. Increasing the pH of the soil caused more of the ions to be released which affected the soil's bio-stability. Whilst it was successful at stabilising caesium in the soil, it decreased the agricultural functionality of the soil (Campbell & Davies, 1997).

Acid mine waste is often contaminated with lead and studies have used natural zeolites to attempt to remediate it. Researchers found that the zeolite they used, clinoptilolite, was stable in acidic solutions and only found to dissolve at a pH of less than 2.00. The addition of zeolite caused the concentration of lead to decrease, however, it was heavily dependent on the pH of the soil and slightly affected by the grain size of the soil, with the smaller particles binding more heavy metals than large particles (Wingenfelder et al., 2005).

Due to the selectivity of clinoptilolite for lead, it is understandably difficult to desorb lead from the zeolite following treatment. The purpose of this would be to regenerate the zeolite. A study has found that the process of desorbing from clinoptilolite was significantly slower than adsorption and that ions that were easily adsorbed were more difficult to desorb (Katsou et al., 2011). This reduces the reusability of the zeolite technique.

Previous research studies have analysed the remediation ability of natural zeolite for lead contaminated soil and researched the many effects achieved by adding zeolite. It was concluded that the addition of zeolite raised the pH, increased the cation exchange capacity and content of organic matter, whilst promoting the aggregate formation. It was determined that only a small addition of zeolite acted to reduce the amount of soluble lead, regardless of the original concentration of lead in the soil. After conducting a variance test, the study reported that the most important factor leading to the immobilisation of lead is the result of an increase in the pH of the soil. Adding zeolite decreased the uptake of lead by plants growing in the soil whilst causing the edible vegetables to be safer to eat and also the quality of the soil to improve (Li et al., 2009; Querol et al., 2006; Ulusoy & Simsek, 2005; Tessier et al., 1979; Theng, 1979; Thornton, 1981; Van Hervijnen et al., 2007; Wang et al., 2003; Zornoza et al., 2002; Winder & Bonin, 1993) (You, 2004).

Addition of natural zeolites also helps to remediate water by acting as adsorbents for the contaminants. A study analysed the cation exchange selectivity for a range of heavy metals on a number of natural zeolites (Wang & Peng, 2010). Pb^{2+} was found to be the cation with the highest selectivity for seven of the nine zeolites.

The research included modifying natural zeolites with methods including acid treatment, ion exchange, and surfactant functionalisation. This caused the modified zeolites to have a higher adsorption capacity for anions and organic compounds.

Natural zeolite from North Sardinia, Italy, was used to adsorb several heavy metals including lead at a controlled pH of 5.5. The slightly acidic pH makes it unlikely that a precipitation of a lead hydroxide was formed, and it was not detected (Castaldi et al., 2008; Araneo, 1987). Zn^{2+} was found to adsorb to the zeolite in higher concentrations than Pb^{2+}. However, in multi-element solutions, lead was more selective due to its sphere of hydration and energy being smaller than those of zinc. This meant that during ion exchange, it was unfavourable for Zn^{2+} to move towards the zeolite. This was exacerbated by the fact that Zn^{2+} was now in competition with Pb^{2+} for the sorption. Pb^{2+} has a greater ionic radius and smaller charge density. This allowed it to bind to the surface of the zeolite with weaker bonds (Castaldi et al., 2008). The research agreed with a previous study that suggested the cations needed to be partially or completely dehydrated to be incorporated into the internal cages and channels of the zeolite (Mon et al., 2005). It was postulated that the aluminium atoms, and not the silicon atoms, in the crystal lattice of the zeolite were being replaced by Pb^{2+} during the ion exchange reaction (Castaldi et al., 2008). This caused an increased disorder to be present in the lattice, referred to as 'microstrain' (Guiner, 1963). This was confirmed by XRD analysis.

2.11.3 Gismondine

Gismondine is a natural zeolite mineral, Figure 2.10, that is found in environments that are under-saturated with silica. Gismondine is often associated with sulphide minerals (International Zeolite Association, 2016). It can form under the common formula of $CaAl_2Si_2O_8{\cdot}4H_2O$, however, calcium ions have been found to undergo ion exchange with Ba^{2+} ions resulting in Ba-rich gismondine (Gismondine-Ba) (Allen et al., 2002). This has been discussed by Braithwaite and collaborators in the analysis of lead smelting slags and proposed that Gismondine-Ba may form in water-

rich weathering environments in the presence of free Ba-ions and silicates (Braithwaite et al., 2001).

Gismondine crystallises in a monoclinic structure and has a pore size of 3.9 x 5.6 Å. The red circles in Figure 2.10 correspond to calcium ions that are located within the central pore of the framework (International Zeolite Association, 2016). Gismondine has a flexible aluminosilicate framework with high selectivity for calcium ions in the ion exchange process. It has, therefore, been suggested that it can be substituted for Zeolite-A in the production of detergents as a water softener (Kecht et al., 2004; Roque-Malherbe & Duconge Hernandez, 2007). This is particularly beneficial for gismondine, as it can allow for a reversible ionic exchange process (Barrer, 1978).

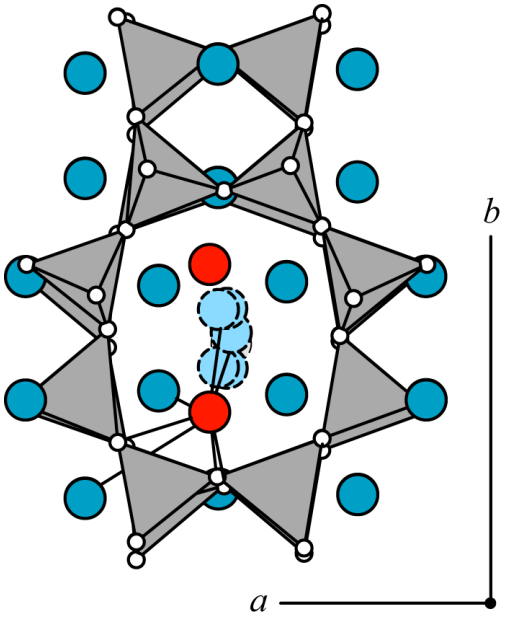

Figure 2.10 - Gismondine structure

Gismondine has been determined to exchange calcium ion with potassium or sodium ions (Bauer & Baur, 1998) but more importantly for this study, the calcium ions will exchange with barium ions in lead smelting slags (Braithwaite et al., 2001). However, as Ba^{2+}ions and Pb^{2+}ions show similar size and charge, they can be expected to replace each other in the environment and in the absence of Ba^{2+}, we can expect Pb^{2+} may exchange with the Ca^{2+} ions.

Research by Roque-Malherbe et al. (2007) determined that not only that gismondine selectively undergoes ionic exchange for divalent cations, but also found

that the ionic exchange process was successful and responsible for removing a number of divalent metal cations from solution. Their results indicated that Pb^{2+} was more selectively exchanged than Cu^{2+}, Co^{2+} and Ni^{2+}. This is due to cations with low hydration enthalpies being favoured for ion exchange (Roque-Malherbe et al., 1987; Colella, 1996; Roque-Malherbe & Duconge Hernandez, 2007).

Physically, calcium ions, Ca^{2+}, have a radius of 114 pm, barium ions, Ba^{2+}, have a radius of 135pm, whilst the radius of lead ions, Pb^{2+}, measures 133 pm (Shannon, 1976). This close similarity allows for an easy exchange to take place, as the lead ions can fit easily in the same atomic site.

2.11.4 Synthetic Zeolites for Remediation

Synthetic zeolites have been used in the remediation of ions. There are several benefits to using synthesised zeolites for remediation. Synthesis allows the experimentalist to: control the purity of the crystalline solids, have uniform particle sizes, select chemical properties and pore sizes, and it allows for greater thermal stability. It also allows for control of the Si/Al ratio which can be altered and further functionalised by adding different inorganic cations. In addition, the use of inorganic precursors causes more hydroxylated surfaces of the zeolite whereas, conversely, organic precursors allow for easy incorporation of metals into the framework. The temperature of the synthesis is important. It has been shown that the rate of crystallisation is directly proportional synthesis temperature, whilst the rate of nucleation and the formation of a new structure, instead, is inversely proportional to the temperature. The phase of the product is controlled by the reaction time and synthesis is carried out at a basic pH (Georgiev et al., 2009).

Synthetic zeolites have been used for long-term studies to determine the immobilisation of cadmium. Zeolite-X (CaX), an aluminium-rich zeolite was chosen. It is most similar to faujasite, a natural mineral. Zeolite-X consists of sodalite cavities that are interconnected. In Ahmed et al. (2009), Extended X-ray Absorption Fine Structure spectroscopy (EXAFS) was used as a technique to determine where the cadmium was interacting with the zeolite. The hypothesis was that that Cd^{2+} ions were first located inside the sodalite cages and then moved via diffusion into the actual zeolite structure,

in the connection between sodalite cages. It was mentioned that EXAFS can only provide an 'average' picture yet the measurements concluded that the hypothesis was correct (Ahmed et al., 2009).

Fly ash is a product of the combustion of coal and presents as a very fine powder. These particles are considered to be highly contaminated. Toxic elements such as lead, mercury, nickel, tin, cadmium, antimony and arsenic (McConnell & Edwards, 2008; Ording, 2009). These can condense whilst being expelled as a gas (Querol et al., 1997; Sout et al., 1988; Klein et al., 1975; Coles et al., 1979). Fly ash is usually calcium, iron, aluminium and silicon rich and works well as a zeolitic material because it resembles volcanic rocks and ash. A study looked particularly at using fly ash to make sodium-based zeolites. They found that it is very important to consider the ratio of SiO_2 to Al_2O_3. Different mineralogical compositions show unalike synthesis behaviour.

Another study used zeolite that was synthesised from coal ash to then immobilise heavy metals in soils. This was directly tested in-situ. The results showed that the untreated reference area had a pH of 3.5 whilst the areas treated with zeolite had a pH of up to 7.5. It was found that there was a considerable reduction in the leaching of several of the heavy metals. The researchers determined that the ion exchange process as well as the precipitation created an affinity of elements for the zeolite addition. Fe^{3+} and Al^{3+} had the highest affinity followed by Cu^{2+} and then Pb^{2+} (Moreno et al., 2001).

Several zeolites are synthesised from coal-fired fly ash, including NaP1, KM, Chabazite and Linde F. The ion exchange capacities of these zeolites were compared and analysed (Querol et al., 1997). NaP1 was investigated in a further study (Garcia-Sanchez et al., 1999). It has the formula: $Na_6Al_6Si_{10}O_{32}{\cdot}12H_2O$. Zeolitic remediation was compared with the abilities of iron oxides and hydroxides. The addition of zeolite allowed for the pH of the soils to increase which, therefore, reduced both the acidity and the amount of toxic materials that were detectable in leachate. Due to the fact that lead can also interact with zeolites via ionic exchange, the mobility of the heavy metals was reduced by over 74%. In the investigation, pyrite slurry was mixed with the

zeolite that resulted in ionic exchange. This also inhibited the increase in pH upon addition of zeolite. The acidity did not change with large variation. This suggests that the precipitation processes caused by a variation in pH are not significant (Garcia-Sanchez et al., 1999).

A two-part study analysed heavy metal-contaminated soils, attempting to remediate them with non-hazardous wastes including fly ash. XRF, XRD and SEM-EDX were used to analyse the materials and study the benefits of using a particular method. The study found that the most efficient material included sugar foam, fly ash and zeolitic material (Gonzalez-Nunez et al., 2011). The second part of the study analysed the efficiency of the materials using leaching tests. It was concluded that zeolites not only increased the pH of the soil, as did the other methods, but it also had the added benefit of increasing the specific sorption capacity. This is the amount of material that is adsorbed by a particular measure of sorbent under known conditions (Kudra & Mujumdar, 2009). Finally, it was noted that the remediation materials are wastes produced from industry, so there is the added positive effect of being able to reuse waste. The treated soil was determined to be acceptable for industrial purposes or the area could be reclassified and further treated at lower cost (Gonzalez-Nunez et al., 2012).

Zeolite Na-A is a synthetic zeolite with the formula $Na_{96}(AlO_2)_{96}(SiO_2)_{96}\cdot 27H_2O$ (Fernandes-Machado & Miotto, 2005). It has been produced by coal ash (Bao et al., 2013) where it was found to be desorbed at a low pH. The framework was partially destroyed and, therefore, the removal rate of metal ions decreased in this acidic environment (Wang et al., 2009). In addition, the functional groups on the surface of the zeolite may dissociate at a higher pH, which would make more anionic sites on the surface available that would aid in metal removal. The pH was found not only to affect the zeolite but was also a variable for the surface charges of adsorbent and the degree of ionisation and speciation of adsorbate during the adsorption process. Contact time was analysed to determine if it was a dominant factor to consider. It was found that for the remediation of lead, the amount of contact time had only minimal effect and was of more importance for some of the other metal ions being analysed (Bao et al., 2013).

Adsorption kinetics and temperature were analysed. Bao, et al. (2013) conducted thermodynamic studies which found that an increase in temperature aided in the removal of heavy metal ions. They suggested that the interaction of metal ions adsorbing onto zeolite is an endothermic reaction. There is a negative adsorption standard free energy change and positive change in entropy. Therefore, the reaction would be spontaneous. An increase in temperature would make the formation of products more likely due to Le Chatelier's Principle.

Their conclusions stated that the synthesised zeolite produced good results for the remediation of heavy metal ions from aqueous solutions. In the first 60 minutes of contact time, 91.87% of Pb^{2+} was removed via adsorption. The Langmuir model and Freundlich isotherm equations were used to describe how the heavy metal ions absorbed onto the zeolite. It was found that the adsorption was spontaneous and that the competitive adsorption ability of heavy metal ions when in a multiple system follows; $Pb^{2+}>Cu^{2+}>Cd^{2+}>Ni^{2+}$, which was determined by correlating the hydrated ionic radii as well as the hydration energies of each species (Bao et al., 2013). Lead had the smallest hydrated ionic diameter of the metal ions analysed. This is relevant because the hydrated ionic diameter and the hydration energies determine the adsorption capacity for the cations.

2.11.5 Zeolite-A as a Remediation Technique

This thesis focuses on the remediation of lead using Zeolite-A, Figure 2.11 (Smart & Moore, 2005). Zeolite-A is of particular interest as it is known to exchange a sodium ion with a calcium ion (Franklin & Townsend, 1985). Lead ions and calcium ions are of equal charge and similar size. Therefore, it is hypothesised in this study that the zeolite may exchange its sodium ion with lead ions and act as a remediation tool. The purpose for choosing Zeolite-A instead of another zeolite, is due to its small pore size and high density of cations. This allows the zeolite to have strong interactions and anchor the adsorbent (Lichtfouse et al., 2013). Zeolite-A has a pore size of approximately 5 Å (as detailed in Table 2.1) whilst a lead ion has an ionic radius of 1.19 Å. This suggests that a lead ion could fit inside the supercage of Zeolite-A.

The synthesis of Zeolite-A follows a simple, low temperature, method using inexpensive and easily obtainable chemicals and would, therefore, be economically suitable for mass production. Zeolite-A crystallises in a cubic structure which is space group 221 and defined as a simple cubic lattice.

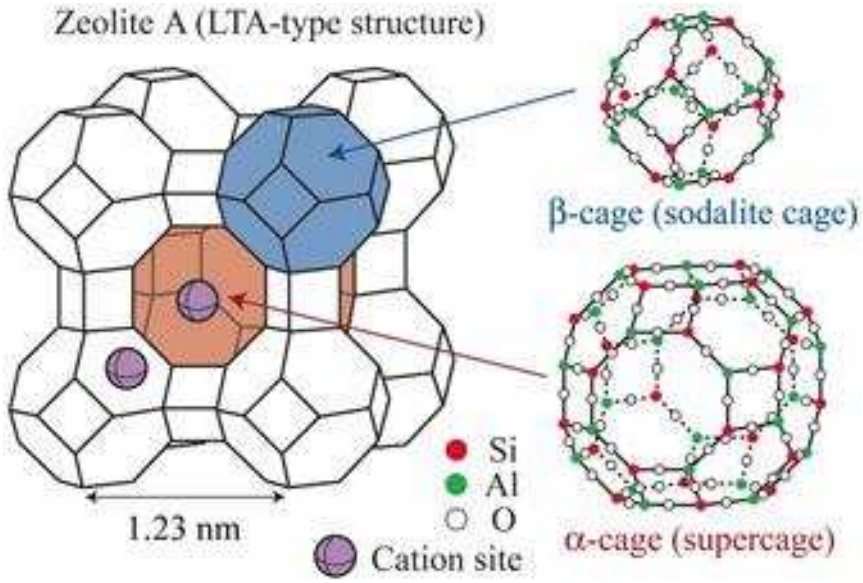

Figure 2.11 - Zeolite-A Structure

Zeolite-A has a pore size of approximately 4 Å whilst a lead ion has an ionic radius of 1.19 Å. This leads to the hypothesis that a lead ion could fit inside the supercage of Zeolite-A. The purpose for choosing Zeolite-A instead of another synthetic type, is due to its small pore size and high density of cations. This allows the zeolite to have strong interactions and anchor the adsorbent (Lichtfouse, et al., 2013).

Querol et al. (2001) synthesised a dehydrated form of Zeolite-A from fly ash and had the formula, $NaAlSi_{1.1}O_{4.2}$. This was attempted due to an earlier study in 1985 finding that fly ash is very similar to some volcanic materials and, therefore, can be used to synthesise zeolites (Querol et al., 2001; Holler & Wirsching, 1985). Several processes exist which involve different zeolites being produced (Kato et al., 1986; Bergk et al., 1987; Mondragon et al., 1990; Larosa et al., 1992; Shigemoto et al., 1992; Kolousek et al., 1993; Catalfamo et al., 1994; Singer & Berkgaut, 1995; Berkgaut & Singer, 1996; Lin & Hsi, 1995) (Park & Choi, 1995; Querol et al., 1995; Shih et al., 1995; Inque et al., 1995; Querol et al., 1995; Querol et al., 1997; Querol et al., 1998). The classic method is alkaline conversion of fly ash, which combines different ratios of SiO_2

and Al_2O_3 with reaction times and conditions. Later, a microwave was introduced into the synthesis, reducing the reaction time considerably (Querol et al., 1997). This type of zeolite has a high Al^{3+}/Si^{4+} ratio, which accounts for the high ion-exchange abilities for heavy metals. This prompted multiple investigations to analyse its ability to decontaminate waste waters.

2.11.6 Computational Background

Zeolite-A is a commonly researched zeolite structure because it is formed of a relatively small number of atoms (672) in its crystallographic unit cell, Figure 5.2. This structure was reported in an experimental study by Pluth and Smith in which Zeolite-A crystallises in the F*m-3c* structure (Pluth & Smith, 1980).

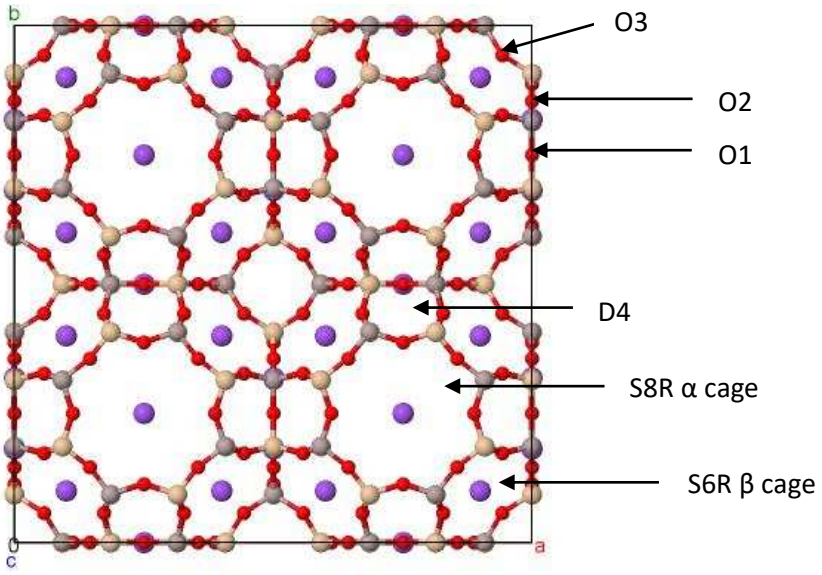

Figure 2.12 - Crystallographic unit cell of anhydrous Zeolite-A containing 672 atoms ($NaSiAlO_{12}$), where red represents oxygen, purple is sodium, grey is silicon and cream is aluminium.

As described shown in detail in Figure 5.1, Zeolite-A is described by sodalite cages, β-cages, which consist of six-membered rings, S6R. These cages are linked by four-membered rings, D4R, to create the Zeolite-A framework, resulting in large super-cages, α-cages, separated by eight-membered rings, S8R. Due to symmetry, three different oxygen sites are present in the structure. The oxygens that build the D4R units in the β-cage are referred to as O(3). The remaining oxygens in S6R units are O(2). The oxygens linking the β-cages are denoted as O(1).

2.12 Conclusions

- As detailed in multiple studies, remediation of soil can be performed with varying methods and techniques.
- Zeolites are particularly a useful soil additive as they have ion exchange properties and are known to reduce the concentrations of hazardous substances whilst restoring friendly biota to the soil.
- Gismondine is a natural zeolite and this study hypothesises that it may exchange calcium ions for lead ions.
- Zeolite-A is a synthetic zeolite that has already been found to be successful in the remediation of hazardous materials.
- Both zeolites will be further investigated throughout this study.
- Pb^{2+} can exchange for Ca^{2+} ions as their charges and ionic radii are similar.

Chapter 3 Area of Study

3.1 Aim

The aim of this section is to detail why the site of analysis was chosen, the background of the site and the hydrology and conditions of the area. This includes the industrial use of the site and the soil reactions believed to have taken place, as this affects the chemistry of the soil and thereby the remediation.

3.2 Introduction

The site selected for study was chosen due to a request from the Swedish Environment Agency to analyse the soil and detect the levels of lead present. It is located in the village of Oskarström at the west coast of Sweden. Synthetic soils could have been used but, to ensure that the results were as realistic as possible, remediation techniques were carried out on the soil samples collected at the site. The material that was investigated is pyrite ash waste, containing elevated levels of lead. The soils, therefore, are expected to contain a high amount of iron oxides with an unknown component of silicate minerals.

3.3 Site Background

In this study, two soil samples, referred to as S1untreated and S2untreated throughout, were collected at the site of a disused industrial paper mill in Oskarström, Halland, Sweden, (Figure 3.1a, b) (Google Maps, 2014; Google Maps Europe, 2011).

The paper mill was closed in 1965 and replaced with a chipboard industry in 1967 that was active until 1986. Currently, the office buildings on the site, marked with 'A', are hosting local small to medium sized enterprises (SMEs) and the large factory building, 'B', is used for storage by the military. The site is located along the Nissan River, a major river in Sweden that has groundwater and surface run-off water diverted towards it because of the nearby geological ridge, causing unusually high ground water levels at the site.

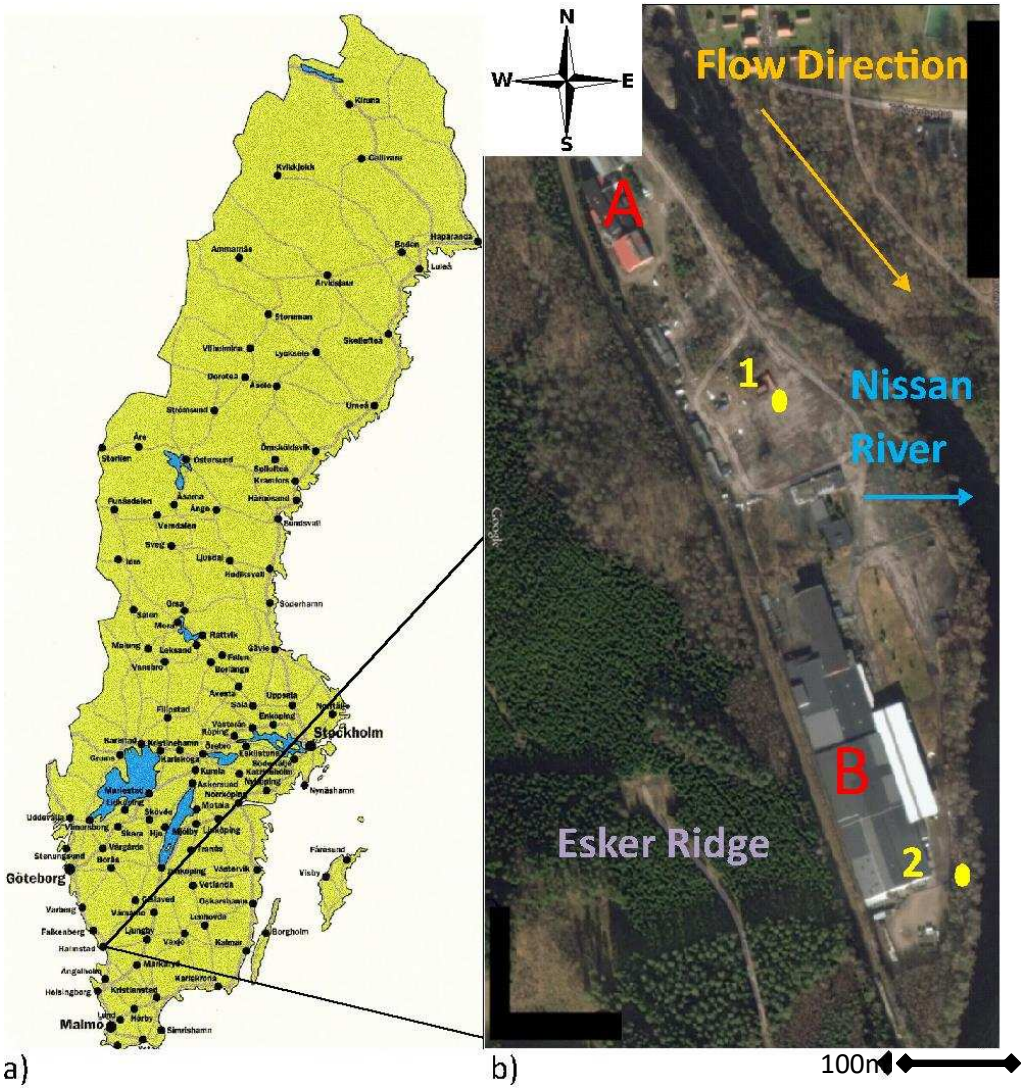

Figure 3.1– a) Map of Sweden and b) Overview of the industrial paper mill current site where samples S1untreated and S2untreated were collected at sites marked “1” and “2”, respectively

The soils analysed in this work were collected from two different locations of the same site. Other locations were also sampled but were found to have low concentrations of lead and, therefore, were not considered in this study. As stated previously, synthetic soils could have been made with a known concentration of lead and remediation analysis could have proceeded. This was not done, in order to mimic more realistic situations. Thus, choosing to use only the soil with considerable concentrations of lead was to produce results that were significant.

Soil 1 was sampled from where the pyrite roasting oven had been located when the mill was still running. Soil 2 was from the area used for discarding the pyrite ash waste as landfill material (Figure 3.1b). The method of disposal used by the industry had been to dump the materials onto the soil with no safety membrane in place. It

has also been speculated that the water used to clean the lead-based pipe system that transported the SO_2 gases may have been disposed of in an inappropriate manner at the site, specifically at the location where Soil 2 was collected. Upon collection at the site, the pH of Soil 1 was below 1.8 and was a purple colour, whilst Soil 2 had a pH of above 5.5 and consisted of a more orange colour.

The nearby road was also analysed as a control. ICP-MS analysis given in Appendix 1 shows that the road did not show levels of lead above the legal limits detailed in Section 6.2.

The mill manufactured paper by producing wood pulp. Wood material is softened by using various salt solutions, for example sulphites (SO_3^{2-}) or bisulphites (HSO^{3-}), which then cause the wood to dissolve and the lignin is separated from the cellulose. The process takes place under pressure, at a pH of 2-3 and with a high temperature of around 130 ^{o}C (Shahzad, 2012; KK, 2012). The two major processes used in wood pulp production are the sulphite and sulphate methods. At the site in Oskarström, the sulphite method was used. The sulphite cooking liquor was produced on site by roasting sulphide minerals, e.g. pyrite (FeS_2), and pure sulphur in order to produce sulphuric acid according to Equation 3.1-3.3 (City Collegiate, 2014; Clark, 2013; O'Leary, 2000).

$$2FeS_2(s) + 5.5O_2(g) \rightarrow 4SO_2(g) + Fe_2O_3(s) \quad (3.1)$$

$$2SO_2(g) + O_2(g) \rightarrow 2SO_3(g) \quad (3.2)$$

$$SO_3^{2-}(aq) + H_2O(l) \rightarrow H_2SO_4(aq) \quad (3.3)$$

The waste product produced in the roasting processes, often referred to as pyrite ash, is known to contain large amounts of heavy metals, including arsenic and lead, as these metals follow the original minerals (Turk, 2016). Pyrite ash is known to be red to purple in colour, owing to the high content of Fe_2O_3 in the soils, and has varying degrees of heavy metal contamination (Oliveira, et al., 2012; Theorin, 2015). At the site in Oskarström, layers of the soil appeared to be dark red to purple, indicating the presence of the ash. The Swedish equivalent of the Environment Agency, Hallands Länstyrelse, was called in to investigate the possibility of heavy metal contamination. In 2007, a potential case was brought against the paper mill regarding

their liability, and whether they could be required to fund the costly clean-up of the site. Due to a legal clause, no contamination prior to 1969 could be considered and the case was lost. There were no requirements for cleaning and remediating the site, therefore, it remains sealed off to the public.

A thorough study was published by the Swedish Environmental Agency based on five industrial sites associated with the manufacturing of paper pulp (Regionalt program, 2005). A site, 'Essevik', was of particular interest as it used the sulphite method for pulp manufacturing. The industry there was active during the same period as Oskarström and had, for a period, the same owners as the site under investigation in this study. At the Essevik site, only elevated zinc concentrations were reported (Nordback, 2004).

3.4 Hydrology of the Site

The weather at the site of study in Sweden involves heavy precipitation of 1014.6 mm per year (Table 3.1, Figure 3.2) (SMHI, 2016). The data in Table 3.1 is for 1970, shortly after the paper mill closed, and therefore after the total contamination would have occurred. The locations, Oskarström and Simlangsdalen, are two villages near Halmstad, shown at close range in Figure 3.3 (Google Maps, 2014). They are less than 15 km distance apart. During the spring, summer and autumn, the precipitation falls as rain, whilst in the winter it takes the form of both rain and snow. As temperatures fall below 0 ^{o}C in December through February, the ground freezes, resulting in large quantities of water being retained in the soil as ice. As the temperatures begin to increase again in March/early April, the ice melts giving rise to highly water logged grounds. The water is quickly flushed out into the river via a drain system located at the industrial site. It is believed that this drain water contains elevated levels of leached metal ions, but this is out of the scope of this project and will, therefore, not be further discussed in the thesis.

Table 3.1– Rain and temperature fluctuations as recorded in the village Oskarström and a nearby village, Simlangsdalen,in 1970

Time period	Rain (mm) – Oskarström	Temperature (ºC) – Simlangsdalen
Jan	82.9	-2.4
Feb	53.6	-2.3
March	70.2	0.6
April	54.9	4.9
May	51.4	10.7
June	80.7	14.3
July	95.3	15.4
August	108.0	14.8
September	107.0	11.3
October	101.8	7.5
November	109.3	2.9
December	99.5	-0.6
Total/Average	1014.6	6.4

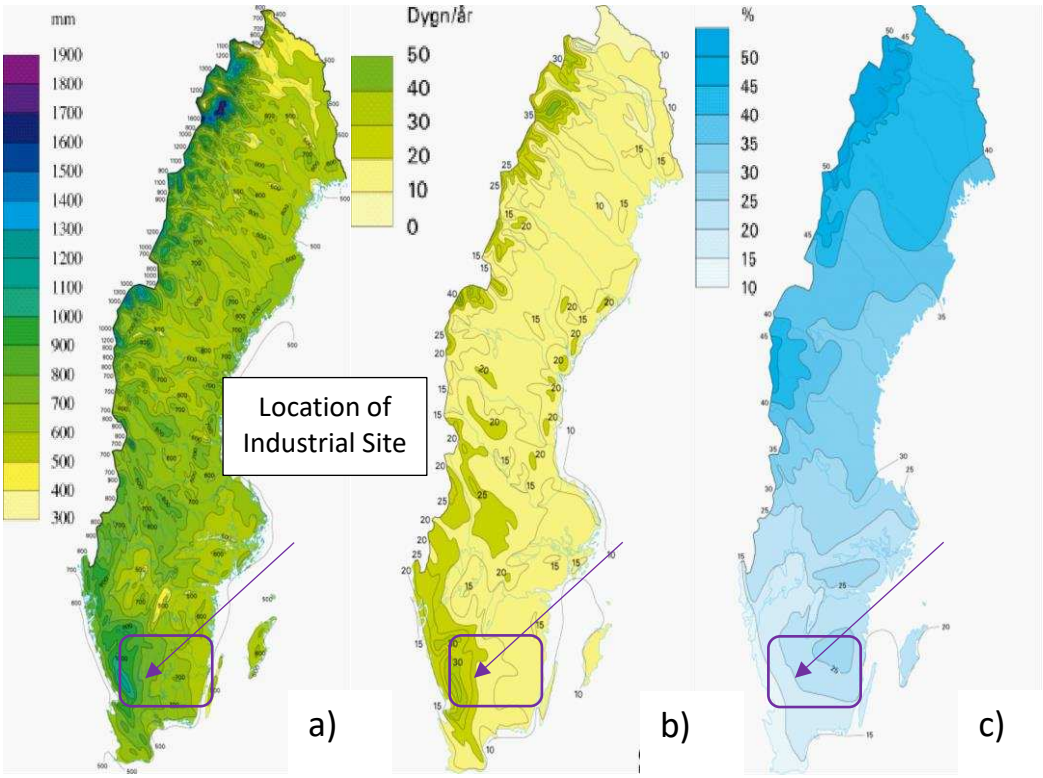

Figure 3.2 – a) Average Rainfall per Year in Sweden: 1961-1990, b) Number of Days with Heavy Rainfall in Sweden: 1961-1990, c) Percentage of Rain as Snow in Sweden: 1961-1990

Figure 3.3 - Zoomed in area showing the location of the site where samples were collected

In the 1970s and early 1980s there were reports of acid rain in Halmstad, Sweden (Moldan, 2013; Mellanby, 1988; Pansar, 2005; Skolvision TM, 2016; Petersson, 2008; Statistiska Centralbyran , 2016). All of this precipitation is believed to have caused heavy metals to be leached into surrounding soils and ultimately into the Nissan River. This led to dire effects including the death of wildlife in large parts of the river and discolouration of the water.

3.5 Conclusions

- Soils were collected from a site in Sweden where industrial processes caused serious lead contamination because of sulphuric acid production.
- The Environment Agency launched an investigation that resulted in this study.
- The area had a notable precipitation that involved acid rain.
- The high levels of precipitation encouraged leaching of the heavy metal.
- Two different areas were analysed that had been inflicted by varying processes. Both sites contained high levels of Pb^{2+}, but showed different pH and colouration suggesting a different mineral composition. This is due to the chemical reactions that are hypothesised to have taken place.

Chapter 4 Experimental Techniques

4.1 Aims

The aim of this section is to provide detailed theory behind each of the techniques used in this project and justify why they were relevant to this study. The specifications of each technique and the preparation of samples for analysis are given, as are reasons for why the particular approaches have been considered.

4.2 Introduction

When analysing soil, it is important to consider the soil residue as well as the liquid leachate. Atomic Absorption Spectroscopy (AAS) allows for the quantitative analysis of soil leachate for a particular element, in this case, lead. X-ray Diffraction (XRD) is used to determine the minerals and crystalline phases present in a solid. Soils are very complex and involve a number of minerals. XRD allows for the determination of any effect that remediation may have. X-ray Fluorescence (XRF) acts as a supportive tool, by providing quantitative elemental analysis. Scanning Electron Microscopy with Energy Dispersive X-ray (SEM-EDX) is also a beneficial supportive technique. It has the ability to analyse solid soil residue by mapping the elemental composition in a sample.

Both SEM and XRF support the XRD results and the combination of techniques allows for a thorough analysis and characterisation of the soil. Whilst XRD determines if remediation has had an effect on the mineral composition of the soil, computational analysis gives insight into the mechanism.

4.3 Atomic Absorption Spectroscopy

Atomic Absorption Spectroscopy (AAS) is a common analytical technique used for the analysis of trace elements. It is a relatively simple setup that allows the user to select an element-specific lamp to analyse a sample for the concentration of that element. It is used in chemical analysis, including the pharmaceutical industry to detect metals in drugs (Lewen, 2011), forensic analysis (Barnett & Buntine, 2008), quality control in the food and beverage industry (Dickson, 2012), the mining industry (Barnett & Buntine, 2008), and by environmental chemists to detect contaminants

(Sharma, 2007), such as the determination of the concentration of cadmium, copper, lead and zinc in phytoremediated soil by using AAS (Chen, et al., 2000).

4.3.1 Flame AAS (FAAS) Theory

AAS is based on the absorption of radiation by free atoms. Elements in their ground states have unique electron configurations based on atomic electron levels, such as 1s, 2s, and 2p. Figure 4.1a shows these levels where the letters K, L, etc. represent electron shells that correspond to atomic orbitals; 1s (K), 2s, and 2p (L), etc. (CLU-IN, US EPA Contaminated Site Clean-up Information, 2015). It also assigns α and β levels which represent electron transitions. A K-transition would imply an excited electron has fallen back into the electron hole created in the K-shell. If it was a transition from the L-shell, it would be denoted K_α, whereas K_β originates from an electron falling back from a higher energy level. As this transition has low probability, it has a lower intensity and is recorded as K_β. K_α is the most probable transition for an electron with the highest intensity. Figure 4.1b is a Jablonski diagram and shows another example of how fluorescence occurs (University of Newcastle Upon Tyne, 2002).

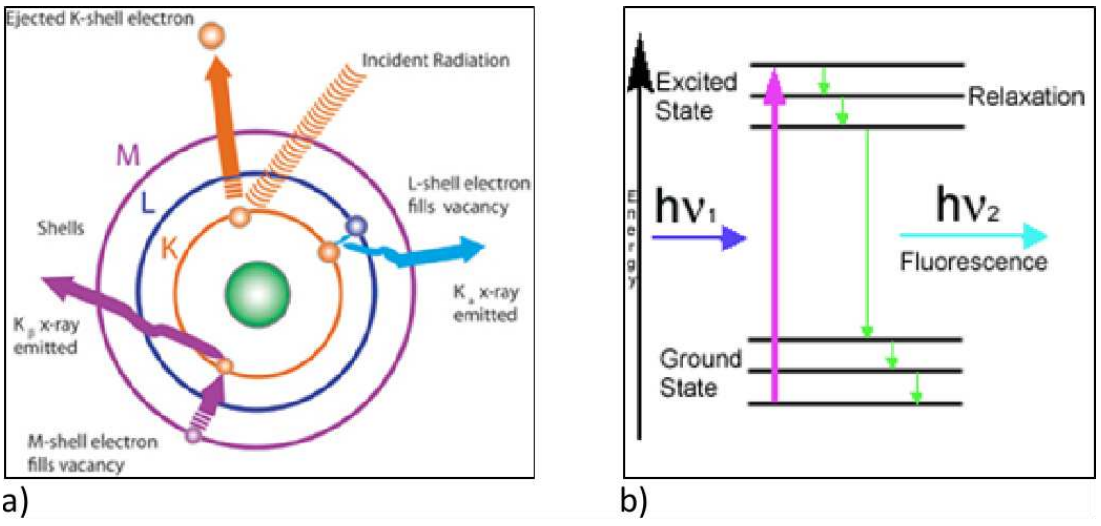

Figure 4.1 - a) Diagram of X-ray electron shell model and b) Jablonski diagram

Atoms will absorb energy in the form of light (photons) when the energy is equal to that of the atom's allowed electronic transitions. Upon relaxing, the electrons will emit photons of light as they fall back to the ground state. The number of atoms that excite is small. Most will stay in their ground state. The number of atoms that excite is obtained from the Boltzmann equation, Equation 4.1.

$$S = k\ lnW \tag{4.1}$$

In this equation, S is the entropy, k is the Boltzmann constant: 1.381×10^{-23} $JK^{-1}$and W is the probability of the electron configurations, i.e. the number of ways electrons can be arranged. This equation describes the possible configurations for electrons to be distributed over energy levels. It also predicts the number and arrangement of atoms excited by applied energy (Chang, 2000; Atkins & de Paula, 2010; Matthews, 1992). As there are always more atoms in their ground state than their excited state, this allows metallic elements to be accurately detected and quantified with very sensitive detection limits.

In FAAS, the sample is dissolved in a chosen solvent, often aqueous based. In the first step during the analysis the solvent evaporates and then the flame causes ions to become atomised. An element-specific lamp applies a voltage, which acts as the energy source. The energy hits the flame that excites electrons out of their core. In this case, a lead-specific lamp was employed. Only in lead will the electrons in their ground state absorb the wavelength specific to lead. As the electrons relax, they will release an X-ray photon. The spectrometer measures the absorption of energy (Hannaford, 2000).

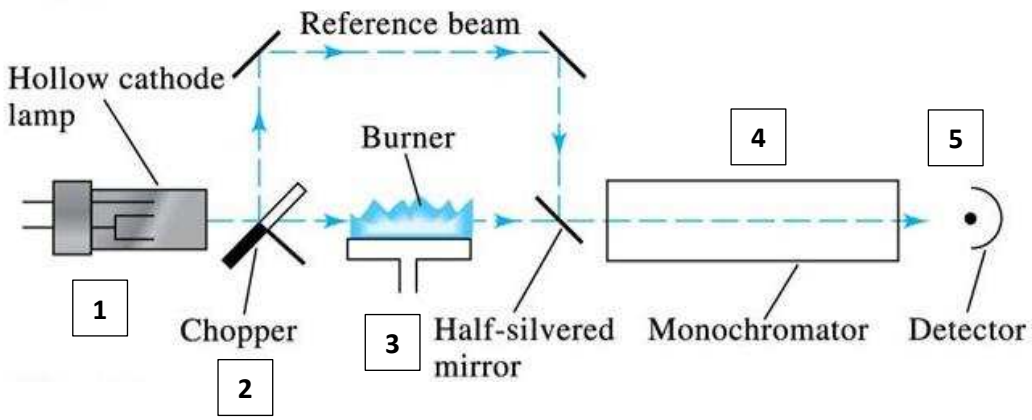

Figure 4.2 – Schematic design of an AAS Spectrometer where the numbers refer to the description in the text

The FAAS apparatus consists of five main components, Figure 4.2 (Holler & Crouch, 2014):

1. A hollow cathode lamp is the source and emits a line spectrum for the analysed element. Each element has its own lamp. The lamp is a cylindrical cathode produced of the metal to be studied and sealed in a glass tube

which contains argon gas. A voltage is applied that electrically excites the cathode's metal atoms and causes photons of light to be emitted as the atoms return to the ground state. This energy can then be absorbed by the free atoms of the element under analysis.

2. A chopper allows energy from the lamp to pass to the detector, not passing through the flame. The path opens and closes very quickly (Dunnivant & Ginsbach, 2009). This generates a reference beam, I_0.
3. The atomiser is the flame, which converts sample ions to free atoms. It does this by evaporating the solvent from the solution of metal ions. All that remains are the crystals of the metal salt. The flame requires an oxidant and fuel (air-acetylene in this experiment) and is at a temperature of approximately 1870K, Figure 4.3 (Garcia & Baez, 2012).
    - An atomiser requires a premix burner. This uses a small plastic tube (nebuliser), which the sample is aspirated through and sprayed into a chamber as a fine mist. Here it is mixed with the oxidant and fuel just before going into the flame. Only the smallest drops of sample reach the flame, as the larger drops contact spoilers in the spray chamber and are transferred to a waste container. The burner head is a 6-10 cm slot where the ignition occurs. The rate of the nebuliser is an adjustable factor.
4. The monochromator selects the wavelength required by eliminating unwanted radiation, originating from sample components as well as the flame. The desired wavelength is isolated until it reaches the detector. Other productions of radiation consist of different wavelengths and are removed by modulating the source energy.
5. A detector with attached amplifier and readout device is the final component. The detector is a photomultiplier tube with a gas source for the flame and vent for exhaust gas. It measures the number of X-ray photons that pass through the flame. This is compared to the reference beam from the lamp.

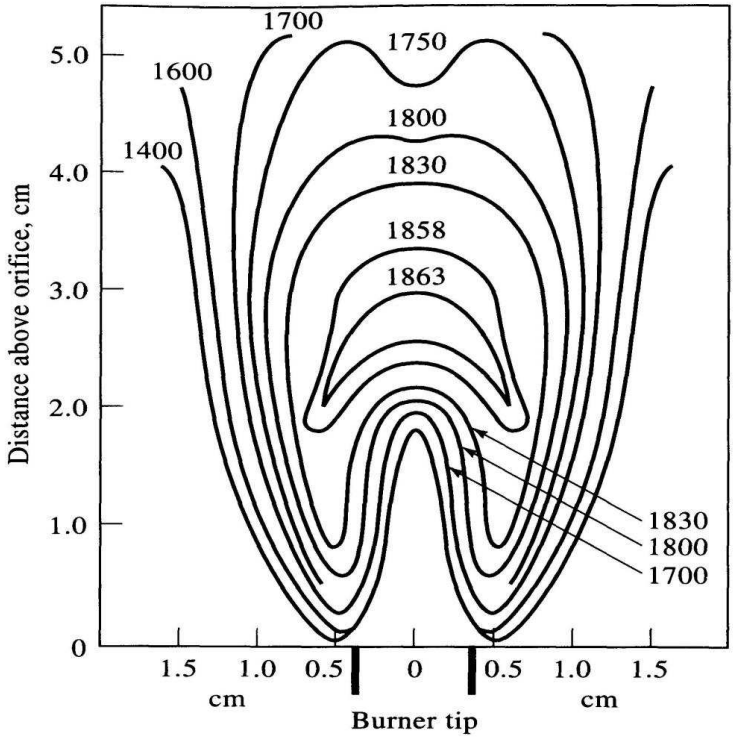

Figure 4.3 – Flame temperature distribution in FAAS

A set of standards with known concentration are run through the AAS. From this, a calibration curve can be plotted using the Beer-Lambert Law. The curve has a linear relationship, which allows the concentration of the unknown sample to be determined. Energy is sent through the already atomised sample, and the amount of light that is absorbed is detected and recorded as a quantity. The absorbance, A, is then entered into Equation 4.2 to determine the concentration of the element under analysis.

$$A = \varepsilon c l = \log\left(\frac{I_0}{I}\right) \tag{4.2}$$

The factors are the absorption of the reference sample, I_0, the absorption passed through the sample, I, ε is the extinction coefficient ($mol^{-1}dm^3cm^{-1}$), l is the path length (cm), and c represents the concentration ($moldm^{-3}$) which in this case, is the number to determine. Figure 4.4 shows the relation of these variables (College of Life Science - National Tsing Hua University, n.d.).

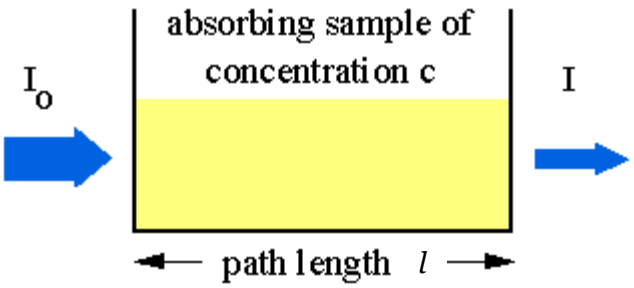

Figure 4.4 - Absorption of Light by a Sample

This means that the absorbance, A, is measured for a set of known concentrations. When absorbance is plotted against concentration, a linear relationship is obtained, (Figure 4.5) fulfilling the Beer-Lambert Law and is due to the fact that absorbance increases proportionally to concentration in this range. From this calibration curve, the concentration of the analyte can be determined (Chang, 2000).

It is important to remember that Beer-Lambert's Law is only valid for an 'ideal' solution, as a non-ideal solution will result in a shift in absorption wavelength of the analyte or a change to the refractive index of the solution (Mehta, 2012). The specific concentration range that follows the Beer-Lambert Law is different for different elements and configurations of the AAS instrument.

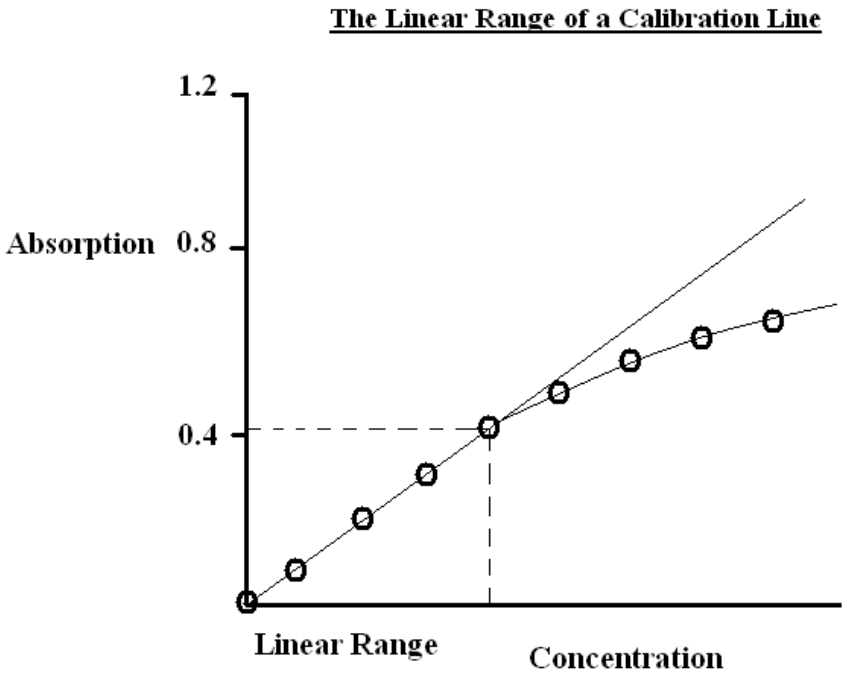

Figure 4.5 - Linear Calibration Line

4.3.2 Furnace AAS Theory

A Graphite Furnace Atomic Absorption Spectrometer, GFAAS, follows the same principle of the FAAS. The main difference is in the temperature that the sample is heated to. The temperature of the flame varies as shown in Figure 4.3, but it does not reach much over 1850 ^{o}C. A graphite furnace involves heating up the sample stepwise to approximately 3000 ^{o}C. The furnace is electrically heated and the sample is placed directly inside. It is dried and vaporised into atoms.

There are several advantages to using GFAAS over traditional FAAS. Those relevant to this study are as follows. Firstly, the detection limit of the GFAAS is two orders of magnitude better. This means that a much lower quantity of substance can be distinguished from the blank value so a smaller sample size is needed. Therefore, this is often used by environmental chemists to analyse samples (Tokman, et al., 2004). Secondly, GFAAS has a more efficient atomiser, allowing the spray of particles to be more homogenous in size and mass. Finally, GFAAS acts as a reducing environment for elements that are easily oxidised. According to a previous study, lead analysis is most commonly conducted using GFAAS due to all of the advantages stated previously (Garcia, et al., 2008).

4.3.3 AAS Specification

A Perkin Elmer AAnalyst800 complete with flame and graphite furnace coupled with an AS 800 auto sampler, atomic absorption spectrometer was used for analysis. The AAS control, data collection, storage and calculation of sample concentrations were performed using software provided by Perkin Elmer, WinLab32 software (version 6.4.0.0191). The Flame Atomic Absorption Spectrometer (FAAS) was initially used to analyse the soil leachates to determine the lead concentrations. A lead lamp was used with a linear range of 20 ppm. The first sequence run in the AAS was always purified water to determine a baseline. The water was re-run until results were constant. Following this, each of the standards prepared earlier on the same day were measured.

The standards were 0.5 ppm to 0.01 ppm and prepared from a lead standard that was 1000 +/- 4mg/L from Sigma-Aldrich. The results were analysed to determine

a calibration curve, Figure 4.6. If there were several 'outliers,' new standards were prepared and the calibration process repeated.

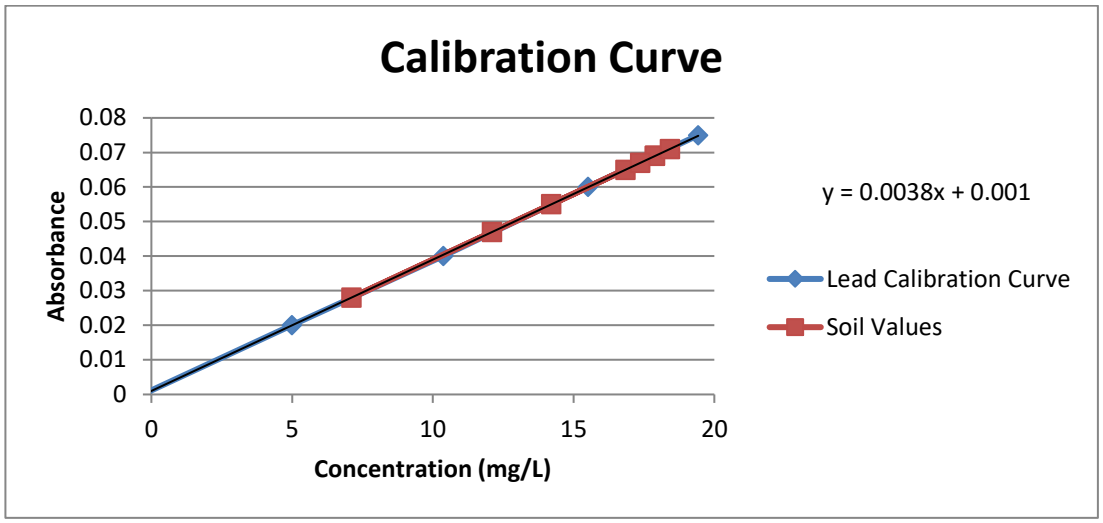

Figure 4.6 - FAAS calibration curve for lead samples with a set of soil results

Between each sample run, purified[2] water was used to wash the nebuliser and clear any trace sample remaining. This prevented any samples from overlapping and producing incorrect results. Samples that contain a concentration greater than the linear range of the elemental lamp must be diluted prior to analysis.

The detection limit for lead was determined to be 1.2×10^{-4} mg/L. This was calculated from 10 blank purified water readings and based on three times the standard deviation of these blank readings, a 98% confidence interval.

The settings for the FAAS are given in Table 4.1, whilst those for Graphite Furnace Atomic Absorption Spectrometer (GFAAS) are given in Table 4.2. The GFAAS had a lead detection limit of 5.0×10^{-5} mg/L which was determined as above.

[2] Deionised water was purified using a Thermo Scientific Barnstead Easy Pure II Reservoir Feed Water Purification System, Series 1305, Model D7031(7133). The system works using a cartridge and filter system.

Table 4.1 - FAAS Spectrometer Settings

Spectrometer settings							
Element	Wavelength (nm)	Slit Width (nm)	Read parameters		Replicate measurements	Lamp parameters	
			Time (sec)	Delay (sec)		Current (mA)	Lamp type
Lead	283.3	0.7H	3.0	0.0	6	10	Hollow Cathode Lamp
Flame settings							
Element	Oxidant	Oxidant flow (L/min)	Acetylene flow (L/min)	Viewing Height (mm)			
Lead	Air	17.0	2.2	0.0			

Table 4.2 - GFAAS Spectrometer Settings

Spectrometer settings							
Element	Wavelength (nm)	Slit Width (nm)	Read parameters		Replicate measurements	Lamp parameters	
			Time (sec)	Delay (sec)		Current (mA)	Lamp type
Lead	283.3	0.7L	5.0	0.0	1	10	Hollow Cathode Lamp
Furnace settings							
Read Step				4			
Injection Temperature (°C)				20			
Step	Temperature (°C)	Ramp Time (sec)	Hold Time (sec)	Internal Flow	Gas Type		
1	110	1	30	250	Normal		
2	130	15	30	250	Normal		
3	850	10	20	250	Normal		
4	1600	0	5	0	Normal		
5	2450	1	3	250	Normal		
Furnace Auto sampler		Sample Volume: 20uL			Diluent Volume: 0uL		
Matrix Modifiers		Volume: 5uL – added to blanks, standards and samples					

4.3.4 ICP-MS vs AAS

Inductively coupled plasma is another analytical technique that could have been employed in place of AAS. There are several reasons why it was not used in this study, which are detailed in the following section.

AAS is a highly specific technique that has low detection limits and requires minimal analyst skill. The running costs are low whilst the size of the equipment is relatively compact. The preparation of the sample is simple and AAS can analyse a small sample size.

The main negative aspect about the AAS compared to ICP is the lack in capability for multi-elemental analysis. This can be dealt with by the ease of changing element lamps and the availability of multi-element lamps. Another disadvantage of AAS is due to the gases required for the flame atomiser, as they are dangerous when mixed. AAS as a technique cannot analyse all elements and it has a lower linear range of 10^3 orders of magnitude (Thermo Elemental, 2001; Tyler & Longjumeau, n.d.).

ICP has a very wide linear range of around 10^5 orders of magnitude. It provides simple and quick qualitative analysis that will simultaneously conduct multi-elemental analysis. The running cost of the apparatus is low. ICP has good precision and low detection limits whilst maintaining high sensitivity. There is minimal chemical interference and over 70 elements can be analysed. The spectra have multiple lines for the determination of each element. As for the chemicals used in analysis, the plasma is much safer and the gases are inert (Thermo Elemental, 2001).

The issues with ICP are due to the multi-line spectra. There are interferences from the multiple elements causing an overlap of the broad lines in the spectrum. As a result, it might be more difficult to positively identify the individual element.

ICP can also be used as a combined technique with Mass Spectrometry (MS). This also demonstrates a rapid multi-elemental analysis but due to the MS, it is possible to have semi-quantitative analysis as well. There are low detection limits, a wide linear range, and short term precision, however there is isotopic analysis including isotope ratio and isotopic dilution analysis (Tyler & Longjumeau, n.d.). Issues

with this dual method involve spectral interference due to ICP, high running costs, but also the fact that much higher user skill is required.

Due to the problems with expensive running costs and the requirement of high user skill, it was decided that instead of finding access to ICP-MS elsewhere along with a skilled user, the benefits of AAS would be suitable. The analysis of the soil was based on lead being the most prominent toxic material. Therefore, it was not a problem that AAS fails to analyse multiple elements, as only lead was needed. Other analytical techniques (e.g. XRF, XRD, SEM-EDX) were used in combination with AAS to analyse the soils and conduct elemental analyses.

4.4 X-ray Diffraction

4.4.1 Introduction

X-ray Diffraction (XRD) is a non-destructive technique that allows for the identification of phases in a solid which can help characterise the material. There are several types, of which powder diffraction is the most common.

XRD analyses solid powders to determine their crystalline structure. From the diffraction pattern, it is also possible to determine the particle size and phase of the sample and is used in environmental analysis to provide mineral composition (Matthews, 1992).

4.4.2 Theory

Powder X-ray Diffraction (XRD) is used to analyse crystalline solids. It produces a unique diffraction pattern for every solid. Consequently, a database can be used to compare the diffraction pattern with known patterns to identify the compounds present in the unknown solid sample. This allows for the composition of mixtures to be analysed. Elements that are heavier will scatter X-rays more effectively than lighter elements. This is due to the scattering of radiation by electrons which is directly proportional to the electron density (Roessle, 2009; Atkins & de Paula, 2010).

Further analysis can be conducted on the peak shape and the standards used can be compared to provide information on the purity of the sample, the particle size and strain.

Bragg's Law states that when a beam of X-rays hits parallel planes of atoms in a crystal, there is a particular angle that will allow for a strong reflection, in the form of X-rays, to be related to the distance between the crystal planes, Figure 4.7 and Equation 3.6 (McGraw-Hill, 2002).

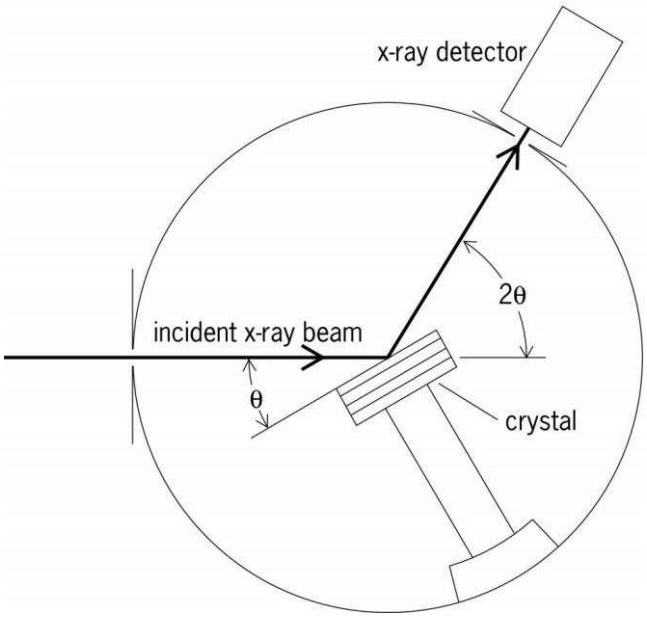

Figure 4.7 - Powder X-ray Diffraction Set Up

Bragg determined that the diffraction process could be represented by a set of lattice planes of atoms located within the crystal, Figure 4.8. Each plane was treated as a mirror that was semi-transparent. X-rays bombard the crystal and an atomic plane reflects some of the beams. Any X-rays that made it through the plane would then reflect off of succeeding planes (Open University, 1996).

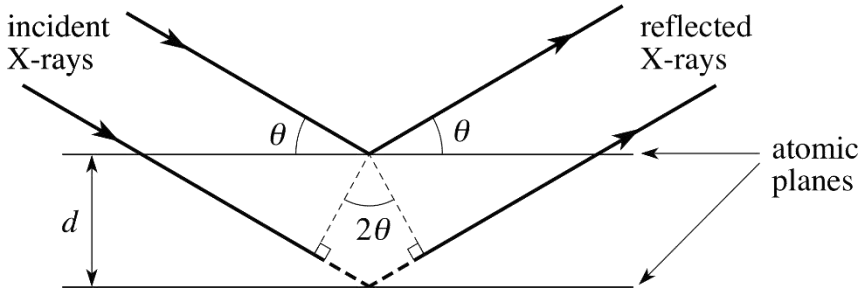

Figure 4.8 - Bragg's Law Diagram

Equation 4.3 is Bragg's equation which shows the relationship between the wavelength of incident X-rays (λ), the angle between the incident or the reflected

beam and the crystal plane (θ), and the distance between the crystal planes (*d*), where *n* is an integer (Matthews, 1992; Atkins, et al., 2006).

$$sin\theta = \frac{n\lambda}{2d} \tag{4.3}$$

Constructive interference occurs when *n* in Bragg's Law is an integer and the reflected waves are in the same phase as each other. The distances that the waves travel must differ by whole number. When *n* is not an integer, the waves are not in the same phase and thereby form destructive interference. This is denoted by nλ, where n is an integer (Open University, 1996).

The setup of a laboratory powder X-ray diffractor has two main components, the X-ray source and the radiation detector. The X-ray source consists of a metal target, copper in this study, and filament that is inside a highly-evacuated tube. The filament will emit an electron beam, which is accelerated towards the metal target. The electron beam will ionize the core electrons in the 1s shell of the metal target. This leaves holes in the 1s shell and causes a transition of electrons. The higher shells which are filled, then drop into the vacant space whilst emitting electromagnetic radiation. This can be compared to Figure 4.1a. In the case of XRD, the energy difference between the higher and lower shell is within the range of X-rays thus producing X-ray radiation. The relaxing of electrons into the lower orbital opening is decided by the transition selection rule. This specifies where a relaxing electron must move from when the vacancy is in a certain location. It results in two intense lines in the spectrum at the corresponding energy (Nave, 2016).

In this study, a copper X-ray source was used with a wavelength of 1.54 Å. In a compound where there is a light element like carbon and a heavy element like bismuth, the heavier element overshadows the lighter one. The beam needs to have a specific size and quality, which is user controlled. Diffraction slits and a monochromator will allow for beam size selection and a single wavelength of radiation (Suryanarayana & Grant Norton, 1998). During analysis, 2θ can be changed by either moving the beam/detector, or moving the sample. The powder diffraction pattern can

be indexed to provide information regarding the material's symmetry and lattice parameters, but in this project, XRD has been used as a purely analytical technique.

4.4.3 XRD Sample Collection

A Bruker D8 Advance X-ray Diffraction (XRD) Diffractometer with a Scintillation detector and a secondary monochromator was used to analyse the soils and their residues both before and after treatment, as well as to obtain a pattern for the Zeolite-A used. This was to determine if the Zeolite-A showed any traces of contaminants and if the heavy metals continued to leach out of the soil.

The results were analysed using the provided evaluation software, EVA, which coupled with the Bruker XRD. Examples of the individual diffraction patterns can be found in Appendix 4. The Search and Match function was used to determine the best material match for each of the peaks. Settings for the XRD are shown in Table 4.3.

Table 4.3- XRD parameter settings

XRD Parameters			
Start	10°	Anode	Copper
End	70°	Wavelength 1	1.5406
Step Size	0.025°	Wavelength 2	1.54439
Time per step	15s	Generator	40kV
Temperature	17°C	K alpha 2 Ratio	0.5
Time started	10s	Divergence slit	0.982°
2θ	10°	Antiscatter slit	0.499°
Θ	5°	Slit measured	fixed

4.5 X-ray Fluorescence

4.5.1 Introduction

X-ray Fluorescence (XRF) is a non-destructive qualitative and semi-quantitative technique providing information with regards to the elemental composition of an unknown sample. It is an extremely fast technique that requires minimal sample preparation and user skill. XRF is an indispensable technique in environmental analysis, being the portable apparatus of choice to take on site to analyse soil quickly for contaminants (Bruker Corporation, 2016). The portable version allows for elements to be detected whilst the full set-up provides more detailed information. This assists researchers by providing preliminary data immediately at the site so that they do not waste valuable time and resources collecting samples that do not contain the elements of interest.

4.5.2 Theory

XRF of an isolated system involves two main steps:

Firstly, an X-ray generator is used to produce primary X-rays by accelerating electrons through a power source whilst being held under vacuum. The electrons collide into the target anode which releases photons that hit the sample. There is energy transferred from incident photons to core electrons, this is known as photo-ionisation of the atom. The requirement is that the photon's energy is enough for the core electron to be ejected, creating an electron hole. The electron ejected becomes a photoelectron. An effect known as the photoelectric effect leads to an ionised atom (Rouessac & Rouessac, 2007).

Secondly, the newly ionised atom must be stabilised as it is in an excited state resulting in several decay events with scattering effects. An electron in the nearest higher energy level will drop down to fill the electron hole and the excess energy is emitted as a photon. There will then be a rearrangement of electrons throughout the shells. Numerous electron relaxations produce element-specific X-ray fluorescence, Figure 4.9 (Rouessac & Rouessac, 2007).

The XRF used in this study used a tungsten anode. Moseley's Law determines that the atomic number of the anode is proportional to the square root of the

frequency of the emitted X-ray (Moseley, 1914). Therefore, tungsten having the atomic number of 74, compared to 29 for copper, will emit X-rays with a higher frequency which are able to excite the fluorescence of any lighter element as intensity and frequency are inversely proportional. This is useful as XRF is used to determine the percentage composition of a sample, rather than the phases of crystals.

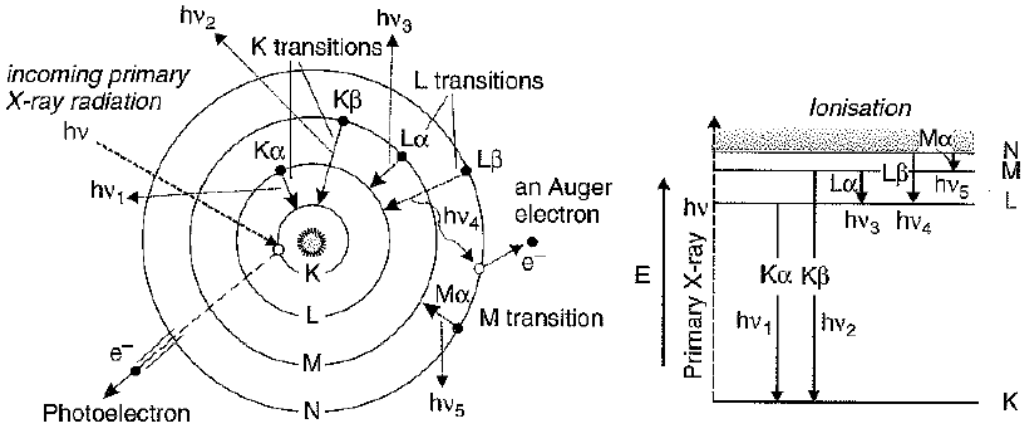

Figure 4.9 - X-Ray Shell Diagrams

X-ray detectors take the energy that the X-ray beam transmitted and convert it into an electrical signal (Yaffe & Rowlands, 1997). These transducers count the individual photons, which have an energy unique to each element. There are two common types of X-ray detectors. The first is a gas transducer most often used in wavelength XRF. The second type of detector is a semi-conductor transducer, also known as a scintillator counter. It is made of a lithium-doped silicon diode and used in XRF and EDX. The conductivity of the active zone is increased by each X-ray photon. The detector provides an impulse, which creates a trace back to the incident photon's energy. The negative of this apparatus is that the background noise is quite high and requires a reduction by being kept at very low temperature (Casas & Sordo, 2006).

The data collected are shown as an emission spectrum. The lines in the spectrum denote the wavelength of intense fluorescence (Rouessac & Rouessac, 2007; Niemantsverdriet, 2007).

The range of fluorescence for all elements is between 40 eV to over 100 eV, which correspond to wavelengths of 31 to 0.012 nm. This calculation is determined

using the Equation 4.4; where h is Planck's constant, c is the speed of light, and λ is the wavelength, and E in the energy. The heavier the element, the higher the number of possible transmissions as there are more energy levels. However, it is important to note that the probability of the occurrence of some of those transmissions is very small (Rouessac & Rouessac, 2007; Niemantsverdriet, 2007).

$$E = \frac{hc}{\lambda} \tag{4.4}$$

4.5.3 XRF Sample Preparation

Solid samples were placed into plastic containers and covered with a 3.6µm Mylar film. The XRF used in this study was a PANalytical Epsilon 3^x spectrometer with a 50 µm beryllium X-ray tube window, max voltage of 50 kV, 135 eV detector with an 8µm thin window. The software employed was Omnian.

The results were tabulated and include the elements present above 0.9%. The purpose for this value is that lead was detected in all samples at or above this value. Full results are available in Appendix 3.

4.6 Scanning Electron Microscope (SEM)/ Energy Dispersive X-ray (EDX)

4.6.1 Introduction

Scanning Electron Microscopy with Energy Dispersive X-ray (SEM-EDX) joins two analytical methods to provide detailed qualitative information. Magnified images of the samples are given and then X-ray spectroscopy can be used to analyse the elements present in the image at specific points and provide a spectrum. SEM-EDX has a wide range of uses as it acts both as a high-powered microscope as well as the EDX.

4.6.2 Theory

Scanning Electron Microscopy (SEM) uses the principles described by the theory of light. Light diverges from a source in several possible ways yet always in a straight line. A beam of light refers to a group of pencils of light originating from all points on a light source. (A pencil of light is a group of rays diverging from a single source, and a ray is a single photon, or particle, of light from a single point). The light can then be absorbed, reflected, or refracted. Absorption implies a photon entering

the material and never coming back out. Reflection is when a ray of light is turned back to its original material and does not enter the new material. Refraction refers to the bending of the direction of light as it goes from one transparent material to another and its velocity changes. Several factors affect refraction: the material, the angle of the incident light ray, and the wavelength of the incident light ray (Dunlap & Adaskaveg, 1997).

SEM operates under the following principles: all specimens are made of atoms described by “clouds” of electrons surrounding them, electrons will be given off the sample if it has an electron probe beam directed at it, and each pixel location has a measurement of electrons (Dunlap & Adaskaveg, 1997).

The source of electrons originates from an ‘electron gun’ consisting of a tungsten filament that is capable of generating a beam of electrons. This beam is then focused by using a series of magnetic lenses (also referred to as coils). This is then rastered, i.e. scanned side to side, across the surface of the sample by the scanning coils (Dunlap & Adaskaveg, 1997; de Gree, 2015).

The benefits of using SEM are that it will analyse textures and small scale features, it can be non-destructive and analyse very small quantities of sample, it rapidly obtains results, and, when coupled with Energy-dispersive X-ray spectroscopy (EDX), it has good detection limits for elements over the atomic number of 5 (Central Facility for Advanced Microscopy and Microanalysis - U.C. Riverside, 2016). SEM is complementary to other techniques. These include those used in the current study, XRF, XRD and AAS.

Non-metallic samples containing organic matter often need to be coated with an unreactive metal, such as platinum or gold, in order to be electrically conductive to provide a high resolution (Australian Microscopy and Microanalysis Research Facility, 2013). Because the sample is run under a vacuum, any liquid will evaporate off during analysis.

The mode of detection used was Secondary Electron. This is the most common detector as it involves an electron being dislodged from the surface, or only a small distance within the sample, due to the beam hitting the sample, Figure 4.10,

(Austrailian Microscopy and Microanalysis Research Facility, 2014). It has low energy which is why SEM must employ the use of a vacuum. The electron is emitted from the material's surface (Dunlap & Adaskaveg, 1997).

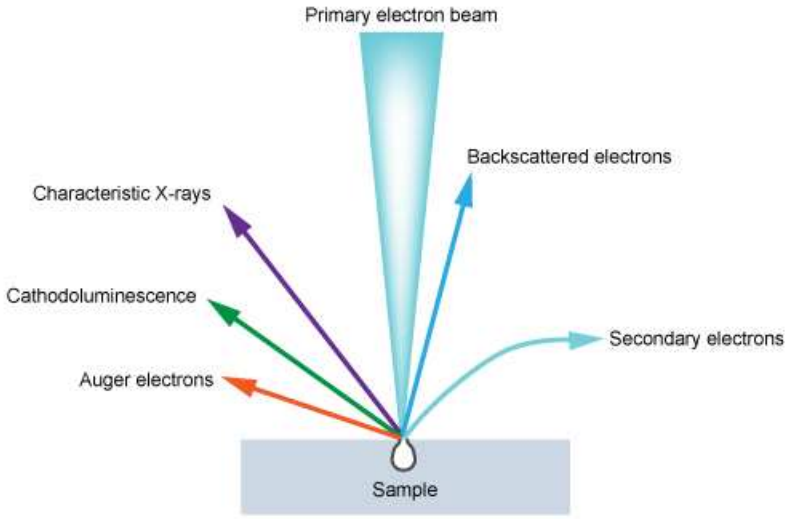

Figure 4.10 – Principles for SEM analysis

The secondary electron has an energy of around 50 eV, whereas the beam is around 20kV. Due to positive electrical bias, around 200-300 V, these electrons are then attracted toward a detector. Not all will make it to the detector as the working distance, surface roughness, and composition affect this. Those that make the journey are then accelerated by a high electrical potential, around 10 kV, to strike a phosphor scintillator. The scintillator will emit light and cause a photoelectric release of electrons from the photomultiplier tube, which are then accelerated to hit another phosphor scintillator. The process continues as would an image amplifier. The brightness on screen is controlled by the current from the photomultiplier tube and a secondary image is produced (Dunlap & Adaskaveg, 1997).

Samples composed of particles can often experience 'charging.' This is due to the number of incident electrons being higher than the number of electrons that are able to escape the sample leading to a build-up of negative charge. Electrons cannot be controlled and, therefore, will discharge randomly, and causing effects such as abnormal contrast, image deformation and shift. The amount of charging that occurs will be related to the energy and number of electrons. This can be decreased slightly by reducing the kV, providing lower energy to the sample. Also, the beam current,

emission level of the electron gun, the spot size and the apertures between the gun and the sample can be adjusted to cause fewer electrons to be discharged (Dunlap & Adaskaveg, 1997).

Fitted with the SEM used for the current project was an Energy Dispersive X-ray (EDX) unit. This unit follows the theory provided for the XRF. Unique for the EDX fitted to the SEM is the ability to create elemental maps of a chosen area of sample.

The detector inside the EDX is a lithium-doped silicon crystal, which must be kept at cold temperatures in order to ensure the reduction of thermally generated signals. The detector used is a Peltier-cooled silicon drift detector with an X-ray capture area of up to 80 mm^2.

4.6.3 SEM-EDX Sample Preparation

A Hitachi S3400 SEM with an Oxford Instruments X-Max 80M50D was used to analyse the soil residue. The residues were mounted onto 12mm stubs that were topped with carbon sticky tabs. This ensured the soil particles would not move during analysis. The residues were tapped over the surface to obtain a thin layer of soil. The mount was then agitated to remove any excess soil.

There are multiple methods that may be used to analyse solid samples. Stubs with carbon sticky tabs are particularly useful for particles and powders that are being analysed with X-rays. A benefit of this method is that there is less interference and low atomic contrast. Polished blocks were not utilised even though they are useful particularly for Wavelength Dispersive X-ray (WDX) rather than EDX, where small phase differences are significant (Central Facility for Advanced Microscopy and Microanalysis, 2016). Polished blocks were not considered for this study as at the start of analysis, the apparatus was not present and available for use. Subsequently, to maintain a consistent method, all of the samples were analysed with carbon-coated stubs.

Several of the samples were gold coated at 10 nm prior to analysis. This helped to ensure the particles did not charge and appear blurry on screen. This was only done to samples that were so highly charged that no analysis could take place.

The height of the sample was recorded and the stub was inserted. The parameters used were: voltage 30.0 kV, emission 90.0 µA[3], and analysis +10 mm.

Point analysis was conducted randomly for each sample to determine the elements present in the area. If lead was identified, further investigations by zooming was performed, and further point analysis done. Some areas of particular interest were mapped out for more detail to understand where the lead was located with respect to each other and with the other elements present. For each element map conducted, a 'blank' was included. This is an element known to be absent in the sample. For this study, uranium was selected. The brightness of the blank speaks to the background reading of the sample. Arsenic was also included as it an element with harmful characteristics and could be chosen for further future analysis. A list of the SEM-EDX settings is given in Table 4.4.

Table 4.4 – Explanation of SEM parameters

SEM PARAMETERS	DESCRIPTION
Magnification	Minimum: x10, Maximum: x300K
Depth of Focus	Dependent on the distance from the sample to the detector. There is better depth of focus at a further distance, however there is also lower resolution.
Resolution	Better resolution closer to the detector, but less depth of focus. This is dependent on the aperture size.
Beam Spot Size (Beam Current)	A smaller spot offers a higher resolution, but less signal and a noisier image is produced
Working Distance	The distance between the pole-piece and the surface of the sample, dependant on the height of the individual sample.
Beam Voltage	A higher voltage gives more signal; however, it also penetrates the sample more.

[3] note that the emission value varied due to the ageing of the filament. The machine was never operated below 70.0 µA to ensure the clearest results.

4.6.4 Limitations of SEM

The quality and representativeness of SEM results have been covered in depth in a study by Michelic et al 2010. It was stated that by taking only a small selection of the overall sample for analysis, the data will be truncated. Changing the analysis of an area significantly does not affect the representative output due to the already truncated data (Michelic, et al., 2011). In the current study, multiple sets of samples were analysed using SEM-EDX and multiple areas of each sample were analysed. The technique was used solely for qualitative purposes to support the results from the XRD. Ideally, further work would include quantitative analysis with more runs on a larger bank of samples. This would ensure more representative results.

4.7 pH Meter

The pH meter used was a Hanna HI98103 Checker® with HI 1270 pH electrode. It has a 0.01 pH resolution with +/-0.2 pH accuracy and 2-point calibration. The pH meter was calibrated using three buffer solutions at a pH of 4, 7 and 10. The pH meter was calibrated before every batch analysis.

4.8 Computational Method

4.8.1 Introduction

Computational simulations are useful to determine the most energetically favourable structures. In this thesis, the simulations work to complement the experimental techniques to determine how lead interacts with Zeolite-A. It may be difficult to obtain atomic information experimentally whilst computational simulations provide a theoretical hypothesis to help interpret experimental observations. In theory, atomistic simulations allow for researchers to model on the atomic scale any type of material.

In this study, ab initio calculations have been employed to study the interaction of lead and barium with Zeolite-A, to establish the probability of lead ion exchange in the Zeolite-A structure.

To model the electronic structure of a material, Schrödinger's equation, Equation 4.5, is applied and based on the description of the system's electrons.

$$\hat{H}\Psi = E\Psi \tag{4.5}$$

Where $\hat{H}$ is the Hamiltonian, Ψ is the total wave function and E is the energy of the system. This energy represents the most stable electronic configuration. In this case, the more negative energy, the higher stability. The operator, $\hat{H}$, produces a value, from the wave function, for energy.

When analysing a single particle or two particles, the exact energy can be determined. Any more than two particles and the precise energy value cannot be calculated. In the current study, a crystal is being analysed, not a single atom, so there are well more than two particles under analysis. This requires an approximation to be made. The two approximations that have been utilised in this project are Hartree-Fock and Density Functional Theory (DFT).

4.8.2 Hartree-Fock Theory

The Hamiltonian that is used to describe the energy can be separated into various contributions. In classical physics, it is common to consider i) kinetic energy, the energy of moving particles, and ii) electrostatic forces, the interaction of charged particles, given by Coulomb's Law, Equation 4.6 (Szabo & Ostlund, 1989; Parr & Yang, 1989; Nave, 2016).

$$F = \frac{q_1 q_2}{4\pi\varepsilon_0 r^2} \tag{4.6}$$

F is the force of interactions, q is the charge on the particle (either positive or negative), ε_0 is the permittivity constant in a vacuum and r is the distance between the particles. The $1/r^2$ value is a larger number than that established in van der Waals forces, ranged at $1/r^6$. Coulomb and van der Waals forces are, therefore, referred to as long and short-ranged, respectively. This implies that Coulomb's Law allows for the particles to be quite a distance away from each other and still be able to be affected by each other (Burgot, 2012; Glasel & Deutscher, 1995).

Hartree-Fock considers electrons to be an electron 'cloud' and the interactions analysed consist of that between an electron and the 'cloud,' with an average electron potential (mean potential), rather than another individual electron. The equation calculates the sum of each electron interacting with the 'cloud'. The more electrons,

the higher the energy. It is important to note that an electron cannot interact with individual electrons, i.e. the Hartree-Fock approximation lacks electron correlation, but calculates an exact exchange term, allowing an electron to interact exactly with an average potential of all of the other electrons. The Hartree-Fock approximation was developed to solve the electronic Schrödinger equation, Equation 4.7 (Sherrill, 2000).

$$H_{eff}(k) = -\frac{\hbar^2}{2m_e}\vec{\nabla}_k^2 - \frac{e^2}{4\pi\varepsilon_0}\sum_g \frac{Z_g}{|\vec{r}_k - \vec{R}_g|} + \frac{e^2}{4\pi\varepsilon_0}\sum_{\substack{i=1 \\ i\neq k}}^{N} \int \frac{|\psi_i(\vec{x}_i)|^2}{|\vec{r}_k - \vec{r}_i|} d\vec{x} - \frac{e^2}{4\pi\varepsilon_0}\sum_{\substack{i=1 \\ i\neq k}}^{N} \int \frac{\psi_i^*(\vec{x}_i)\psi_i(\vec{x}_k)}{|\vec{r}_k - \vec{r}_i|} d\vec{x} \quad (4.7)$$

In this equation, the terms are as follows; r represents electronic degrees of freedom, R is the nuclear degrees of freedom, Z is the charge of the nuclei, ε_0 is the dielectric constant, ψ_i is the wave function, h is Planck's constant divided by 2π, m_e is the mass of the electron, and e is the charge of the electron.

∇^2 is defined in Equation 4.8.

$$\nabla^2 = \frac{\partial^2 x}{\partial t^2} + \frac{\partial^2 y}{\partial t^2} + \frac{\partial^2 z}{\partial t^2} \quad (4.8)$$

Kinetic energy is represented by Equation 4.9.

$$\hat{T}^E = -\sum_{i=1}^{I} \frac{\hbar^2}{2m_e}\nabla_i^2 \quad (4.9)$$

Several factors have not been accounted for by the Hartree-Fock approximation. The fact that the atoms are moving needs to be addressed. Electrons move extremely fast, at the speed of light, whilst atoms move significantly slower. The Born-Oppenheimer approximation addresses the movement of atoms. It assumes that nuclei are fixed in position, allowing for the electrons to be treated separately from the nuclei. This allows the focus of calculations to remain on the distribution of electrons.

A wave function tells where there are electrons located. It is, therefore, related to the electron density. Equation 4.10 shows that the electron density is equal to the probability of finding an electron in a specific location.

$$[\rho] = |\psi(r)|^2 \tag{4.10}$$

The variable 'r' is the radial distance of the electron from the centre of the atom, therefore ψ(r) is the wave function at a specific point, and can be changed which allows for an electron distribution to be built up to show where all of the electrons are located, Equation 4.11.

$$\phi_j(r) = \sum_{i=1}^{N} c_i \psi_i \tag{4.11}$$

ϕ_i is the atomic orbital under investigation, i denotes the specific orbital, and c_i is the coefficient for that orbital. In order to describe ϕ_i one must apply a linear combination of atomic orbitals, LCAO, which define the combination coefficient, Equation 4.12.

$$\psi_{MO}(\vec{r}) = \sum_{i=1}^{n} c_i \varphi_i(\vec{r}) \tag{4.12}$$

There are several methods of describing atomic orbitals mathematically. Radial distribution depends on the distance of an electron from the core and angular distribution considers the 3D shape of the orbital i.e. sphere for s, dumbbell for p, etc. Radial distribution can be plotted as a graph of wave function versus distance between particles. This graph has a similar form to a Gaussian function, Figure 4.11.

In this work the atomic orbitals are described by Gaussian functions that are used to build up basis sets, Equation 4.13. A Gaussian is an exponential function that depends on an exponent and the distance between an electron and the core, e^{r^2}.

$$\varphi_i = Be^{-Ar^2} \tag{4.13}$$

The method employed plots a Gaussian that fits part of the original curve. The area of the Gaussian that does not fit is considered to have failed, the remainder is kept. A new Gaussian is made to fit a different part of the original curve to build up a linear composite of Gaussian functions. This then follows the same method. The area that correlates is kept, the failure is discarded. This is repeated until a number of Gaussian curves fit the original curve. Despite using many Gaussian curves, it is very difficult to fit the origin of the curve, representing the electrons nearest to the core. The reason being that a Gaussian begins with a curve whilst radial distributions start with a straight line in immediate downward slope, Figure 4.11 (Leach, 2001).

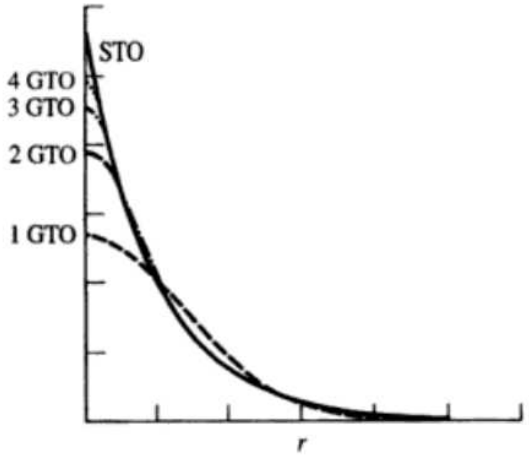

Figure 4.11 - Plot showing 1s atomic orbital (Slater type orbital, STO) in comparison with Gaussian type orbitals (GTO) up to a 4th term linear combination

Basis sets describing core electrons often have six to eight Gaussians because there are many needed to describe the electrons close to the core. Basis sets are sets of atomic functions, which include atomic orbitals centred on atoms, bonds and lone pairs. This creates the molecular structure. There are many different types and they are approximations. When many basis functions are used in a crystalline, densely packed system, the basis functions can overlap.

Large basis sets are beneficial because they allow for more accurate calculations, but they use diffuse functions which are wasteful for computer resources. Simple basis sets are minimal. They only contain the functions required to accommodate every occupied orbital in each individual atom in their ground state. It will usually contain every atomic orbital in the shell. A compromise between computer time and accuracy is required.

Self-Consistent Field (SFC) cycles are as described in Figure 4.12. The quantum-mechanical program starts by taking the provided basis set Gaussian function and guessing 'c' for the atomic orbital based on this. From this it calculates an energy. The new ψ_i gives information of where the electrons can be found in space and a new set of coefficients, 'c', are derived from which a new energy can be calculated. This energy is compared to the previous energy calculated. If the new energy is lower, it is kept. If not, it is discarded and the previous energy is maintained. c_i is then changed again and

the process is repeated until the difference in energy is not changing by more than a given value. The calculations in the current study used a cut off of 10^{-6} Hartree.

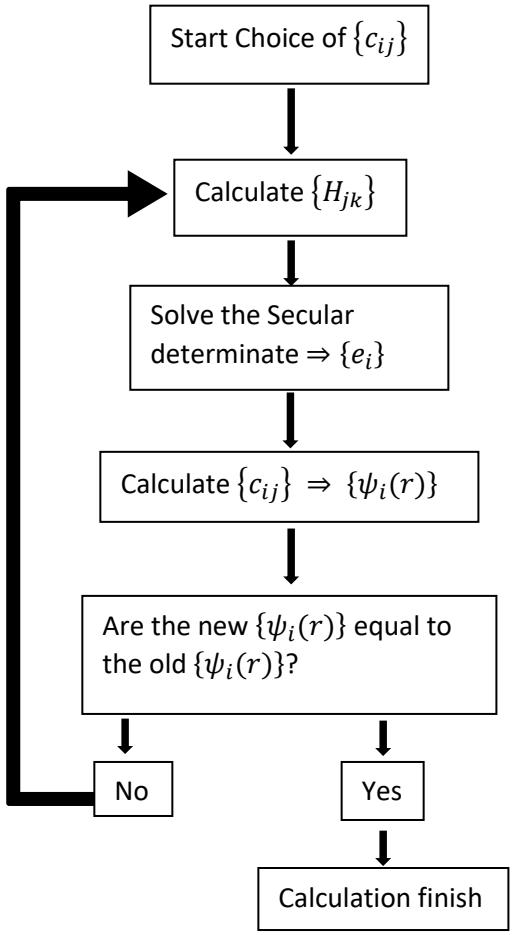

Figure 4.12 - Self Consistent Field Cycle (SCF)

To find the energetically most stable geometry, a geometry optimisation is undertaken. In this study the Broyden-Fletcher-Goldfarb-Shanno, BFGS, approximation has been used. This is an iterative process that is based on an improved version of the Newton-Raphson algorithm. The algorithm is used to find minimum potential energy surfaces (PES) (Canepa, 2011). The SCF energy must converge in each point investigated on the PES in order to finish. This requires many small steps and a gradient of zero marks the minimum. However, if the minimum is very flat then it would take an extremely long time to calculate the lowest point because the steps would be incredibly small.

4.8.3 Density Functional Theory (DFT)

Density Functional Theory disregards atomic orbitals. It instead describes an electron density. In DFT, the electrons are able to see each other specifically as

opposed to only being able to determine an electron cloud, therefore it contains a correlation term as described in Equation 4.14.

$$\left(-\frac{1}{2}\nabla^2 + v_{ext} + v_{ee} + v_{xc}\right)\psi_j(\vec{r}) = \varepsilon_j\psi_j(\vec{r}) \quad (4.14)$$

v_{ext} is the positive interaction with negative (the core protons interacting with electrons). v_{ee} is the interaction between two electrons, and v_{xc} is the exchange correlation term.

A well-known problem with DFT is the fact that an electron can interact with itself, known as self-interaction. This is not the case in Hartree-Fock, where exchange described is exact. DFT corrects the problem by the Self-Interaction Correction (SIC) or by using Hybrid Functional Theory. In this thesis, the latter approach has been employed.

Hartree-Fock perfectly describes the exchange of electrons exactly, even for solid systems. However, it does not consider the correlation. In DFT, various functionals are used to describe the exchange and the correlation terms. It is necessary to have a mathematical ability to describe electron density, which allows a certain empirical guessing.

The first method is the Local Density Approximation (LDA), which describes the density as being 'perfectly' uniform, working well for metals. It does not account for orbital overlap with higher electron density.

The second method is the General Gradient Approximation (GGA). This allows a functional to be chosen for exchange and another for correlation. This involves multiple mathematical equations. There are a number of possibilities. One is chosen based on the similarity of the system it was designed for. In this study, Becke (Becke, 1988) was chosen for the exchange functional and Lee-Yang-Par (Lee, et al., 1988) was used for the correlation functional. This results in the well-known BLYP functional (Finley, 2004).

Becke dealt with the self-interaction issue by using parts of Hartree-Fock and combined Hartree-Fock with DFT to create a hybrid functional theory. He used his own functional combined with LYP and added what he found to be an ideal 20% of Hartree-

Fock, which resulted in B3LYP (Finley, 2004). The percentage is an empirical value that is subject to discussion. B3LYP is a hybrid described by 20% Hartree-Fock (B3LYP) and 80% DFT (Becke). The B3LYP functional was employed as it is known to work well on molecular systems. Zeolites are open framework structures, i.e. not dense, allowing them to be treated as molecular systems rather than highly packed crystal structures.

4.8.4 CRYSTAL09

CRYSTAL09 is a quantum chemistry program that is designed to run ab initio calculations on crystalline solids. It computes the structures electronically and produces an output file that contains the amount of cycles calculated as well as the amount of energy required for formation of the molecule. CRYSTAL09 investigates the chemical and physical properties which include structural, vibrational, and dielectric properties (CRYSTAL, 2016). This software uses Gaussian basis functions to create the electron charge density, allowing it to build crystalline orbitals, i.e. molecular orbitals.

4.9 Conclusions

In this section the techniques employed in this study have been described with their theory. They include:

- Atomic Absorption Spectroscopy (AAS) – gives elemental concentrations in the leachates (liquid samples)
- X-Ray Diffraction (XRD) – provides solid compositions by determining the minerals present in the sample
- X-Ray Fluorescence (XRF) – provides composition in solids based on percentage
- Scanning Electron Microscopy with Energy Dispersive X-Ray (SEM-EDX) – gives elemental composition as well as microscopic zoom capabilities
- Computational – provides adsorption energies and structures

Chapter 5 Materials and Methods

5.1 Aim

The aim of this section is to introduce, in more detail, the properties of the locations of the sites analysed, state the field sampling and collection methods, and to detail the lab work done to assure quality in results. The synthesis of Zeolite-A and the method of addition to samples are also described.

5.2 Introduction

The samples were all collected in a manner acceptable to quantitative trace analysis. However, this was not a geological survey but the aim of the project was to undertake a chemical study of Zeolite-A to determine if it could be used on natural soil samples with high levels of lead. This project will, therefore, not include any discussion on comparative control samples.

5.3 Sample Collection

Approximately 1 kg of each sample was collected using a mini-digger and a stainless-steel trowel, and directly placed into labelled plastic bags and sealed. The bags were then immediately placed into another empty bag and sealed. The bags were stored at approximately 18 ^{o}C and out of direct sunlight. Note that that the samples were not kept in inert atmosphere but the bags were airtight until analysis commenced.

The military allowed access to the site for sample collection for only a limited time. A mini-digger was used to extract the soil. Each layer was analysed visually, measured and noted. It was clear that the leaching processes had occurred as the layers maintained a red colouring throughout several layers.

Stones and organic materials were removed from the soil samples, which were then bagged and numbered based on location and layer depth. Soil 1 was retrieved from a visible pyrite ash layer that spanned from the surface to 20 cm below. In Soil 2, the pyrite ash layer appeared approximately 60 cm from the surface and was a thickness of 18 cm. These layers were chosen for analysis because they appeared to have the brightest red and orange colouring, which would imply that they contained

the highest concentration of pyrite ash waste and thereby also the highest heavy metal contamination. This has been confirmed by ICP-MS analysis presented in Appendix 1.

5.4 Quality Assurance and Statistical Testing

As previously mentioned, the purpose of this investigation did not centre on the geological aspects. As such, the quality assurance for geochemical analysis was not considered. The quality assurance that was factored was centred on the analysis undertaken regarding the remediation of soil technique.

Multiple samples of remediated soils were run for each experimental method detailed. Machines were calibrated and errors bars and statistical tests were carried out. Error bars were calculated using the standard deviation of the measurements, as provided by the instrument's output data. This also involved calculating the mean absorbance using Equation 5.1, where x is each value and n is the number of values.

$$\bar{x} = \frac{1}{n}\sum_{i=1}^{n} x_i \tag{5.1}$$

The standard deviation of the absorbance values uses Equation 5.2.

$$\sigma = \sqrt{\frac{1}{n-1}\sum_{i=1}^{n}(x_i - \bar{x})^2} \tag{5.2}$$

A t distribution based 95% confidence interval for the mean of the samples run was calculated. Equation 5.3 was used, where $t_{\frac{\alpha}{2},n-1}$ is the t distribution coefficient for a (1-α)% confidence interval for a sample of size n.

$$\bar{x} \pm t_{\frac{\alpha}{2},n-1}\frac{\sigma}{\sqrt{n}} \tag{5.3}$$

Due to the number of samples that were run, the interval was less than the standard error bars calculated using sample standard deviation. Therefore, in all of the data provided, the error bars are shown to represent the greatest error calculated.

5.5 Sample Preparation

The soil samples were weighed, placed on large numbered Petri dishes and dried in an oven at 70 ^{o}C. The samples remained in the oven until they were found to have reached constant mass. This ensured that any residual moisture was removed.

The samples were ground with a pestle and mortar and then sieved using 1 mm mesh to remove any remaining stones and organic matter. Finally, the samples were put into sealed and labelled plastic containers.

The purpose of grinding the soils was to ensure a higher surface area, allowing a higher dissolution rate and a more homogeneous material. It is possible that the heating and grinding of the soil modified the sample. However, this aspect has not been considered in the project as the matrix was assumed to be insignificant because of the low probability of phase change due to the sample preparation.

5.6 Lead Standards for AAS Calibration

Lead standard was purchased from Sigma Aldrich as a 1000 +/- 4 mg/L, calibration stock solution. Calibration standards were prepared by diluting the stock solution in 0.25M HNO_3 as shown in Table 5.1. Lead has a working linear concentration range of 20 ppm for use in Atomic Absorption Spectroscopy (AAS).

Table 5.1 - FAAS calibration standards

Calibration Standard Number	Concentration of Lead (mg/L)	Volume of Stock Solution (mL)	Volume of 0.25MHNO_3 (mL)	Final Volume (mL)
1	0.25	0.0125	49.9875	50
2	0.5	0.025	49.975	50
3	1	0.05	49.95	50
4	2	0.1	49.9	50
5	5	0.25	49.75	50
6	10	0.5	49.5	50
7	15	0.75	49.25	50
8	20	1	49	50

5.7 Difficulties Using Flame Atomic Absorption Spectroscopy (FAAS)

A previous study of the same soil samples, using ICP-MS (Appendix 1), produced data providing initial concentrations of lead present in the untreated soils. These concentrations were over 20,000 ppm for both soils. The results produced by FAAS showed a significantly lower concentration. This caused speculation as to whether FAAS was producing incomplete results. The theory was that the temperature of the

flame was not high enough, or the sample was not held over the flame for long enough to separate the lead from the matrix. To test this hypothesis, GFAAS was used, and it was decided that FAAS results should only be used as an indication of general trends.

It was also determined that there was lead present in standards, thought to have originated from the HNO_3 stock which was suspected to be contaminated. The stock was, therefore, compared to another laboratory-grade stock solution and also to an analytical stock. The analysis grade was found to give significantly lower readings of lead, below the detection limit.

Table 5.2 - FAAS of various nitric acid samples

Nitric Acid	FAAS Absorbance
Blank (purified water)	0.0016
Contaminated laboratory-grade HNO_3	0.9033
Laboratory-grade HNO_3	0.1049
Analysis-grade HNO_3	0.0559

Due to this data, all further analysis was conducted using the analytical grade HNO_3.

5.8 Zeolite-A Synthesis

The Zeolite-A used in this study was synthesised using the following method (Alfredsson, 2010):

1. Approximately 6.75 g of sodium aluminate and 12.50 g of sodium hydroxide were dissolved in 150 cm^3 of water and brought to boil in a magnetically stirred beaker.
2. Separately, around 7.25 g sodium silicate in 100 cm^3 of water was heated and once it reached 85 ^oC, the two solutions were added together and a white suspension was formed. The mixture was stirred at ca. 90 ^oC for approximately 2 hours.
3. The solution was monitored until the white suspension was found to settle out quickly once stirring was stopped. The mixture was then cooled to room temperature, decanted and re-suspended in 200 cm^3 of water, twice, for washing.

4. A Büchner filter and sintered funnel were used to retrieve the suspension with ca. 10 cm^3 of water for further washing.
5. Finally, the product was dried for 12 hours at 100 ^oC.

5.9 Digestion of Soil Samples

Purified water and analytical grade 0.25M HNO_3 were used to digest the contaminated soils. The latter was chosen as it acts both as an oxidising reagent as well as an acid, causing the pH to decrease. It is also a common reagent when digesting soils (Zeng-Yei & Zueng-Sang, 2002). Aqua regia was not used even though it is both complex binding and an oxidising agent as an early study undertaken on these soils showed that digestion in aqua regia and HNO_3 gave similar overall lead concentrations (Collins, 2009). The use of nitric acid also mimics the rainfall of the particular situation in Sweden more closely as HNO_3 is one of the components in acid rain (Ivezic, et al., 2013).

Following this, the soils were mixed with varying amounts of zeolite (as described in the method below). Samples were mechanically stirred in purified water or analytical grade 0.25M HNO_3 as described below. A table of samples is displayed in Appendix 2.

5.9.1 Analysis in 0.25M HNO_3

To make the 0.25M HNO_3 stock solution, 8 ml of HNO_3 solution (69% laboratory analysis grade nitric acid) was made up to 500 ml with purified water, prepared as described above. This gave rise to a solution that was found to have a pH of 0.20.

All of the analyses using dilute nitric acid and purified water followed the same method which is as follows:

1) Approximately 1 g of the designated soil sample was placed in a glass conical flask and 15 ml of purified water was added to it. Depending on the sample, 0 g, 0.25 g, or 0.50 g of Zeolite-A were added before the flask was covered with Parafilm® M (2in) and shaken for 24 hours.
2) The resulting mixture was gravity filtered using Whatman Grade 1 filters. The leachate was further filtered by using a syringe to inject the leachate into

Minisart®NML Syringe Filters 16534 with cellulose acetate membrane, gamma-sterile, 28 mm diameter, 0.2 um pore size, filtration area 6.2 cm^2, hold up volume 0.15 ml maximum pressure 4.5 bar, max temp 50 ^oC (Sartorius, 2016). This was used to ensure that any particles would not get stuck in the nebuliser tube for the flame AAS.

3) The leachate samples were transferred to PVP sample tubes, diluted as necessary, and immediately analysed by AAS.
4) The solid residue was left to dry at room temperature before being weighed and collected.

Teflon flasks were not used due to availability, but to account for the possibility of glass absorbing metal cations, the flasks were cleaned in acid baths. There is a possibility that this affected the total lead level measured, however all soils were analysed following the same method and, therefore, the amount of lead being absorbed by the flask would remain constant and not affect the individual amounts. The possible amount absorbed would be within the error taken into consideration.

5.9.2 Analysis in Purified Water

The soil samples were analysed with purified water. This was in order to mimic rainfall whilst removing any contaminants that could be present in tap water (Russell, 2016). Purified water was obtained by filtering deionised water through a ThermoScientific Barnstead EasyPure II Reservoir Feed Water Purification System, Series 1305. Originally, the soils were analysed in deionised water as a preliminary test to detect any changes in lead concentration. Further analyses were then conducted with purified water.

5.9.3 Naming of Samples

S1untreated and S2untreated refer to Soil 1 and Soil 2, respectively, after the samples were collected, dried, and sieved, as detailed in Section 5.5. S1w refers to ca. 1 g of Soil 1 washed in 15 ml of purified water. S1wZA25 corresponds to an addition of ca. 0.25 g of Zeolite-A and S1wZA50 adds 0.50 g to the sample prior to washing in purified water. The same method was followed for Soil 2. For the soils washed in 0.25M HNO_3 instead of purified water, S1a refers to ca. 1 g of Soil 1

washed in 15 ml of 0.25M HNO_3. S1aZA25 corresponds to an addition of ca. 0.25 g of Zeolite-A and S1aZA50 adds 0.50 g to the sample prior to washing in purified water. The same method was followed for Soil 2

5.10 Conclusions

- The soils were collected from a site in Sweden where high levels of lead contamination was suspected to have occurred. This was confirmed by ICP-MS (Appendix 1).
- A chemical analysis was undertaken, taking into account a strict analytical quality assurance in which statistical testing was carefully considered.
- It was found that FAAS is not a suitable technique for analysis of Pb-containing soil leachate with an acidic HNO_3 matrix. Instead, GFAAS was employed.
- All leachates were prepared with analytical grade HNO_3 and analysed within 24 hours of preparation to minimise a decay of the samples.
- Zeolite-A was synthesised and used for remediation by addition to soil samples.
- The zeolite was added to soils that were washed in dilute acid or purified water. This mimicked the conditions that affected the site in the form of precipitation and acid rain.

Chapter 6 Results and Discussion

6.1 Aim

There are two aims of this chapter. The first aim is to characterise the properties of the two untreated soil samples, S1untreated and S2untreated, and those washed in purified water and dilute acid, S1w, S1a, S2w and S2a, using qualitative as well as quantitative techniques. Visual techniques are an example of qualitative methods used to determine the colours of the samples. Quantitative methods included XRF and XRD to measure the concentration of lead in the untreated samples.

The second aim is to analyse Zeolite-A as a suitable remediation technique for lead in soil. This is done first by analysing the effect of pH on Zeolite-A to understand its stability and ability to form secondary minerals as well as the effect the pH will have on the solid residue. Moreover, the solid soil residues obtained after washing the soil samples, named as detailed in Section 5.9.3, were analysed using XRD, SEM-EDX and XRF. This was to determine what remediation effect, if any, the addition of Zeolite-A, in varying amounts, had on the lead contamination and mineral composition.

6.2 Introduction

The US Environment Protection Agency (EPA) states that 'safe' levels of lead present in residential areas, that are designated as 'play areas,' is less than 400ppm whilst 'non-play areas' is under 1,200 ppm (Centers for Disease Control and Prevention, 2007). The levels adopted by the Swedish Environment Agency are higher, citing the poisonous level of lead to be 2,500 ppm (Rylander, 2007). Soil 1 tested below the EPA suggested limits for 'non-play areas', whilst Soil 2 was significantly above both of the EPA recommended values. Further, the pH of the two soil samples demonstrated large differences proposing that they represent two different environments.

The remediation of contaminated soil involves considering multiple factors. One of these is the affect that an additive will have on the soil and surrounding environment. Various methods have been investigated to use minerals as well as

organic materials for cation exchange or adsorption at heavy metal-contaminated industrial sites (Bailey et al., 1999). Zeolites have proven to show high selectivity towards lead (Babel & Kurniawan, 2003) and also be independent of the choice of zeolite structure. Bearing this in mind, Zeolite-A, a synthetic zeolite with small pore sizes that is low cost and easy to synthesise, was chosen as the remediation method of the lead-contaminated site in Oskarström. Zeolite-A has also been shown to increase the pH of soils where it has been added, and is known to decrease heavy metal leaching (Hamon et al., 2007; Oste et al., 2002), and was analysed in relation to the positive affect it could have on the remediation process.

6.3 Identification of Zeolite-A

Zeolite-A was synthesised as described in Section 5.8.3. Figure 6.1, an XRD pattern of the synthesised Zeolite-A, shows that all peaks are associated with the red lines representing the pattern for sodium aluminium silicate hydrate, ($Na_{12}[(AlO_2)_{12}(SiO_2)_{23}]\cdot 27H_2O$) as reported in the EVA database (PDF Card Number: 01-073-2340) which corresponds to Zeolite-A. No additional peaks were identified arising from contaminants in the sample. All batches of Zeolite-A used in this study were characterised in this way and discarded if they showed any contamination.

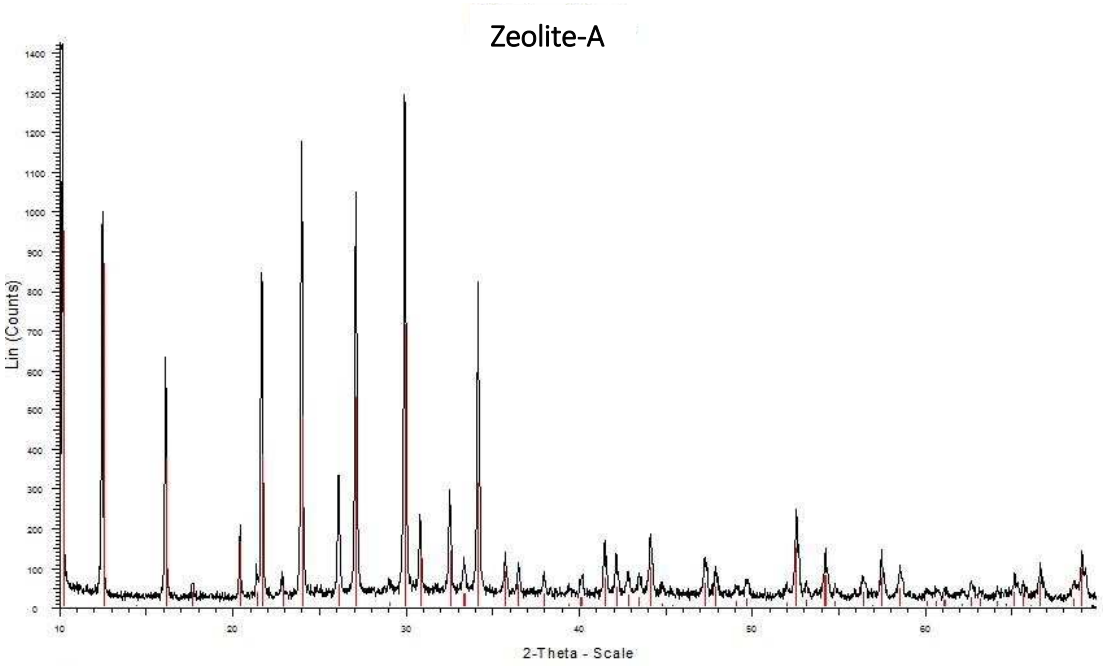

Figure 6.1 - XRD pattern of Zeolite-A and red peaks corresponding to Zeolite-A in database

Analysing the crystal particles using SEM (Figure 6.2a) clearly shows the cubic crystal morphology of Zeolite-A (space group Fm-3c). The particle sizes of the Zeolite-A cubes are approximately 620 nm in width. The EDX spectrum, Figure 6.2b, shows that the elements present in the Zeolite-A sample correspond with those in the molecular formula of Zeolite-A and that no contaminants were detected. Note that the carbon peaks arise from the carbon sticky tab used in the setup of the experiment.

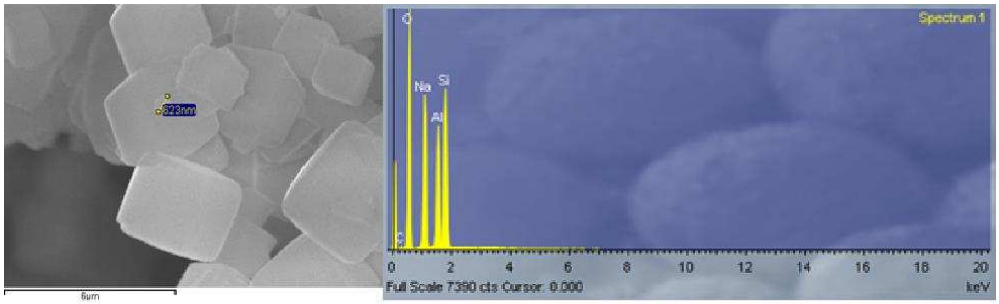

a) b)

Figure 6.2 - a) SEM Image of Zeolite-A as synthesised, b) EDX Spectrum of the sample

6.3.1 Ball milling of Zeolite-A

In an attempt to create a homogenous powder of smaller particle size, Zeolite-A was ball milled, using a Glen Creston Ltd. 8000M mixer/mill. The benefit of this would be that there would be a larger surface area capable of interacting with lead. The settings were to grind the samples for 30 minutes and then pause for 5 minutes. After 5 separate runs on settings of 8 repetitions, the number of repetitions was increased to 24 for three more attempts. SEM analysis showed the particles to be approximately 300nm and larger, but the size was not homogenous. It was not possible to achieve smaller particles with this method. Hence, no further analyses were undertaken with these samples.

6.3.2 Determining the solubility and pH dependence of Zeolite-A

It is known that the solubility of Zeolite-A is dependent on pH (Hartman & Fogler, 2007; Munthali et al., 2014). This is because a lower pH causes particles of Zeolite-A to dissolve, as it is soluble in acidic solutions. It was important to determine, regardless of soils, how the acid and purified water affected Zeolite-A.

To test the solubility, concentrated HNO_3 was used to control the pH of a Zeolite-A solution. Approximately 0.25 g of Zeolite-A was mixed with 15 ml of 0.25M HNO_3 as was used in the washing of soil. The solution had a pH of 1.40. The low pH of the acid was to mimic the effect of acid rain on already acidic soils, as detailed in Section 3.4.

It was found that a significant amount of zeolite dissolved immediately but with larger agglomerations staying solid. Over time and with stirring with a glass rod, the solution became clear to the naked eye. These results agree with previous studies that reported similar pH dependence for Zeolite-A (Chantiwas et al., 2000; Schwuger, 1997).

After observing the dissolving of Zeolite-A in 0.25M HNO_3, further testing was undertaken to analyse the pH dependency of Zeolite-A and its remediation capabilities for lead in the form of lead nitrate, $Pb(NO_3)_2$. This was conducted in order to have a hypothesis how Zeolite-A would act in an acidic environment, caused by acid rain and by the soils.

A series of solutions were made that covered the pH spectrum:

1. The blank sample was 0.1 g of $Pb(NO_3)_2$ mixed with 15 ml of deionised water. The pH of this solution was 3.54.
2. Approximately 1 g of Zeolite-A was added to 0.1 g of $Pb(NO_3)_2$ and 15 ml of deionised water.
3. Addition of Zeolite-A resulted in the samples having a pH of approximately 9.42. To this, either concentrated HNO_3 or NaOH was added, dropwise with a plastic pipette, until the desired pH was reached.
4. The solution of NaOH was made by taking 1.03 g of NaOH and mixing it with 10 ml of deionised water. This solution had a NaOH concentration of 2.58M and a pH of 13.12.

Table 6.1 displays the details of each sample. The name of each sample states the pH of the solution.

Table 6.1 - Zeolite-A as a remediation technique at varying pH

Sample Name	Mass of Zeolite-A (g)	Mass of $Pb(NO_3)_2$ (g)	Deionised Water (ml)	Drops of HNO_3/NaOH Added	Final pH	Mass of Solid Residue (g)
ZAPbBlank	0	0.103	15	0	3.54	0
ZAPbpH2	1.002	0.110	15	51 (HNO_3)	2.06	0.050
ZAPbpH4	1.004	0.109	15	9 (HNO_3)	3.99	0.837
ZAPbpH6	1.008	0.107	15	3 (HNO_3)	6.03	0.992
ZAPbpH8	1.004	0.104	15	1 (HNO_3)	7.79	0.930
ZAPbpH10	1.006	0.105	15	1 (NaOH)	10.24	0.971
ZAPbpH12	1.003	0.110	15	6 (NaOH)	12.13	0.955

Figure 6.3 shows the results of FAAS on the solutions. It is clear that Zeolite-A aids in confining lead to the solid residue when in a solution at a pH of greater than 4. It is less efficient at a lower pH. This could be due to the solubility of Zeolite-A at low pH. Above a pH of 4, the Zeolite-A is not dissolving and is interacting with the lead in a way that keeps the heavy metal in the solid residue. This implies that Zeolite-A is best used in conditions where the pH is higher than 4. In the current study, Soil 1 washed in water is at a pH below 4, and Soil 2 washed in water is above the pH of 4. This allows for a comparison of remediation with other minerals present. Whilst this study considered Zeolite-A mixed with lead nitrate at a range of pH values, this created a situation where no other compounds or minerals were present for the zeolite or lead to interact with, unlike in soil samples containing pyrite ash. As the pH decreased, there was not enough solid residue to perform further analysis, which would have given information regarding the amount of lead still present with the remaining zeolite structures. Hence, this will not be discussed in this project.

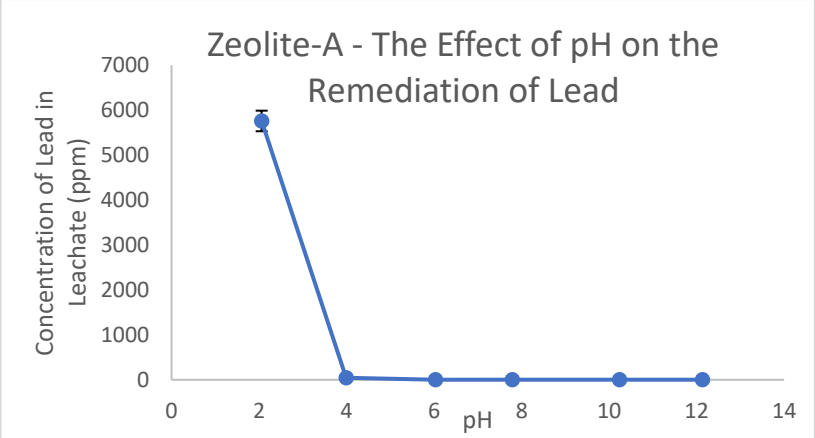

Figure 6.3 - Zeolite-A – The Effect of pH on the Remediation of Lead

6.4 Soil Classification

The grain size of the soils under analysis in this project were determined by using an XTL-101 series light microscope. The limitations of this apparatus include the low resolution and magnification. In addition, soils are often agglomerations of smaller particles which would be difficult to detect with these limiting factors. The general properties of the soils are summarised in Table 6.2 along with their British soil classification.

Table 6.2 - Soil classification according to British soil classification

Soil Sample	1	2
Appearance	Coarse, range of grain size, deep red/brown with yellow and white deposits	Fine particles. The majority of particles were small with some large grains, light brown.
Measured Grain Size (mm)	2-6	0.15-0.72
British Soil Classification	Fine Gravel	Fine, Medium, and Coarse Sand

Organic material and colloidal organic material can affect the interaction of soil with heavy metals. These materials have a high affinity for heavy metals and as a result, metal-organic complexes are formed (Christensen et al., 1996; Gounaris et al., 1993). This interaction affects the overall concentration of toxic heavy metals in the soil. If the organic material is soluble, then it can facilitate the mobility of heavy metals. Conversely, insoluble organic material would cause the heavy metals to be retained in the soil.

Both soils had 2% of their total weight accounted for by organic matter via direct measure of the Loss on Ignition (LoI), which was an analytical service conducted by the laboratory services company, LGC (Jeffrey, 2011). LoI calculates the percentage of organic matter in the soil based on the weight of the soil before putting it into a furnace to burn off the organic material, leaving only the minerals and the subsequent final weight. 2% of organic matter is understandable for sandy soils as the samples are well aerated, and organic matter decomposes at a fast rate. Due to the low amount of organic matter, it is easier for heavy metals to leach into groundwater as there is less possibility of organic material retaining the toxic substances.

6.5 Mineral Characterisation of Soil 1

The visual analysis of Soil 1 proposed that the grain size of the soil sample was in the region of millimetres (Table 6.2). Using SEM to obtain a higher magnification, Figure 6.7, it is evident that the grains consist of many smaller particles. However, the SEM was not capable of zooming in enough to determine if the individual particles were nanoparticles and the Malvern Zetasizer Nano ZS available in the department was not able to separate the agglomerated particles.

6.5.1 XRD of S1untreated, S1w and S1a

X-ray diffraction was used to produce a diffraction pattern. This pattern was collected and indexed using the EVA XRD software, which provides a database available through the Bruker package. By coupling the EVA database with XRF Omnian software, a list of plausible minerals was compiled, Table 6.3. This list was compared with the minerals detected in other studies that have been analysed in pyrite-rich soils. To display the XRD patterns, Panalytical software was used. The XRD pattern for S1untreated is displayed in Figure 6.4. It was matched with minerals that are very common in pyrite-rich soil.

Table 6.3 - Mineral components of S1untreated, S1w, and S1a identified using the EVA database by Bruker

S1untreated		S1w/S1a	
Chalcopyrite	$CuFeS_2$	Chalcopyrite	$CuFeS_2$
Copper Antimony Sulphide	Cu_3SbS_3	Copper Antimony Sulphide	Cu_3SbS_3
Cubanite	$CuFe_2S_3$	Cubanite	$CuFe_2S_3$
		Gismondine	$CaAl_2Si_2O_8 \cdot 4H_2O$
Hematite	α-Fe_2O_3	Hematite	α-Fe_2O_3
Illite	$K(Al,Fe)_2AlSi_3O_{10}(OH)_2 \cdot H_2O$	Illite	$K(Al,Fe)_2AlSi_3O_{10}(OH)_2 \cdot H_2O$
Koninckite	$FePO_4 \cdot 3H_2O$	Koninckite	$FePO_4 \cdot 3H_2O$
Lead silicate	Pb_3SiO_5		
Lead Sulphate	$PbSO_4$	Lead Sulphate	$PbSO_4$
Magnesium phosphate	MgP_4O_{11}	Magnesium phosphate	MgP_4O_{11}
Phosphoferrite	$(Fe,Mn)_3(H_2O)_3(PO_4)_2$	Phosphoferrite	$(Fe,Mn)_3(H_2O)_3(PO_4)_2$
Plumbojarosite	$PbFe_6(SO_4)_4(OH)_{12}$		
Pyrite	FeS_2	Pyrite	FeS_2
Quartz	SiO_2	Quartz	SiO_2
Segnitite	$PbFe_3(AsO_4)(AsO_3OH)(OH)_6$	Segnitite	$PbFe_3(AsO_4)(AsO_3OH)(OH)_6$
Sphalerite	ZnS	Sphalerite	ZnS

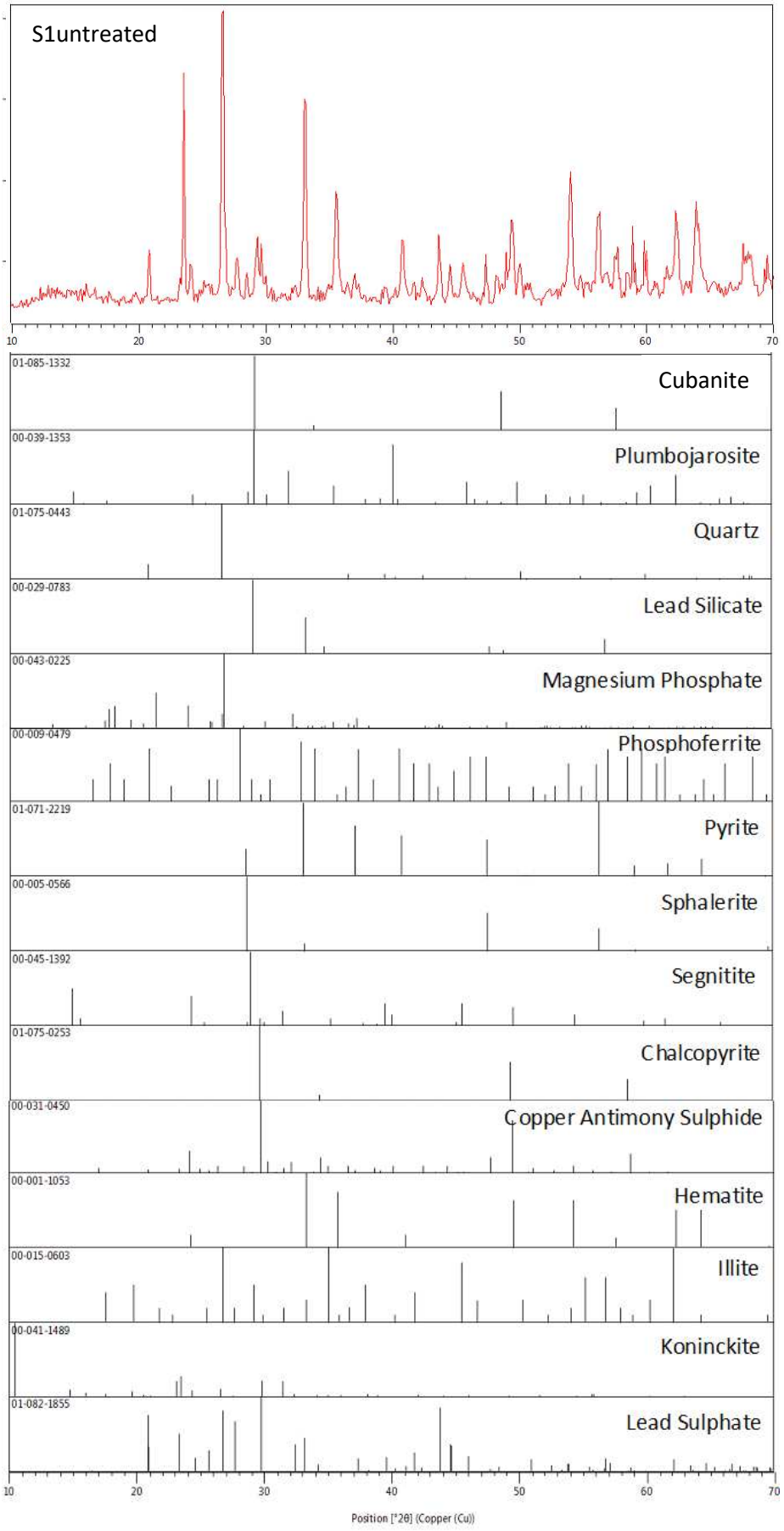

Figure 6.4 - XRD Pattern for S1untreated and corresponding minerals

Regarding Figure 6.4, the XRD pattern for S1untreated, it is clear that Soil 1 is a hematite-based soil, thus the most prominent peaks in the XRD pattern are due to this mineral. Hematite is a product of the roasting of pyrite, as shown in Chapter 3, Equation 3.1 (Oliveira et al., 2012). Quartz also makes up a large amount of the composition. This is unsurprising as quartz is one of the major minerals in the Earth's crust. In fact, it is the second most common mineral on Earth (Sandatlas, n.d.). Other common minerals in Soil 1 include segnitite and sphalerite. Segnitite is an arsenate analogue of kintoreite, that forms due to the oxidation of lead zinc sulphide ore (Birch et al., 1992). Sphalerite is a major ore of zinc and common in soil.

There were several copper-based compounds detected. Chalcopyrite is the most common of copper ores, copper antimony sulphide is known as 'skinnerite' and cubanite is a common copper mineral that is very similar to chalcopyrite (Alloway, 1995). Cubanite occurs in soils that have experienced high temperatures (mindat.org, 2016) in accordance with the processing method applied at the site.

Specific to Soil 1, plumbojarosite is a common secondary mineral found in soils that contain oxidised lead minerals. It is soluble and forms under acidic conditions. Pyrite is also detected due to the nature of the site. Soil 1 was taken from the location of the roasting furnace and, therefore, pyrite is expected in this area as it is one of the side products in the production the sulphuric acid. It is possible that pyrite and cubanite were both present in the original material roasted at the site.

Lead silicate and lead sulphate were identified. These are possible considering the high levels of lead detected by ICP-MS (Appendix 1). The following are minerals detected in the soil. Illite is a mineral containing an aluminosilicate that is present in a wide variety of environments and common in sediments and clays. It can be formed by weathering or hydrothermal alteration (mindat.org, 2016). Koninckite is a hydrated iron phosphate. Magnesium phosphate needs an acidic environment for its formation (Stachel et al., 1992). Phosphoferrite can be found with iron, manganese, or a mixture of the two metals in its formula. It forms

from hydrothermal alteration of graftonite, $(Fe^{2+}, Mn, Ca)_3(PO_4)_2$, in silicate structures (Nriagu & Moore, 1984).

The main difference in the XRD patterns of the untreated soil compared to the acid-washed soil, Figure 6.5, is the potential appearance of gismondine in the latter. The XRD pattern for S1w is not detailed as it has identical minerals detected as those in S1a and is therefore included in Appendix 4.

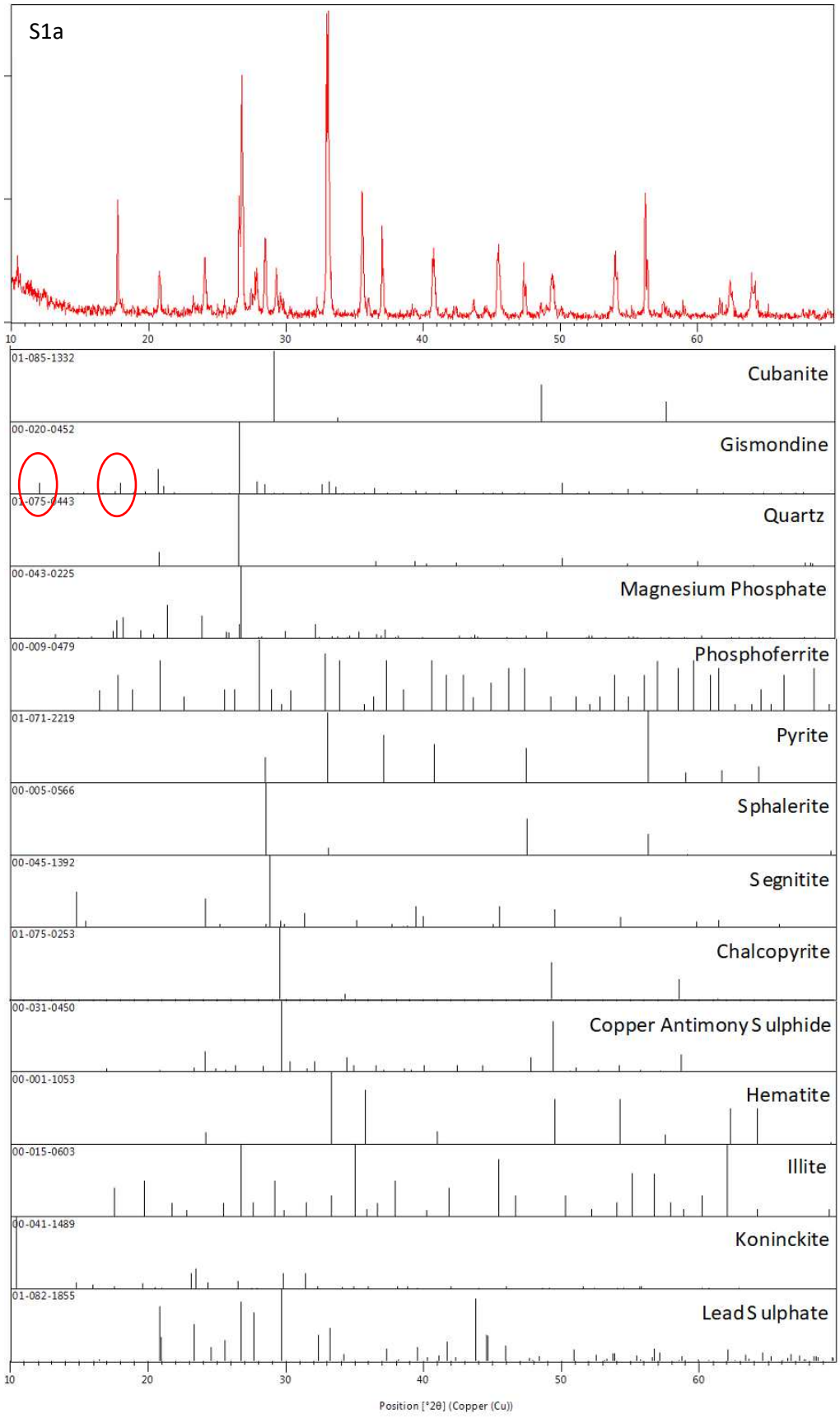

Figure 6.5 - XRD Pattern for S1a and corresponding minerals

The XRD pattern representing the washed soils, Figure 6.5, indicate that lead silicate and plumbojarosite disappear and a secondary mineral is formed, possibly gismondine. This formation of gismondine could be understood if the Ca^{2+} and Al^{3+} ions in the generally reported formula for gismondine are replaced by Pb^{2+} and Fe^{3+} according to the unbalanced Equation 6.1.

$$Pb_3SiO_5 + PbFe_6(SO_4)_4(OH)_{12} + H_2O \text{ (in excess)} \rightarrow PbFe_2Si_2O_8{\cdot}4H_2O \qquad (6.1)$$

The secondary mineral is detected in both washed soils, S1w and S1a. The hypothesis in this study is that the mineral is gismondine. The red circles show that there are several peaks that do not align completely with the soil pattern when using the typical Ca-gismondine data. A more in-depth view of this is seen in Figure 6.6. This shows the pattern for S1a with the red peaks for gismondine overlaid. The arrows in blue show slight shifts that do not perfectly align with the soil pattern. The arrow pointing at around 18° 2θ does align with the shoulder of the soil peak, but not with the main peak, and it has a high intensity. The pattern for S1w showed the same peaks not aligning, therefore, it is in Appendix 4.

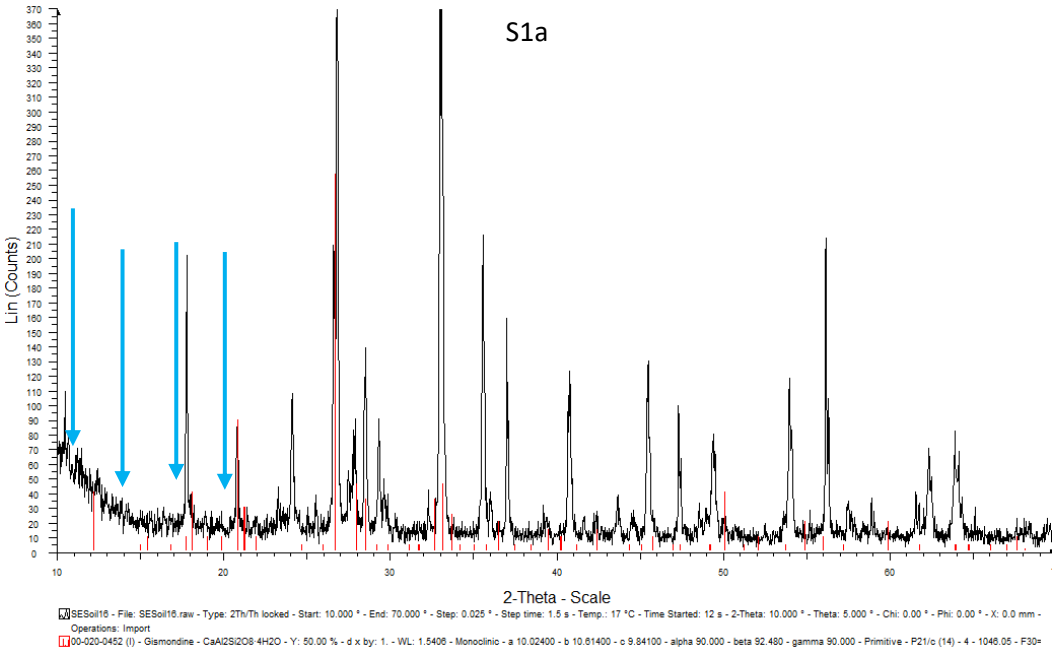

Figure 6.6 - XRD Pattern of S1a with gismondine peaks overlaid in red

A possible explanation for the shift of the peaks could be due to the structure of zeolites. It has been found that the framework of zeolites can be influenced by subtle changes which then affect the observed intensities and symmetry (van

Koningsveld & Bennett, 1999). Possible changes include when non-framework species are disordered or there is an isomorphous replacement of framework atoms. Depending on how lead interacts with the zeolite, either or both of these issues could be causing a shift in the XRD pattern. Importantly, it is known that the gismondine-type framework arrangement (GIS) is extremely flexible and is classified as a collapsible framework. Oxygen atoms acting as flexible hinges and the angles around the oxide tetrahedra can co-rotate which causes non-framework species to be wrapped around the tetrahedra or a collapse is caused, resulting in the formation of the smallest angle of the oxygen hinges (Baur, 1992; Baur, 1995). Therefore, changing of either framework or non-framework atoms causes structural changes. In particular, powder XRD is complicated when cell dimension and symmetry changes occur, resulting in similar arrangements with new atoms not being recognised. Using lead specifically, it was found that after exchange into Zeolite-A, a zeolite known to have a non-collapsible framework, the result was a distortion of each sodalite cage. Consequently, it is hypothesised in the current study, that gismondine would almost certainly experience distortion upon exchange with lead ions, leading to a change in framework, thus causing XRD patterns to alter slightly from the standard Ca-gismondine pattern.

It has been proposed by Braithwaite and collaborators that gismondine can form easily under mild hydrothermal conditions (Braithwaite et al., 2001). As evidence for their statement, they refer to 'Zeolite MAP' (Na-Gismondine) commercially used as a water softener in, for example, washing powders (Adams et al., 1997). Braithwaite et al studied the formation of barium-rich gismondine in lead smelting slags and reported that the dissolved Ba ions would interact with silicates from the slag in the water-rich weathering conditions, forming gismondine. This can be further justified by a study in which it was demonstrated that barium ions are more stable than sodium ions in gismondine, which are easily exchanged (Allen et al., 2002). As the pyrite waste analysed in the current study shows a very low barium ion concentration, it can be proposed that Pb^{2+}, with a similar charge and ionic radii to Ba^{2+}, could form Pb-gismondine as the conditions are similar to those described.

6.5.2 Microscopy of Soil 1 – Zooming

Figure 6.7a shows a scale of 1 mm, where there are large particles of the soil that are visible to the naked eye. The area marked by a blue circle is analysed further at a five times higher magnification (200 µm). Figure 6.7b shows that the area is a clustering of smaller particles. The orange area was selected for 100 times larger magnification (Figure 6.7c) than the original figure. There are still significantly smaller particles present that appear to be agglomerations of particles. However, it was not possible to use higher magnification as there was significant sample charging rendering the images unclear.

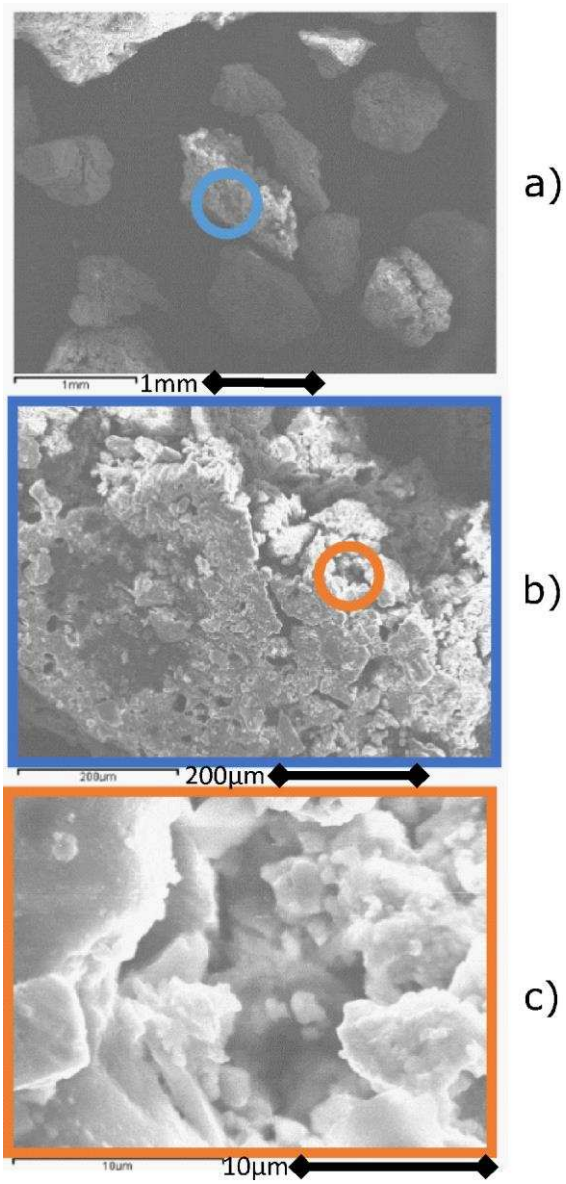

Figure 6.7 – a) SEM image showing S1untreated, b) image of blue circle in (a) enlarged, and c) image of orange circle in (b) enlarged

6.5.3 SEM-EDX of S1untreated – Soil 1 after drying and sifting

The SEM coupled with EDX can be used to determine the elemental composition of the samples. Figure 6.8a shows an SEM image of S1untreated after drying and sifting as described in Section 5.5. Multiple samples and sites were analysed and results obtained. These images, spectra, and maps are not included as they are superfluous and match the provided data.

It is important to note that due to the carbon sticky tab used, carbon will be detected regardless of whether it is present in the actual sample. The brighter areas on the map denote a higher concentration of the element being analysed in that particular area.

The area analysed, indicated by the red arrow in Figure 6.8a, was a crude cube-like structure that appeared to be a single compound rather than a cluster of particles. The resulting EDX spectrum, Figure 6.8b shows that the elements present are lead, iron, and sulphur, suggesting the area could be plumbojarosite or lead sulphate.

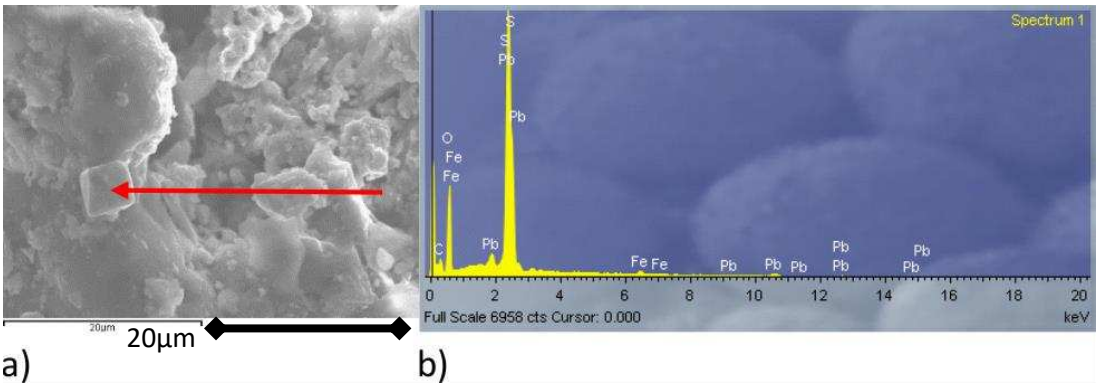

Figure 6.8 - a) SEM image showing S1untreated and b) EDX spectrum corresponding to the point marked with a red arrow

An alternative area of Soil 1, composed of several particles that are each made up of many agglomerations of smaller particles, was also analysed, Figure 6.9a. The EDX sum spectrum, Figure 6.9b, shows a wide range of elements present. It is important to note that there are some elements shown in the spectrum that may not be present in large quantities, but have overlapping keV values with other more intense peaks. This mostly occurs towards the lower end of the range, between 0 and 2 keV.

From the elemental map of the area, Figure 6.9c, it can be determined that there is sulphur present, probably due to pyrite, FeS_2, which is plentiful in Soil 1. Arsenic and lead seem to be following each other and appear nearly identical. The blue circles represent a correlation between oxygen, silicon and iron. This could indicate a piece of quartz and iron oxide. The orange circles show a region that is showing a rather concentrated area of arsenic and lead as well as all of the other elements that were mapped. The areas indicated by green circles are associated with lead, arsenic, iron and oxygen.

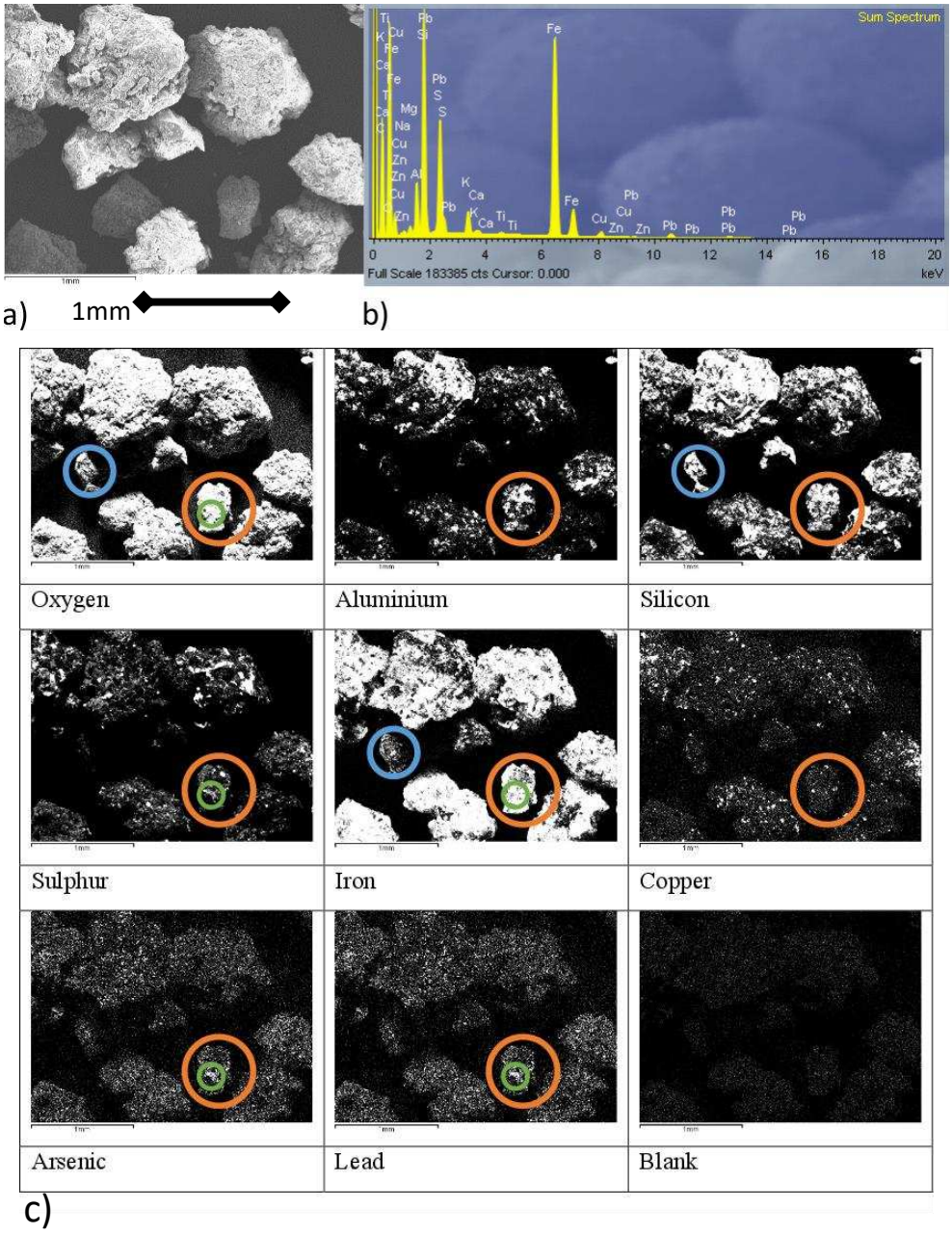

Figure 6.9 – a) SEM map area image showing S1untreated, b) Corresponding EDX sum spectrum, and c) Corresponding EDX element map

6.5.4 SEM-EDX of S1w – Soil 1 washed in deionised water

When washing Soil 1 with deionised water, the EDX spectrum changes, Figure 6.10b. The peaks for silicon and sulphur have decreased. In addition, the peaks for copper and zinc are gone entirely. It is now possible to see peaks for arsenic. This could be due to the fact that a small amount of sample is being analysed, indicated by the arrow in Figure 6.10a, and, therefore, this area may not be representative of the entire sample and these missing elements may still be present in the overall sample. It is important to evaluate the maps as well, which analyse a larger area.

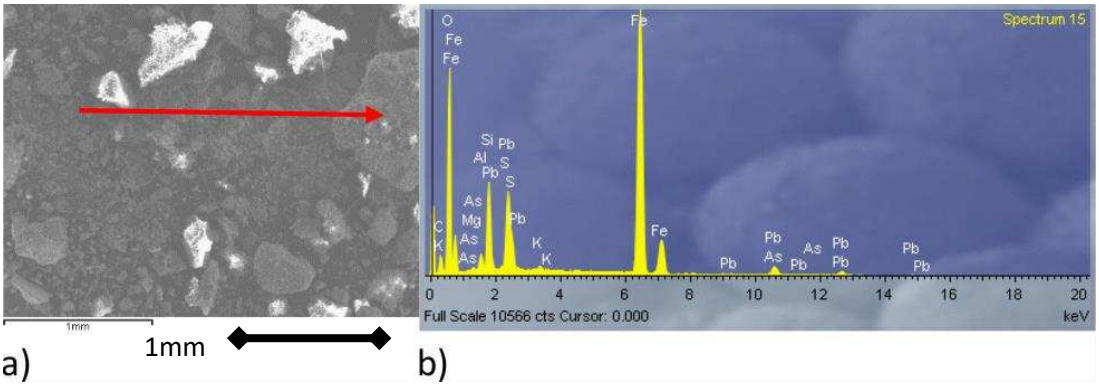

Figure 6.10 - a) SEM image showing S1w and b) EDX spectrum corresponding to the point marked with a red arrow

Figure 6.11b, the EDX spectrum of another area of S1w, shows that copper is still present. The element map, Figure 6.11c, shows that copper clearly follows sulphur and iron, shown by the orange circles. This could indicate a piece of cubanite.

The presence of iron seems to be inversely related to that of silicon whilst iron and oxygen show a positive correlation, forming iron oxides as highlighted with the blue circles. Aluminium is very difficult to detect and the amounts of lead and arsenic are negligible. The bright areas are only slightly brighter than in the blank. The green circles show a large piece of quartz. The concentrated areas of lead and arsenic are denoted by the yellow circles and red arrows. The only other elements in the map that are present in this area are iron and oxygen.

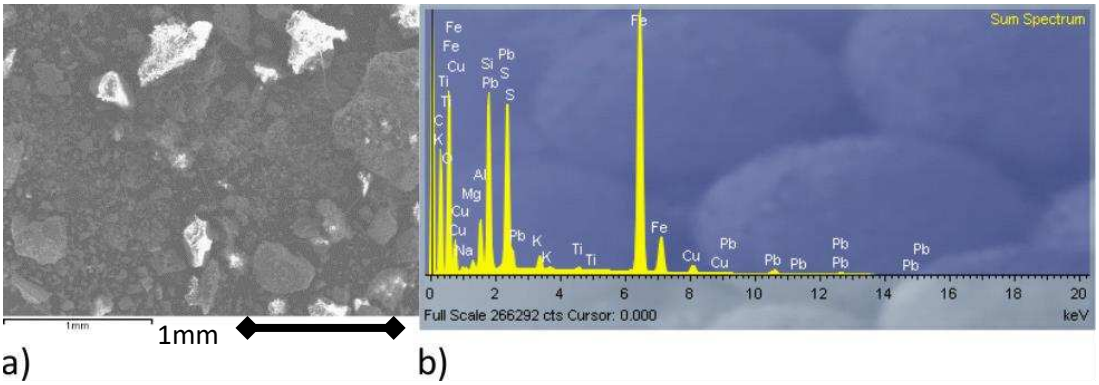

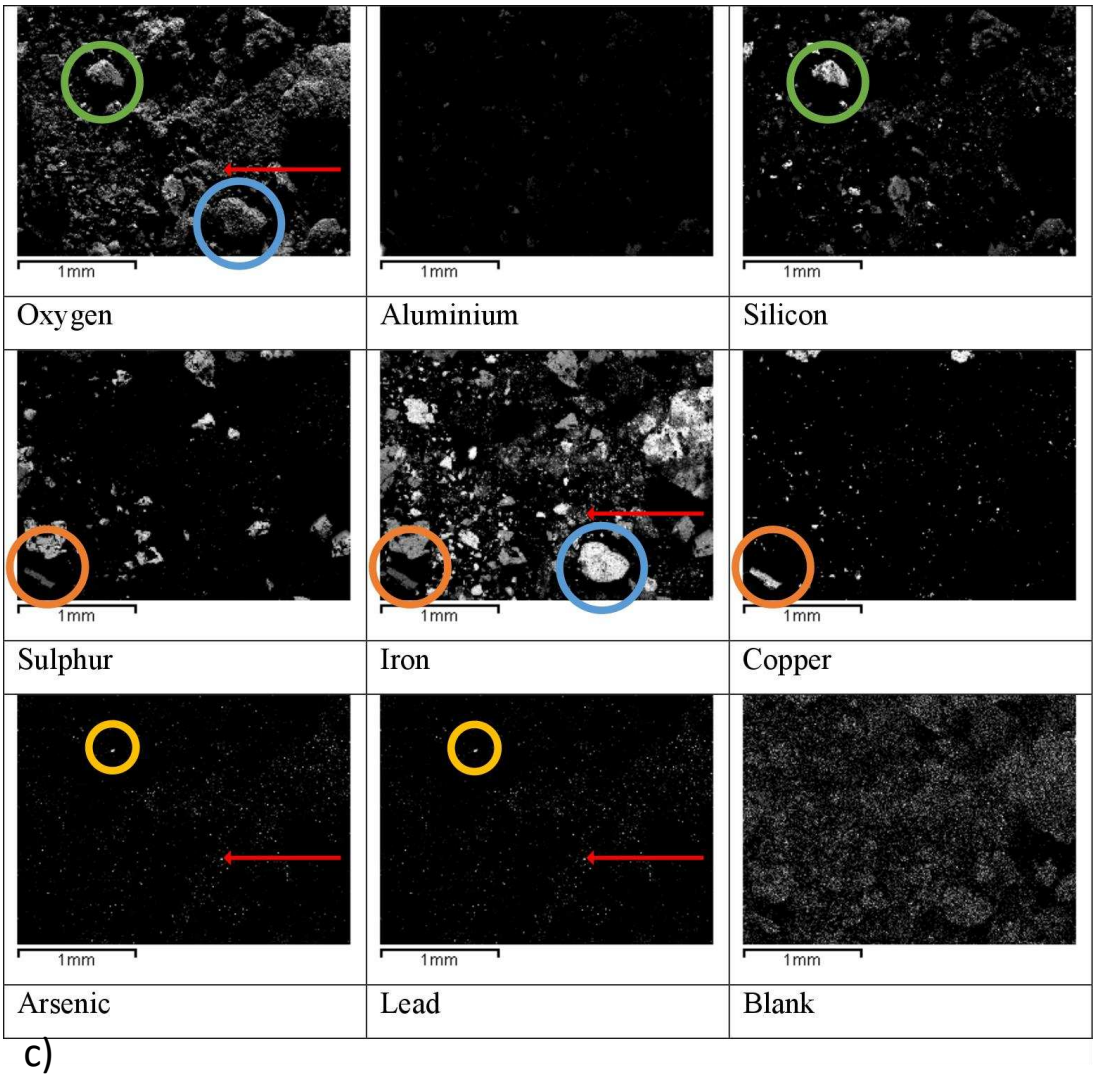

Figure 6.11 – a) SEM map area image showing S1w, b) Corresponding EDX sum spectrum, and c) Corresponding EDX element map

6.5.5 SEM-EDX of S1a – Soil 1 washed in 0.25M HNO_3

The point-analysis in Figure 6.12a shows the particles are not of homogenous size and some are clearly agglomerations of smaller particles, whilst others seem to be singular structures. The spectrum, Figure 6.12b, appears quite simple. Lead is still present, forming the most abundant peak, with iron represented by a smaller peak.

This is probably due to the point-placement of the analysis. Copper is seen to be detected again.

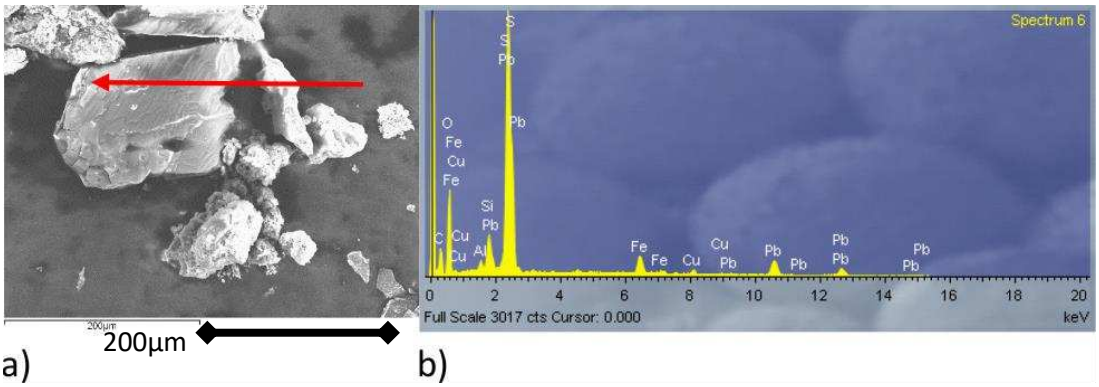

Figure 6.12 - a) SEM image showing S1a and b) EDX spectrum corresponding to the point marked with a red arrow

Figure 6.13c, the EDX element map of a subsequent area, is extremely blurry, caused by the particles charging during analysis. The sum spectrum, Figure 6.13b, agrees with the previous point-analysis and includes peaks for iron and lead. It differs from the previous spectrum of S1a by showing a higher intensity peak for iron and includes peaks for magnesium. Although the map is extremely blurred, it is still possible to see that lead and arsenic are present but now in larger, specific areas, rather than evenly dispersed.

The blue and orange circles show a positive correlation between arsenic, lead, sulphur and copper. There is a distinct dark area in the map of iron, in the same location as the blue circles, denoted by a red circle, demonstrating the absence of this element.

Analysing the original scan, there are areas of material that are obviously different in structure to the smooth area around and underneath the clusters. It is not possible to determine explicitly if lead and arsenic are bonded to both sulphur and copper or if there are two different minerals that have overlapping bright areas on the map.

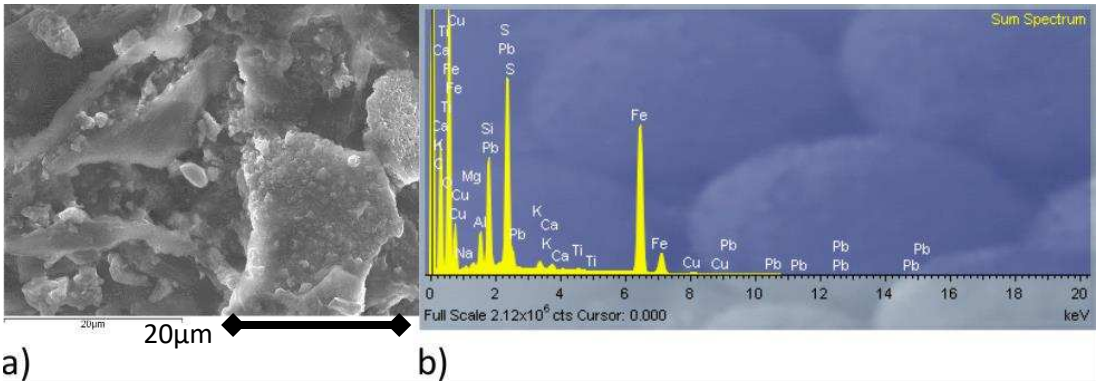

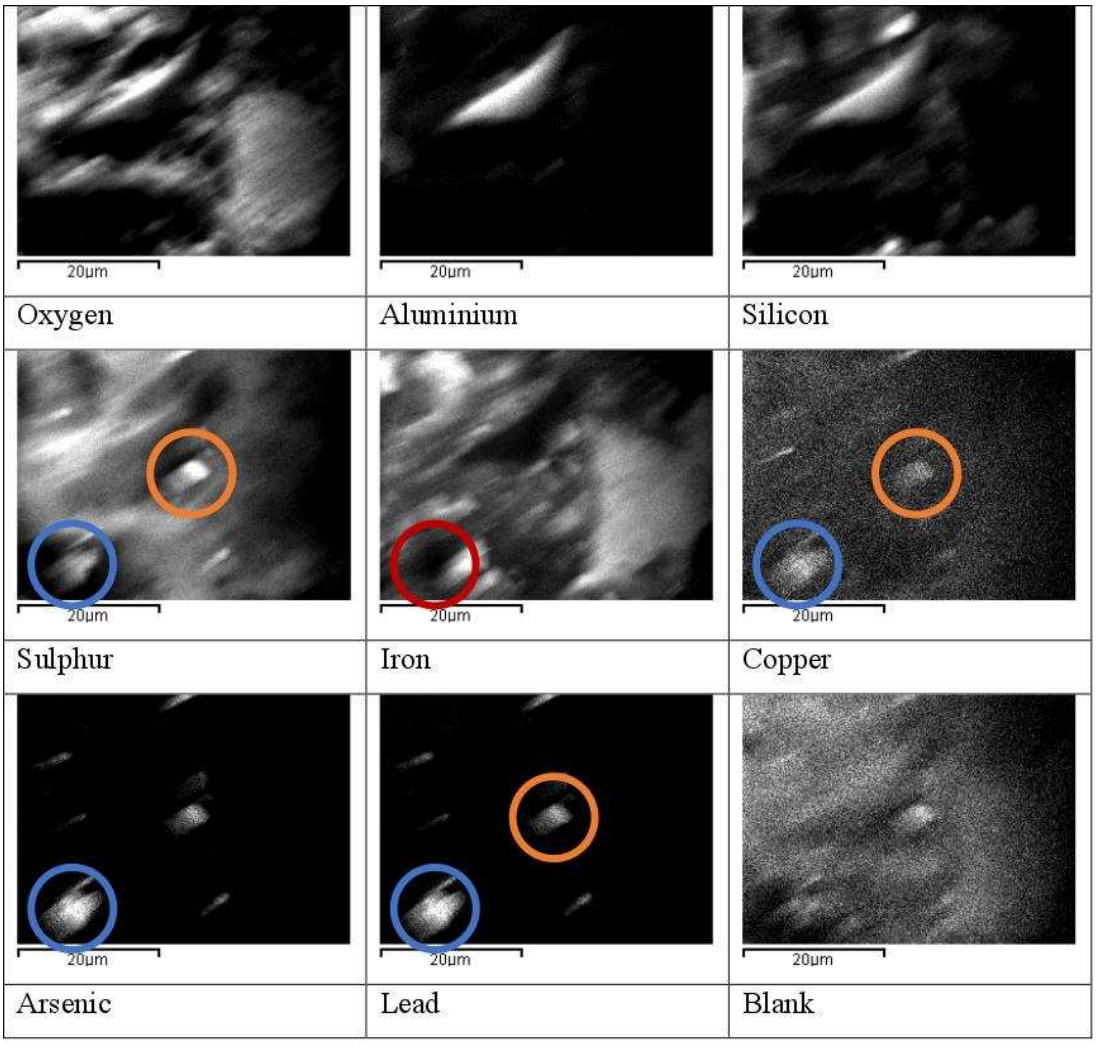

Figure 6.13 – a) SEM map area image showing S1a, b) Corresponding EDX sum spectrum, and c) Corresponding EDX element map

6.5.6 XRF Analysis of S1untreated with S1w and S1a

The Omnian XRF software allows the user to identify the amount of the individual elements based on sample origin, for example, oxides, minerals etc. In this study, the percentage of relative amounts of elements in the sample were

based on mineral components. By determining the elemental composition of the soil before and after washing, it is also possible to determine the mineral components of the soils and the effect that the washing had on each sample.

The XRF data of elements present over 0.9%. The reason for the percentage shown is explained in Section 4.5.3. Table 6.4, shows the same elements for S1w and S1a. It is important to remember that each sample is from a different selection of soil, explaining the reason for the slight changes in elemental compositions. However, both S1w and S1a differ from the untreated soil by phosphorus falling from nearly 6% to below the detection limit. Phosphorus was present in the minerals detected with XRD. Therefore, it is likely that the phosphate compounds are only present in small quantities.

Table 6.4 - XRF elemental composition above 0.9% for S1untreated, S1w, and S1a

S1untreated		S1w		S1a	
Element	Percentage (%)	Element	Percentage (%)	Element	Percentage (%)
Fe	54.95	Fe	57.72	Fe	60.08
S	12.77	Si	16.21	Si	14.87
Si	10.10	S	11.50	S	12.19
K	6.25	Al	4.64	Al	3.67
P	5.97	Pb	2.83	Pb	2.80
Cu	2.86	Cu	2.38	Cu	2.64
Al	2.70	K	1.76	K	1.37
Pb	1.85	P	< det limit	P	< det limit

6.6 Mineral Characterisation of Soil 2

The same analyses were carried out on samples involving Soil 2 in an effort to determine the different minerals present and how this affects the soil chemical properties prior to remediation treatment.

6.6.1 XRD of S2untreated, S2w and S2a

As with Soil 1, the XRD measurements were undertaken on the untreated Soil 2 (Figure 6.14). The matched minerals are given in Table 6.5.

Table 6.5 - Mineral components of S2untreated, S2w, and S2a identified using the EVA database by Bruker

S2untreated		S2w/S2a	
Albite	$K_{0.2}Na_{0.8}AlSi_3O_8$	Albite	$K_{0.2}Na_{0.8}AlSi_3O_8$
Chalcopyrite	$CuFeS_2$	Chalcopyrite	$CuFeS_2$
Copper Antimony Sulphide	Cu_3SbS_3	Copper Antimony Sulphide	Cu_3SbS_3
		Gismondine	$CaAl_2Si_2O_8{\cdot}4H_2O$
Hematite	α-Fe_2O_3	Hematite	α-Fe_2O_3
Illite	$K(Al,Fe)_2AlSi_3O_{10}(OH)_2{\cdot}H_2O$	Illite	$K(Al,Fe)_2AlSi_3O_{10}(OH)_2{\cdot}H_2O$
Koninckite	$FePO_4{\cdot}3H_2O$	Koninckite	$FePO_4{\cdot}3H_2O$
Lead silicate	Pb_3SiO_5		
Lead Sulphate	$PbSO_4$	Lead Sulphate	$PbSO_4$
Quartz	SiO_2	Quartz	SiO_2
Segnitite	$PbFe_3(AsO_4)(AsO_3OH)(OH)_6$	Segnitite	$PbFe_3(AsO_4)(AsO_3OH)(OH)_6$

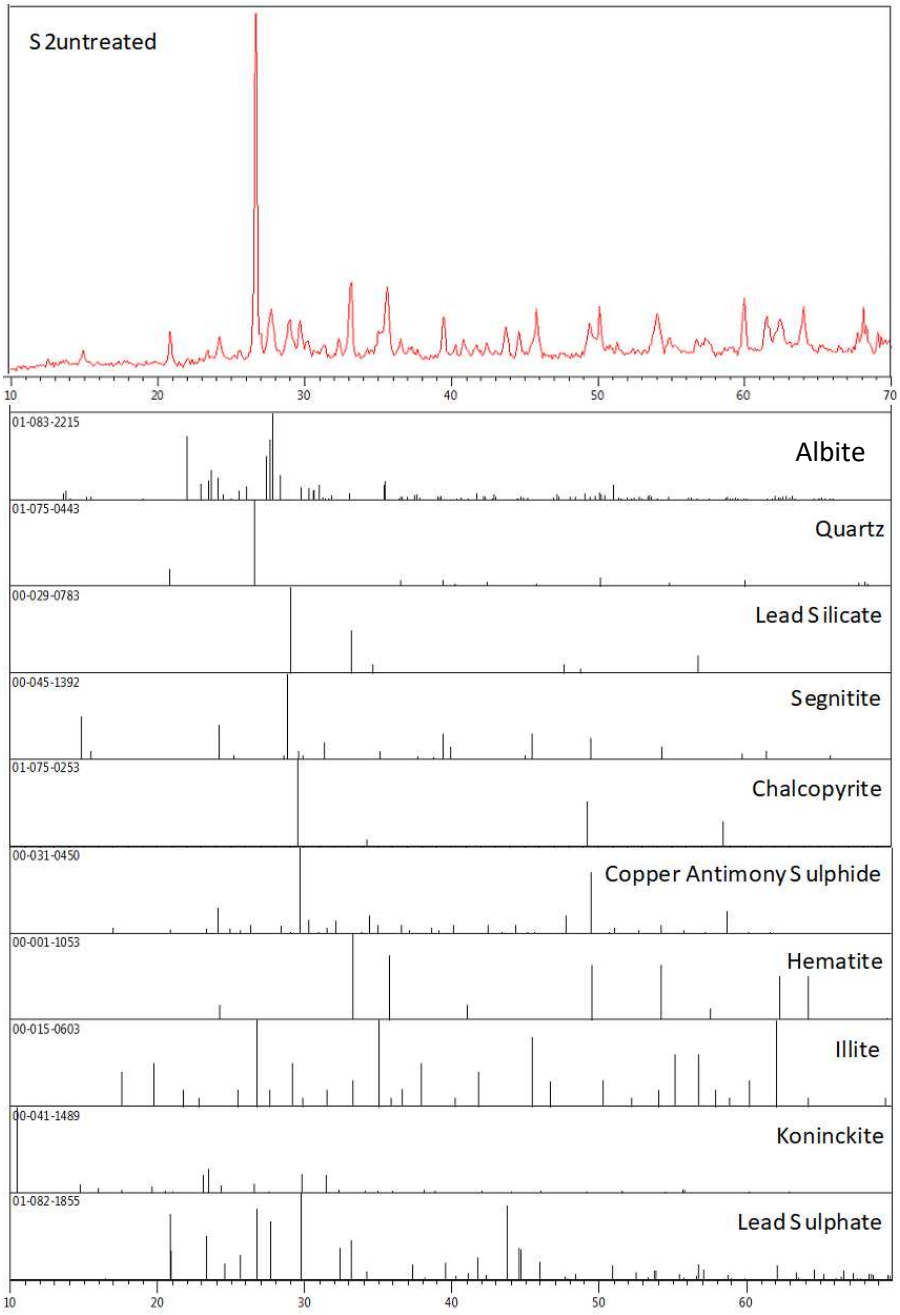

Figure 6.14 - XRD Pattern for S2untreated and corresponding minerals

As with Soil 1, Soil 2 is also a hematite-based soil with many of the same minerals present. Uniquely for Soil 2, there is no plumbojarosite or pyrite, instead albite is detected. The formula of albite is that reported on the PDF card (01-083-2215) and detected using the software. It is not the conventional formula for albite, usually found without potassium.

The pattern for S2a, Figure 6.15 showed identical mineral compositions to S2w (Appendix 4). Lead silicate is not present in the washed soils and the XRD patterns for S2a matched approximately, as they did with Soil 1, with gismondine.

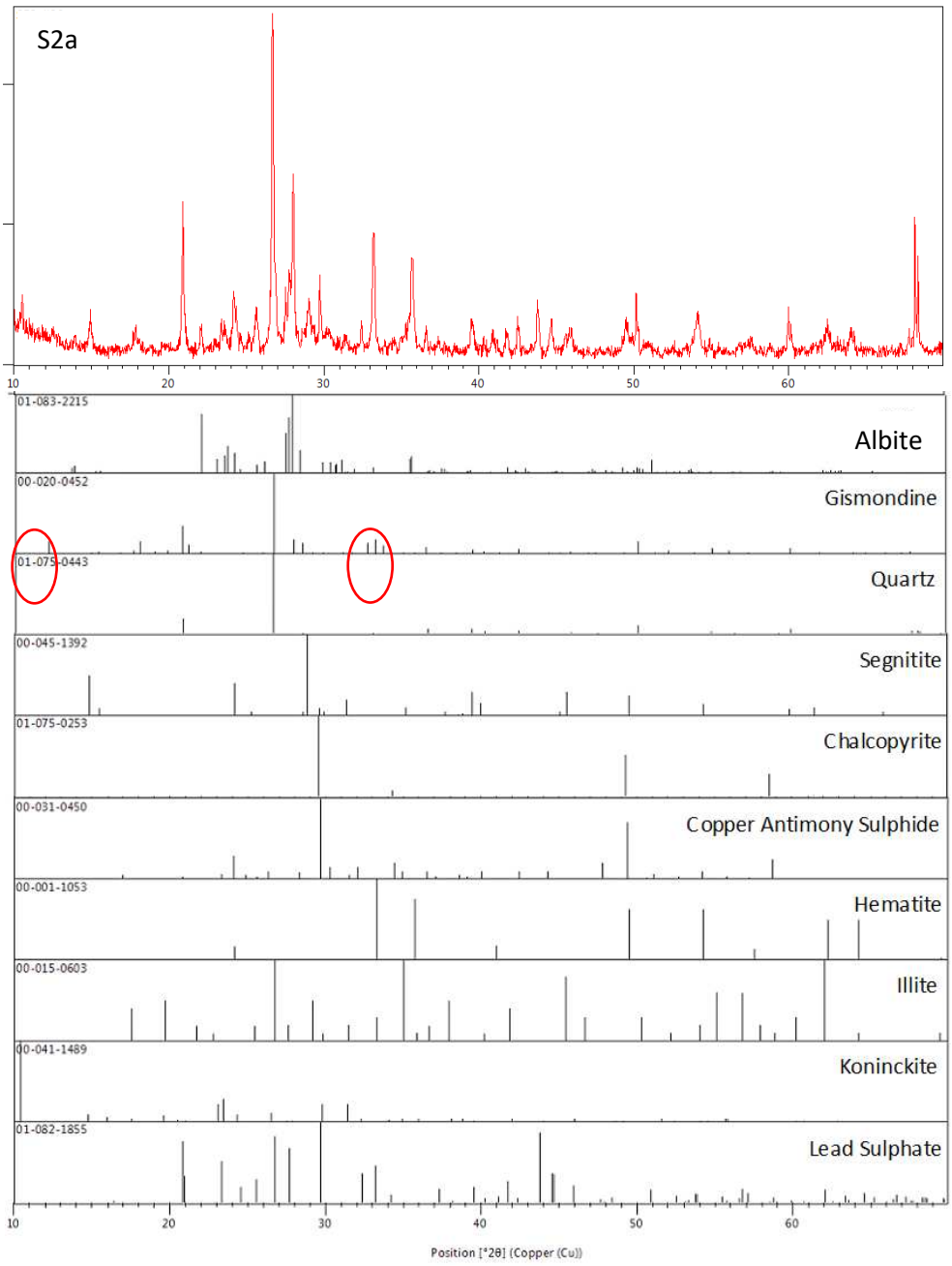

Figure 6.15 - XRD Pattern for S2a and corresponding minerals

In an attempt to make clear the similarity between the matching of gismondine in Soil 1 washed samples with Soil 2 washed samples, another matched XRD pattern is given in Figure 6.16. It shows that there are deviations in the matching at the same four places as before with Soil 1, which would be the expected result if framework changes have occurred due to the exchange with lead ions. The equivalent figure for S2w is in Appendix 4.

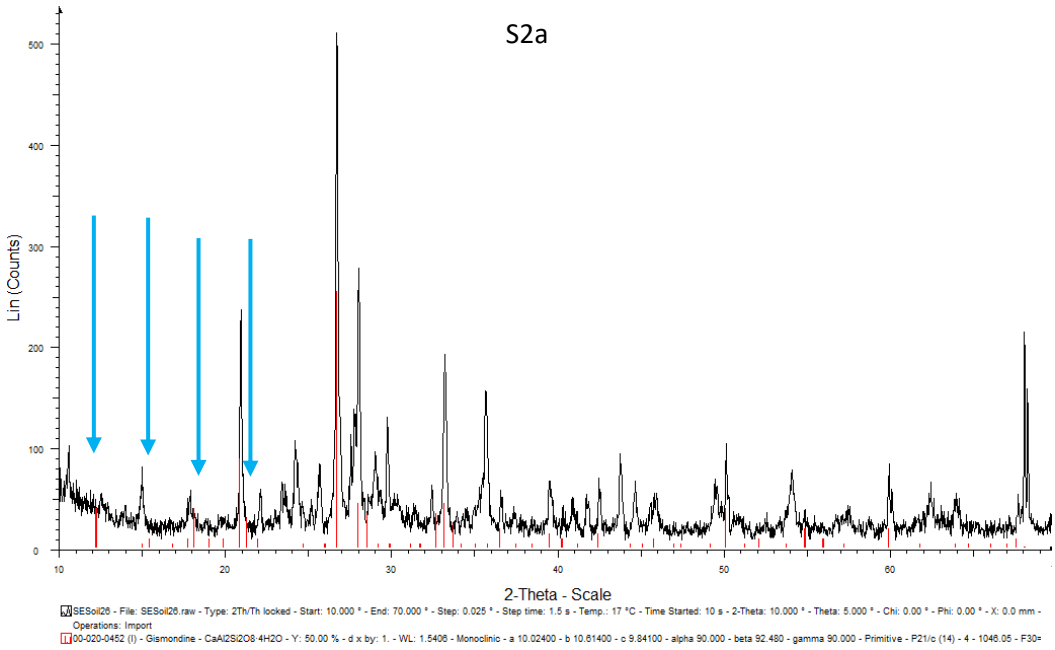

Figure 6.16 - XRD pattern for S2awith gismondine peaks overlaid in red

6.6.2 SEM-EDX of S2untreated – Soil 2 after drying and sifting

Figure 6.17a shows a clustering of particles and it is important to note the appearance of arsenic in the corresponding spectrum, Figure 6.17b. Arsenic shares similar keV values with lead for values around 10 keV. This can act in a detrimental way, hiding the lead peaks and only showing a positive result for arsenic (Olympus Corporation, n.d.). However, it is possible to determine that this is not a 'false positive' result because of the strong peaks for arsenic around 1.5 keV, which do not include lead. This gives proof that arsenic is being detected, as well as lead, in high quantities. Sulphur is still detected, as is aluminium and iron.

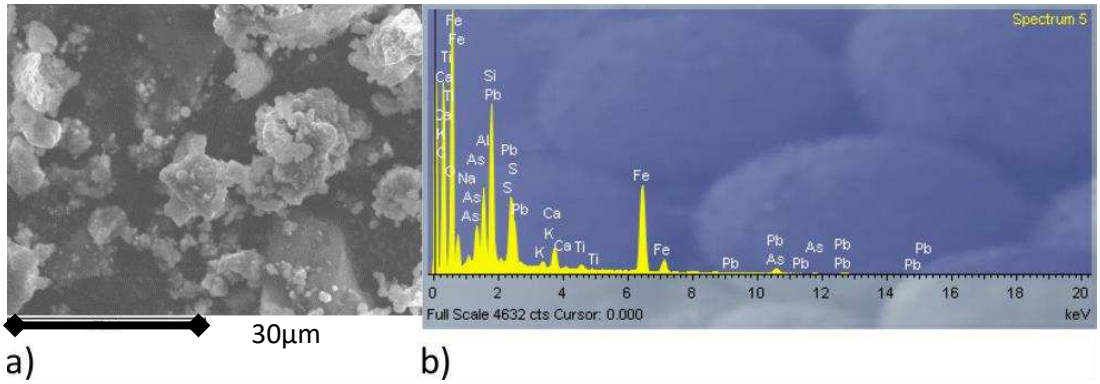

Figure 6.17 - a) SEM image showing S2untreated and b) Corresponding EDX Spectrum

Figure 6.18c shows the EDX elemental maps of S2untreated, suggesting copper was not detected in high amounts in the mapping area and, therefore, not automatically selected in the map by the software, which only detects the most plentiful elements. Copper is, however, shown on the sum spectrum, Figure 6.18b, overlapping with zinc. This is due to similar keV values; 8.046 for copper, and 8.637 for zinc. Therefore, it is possible that there is only copper, and the detection of zinc is not accurate.

The map confirms that although sulphur is present in Soil 2, it is in far lower quantity and concentration than in Soil 1. This is due to the nature of the industrial site. The purpose of the industry was to oxidise the sulphur in pyrite into sulphuric acid, H_2SO_4. Therefore, the majority of sulphur would have been oxidised when the pyrite ash was dumped at Site 2.

The blue areas are found to be extremely concentrated in lead and arsenic, as well as iron and oxygen. This is probably due to segnitite. Aluminium oxide is shown clearly with the orange circle. Lead is again following arsenic, and it appears that they are more concentrated in some areas, i.e. not homogeneously distributed within the soil. Iron seems to be spread evenly throughout the sample area and followed by arsenic and lead, but with higher concentrations in different areas. An aluminium silicate is denoted by the yellow circles.

It is important to note that there are 'shadows' in the sample, caused by the direction of light hitting the particles which results in 'black-out zones' where 'nothing' is detected because the beam could not reach those areas of sample.

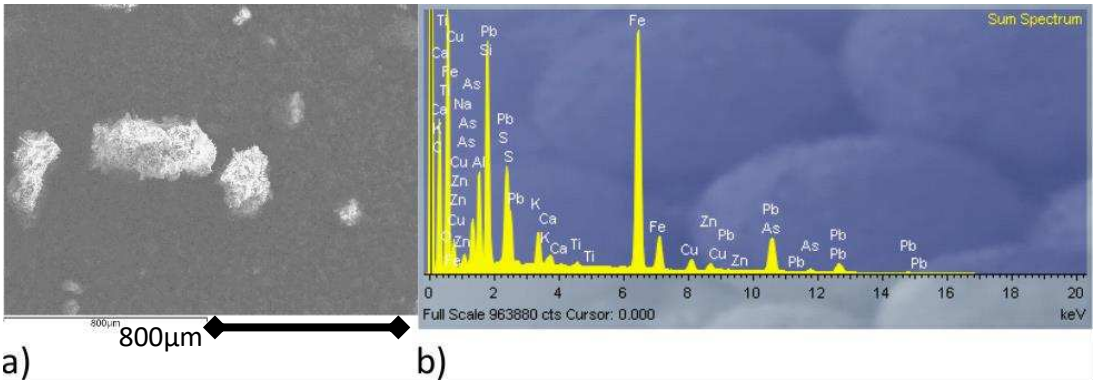

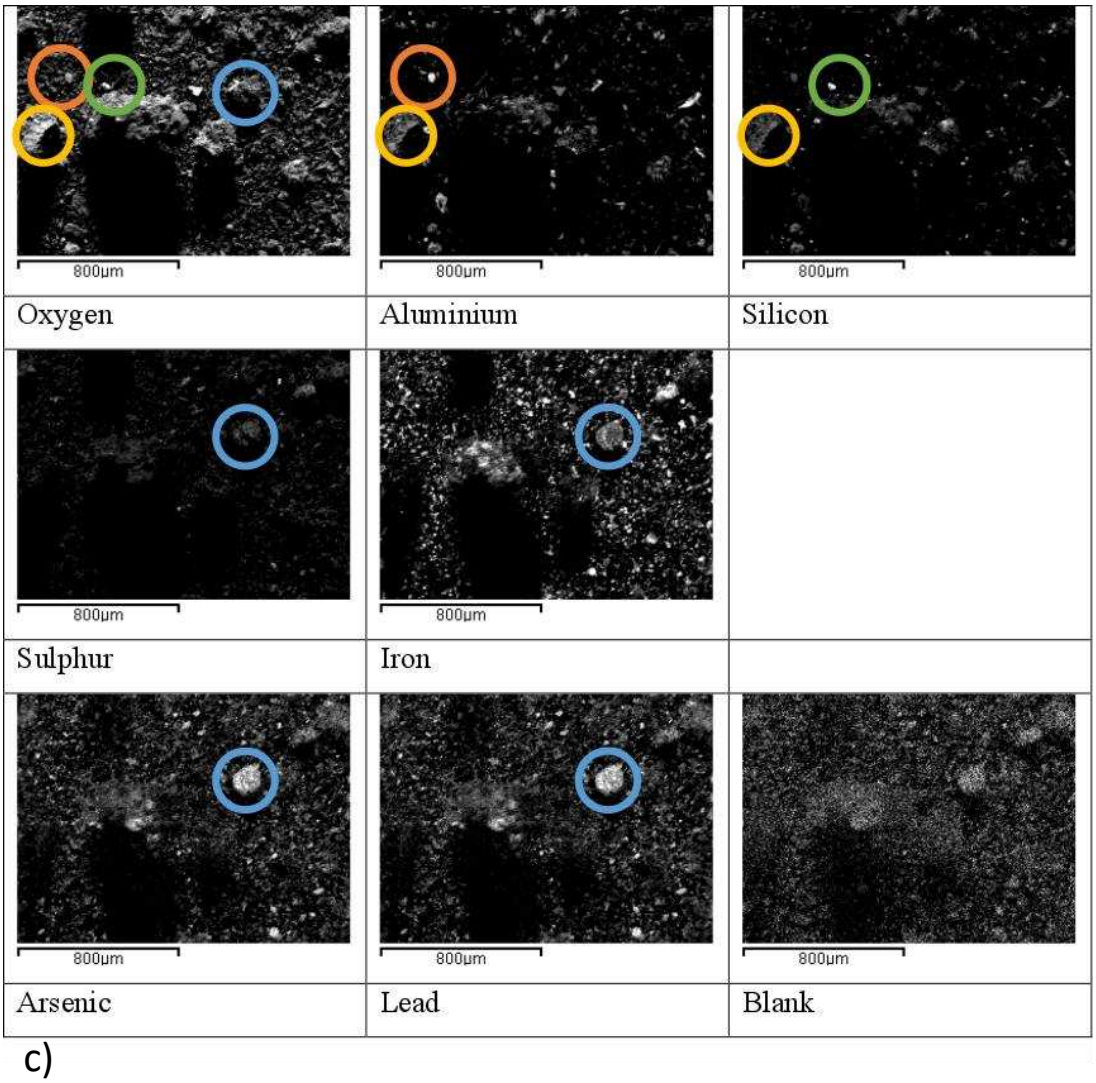

Figure 6.18 – a) SEM map area image showing S2untreated, b) Corresponding EDX sum spectrum, and c) Corresponding EDX element map

6.6.3 SEM-EDX of S2w – Soil 2 washed with deionised water

The point-analysis of this material, Figure 6.19a, provides an elemental spectrum, Figure 6.19b that is nearly identical to the overall sum spectrum

obtained from the mapping, Figure 6.19b. This suggests that lead and arsenic are dispersed throughout the soil in a homogeneous manner.

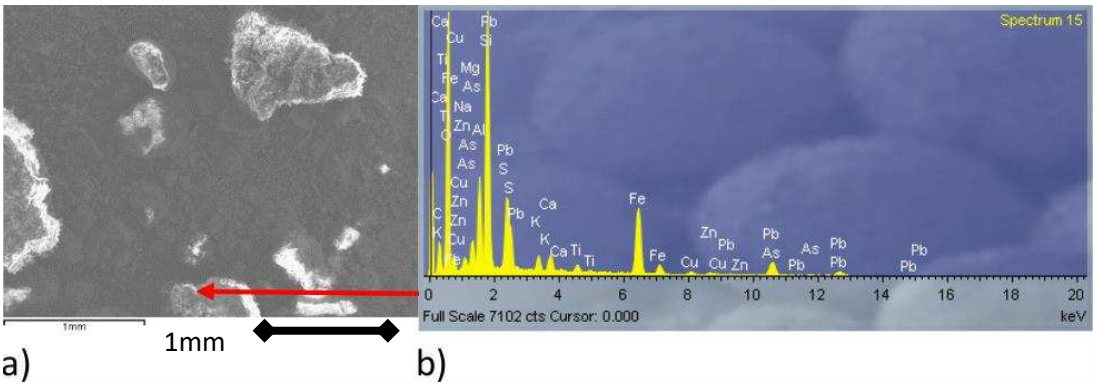

Figure 6.19 - a) SEM image showing S2w and b) EDX spectrum corresponding to the point marked with a red arrow

From the elemental map, Figure 6.20c, it can be seen that lead and arsenic are again present in quantities similar to the blank and, therefore, are not high in concentration. They do register on the sum spectrum, Figure 6.20b, and the element map shows that several areas contain slightly higher concentration of the two heavy metals analysed. These areas are marked with orange circles. They do not match the other elements, although their low concentration makes this difficult to determine definitively. The green circles show a piece of iron oxide, whilst the blue circles show quartz. This is not an aluminosilicate structure as there is an absence of aluminium at this location, highlighted by the red circle. Instead, the yellow circles indicate a large area with aluminium silicate, which could be indicative of gismondine. The pink circles show a positive correlation between lead, arsenic, silicon, aluminium, and oxygen. This could be due to lead interacting with gismondine, forming Pb-gismondine.

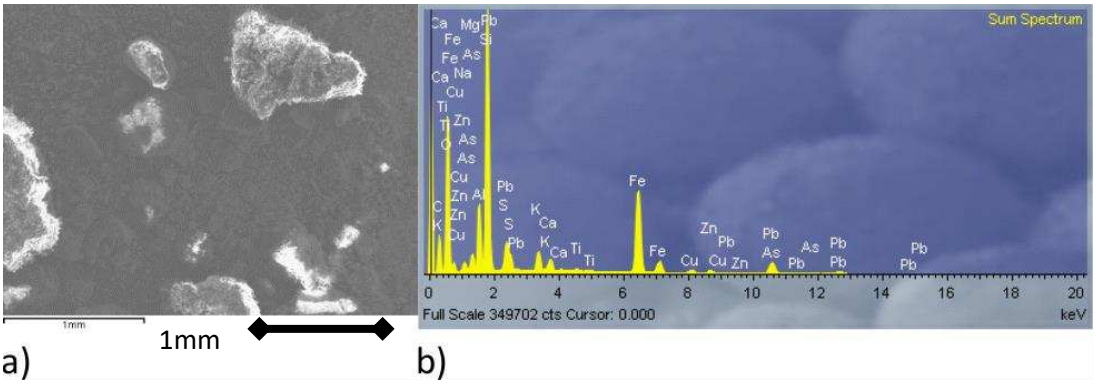

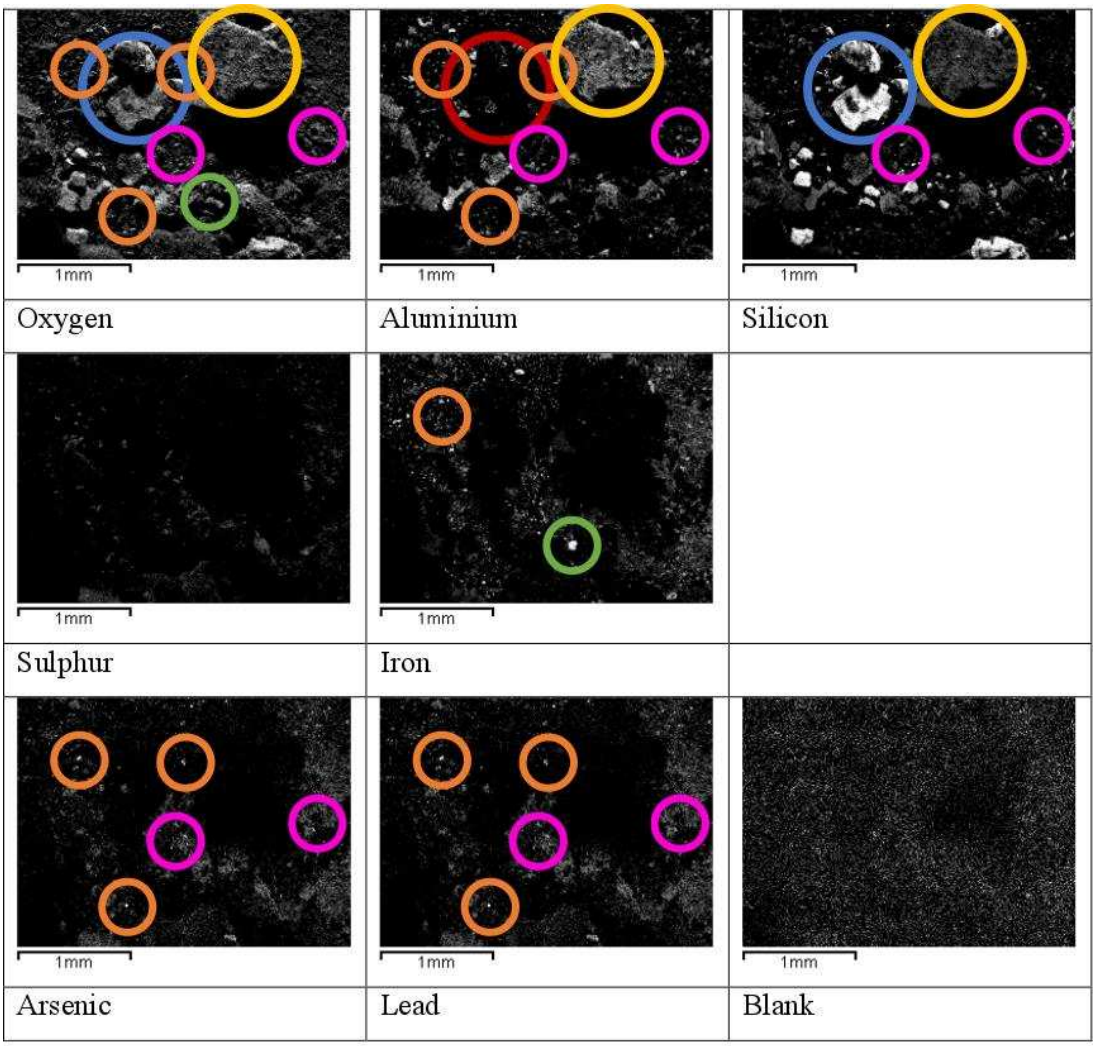

Figure 6.20 – a) SEM map area image showing S2w, b) Corresponding EDX sum spectrum, and c) Corresponding EDX element map

6.6.4 SEM-EDX of S2a – Soil 2 washed with 0.25M HNO_3

Again, for S2a, the agglomeration of particles is visible. The point-analysis, Figure 6.21a, detected a large amount of iron and arsenic as well as lead in its corresponding spectrum, Figure 6.21b. Copper also appears in the spectrum.

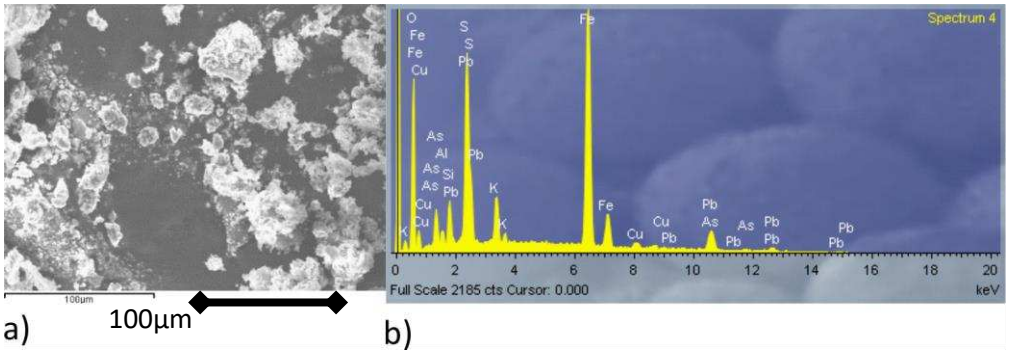

Figure 6.21 - a) SEM image showing S2w and b) Corresponding EDX spectrum

The EDX sum spectrum, Figure 6.22b, of a subsequent area of the same soil sample, detected a much lower amount of iron and arsenic and does not show any lead. However, lead is clearly visible in the element map, Figure 6.22c. For the first time, it appears that the lead and arsenic have more bright areas than iron, implying a higher concentration. The map shows lead following arsenic, as in the previous samples, however they are also aligned with iron and copper, as shown by the purple circles. In addition, another area shows correlation between the heavy metals and sulphur, denoted by blue circles. These do not correlate with silicon and aluminium which are, again, following each other together with oxygen. There are yellow circles indicating the presence of an aluminosilicate structure. There is also an area of iron that does not align with any other of the elements mapped, marked by a green circle.

The pink circles draw attention to a particular area found in all of the maps except for copper. Within the pink circle there are two arrows. The blue arrow indicates the presence of oxygen, iron, arsenic, and lead. The red arrow shows the absence of the elements sulphur, aluminium and oxygen. The yellow arrow shows the presence of oxygen, sulphur, arsenic and lead. The white arrow shows the absence of iron, aluminium, and silicon in this area. The brown circles show areas that are bright for oxygen, aluminium, silicon, lead, and oxygen. This may be due to gismondine interacting with lead and not to plumbojarosite because of the solubility of the latter, suggesting it to have dissolved.

It is interesting to see that arsenic and lead either follow iron, or sulphur. However, the iron and sulphur will not overlap. This confirms the absence of

plumbojarosite, which has iron, sulphur, and lead in its overall composition. Segnitite is a mineral that contains lead, iron and arsenic oxides as well as hydroxides.

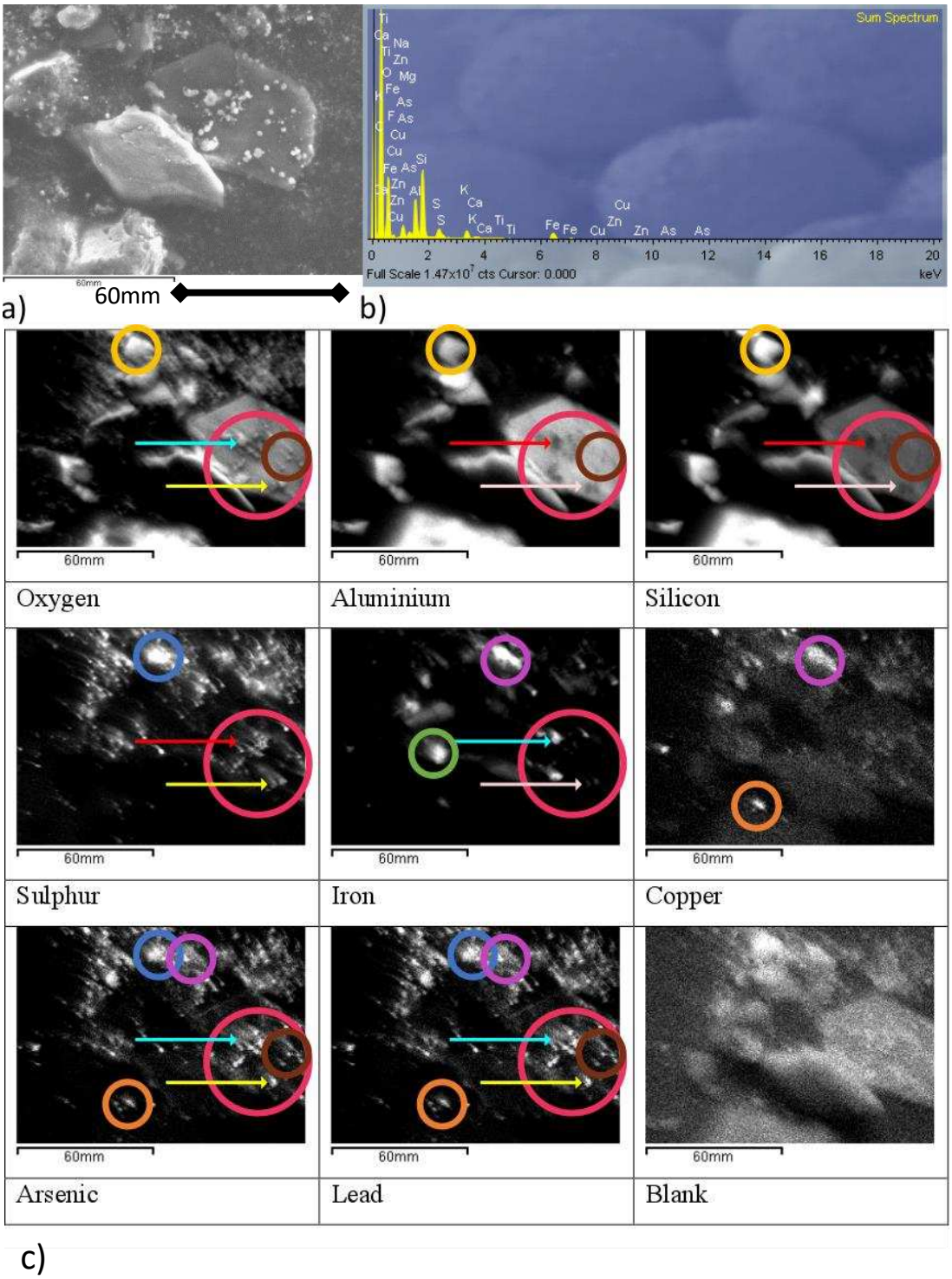

Figure 6.22 – a) SEM map area image showing S2a, b) Corresponding EDX sum spectrum, and c) Corresponding EDX element map

6.6.5 XRF Analysis of S2untreated with S2w and S2a

The XRF data, Table 6.6, for S2untreated differs from S1untreated by the absence of sulphur and the detection of arsenic. This fits with the XRD data, Table 6.6,

that shows the absence of sulphur-containing compounds pyrite and cubanite and the addition of the arsenic-rich compound segnitite. Because chalcopyrite and copper antimony sulphide remain present, whilst pyrite and cubanite are missing, the amount of sulphur has decreased to below 0.9%. S2w and S2a had the same elements present over the threshold with the similar trend of phosphorus falling below the detection limit after washing, yet being present in the XRD minerals list. This is discussed further in Section 6.5.6.

Table 6.6 - XRF elemental composition above 0.9% for S2untreated, S2w, and S2a

S2untreated		S2w		S2a	
Element	Percentage (%)	Element	Percentage (%)	Element	Percentage (%)
Fe	39.36	Fe	39.30	Fe	39.18
Pb	14.97	Si	18.81	Si	23.88
Si	14.85	Pb	16.04	Pb	11.72
K	8.22	As	6.89	Al	6.60
As	6.07	Al	5.76	As	6.04
Al	5.33	K	4.16	K	4.50
P	3.14	Ca	2.13	Zn	1.63
Zn	1.69	Zn	1.71	Ca	1.62
Ca	1.64	Cu	1.47	Cu	1.34
Cu	1.50	P	< det limit	P	< det limit

6.7 Comparison of Soil 1 and Soil 2

XRD data in Table 6.7 shows that in Soil 1, pyrite is identified, unlike in Soil 2. This is because Soil 1 was taken from the roasting site and will, therefore, have both the starting materials and waste products of the roasting procedure. Conversely, Soil 2 is the waste product that should no longer contain any pyrite.

Table 6.7 – Mineral components of S1untreated and S2untreated identified using the EVA database by Bruker

S1untreated		S2untreated	
		Albite	$K_{0.2}Na_{0.8}AlSi_3O_8$
Chalcopyrite	$CuFeS_2$	Chalcopyrite	$CuFeS_2$
Copper Antimony Sulphide	Cu_3SbS_3	Copper Antimony Sulphide	Cu_3SbS_3
Cubanite	$CuFe_2S_3$		
Hematite	α-Fe_2O_3	Hematite	α-Fe_2O_3
Illite	$K(Al,Fe)_2AlSi_3O_{10}(OH)_2 \cdot H_2O$	Illite	$K(Al,Fe)_2AlSi_3O_{10}(OH)_2 \cdot H_2O$
Koninckite	$FePO_4 \cdot 3H_2O$	Koninckite	$FePO_4 \cdot 3H_2O$
Lead silicate	Pb_3SiO_5	Lead silicate	Pb_3SiO_5
Lead sulphate	$PbSO_4$	Lead sulphate	$PbSO_4$
Magnesium phosphate	MgP_4O_{11}		
Phosphoferrite	$(Fe,Mn)_3(H_2O)_3(PO_4)_2$		
Plumbojarosite	$PbFe_6(SO_4)_4(OH)_{12}$		
Pyrite	FeS_2		
Quartz	SiO_2	Quartz	SiO_2
Segnitite	$PbFe_3(AsO_4)(AsO_3OH)(OH)_6$	Segnitite	$PbFe_3(AsO_4)(AsO_3OH)(OH)_6$
Sphalerite	ZnS		

6.7.1 XRF Analysis Comparing S1untreated and S2untreated

From the XRF results Table 6.8, it is concluded that the major compound in both soils is an iron-based mineral. There is a distinct difference between the two soils, which may affect their response to remediation techniques. Soil 1 had a large component of sulphur whilst Soil 2 had a much higher lead content.

Table 6.8 - XRF elemental composition above 0.9% for S1untreated and S2untreated

S1untreated		S2untreated	
Element	Percentage (%)	Element	Percentage (%)
Fe	54.95	Fe	39.36
S	12.77	Pb	14.97
Si	10.10	Si	14.85
K	6.25	K	8.22
P	5.97	As	6.07
Cu	2.86	Al	5.33
Al	2.70	P	3.14
Pb	1.85	Zn	1.69
		Ca	1.64
		Cu	1.50

The amount of lead detected by the XRF was quite different for the two samples with considerably more being present in Soil 2. Arsenic also showed a higher percentage concentration in Soil 2. This is logical as the two elements appear to follow each other in the previous SEM-EDX results. Sulphur, conversely, is only detected above 0.9% in Soil 1, as it would be present in pyrite, plumbojarosite, copper antimony sulphide and chalcopyrite. Plumbojarosite is formed in acidic sulphide-rich environments, in this case, as a result of the roasting process. Soil 2 does not show XRF results for sulphur, but it does consist of sulphur compounds, detected by the XRD, Table 6.9. These are in the form of copper antimony sulphide and chalcopyrite. The EDX element maps agreed that sulphur was present, especially in S2a. It was not detected by the XRF probably due to its low concentration. The full results, shown in Appendix 3, detail that sulphur is detected at 0.75%. Zinc is detected in S2untreated, but this does not agree with the XRD results, which show that sphalerite is present in Soil 1 samples, and not Soil 2. From the XRF data, it is detected that phosphorus is found at a higher percentage in S1untreated than S2untreated which agrees with the XRD data showing that koninckite, magnesium phosphate and phosphoferrite are present in Soil 1 whilst koninckite is the only phosphate-containing mineral in Soil 2.

Figure 6.23 shows an XRF graph of both untreated soils that has been normalised to 100%. It is clear that the XRF confirms that Soil 2 has a much higher concentration of lead. It also has more aluminium, arsenic, calcium, potassium, silicon and zinc. This confirms with the results previously discussed from XRD and SEM-EDX analysis.

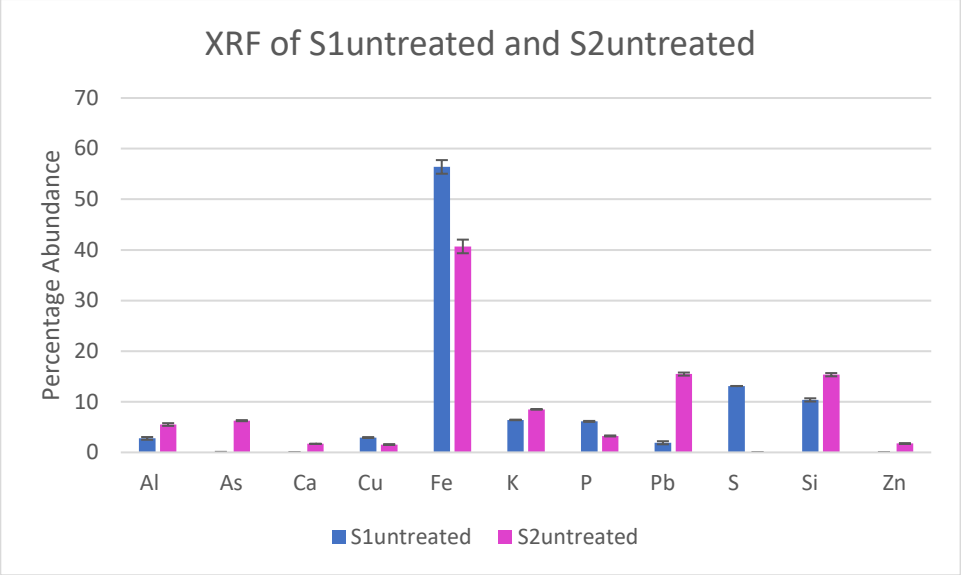

Figure 6.23 – Normalised XRF data of S1untreated and S2untreated

6.8 Analysis of Treated Soils

XRD, SEM-EDX and XRF were also used to analyse the treated samples. The addition of Zeolite-A and its effect on the solid residues was determined.

6.8.1 XRD of Soil 1 in Water

The XRD results in Table 6.9 show that, as seen with S1w, plumbojarosite is no longer identified in the spectrum after washing. Zeolite-A is detected in S1wZA25 and S1wZA50, showing that the zeolite remains in the soil and is not leaching or dissolving. This is confirmed in the XRD pattern for S1wZA25, Figure 6.24. The XRD pattern for S1wZA50 is in Appendix 4, as the minerals detected are identical. The pattern for gismondine overlaid on the pattern for S1wZA25 is in Figure 6.25.

Table 6.9 - Mineral components of S1untreated, S1w, S1wZA25, and S1wZA50 identified using the EVA database by Bruker

S1untreated		S1w	
Chalcopyrite	$CuFeS_2$	Chalcopyrite	$CuFeS_2$
Copper Antimony Sulphide	Cu_3SbS_3	Copper Antimony Sulphide	Cu_3SbS_3
Cubanite	$CuFe_2S_3$	Cubanite	$CuFe_2S_3$
		Gismondine	$CaAl_2Si_2O_8 \cdot 4H_2O$
Hematite	α-Fe_2O_3	Hematite	α-Fe_2O_3
Illite	$K(Al,Fe)_2AlSi_3O_{10}(OH)_2 \cdot H_2O$	Illite	$K(Al,Fe)_2AlSi_3O_{10}(OH)_2 \cdot H_2O$
Koninckite	$FePO_4 \cdot 3H_2O$	Koninckite	$FePO_4 \cdot 3H_2O$
Lead silicate	Pb_3SiO_5		
Lead Sulphate	$PbSO_4$	Lead Sulphate	$PbSO_4$
Magnesium phosphate	MgP_4O_{11}	Magnesium phosphate	MgP_4O_{11}
Phosphoferrite	$(Fe,Mn)_3(H_2O)_3(PO_4)_2$	Phosphoferrite	$(Fe,Mn)_3(H_2O)_3(PO_4)_2$
Plumbojarosite	$PbFe_6(SO_4)_4(OH)_{12}$		
Pyrite	FeS_2	Pyrite	FeS_2
Quartz	SiO_2	Quartz	SiO_2
Segnitite	$PbFe_3(AsO_4)(AsO_3OH)(OH)_6$	Segnitite	$PbFe_3(AsO_4)(AsO_3OH)(OH)_6$
Sphalerite	ZnS	Sphalerite	ZnS

S1wZA25/S1wZA50	
Chalcopyrite	$CuFeS_2$
Copper Antimony Sulphide	Cu_3SbS_3
Cubanite	$CuFe_2S_3$
Gismondine	$CaAl_2Si_2O_8 \cdot 4H_2O$
Hematite	α-Fe_2O_3
Illite	$K(Al,Fe)_2AlSi_3O_{10}(OH)_2 \cdot H_2O$
Koninckite	$FePO_4 \cdot 3H_2O$
Lead Sulphate	$PbSO_4$
Magnesium phosphate	MgP_4O_{11}
Phosphoferrite	$(Fe,Mn)_3(H_2O)_3(PO_4)_2$
Pyrite	FeS_2
Quartz	SiO_2
Segnitite	$PbFe_3(AsO_4)(AsO_3OH)(OH)_6$
Sphalerite	ZnS
Zeolite-A	$Na_{12}[(AlO_2)_{12}(SiO_2)_{23}] \cdot 27H_2O$

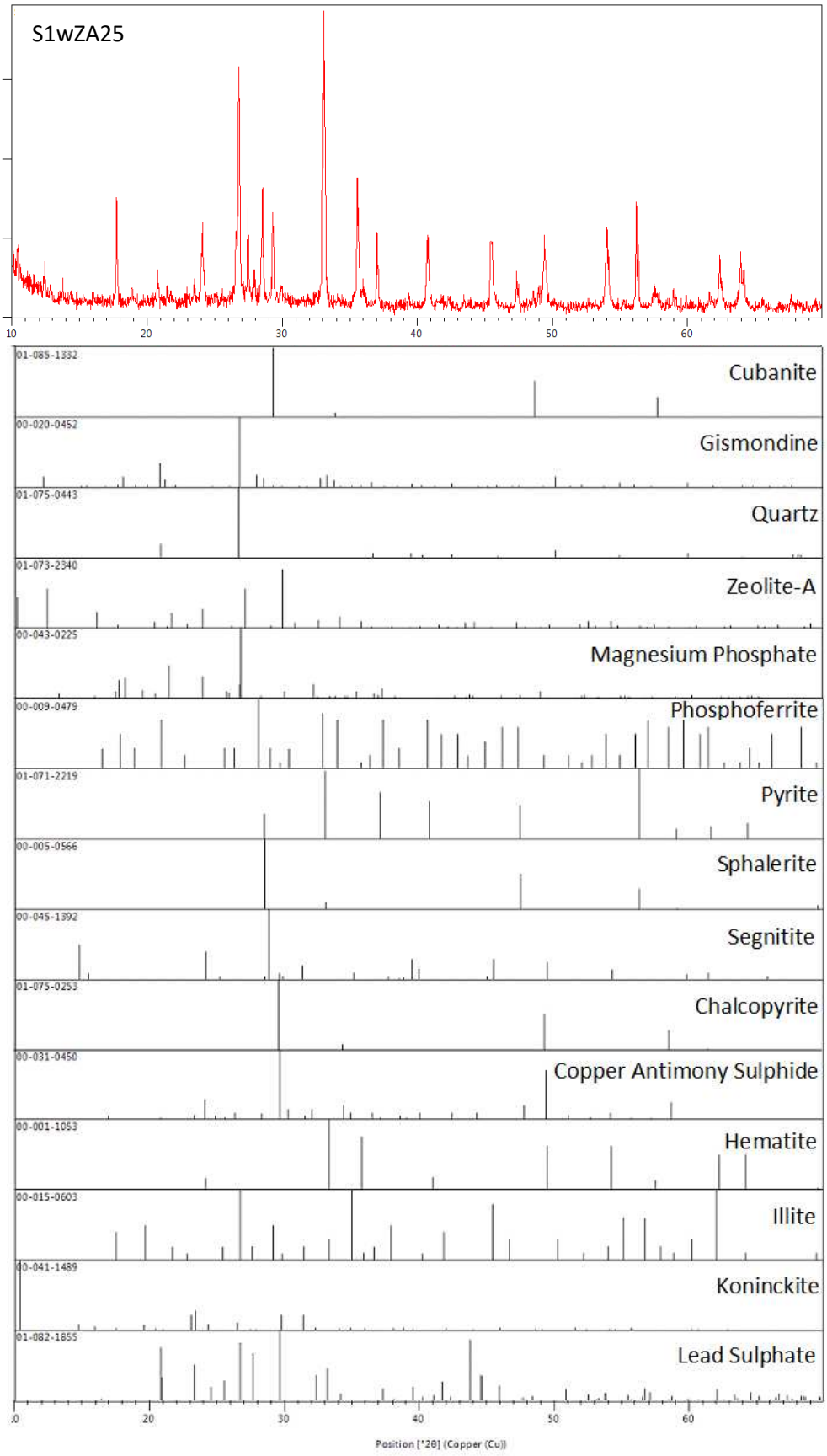

Figure 6.24 - XRD Pattern for S1wZA25 and corresponding minerals

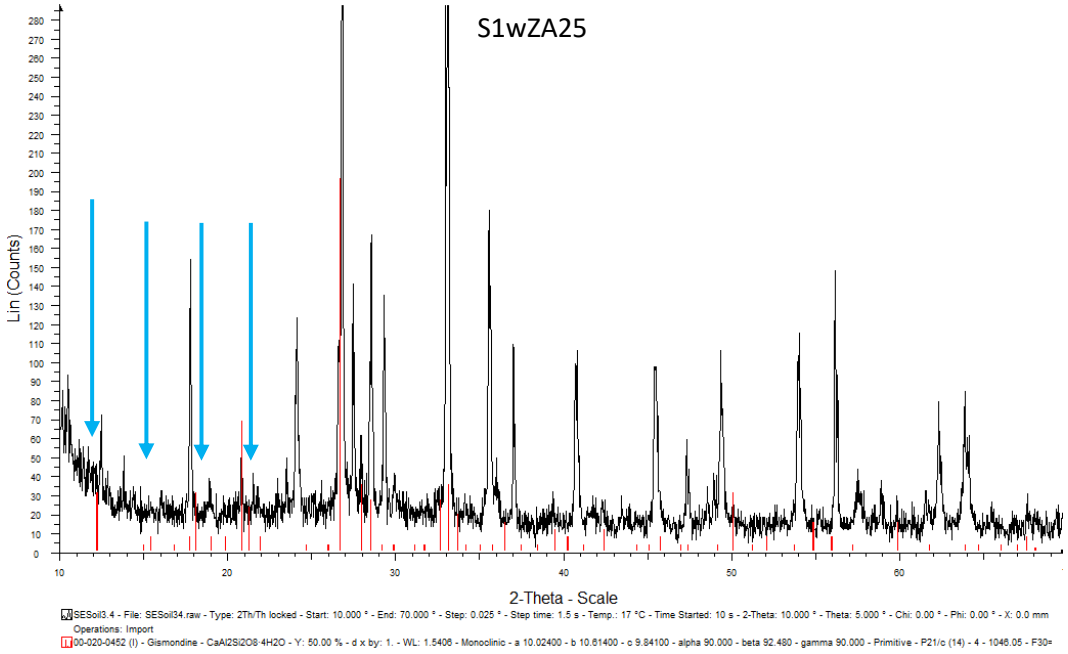

Figure 6.25 - XRD pattern of S1wZA25with gismondine peaks overlaid in red

6.8.2 SEM-EDX of S1wZA25 – Soil 1 in Water with 0.25 g of Zeolite-A

To better understand what minerals were left in the soil residues and to track any differences in lead remediation by the addition of Zeolite-A, SEM-EDX measurements were undertaken to identify residues of Zeolite-A, observed as cubes of non-homogeneous size, as well as the elemental composition of the soils. The analysis of Soil 1 started with 0.25 g of Zeolite-A added to the washing procedure. This was in an attempt to collect data regarding the synthetic zeolite and any elements interacting with it. Figure 6.26a shows cube-like morphologies, characteristic of Zeolite-A.

The EDX spectrum (Figure 6.26b) shows aluminium, silicon, sodium and oxygen peaks. There are also peaks for iron and lead. The pH of this solution was 4.06 and the spectrum shows that the Zeolite-A did not dissolve in the solution, as the zeolite particles are still intact. However, it is difficult to judge whether the lead is exchanging with sodium ions in Zeolite-A as the presence of lead could be due to the beam detecting soil around the cube.

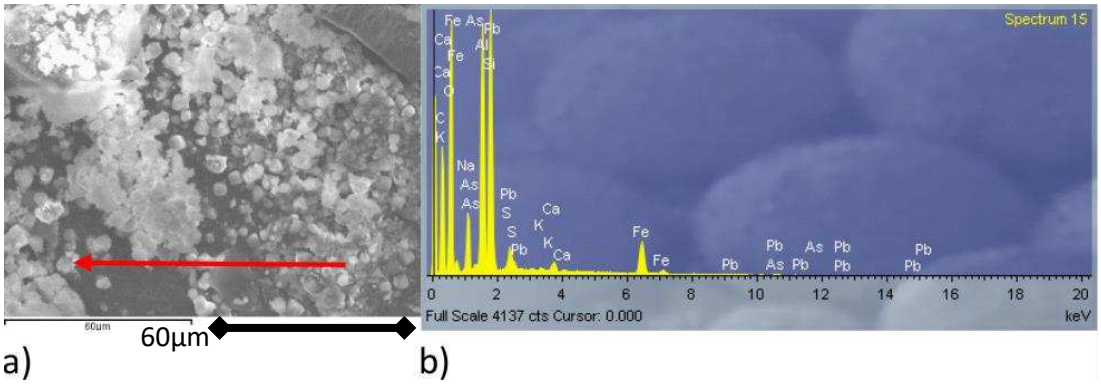

Figure 6.26 - a) SEM image showing S1wZA25 and b) EDX spectrum corresponding to the point marked with a red arrow

Another area is presented in Figure 6.27a. It is difficult to see the individual Zeolite-A cube-like structures because the image is zoomed out to 1 mm, over 16.5 times greater distance than Figure 6.26a. The resulting map, Figure 6.27c is extremely pixelated but still shows valuable information. Lead is present, as well as arsenic, and they are in the same positions as shown by the orange circles. There is overlap between the lead, arsenic, sulphur and iron. Within the orange circle, which these elements share in common, there is an area, denoted with an arrow, that is present in the analysis for heavy metals as well as silicon and oxygen but not in sulphur or iron. This suggests that the heavy metals could be formed around a silicate structure, possibly gismondine or Zeolite-A.

Silicon has several areas that overlap with oxygen, probably due to quartz, the presence of aluminium appears below the level of the blank, and sulphur appears in specific locations that are matched by iron, denoted by the blue circles. This is probably the detection of pyrite. It is important to note how strong the results for the blank are, as this implies that most of the mapping data falls within that error. The overall spectrum, Figure 6.27b, shows peaks for silicon, magnesium, and sodium.

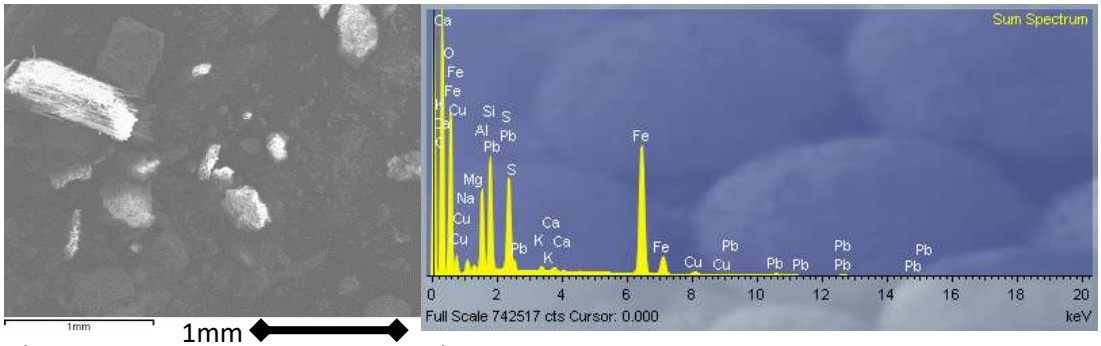

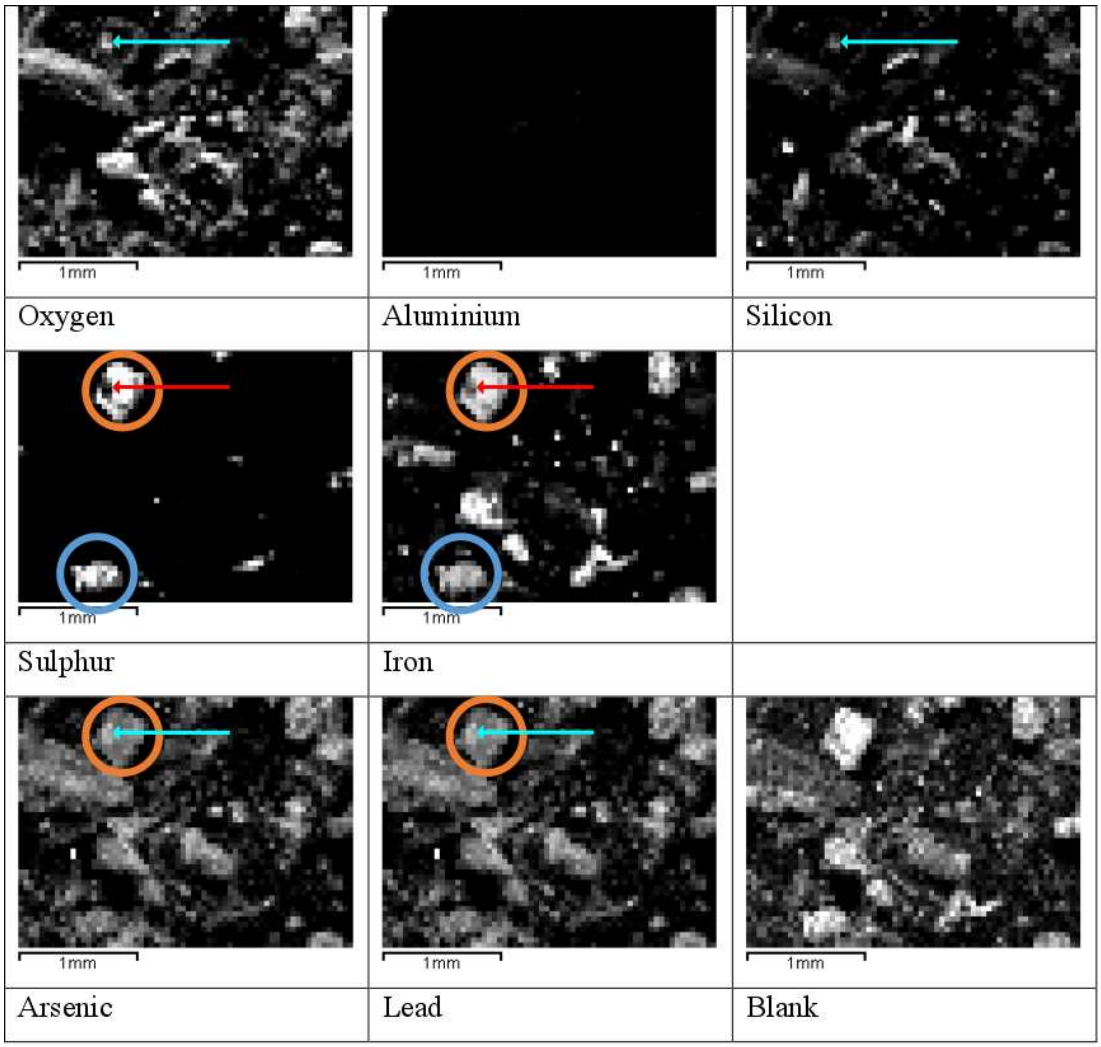

Figure 6.27 - a) SEM map area image S1wZA25, b) Corresponding EDX sum spectrum, and c) Corresponding EDX element map

6.8.3 SEM-EDX of S1wZA50 – Soil 1 in Water with 0.50 g of Zeolite-A

To fully understand the importance of Zeolite-A in the remediation process, the amount of zeolite was increased and resulted in the cube-like structures being distributed homogeneously across and throughout the soil. From Figure 6.28 it can be

seen that the structures are easily visible even from a scale of 200 µm. It is also possible to see detritus that made it through the sifting process due to its small size.

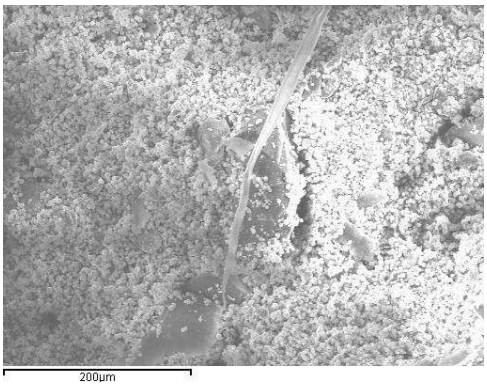

Figure 6.28 - SEM image showing S1wZA50: 200 µm

Zoomed in to a scale of 50 µm, a cube was selected for analysis, Figure 6.29a. Strong peaks for lead, sulphur and arsenic as well as the typical Zeolite-A peaks were identified in the corresponding point EDX spectrum, Figure 6.29b.

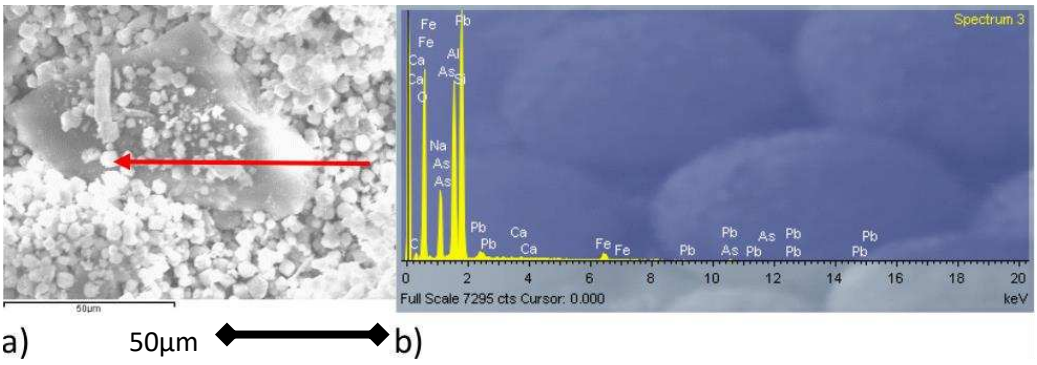

Figure 6.29 - a) SEM image showing S1wZA50 and b) EDX spectrum corresponding to the point marked with a red arrow

In the EDX element map, Figure 6.30c, aluminium is blank. This is due to a small amount of the metal stub being visible in the top right corner. Because the base is partially composed of aluminium, any of this element in the solid sample would be completely overshadowed by the high concentration detected in the base.

The sum spectrum, Figure 6.30b, shows aluminium and lead to be present, however the element map shows only a few select areas of lead. Again, the lead and arsenic maps appear identical and the blue circles show correlation between the heavy metals along with silicon and oxygen. This is a similar result to S1wZA25, where it was proposed that lead and arsenic are interacting with gismondine or Zeolite-A.

Sulphur seems to be directly following iron, as shown by the yellow circles, in the form of pyrite, and iron seems to be following oxygen, as hematite, with an important exception; where sulphur and iron are both found, oxygen is missing, shown by the red circle. This would show that pyrite and iron oxide are both present as separate minerals.

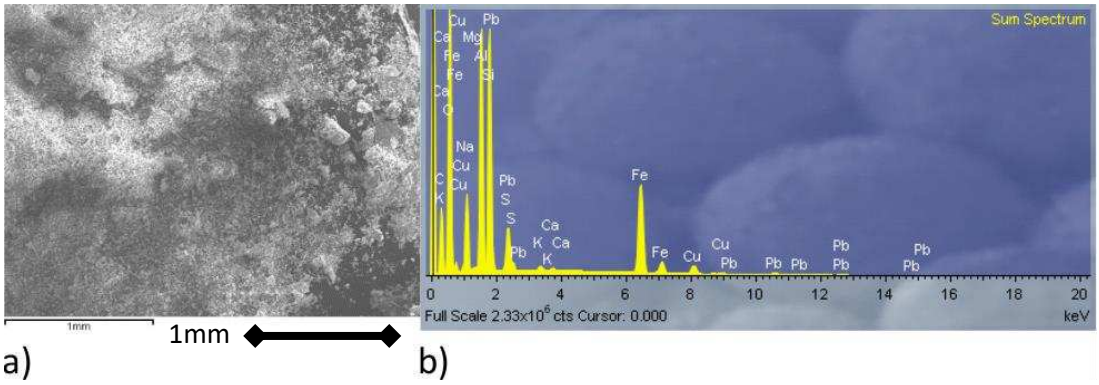

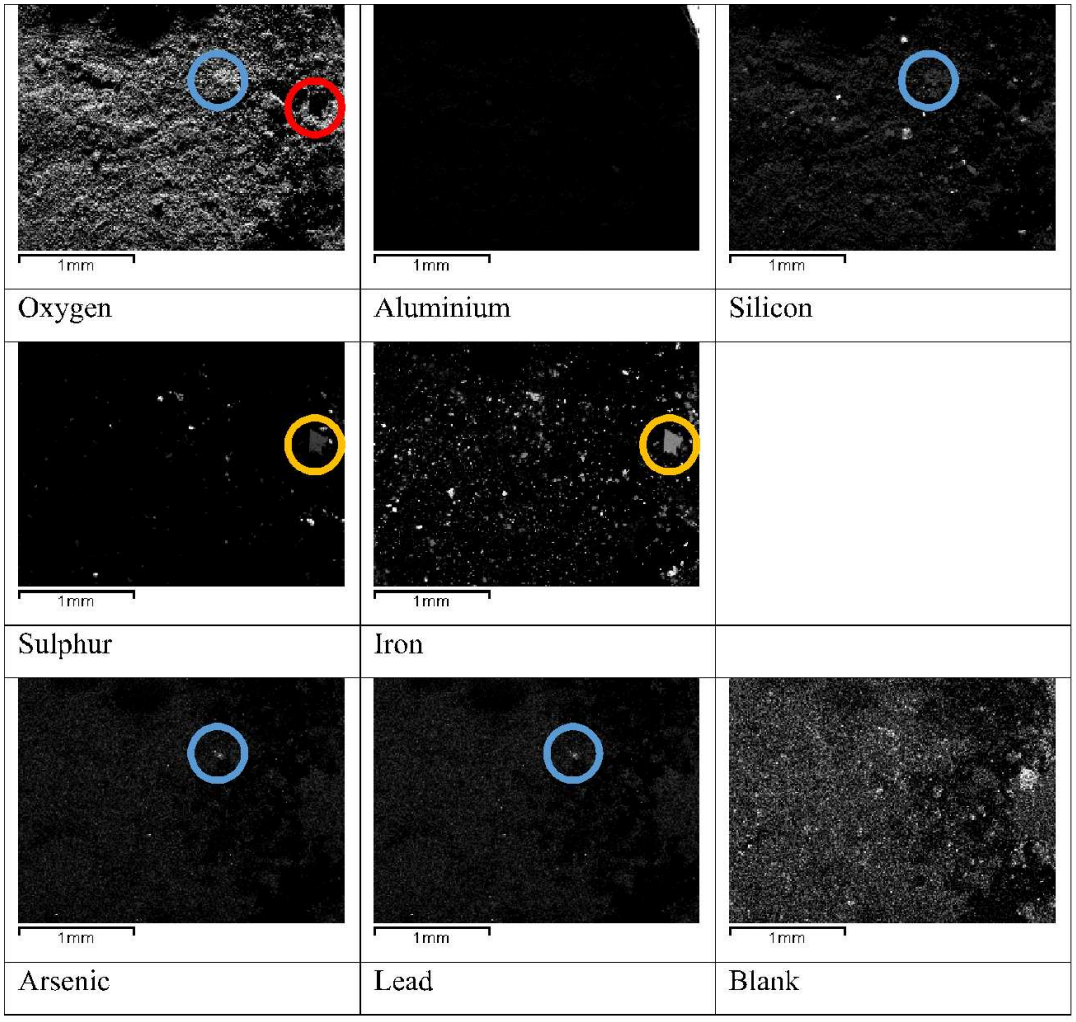

Figure 6.30 - a) SEM map area image showing S1wZA50, b) Corresponding EDX sum spectrum, and c) Corresponding EDX element map

6.8.4 XRF of Soil 1 in Water with Increasing Zeolite-A

The untreated and unwashed soil, S1untreated, shows approximately 1.8% of lead present in the solid residue, Figure 6.31. The sample has not been washed and therefore, the lead will not have had the ability to leach, allowing it to be fully present in the solid. The samples were then washed, resulting in a decrease in the percentage of lead detected in the solid. This is due to lead leaching. The addition of Zeolite-A does not appear to change the amount of lead that leaches out of the solid residue. This could be due to the small concentrations and thereby difficulty in detection.

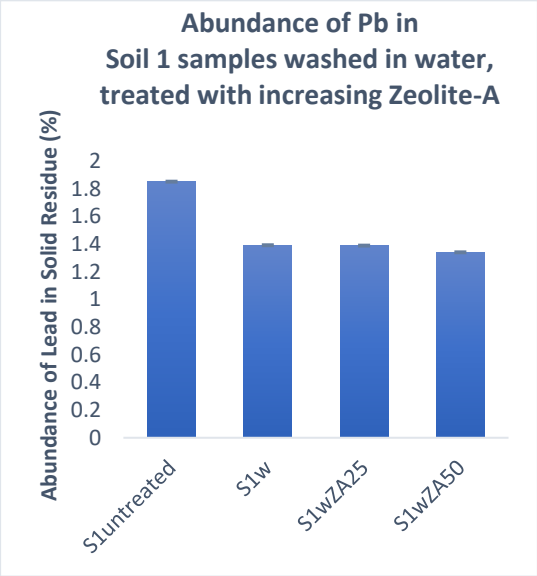

Figure 6.31 - XRF percentage composition of lead for Soil 1 (water)

The XRF data (Table 6.10) shows the only change between S1wZA25 and S1w is the absence of potassium in the former. S1wZA50 lacks potassium above 0.9%, possibly due to a decrease in illite, but shows increased levels of sodium, possibly caused by the additional Zeolite-A added. An increased amount of sodium ions means that more lead ions can potentially undergo ion exchange to be incorporated into the zeolite structure. This is difficult to prove from the XRF measurements as the percentage concentrations are low.

Table 6.10 - XRF elemental composition above 0.9% for S1untreated, S1w, S1wZA25, and S1wZA50

S1untreated		S1w		S1wZA25		S1wZA50	
Element	Percentage (%)	Element	Percentage (%)	Element	Percentage (%)	Element	Percentage (%)
Fe	54.95	Fe	57.72	Fe	55.64	Fe	43.67
S	12.77	Si	16.21	Si	17.04	Si	22.85
Si	10.10	S	11.50	Al	10.15	Al	16.40
K	6.25	Al	4.64	S	7.98	S	5.51
P	5.97	Pb	2.83	Pb	2.84	Na	3.46
Cu	2.86	Cu	2.38	Cu	2.69	Pb	2.99
Al	2.70	K	1.76	K	1.11	Cu	2.02
Pb	1.85	P	< det limit	P	< det limit	Ca	0.93

6.8.5 XRD of Soil 1 in Acid

Table 6.11 shows that both before and after treatment with Zeolite-A, all Soil 1 samples investigated with XRD displayed high content of sulphide-rich minerals. These sulphide minerals remain after agitation, suggesting that they have lower solubility in acid than the sulphate minerals, for example, plumbojarosite. The addition of dilute acid causes the removal of lead silicate and plumbojarosite. Aside from the formation of gismondine, no other minerals are introduced resulting in the washed and treated soil residues showing the same minerals present as also shown in Figure 6.32 for S1aZA25. The diffraction pattern for S1aZA50 is in Appendix 4.

Table 6.11 - Mineral components of S1untreated, S1a, S1aZA25, and S1aZA50 identified using the EVA database by Bruker

S1untreated		S1a/S1aZA25/S1aZA50	
Chalcopyrite	$CuFeS_2$	Chalcopyrite	$CuFeS_2$
Copper Antimony Sulphide	Cu_3SbS_3	Copper Antimony Sulphide	Cu_3SbS_3
Cubanite	$CuFe_2S_3$	Cubanite	$CuFe_2S_3$
		Gismondine	$CaAl_2Si_2O_8{\cdot}4H_2O$
Hematite	α-Fe_2O_3	Hematite	α-Fe_2O_3
Illite	$K(Al,Fe)_2AlSi_3O_{10}(OH)_2{\cdot}H_2O$	Illite	$K(Al,Fe)_2AlSi_3O_{10}(OH)_2{\cdot}H_2O$
Koninckite	$FePO_4{\cdot}3H_2O$	Koninckite	$FePO_4{\cdot}3H_2O$
Lead silicate	Pb_3SiO_5		
Lead Sulphate	$PbSO_4$	Lead Sulphate	$PbSO_4$
Magnesium phosphate	MgP_4O_{11}	Magnesium phosphate	MgP_4O_{11}
Phosphoferrite	$(Fe,Mn)_3(H_2O)_3(PO_4)_2$	Phosphoferrite	$(Fe,Mn)_3(H_2O)_3(PO_4)_2$
Plumbojarosite	$PbFe_6(SO_4)_4(OH)_{12}$		
Pyrite	FeS_2	Pyrite	FeS_2
Quartz	SiO_2	Quartz	SiO_2
Segnitite	$PbFe_3(AsO_4)(AsO_3OH)(OH)_6$	Segnitite	$PbFe_3(AsO_4)(AsO_3OH)(OH)_6$
Sphalerite	ZnS	Sphalerite	ZnS

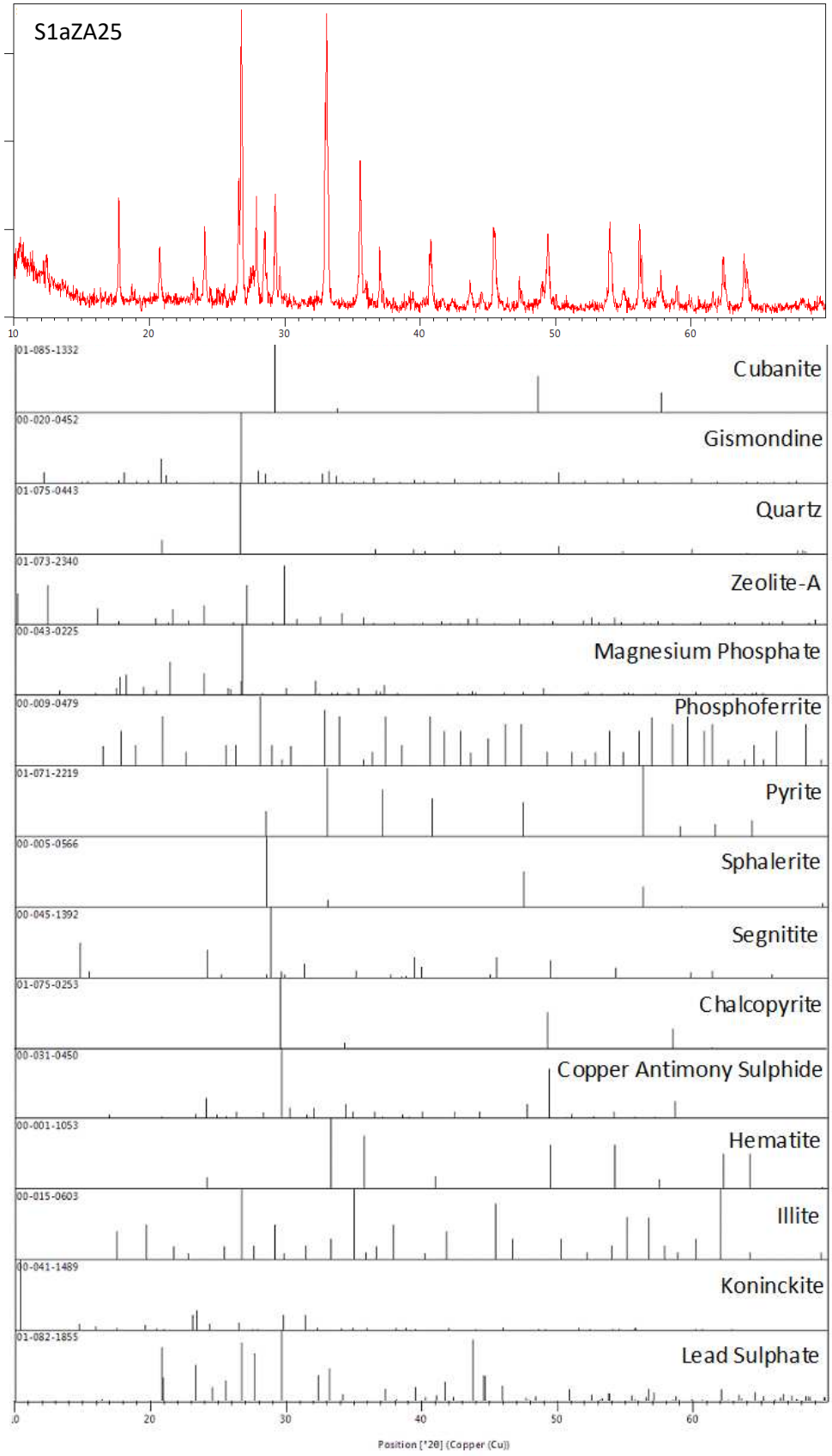

Figure 6.32 - XRD Pattern for S1aZA25 and corresponding minerals

In Figure 6.33, it can be seen that a fourth blue arrow is present. This is due to a peak in the soil pattern that has diminished upon addition of Zeolite-A. In the pattern for S1a, a peak matching with the gismondine peak was present. This could be due to the addition of Zeolite-A having an effect on the secondary mineral present.

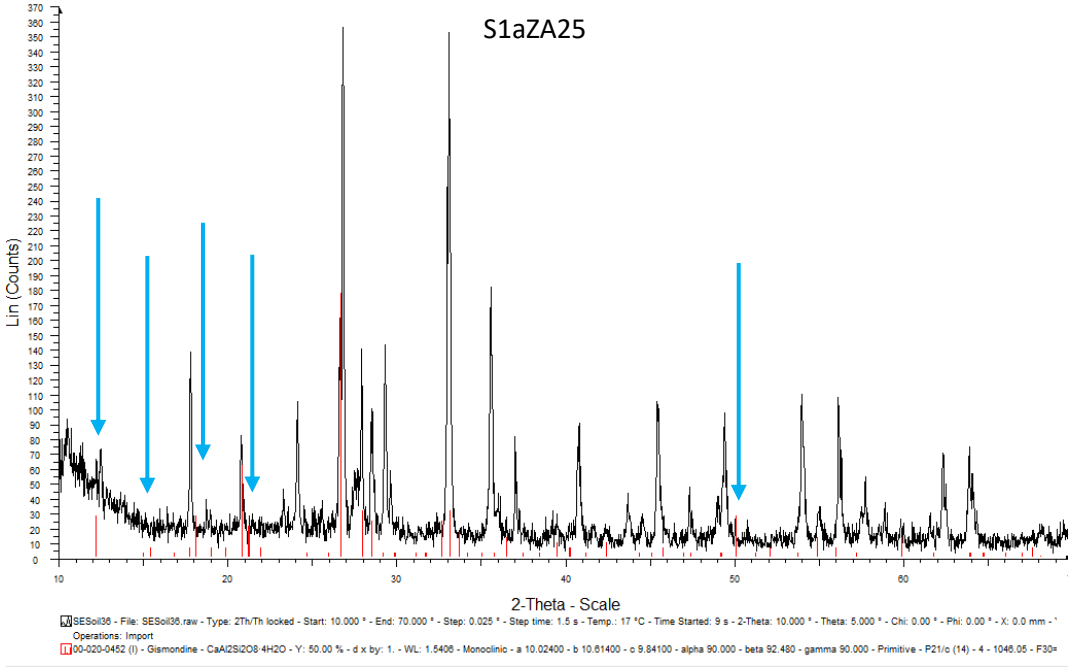

Figure 6.33 - XRD pattern for S1aZA25with gismondine peaks overlaid in red

6.8.6 SEM-EDX of S1aZA25 – Soil 1 in Acid with 0.25 g of Zeolite-A

The soil residues were also studied in detail by SEM-EDX. Initially, it is clear that the cube-like structures are not visible, Figure 6.34a. As discussed under the previous XRD section, it is proposed that the acidic pH of the solution causes the Zeolite-A to dissolve.

Spectrum, Figure 6.34b, shows that Al, Si, O and Na are still detected, inferring that whilst Zeolite-A has broken down in structure, it is not escaping into the leachate. The elements are possibly due to the formation of gismondine.

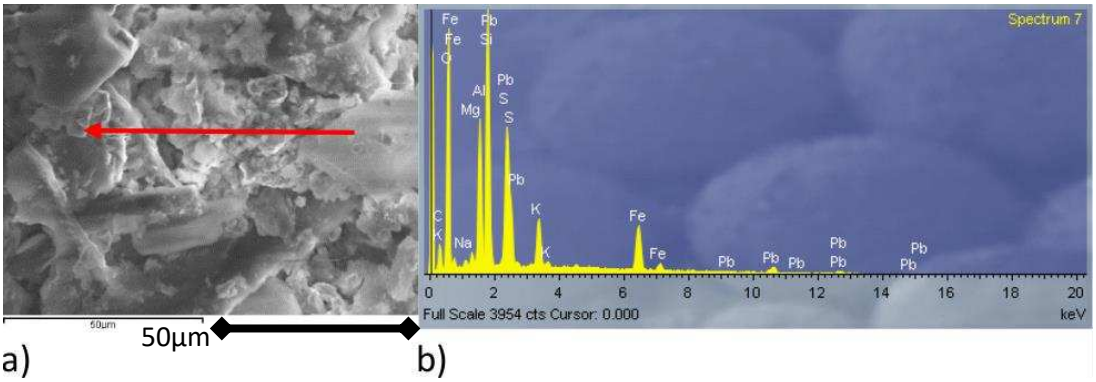

Figure 6.34 - a) SEM image showing S1aZA25 and b) EDX spectrum corresponding to the point marked with a red arrow

Figure 6.35c, the element map for S1aZA25, shows that lead and arsenic are quite difficult to detect in this map and the blank is very bright. Regardless, the heavy metals appear on the sum spectrum, Figure 6.35b, and they seem evenly distributed in the sample.

Sulphur and copper are also sparse in the map. Sulphur is bright in one area, circled in yellow, that aligns with an area in the iron map. This is probably due to pyrite being present. Iron is particularly concentrated in a central area along with oxygen, suggesting that the middle area is a large piece of iron oxide or hydroxide, shown by the blue circles. Silicon shows brightness in this area, whilst aluminium only shows a few bright fragments. The blue and red arrows show an area in which aluminium and iron are negatively correlated, whilst the pink arrows show a connection between lead, arsenic, oxygen, aluminium, and silicon. This could be due to gismondine interacting with lead.

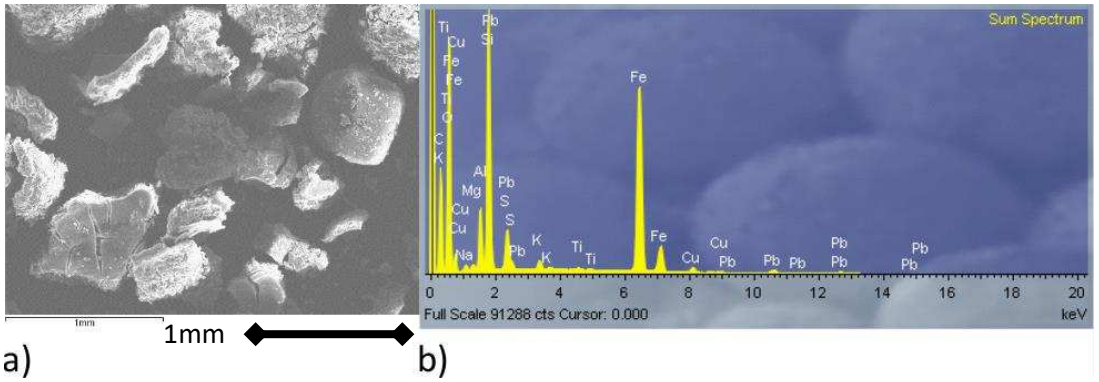

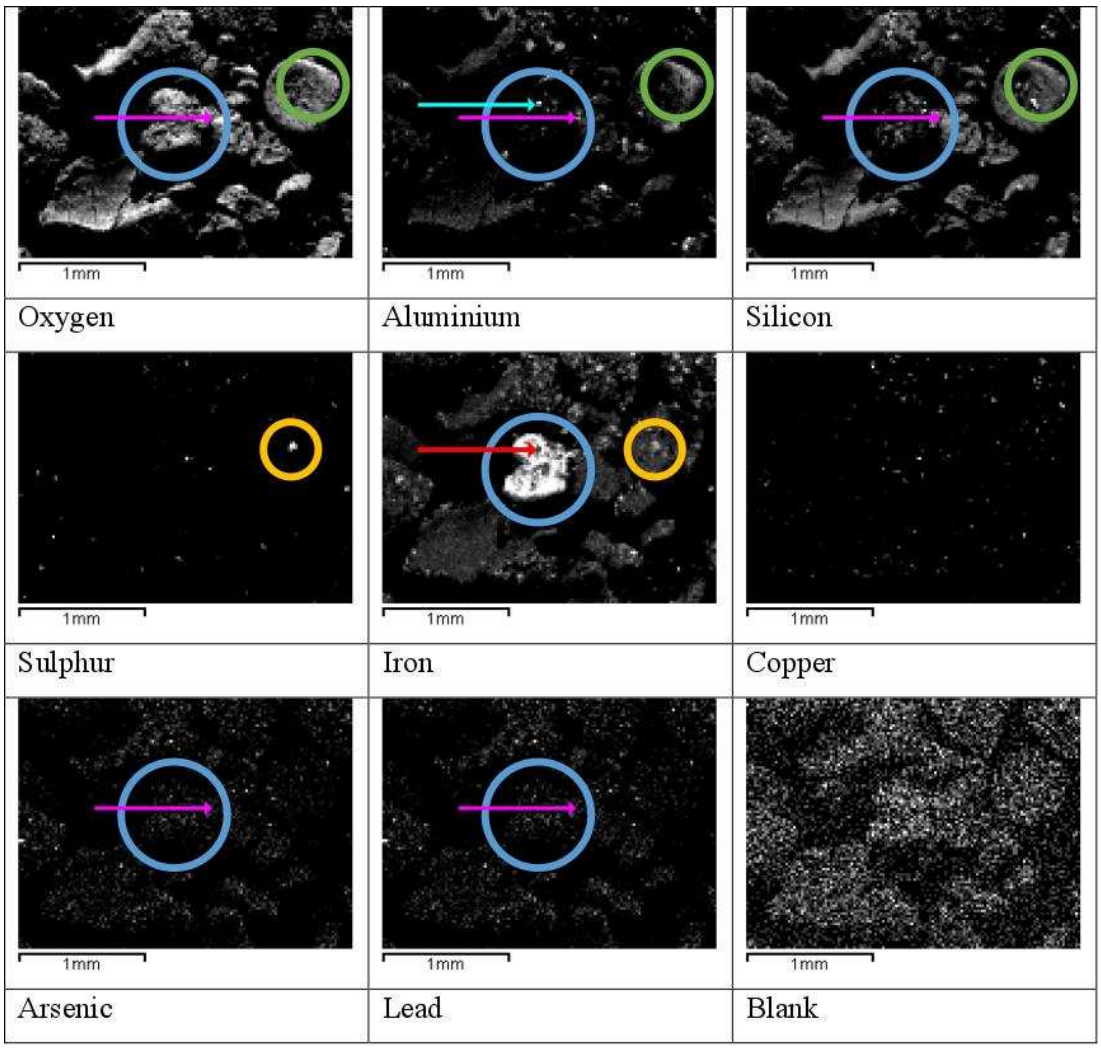

Figure 6.35 - a) SEM map area image showing S1aZA25, b) Corresponding EDX sum spectrum, and c) Corresponding EDX element map

6.8.7 SEM-EDX of S1aZA50 – Soil 1 in Acid with 0.50 g of Zeolite-A

Two different point analyses were undertaken using SEM-EDX, Figure 6.36a. It was found that there are no indications of Zeolite-A being present, as the large agglomerations present are over 1 mm in size. No micro-sized cube-like structures are visible, even with the increased amount of synthetic zeolite. It is clear from the point analysis that there is a higher concentration of iron than lead. The red arrow spectrum, Figure 6.36b, shows that both lead and iron are present as well as aluminium and silicon. The orange arrow spectrum, Figure 6.36c, shows that no lead is present at the second analysed location, however, sodium, aluminium and silicon are detected.

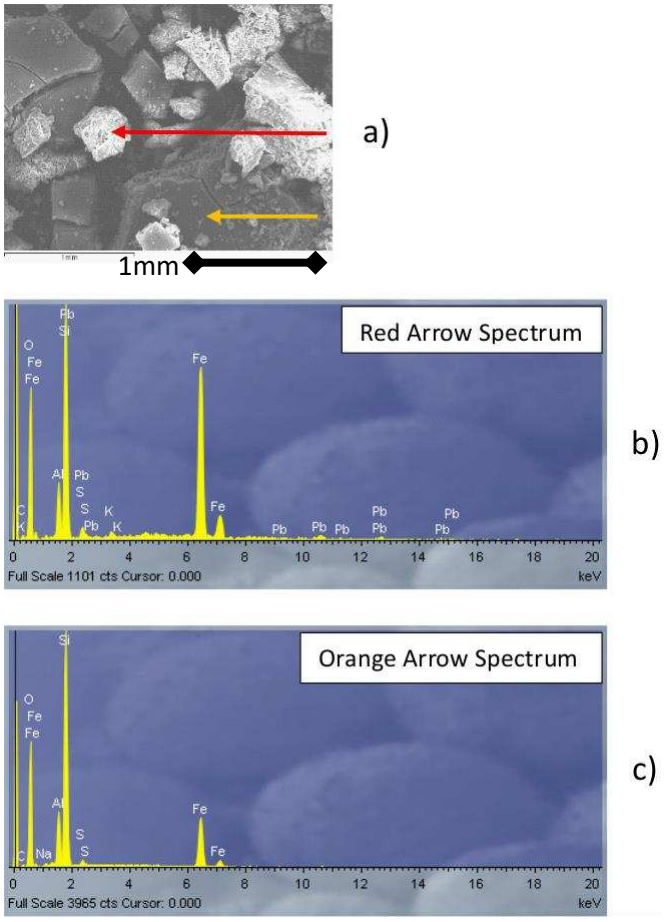

Figure 6.36 - a) SEM image showing S1aZA50, b) EDX spectrum corresponding to the point marked with a red arrow, and c) EDX spectrum corresponding to the point marked with an orange arrow

The element map, Figure 6.37c, is quite saturated, having run for longer than necessary, and appears slightly fuzzy. There are two large areas containing sulphur, arsenic and lead, circled in blue and green. The red circles, at the same location as the blue circles, show an absence of iron, aluminium and silicon. It is possible that lead

sulphate is detected. Arsenic and lead have very similar keV values, 10.543 keV and 10.551 keV, respectively, that could be overlapping.

The blue arrows are pointing at an area that is bright for sulphur, lead and arsenic. It is somewhat present in silicon and missing in the maps of aluminium and iron. This could be another piece of lead sulphate, or possibly pyrite overlapping with lead-gismondine.

Pyrite can be identified by the yellow circles, showing an overlapping area between iron and sulphur that is absent in the other element maps. The orange areas are a small piece of material that is present in oxygen, aluminium, silicon, sulphur and iron, albeit very light in the latter. This could be due to pyrite being present as well as a silicate structure, occupying the same area.

The sum spectrum, Figure 6.37b, shows that the entire area analysed has been positively identified to contain lead, silicon and aluminium. This agrees with the previous point-analysis that showed lead and sodium both being present in the sample but not necessarily at the same location and thereby not in the same mineral.

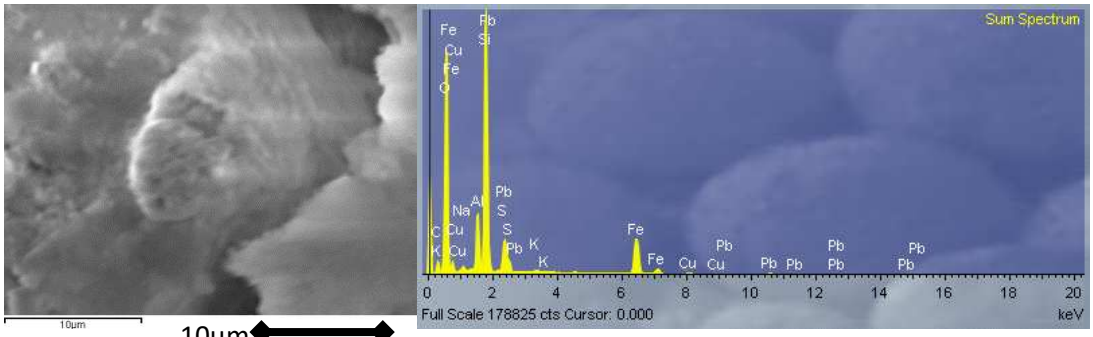

a) b)

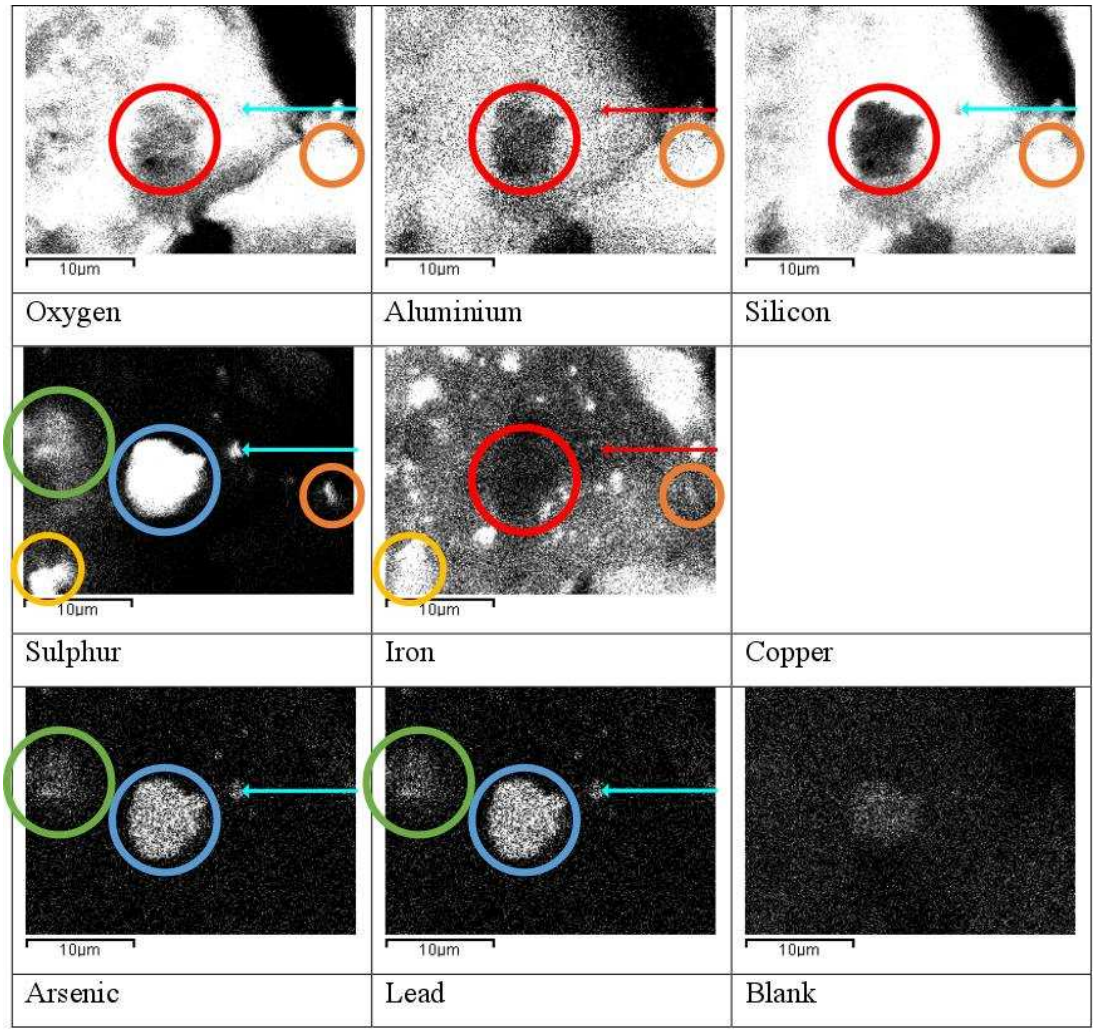

c)

Figure 6.37 - a) SEM map area image showing S1aZA50, b) Corresponding EDX sum spectrum, and c) Corresponding EDX element map

6.8.8 XRF of Soil 1 in Acid with Increasing Zeolite-A

Analysing the soil residues after washing in acid shows a decrease in the concentration lead, which is expected after washing due to leaching, Figure 6.38. After treatment, there appears to be a small change in percentage of lead detected, however all of the values are low and, therefore, difficult to detect accurately. There

is a marked decrease in lead when further zeolite is added. This is still a difference of less than 1% and is for a completely different sample of soil, which makes the comparison difficult with such small percentages.

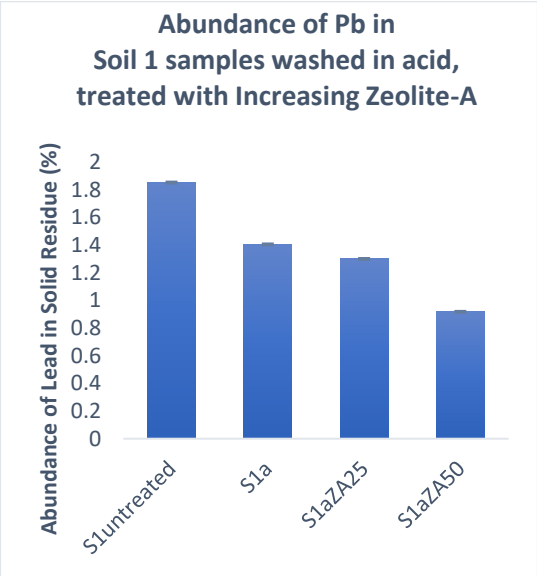

Figure 6.38 - XRF percentage composition of lead for Soil 1 (acid)

The XRF identified the elements present over 0.9% in the washed and treated soils, Table 6.12. This suggests that for Soil 1 when washed with dilute acid, the amount of Zeolite-A added does not have an effect on the minerals formed and detected.

Table 6.12 - XRF elemental composition above 0.9% for S1untreated, S1a, S1aZA25, and S1aZA50

S1untreated		S1a		S1aZA25		S1aZA50	
Element	Percentage (%)	Element	Percentage (%)	Element	Percentage (%)	Element	Percentage (%)
Fe	54.95	Fe	60.08	Fe	57.69	Fe	51.04
S	12.77	Si	14.87	Si	17.99	Si	21.26
Si	10.10	S	12.19	S	10.53	S	11.05
K	6.25	Al	3.67	Al	5.29	Al	9.26
P	5.97	Pb	2.80	Pb	2.64	Cu	2.23
Cu	2.86	Cu	2.64	Cu	2.39	Pb	2.02
Al	2.70	K	1.37	K	1.37	K	1.15
Pb	1.85	P	< det limit	P	< det limit	P	< det limit

6.8.9 XRD of Soil 2 in Water

As with Soil 1, the XRD data of Soil 2 shows a mixture of sulphides and oxide minerals, Table 6.13. The main difference between Soil 1 and Soil 2, is the presence of albite in Soil 2, which remains unaffected by washing in water. There is also a lack of pyrite. Lead silicate disappears in the washed and treated soils and gismondine appears in the samples after washing and addition of Zeolite-A. Figure 6.39 shows the matching patterns for S2wZA25. The pattern for S2wZA50 is in Appendix 4. Figure 6.40 shows the XRD pattern for S2wZA25. There are still several peaks of gismondine that do not align with the diffraction pattern of the soil. These are highlighted in blue.

Table 6.13 - Mineral components of S2untreated, S2w, S2wZ25, and S2wZ50 identified using the EVA database by Bruker

S2untreated		S2w	
Albite	$K_{0.2}Na_{0.8}AlSi_3O_8$	Albite	$K_{0.2}Na_{0.8}AlSi_3O_8$
Chalcopyrite	$CuFeS_2$	Chalcopyrite	$CuFeS_2$
Copper Antimony Sulphide	Cu_3SbS_3	Copper Antimony Sulfide	Cu_3SbS_3
		Gismondine	$CaAl_2Si_2O_8{\cdot}4H_2O$
Hematite	α-Fe_2O_3	Hematite	α-Fe_2O_3
Illite	$K(Al,Fe)_2AlSi_3O_{10}(OH)_2{\cdot}H_2O$	Illite	$K(Al,Fe)_2AlSi_3O_{10}(OH)_2{\cdot}H_2O$
Koninckite	$FePO_4{\cdot}3H_2O$	Koninckite	$FePO_4{\cdot}3H_2O$
Lead silicate	Pb_3SiO_5		
Lead Sulphate	$PbSO_4$	Lead Sulphate	$PbSO_4$
Quartz	SiO_2	Quartz	SiO_2
Segnitite	$PbFe_3(AsO_4)(AsO_3OH)(OH)_6$	Segnitite	$PbFe_3(AsO_4)(AsO_3OH)(OH)_6$

S2wZA25/S2wZA50	
Albite	$K_{0.2}Na_{0.8}AlSi_3O_8$
Chalcopyrite	$CuFeS_2$
Copper Antimony Sulfide	Cu_3SbS_3
Gismondine	$CaAl_2Si_2O_8{\cdot}4H_2O$
Hematite	α-Fe_2O_3
Illite	$K(Al,Fe)_2AlSi_3O_{10}(OH)_2{\cdot}H_2O$
Koninckite	$FePO_4{\cdot}3H_2O$
Lead Sulphate	$PbSO_4$
Quartz	SiO_2
Segnitite	$PbFe_3(AsO_4)(AsO_3OH)(OH)_6$
Zeolite-A	$Na_{12}[(AlO_2)_{12}(SiO_2)_{23}]{\cdot}27H_2O$

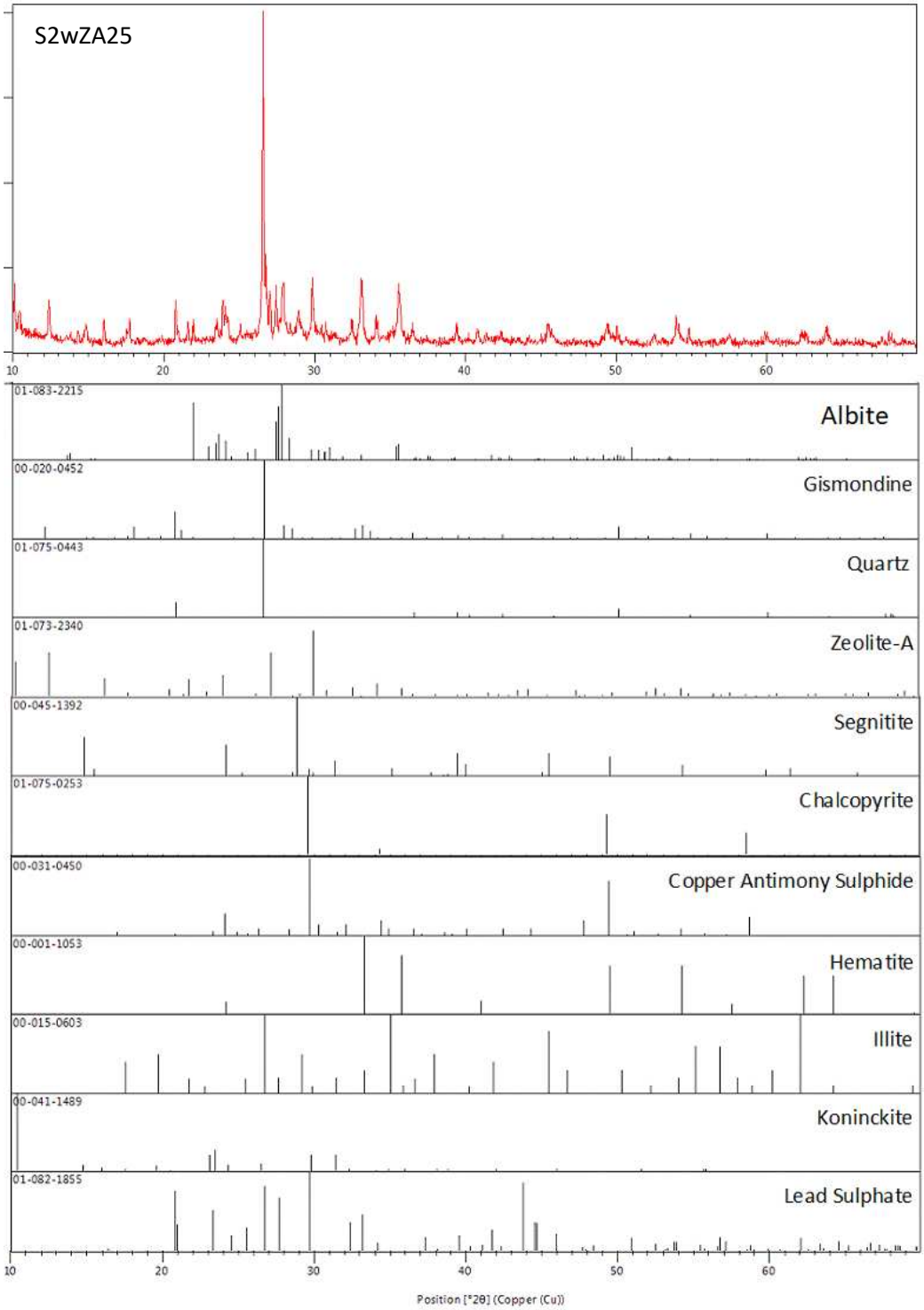

Figure 6.39 - XRD Pattern for S2wZA25 and corresponding minerals

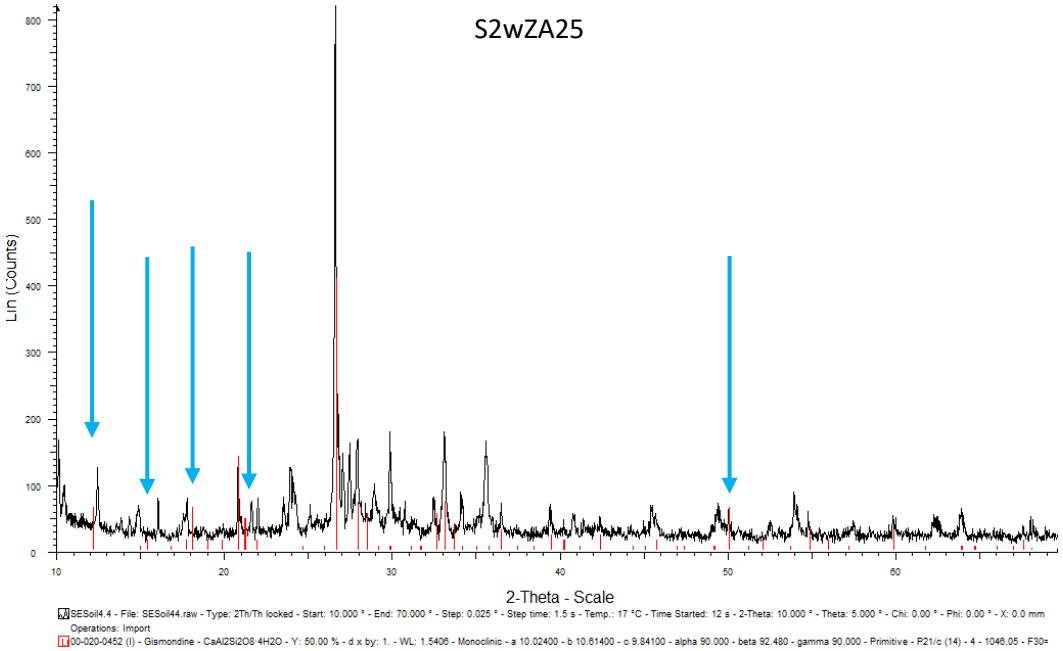

Figure 6.40 - XRD pattern of S2wZA25with gismondine peaks overlaid in red

6.8.10 SEM-EDX of S2wZA25 – Soil 2 in Water with 0.25g of Zeolite-A

SEM-EDX was undertaken to determine the elemental composition of the soil residues, and to see if cube-like particles were present in the sample after adding Zeolite-A.

As with Soil 1, cube-like particles were detected in the SEM image, Figure 6.41a. Point-analysis of a cube-shaped particle shows a large amount of iron, lead, and arsenic as well as increased amounts of copper and possibly calcium, Figure 6.41b. Aluminium, silicon and oxygen are also detected. It is clear that the Zeolite-A structure has not dissolved. This is unsurprising due to the higher pH of Soil 2 compared to Soil 1 and, therefore, increased stability of zeolite structure.

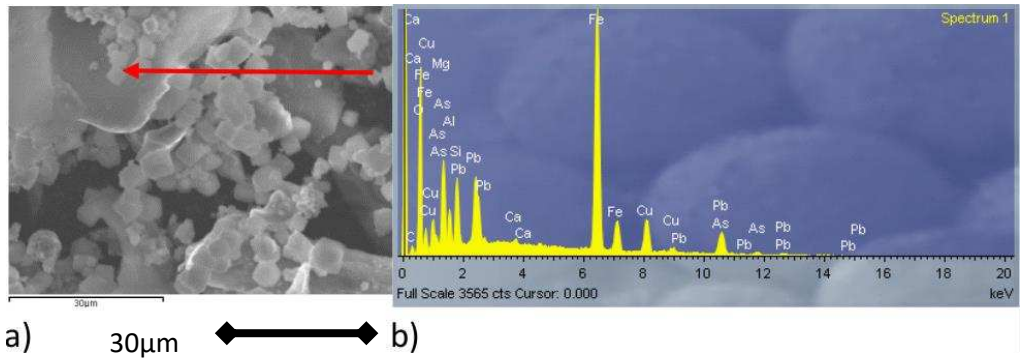

Figure 6.41 - a) SEM map area image showing S2wZA25 and b) EDX spectrum corresponding to the point marked with a red arrow

The peaks in the sum spectrum, Figure 6.42b, for lead and sulphur are not intense. The amount of sulphur, lead and arsenic detected in the total element map, Figure 6.42c, is low. The orange circled areas show a connection between silicon, aluminium and oxygen. This is evidence of an aluminium silicate. There is lead, arsenic, iron and oxygen, denoted by the green circles, which is possibly caused by segnitite. The blue circles show a connection between lead, arsenic, oxygen, aluminium and silicon. This could be due to the interaction of lead with gismondine.

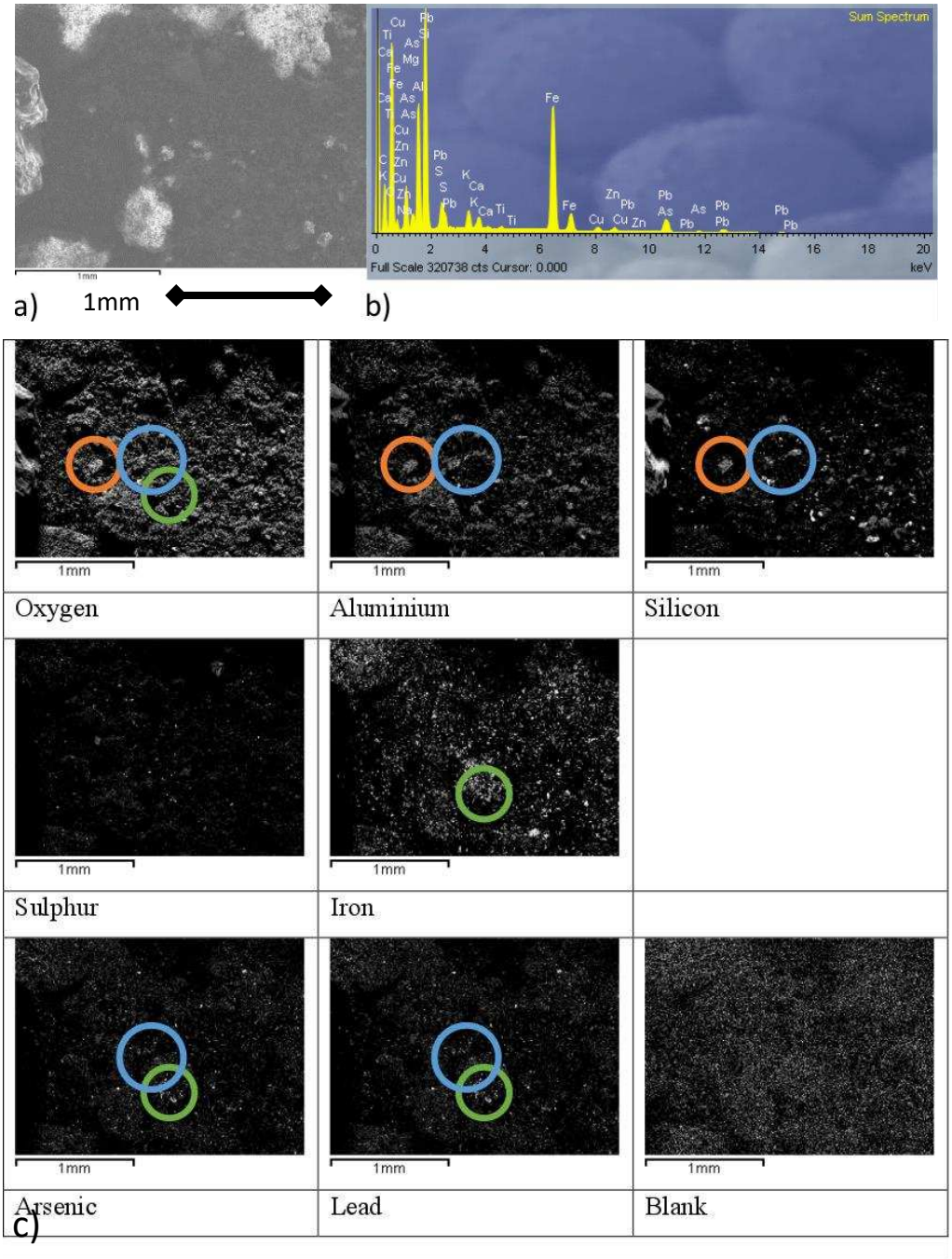

Figure 6.42 - a) SEM map area image showing S2wZA25, b) Corresponding EDX sum spectrum, and c) Corresponding EDX element map

6.8.11 SEM-EDX of S2wZA50 – Soil 2 in Water with 0.50g of Zeolite-A

SEM images after the addition of 0.50 g of Zeolite-A in Soil 2 residues are depicted in Figure 6.43. This array of images shows the sample from a distance and then how it appears as the microscope zooms. A piece of detritus was focused on in Figure 6.43a, denoted by the blue circle, due to the coating of fine particles over the surface, some of which appeared to be cube-like zeolite structures. This is shown more closely in the Figure 6.43b, surrounded in a blue border. This was then zoomed into again, at the site of the green circle, to determine the particle size and it is possible to see that the particles are agglomerated. This is shown by the green-bordered image, Figure 6.43c. Finally, the orange selection in the original image, a), was analysed in more detail. The result, Figure 6.43d, has an orange border and shows similar agglomerations as in Figure 6.44b.

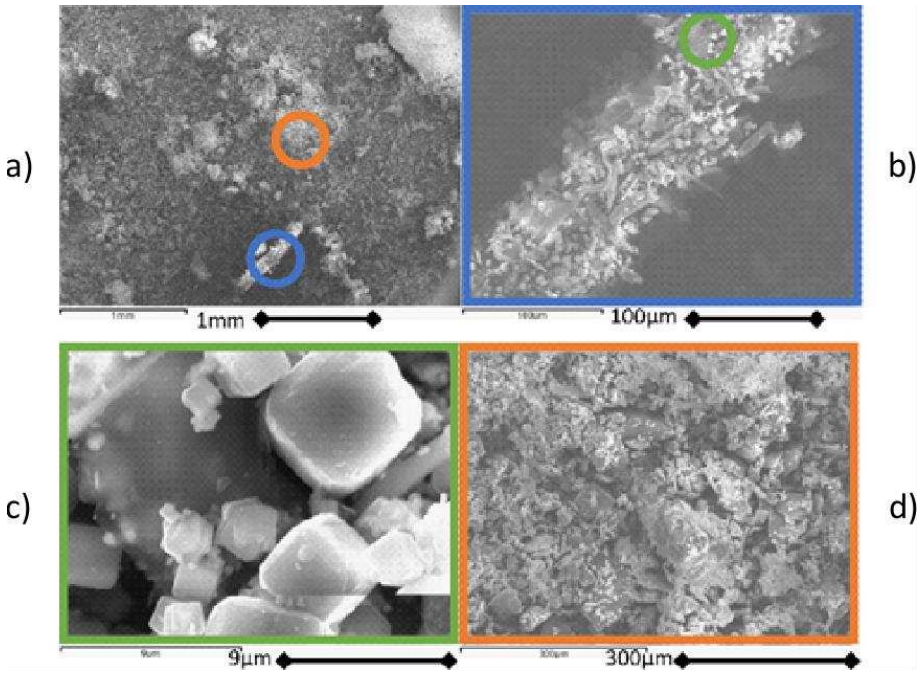

Figure 6.43 - a) SEM initial image showing S2wZA50, b) image of blue circle in (a) enlarged, c) image of green circle in (b) enlarged, and d) image of orange circle in (a) enlarged

Point-analysis of two distinctly different areas was completed, Figure 6.44a. The red arrow spectrum, Figure 6.44b, was of a cube-shaped particle. The spectrum shows very low intensity for iron but quite a significant amount of arsenic and lead. This suggests that an iron mineral is not the primary location for lead and arsenic to be located after remediation. The orange arrow, Figure 6.44a, points at a darker, more flat area and shows a different spectrum, with the focus on iron and only small peaks

present for lead. This area appears to be a darker colour and not to have the cube-like morphology. In the corresponding spectrum, Figure 6.44c, lead seems to still be present with iron, as in the original untreated soil.

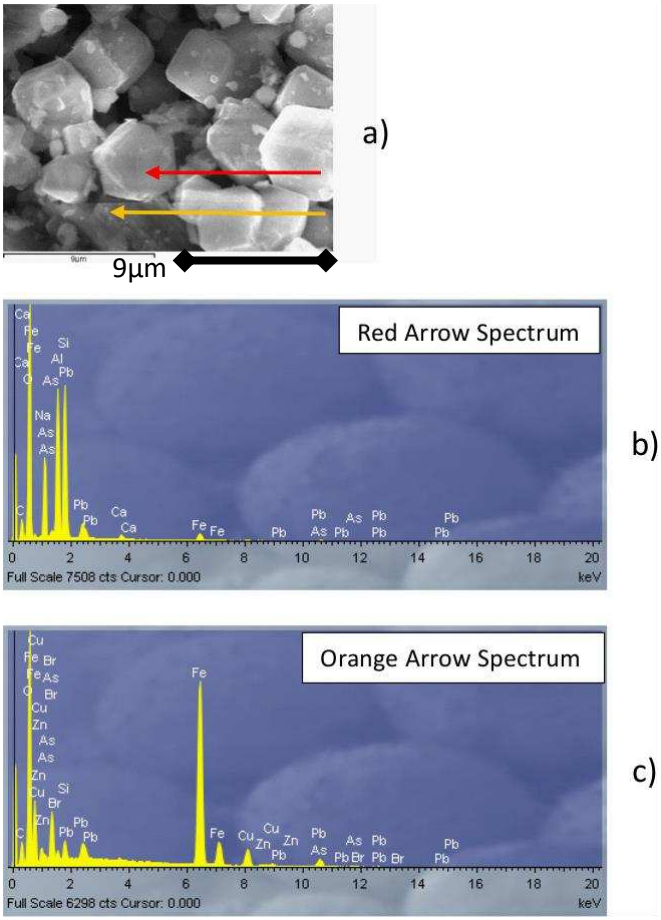

Figure 6.44 - a) SEM image showing S2wZA50, b) EDX spectrum corresponding to the point marked with a red arrow, and c) EDX spectrum corresponding to the point marked with an orange arrow

The element map, Figure 6.45c, suggests that oxygen, aluminium and silicon are all directly interacting. Iron is rather evenly dispersed, whilst sulphur and copper are difficult to detect. Lead and arsenic show areas of brightness, but all seem to be less than or equal to the brightness of the blank. The sum spectrum, Figure 6.45b, shows lead to be present as well as iron.

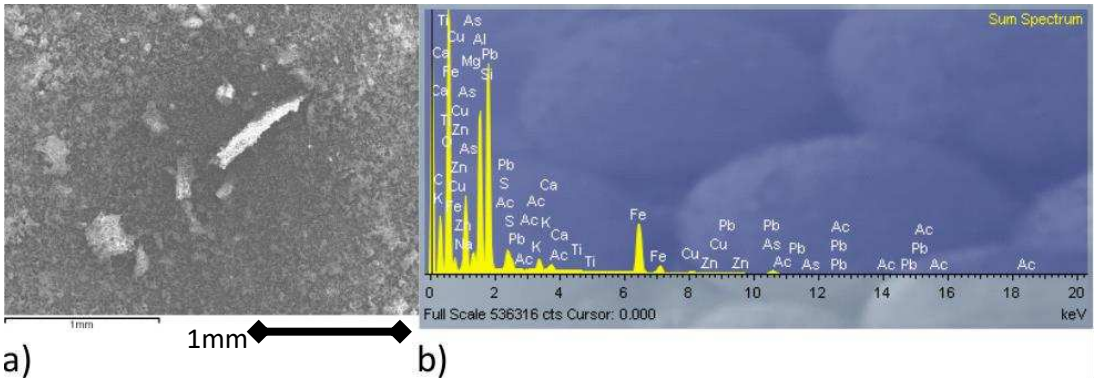

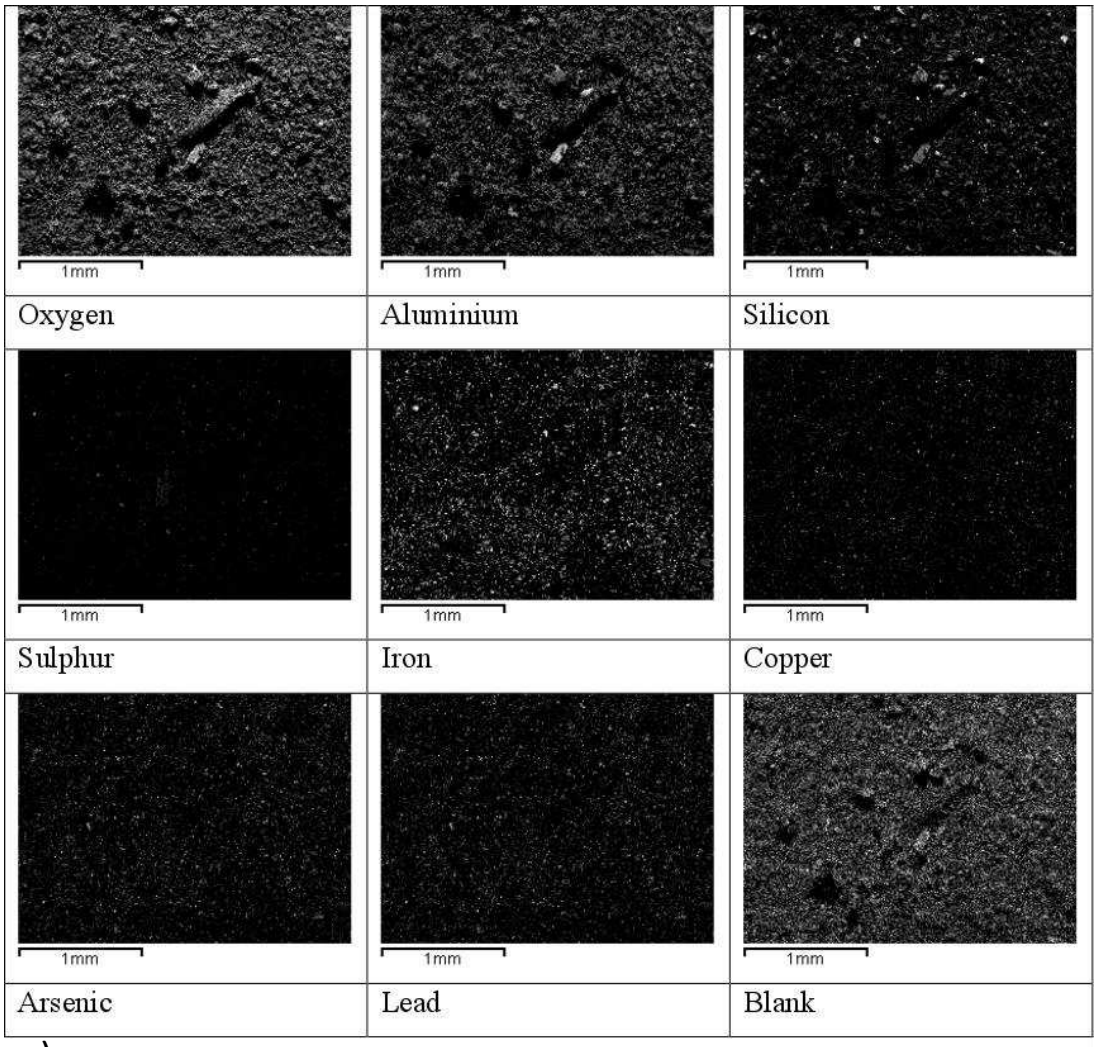

Figure 6.45 - a) SEM map area image showing S2wZA50, b) Corresponding EDX sum spectrum, and c) Corresponding EDX element map

6.8.12 XRF of Soil 2 in Water with Increasing Zeolite-A

The data presented in Figure 6.46 follows a similar trend to that observed for Soil 1, i.e. washing causes lead to be leached from the soil, but the extent to which the addition of zeolite affects the amount of lead in the soil residues is difficult to determine as the values are extremely low.

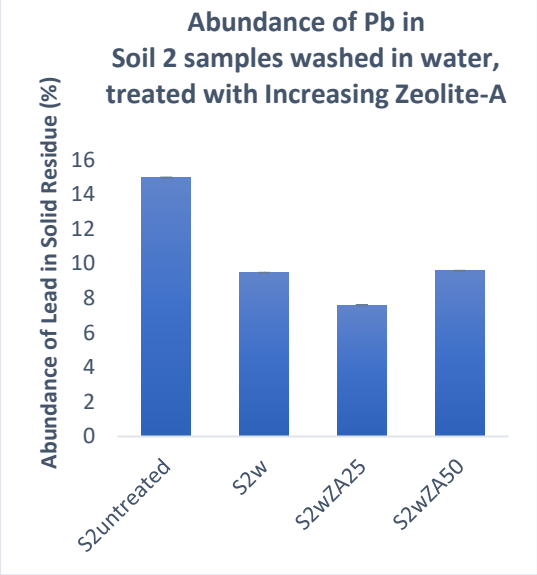

Figure 6.46 - XRF percentage composition of lead for Soil 2 (water)

The XRF data, Table 6.14, shows differences between the Soil 2 samples washed in water and treated with Zeolite-A. S2wZA25 and S2wZA50 both show the same elements present, and sodium now registers, unlike in S2untreated and S2w. This must be due to the addition of Zeolite-A. Silicon is decreasing between S2wZA25 and S2wZA50 due to the fact that the soils samples are not identical. Therefore, they will show varying percentage abundance. The purpose of this analysis was not to detect exact values, conversely, to determine if there was a significant abundance increase or decrease caused by leaching.

Table 6.14 - XRF elemental composition above 0.9% for S2untreated, S2w, S2wZA25, and S2wZA50

S2untreated		S2w		S2wZA25		S2wZA50	
Element	Percentage (%)	Element	Percentage (%)	Element	Percentage (%)	Element	Percentage (%)
Fe	39.36	Fe	39.30	Fe	32.03	Fe	27.41
Pb	14.97	Si	18.81	Si	25.12	Si	20.47
Si	14.85	Pb	16.04	Pb	14.47	Pb	17.89
K	8.22	As	6.89	Al	10.24	Al	14.06
As	6.07	Al	5.76	As	5.30	Na	6.04
Al	5.33	K	4.16	K	3.83	As	5.78
P	3.14	Ca	2.13	Na	2.12	K	2.33
Zn	1.69	Zn	1.71	Ca	1.94	Ca	1.50
Ca	1.64	Cu	1.47	Zn	1.34	Zn	1.35
Cu	1.50			Cu	1.13	Cu	1.08

6.8.13 XRD of Soil 2 in Acid

Table 6.15 shows the minerals present in each of the samples as detected with XRD. All of the washed and treated soils contained the same minerals. The lead silicate detected in S2untreated disappeared after treatment with acid. Instead, gismondine is identified, as it was for samples of Soil 2 washed in water. The peaks present for gismondine are able to be distinguished in Figure 6.47, the diffraction pattern for S2aZA25. The diffraction pattern for S2aZA50 is in Appendix 4. The pattern for S1aZA25 with gismondine overlaid is given in Figure 6.48.

Table 6.15 - Mineral components of S2untreated, S2a, S2aZA25, and S2aZA50 identified using the EVA database by Bruker

S2Untreated		S2a/S2aZA25/S2aZA50	
Albite	$K_{0.2}Na_{0.8}AlSi_3O_8$	Albite	$K_{0.2}Na_{0.8}AlSi_3O_8$
Chalcopyrite	$CuFeS_2$	Chalcopyrite	$CuFeS_2$
Copper Antimony Sulphide	Cu_3SbS_3	Copper Antimony Sulphide	Cu_3SbS_3
		Gismondine	$CaAl_2Si_2O_8{\cdot}4H_2O$
Hematite	α-Fe_2O_3	Hematite	α-Fe_2O_3
Illite	$K(Al,Fe)_2AlSi_3O_{10}(OH)_2{\cdot}H_2O$	Illite	$K(Al,Fe)_2AlSi_3O_{10}(OH)_2{\cdot}H_2O$
Koninckite	$FePO_4{\cdot}3H_2O$	Koninckite	$FePO_4{\cdot}3H_2O$
Lead silicate	Pb_3SiO_5		
Lead Sulphate	$PbSO_4$	Lead Sulphate	$PbSO_4$
Quartz	SiO_2	Quartz	SiO_2
Segnitite	$PbFe_3(AsO_4)(AsO_3OH)(OH)_6$	Segnitite	$PbFe_3(AsO_4)(AsO_3OH)(OH)_6$

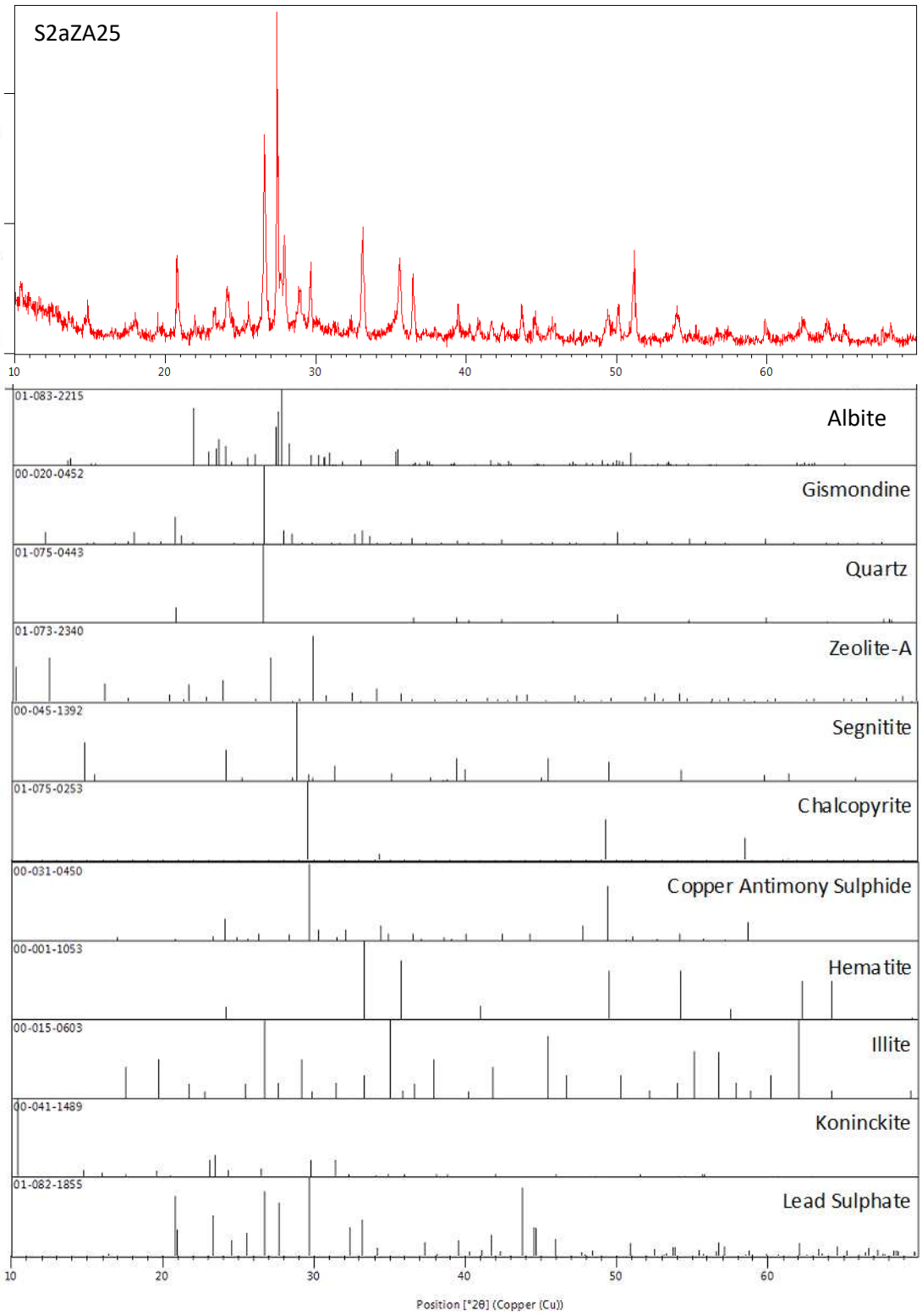

Figure 6.47 - XRD Pattern for S1aZA25 and corresponding minerals

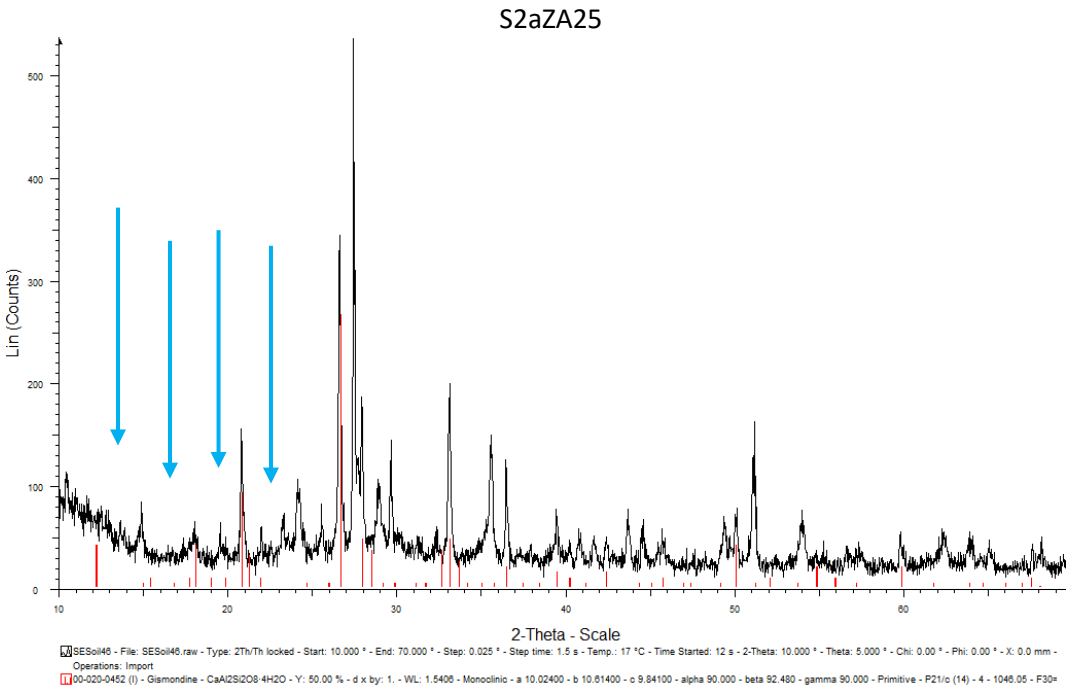

Figure 6.48 - XRD pattern of S2aZA25with gismondine peaks overlaid in red

6.8.14 SEM-EDX of S2aZA25 – Soil 2 in Acid with 0.25g of Zeolite-A

To determine the presence of Zeolite-A in the acid-treated samples, SEM-EDX was conducted. As in the other acid treated samples, cube-like particles of Zeolite-A are not visible in Figure 6.49a, which suggests that the material has dissolved and formed secondary minerals. The point-analysis spectrum, Figure 6.49b, shows that iron, lead and arsenic are still present as well as aluminium and silicon. There seems to be a considerable amount of potassium detected.

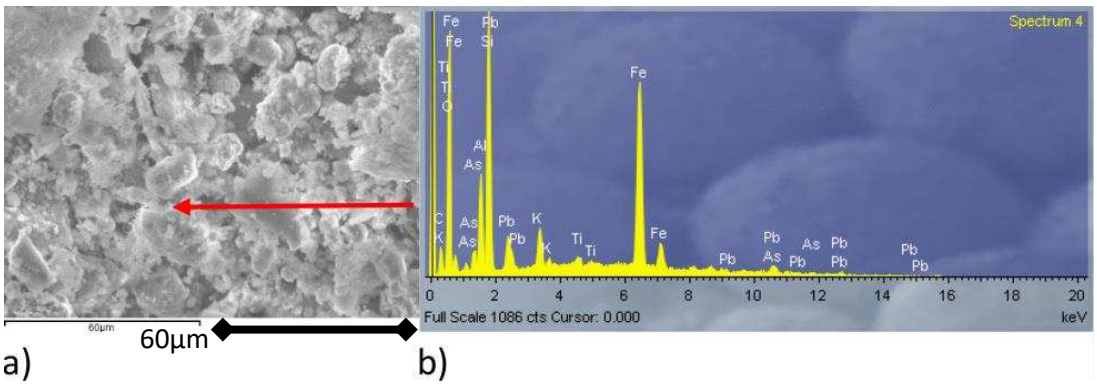

Figure 6.49 - a) SEM image showing S2aZA25 and b) EDX spectrum corresponding to the point marked with a red arrow

The element map, Figure 6.50c, did not detect significant sulphur or copper in this sample. Instead, both the sum spectrum, Figure 6.50b, as well as the map, showed

elevated amounts of potassium present. The blue circles show an area of potassium, oxygen, aluminium and silicon but not iron, the latter of which is marked with a red circle to show its absence. This suggests the presence of albite.

There is evenly dispersed arsenic and lead throughout the sample as opposed to being located in specific regions in high concentration. They appear to be a similar concentration to the blank.

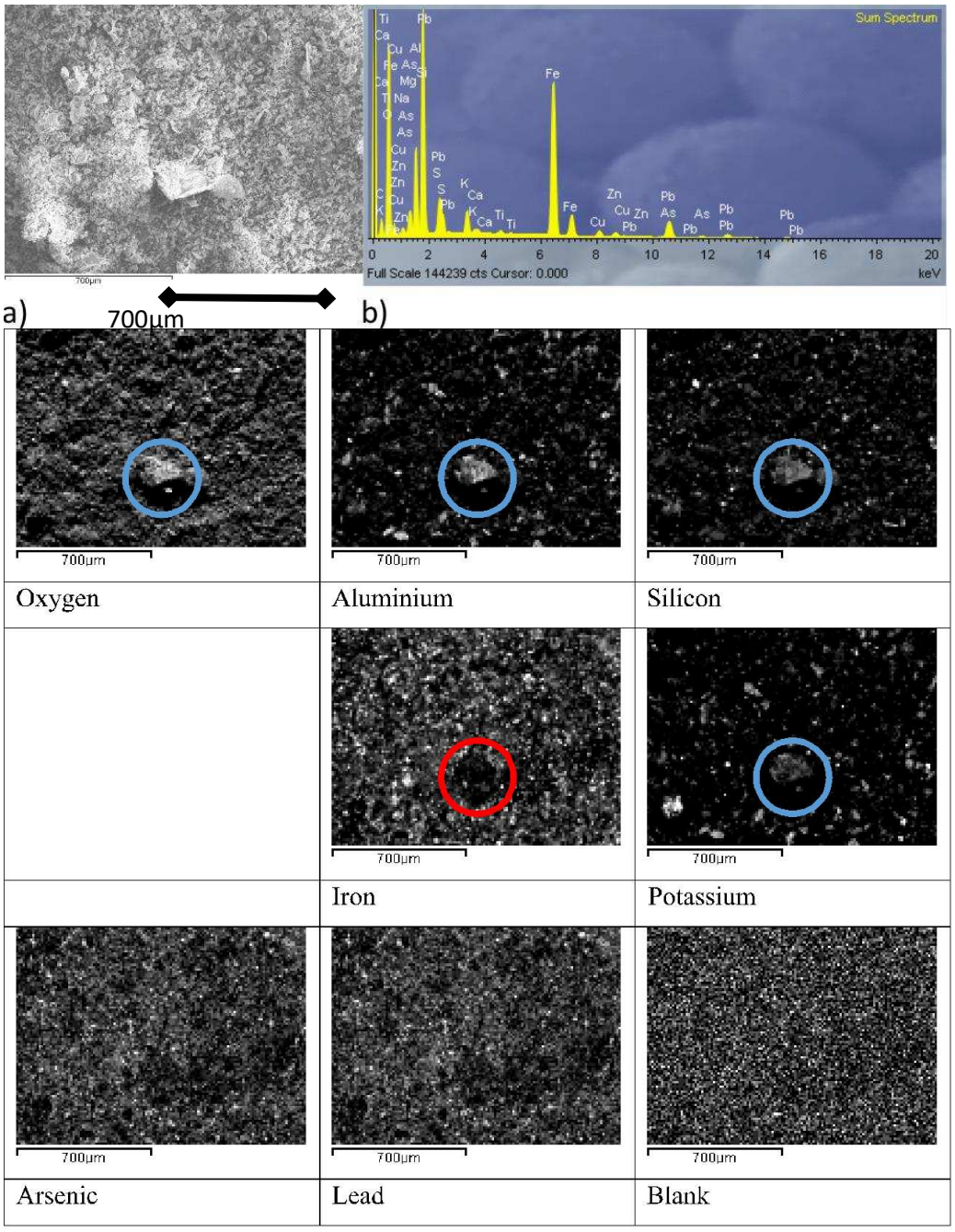

Figure 6.50 - a) SEM map area image showing S2aZA25, b) Corresponding EDX sum spectrum, and c) Corresponding EDX element map

6.8.15 SEM of S2aZA50 – Soil 2 in Acid with 0.50g of Zeolite-A

As with Soil 1, the higher Zeolite-A addition does not result in the presence of cube-like morphologies associated with Zeolite-A, Figure 6.51a. The point analysis of this area shows a high concentration of iron, lead and arsenic, Figure 6.51b. There is also silicon, aluminium and copper present. Sodium does not appear.

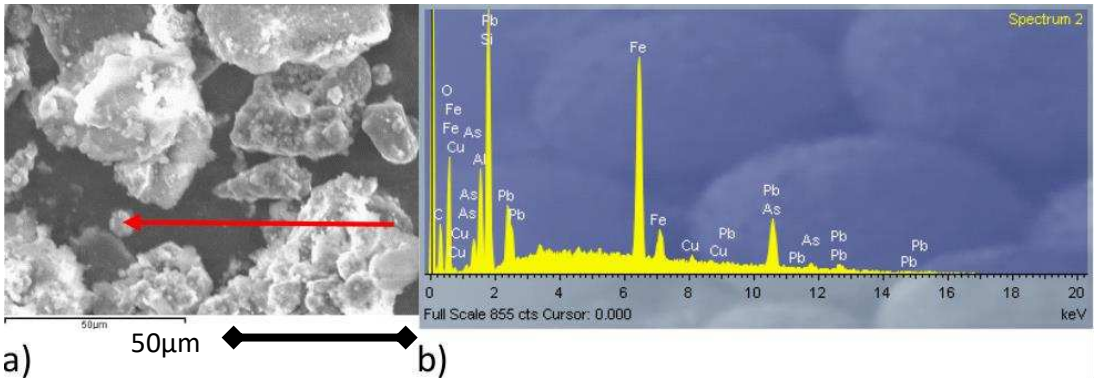

Figure 6.51 - a) SEM image showing S2aZA50 and b) EDX spectrum corresponding to the point marked with a red arrow

Figure 6.52a shows a range of different looking particle agglomerations. Some particles appear darker and with a flat surface, whilst others are white and grainy. The latter appears to be related to iron oxide whilst the former is followed by aluminium, oxygen and silicon, denoted by the blue circles. Lead and arsenic are present in the area composed of iron oxide as shown by the red rectangle.

There appears to be only a very small amount of sulphur present in the map, which falls below the detection limit shown for the blank. Arsenic and lead appear in a low concentration with some higher concentrations in particular regions. The same can be said for iron that appears inversely related to both aluminium and silicon.

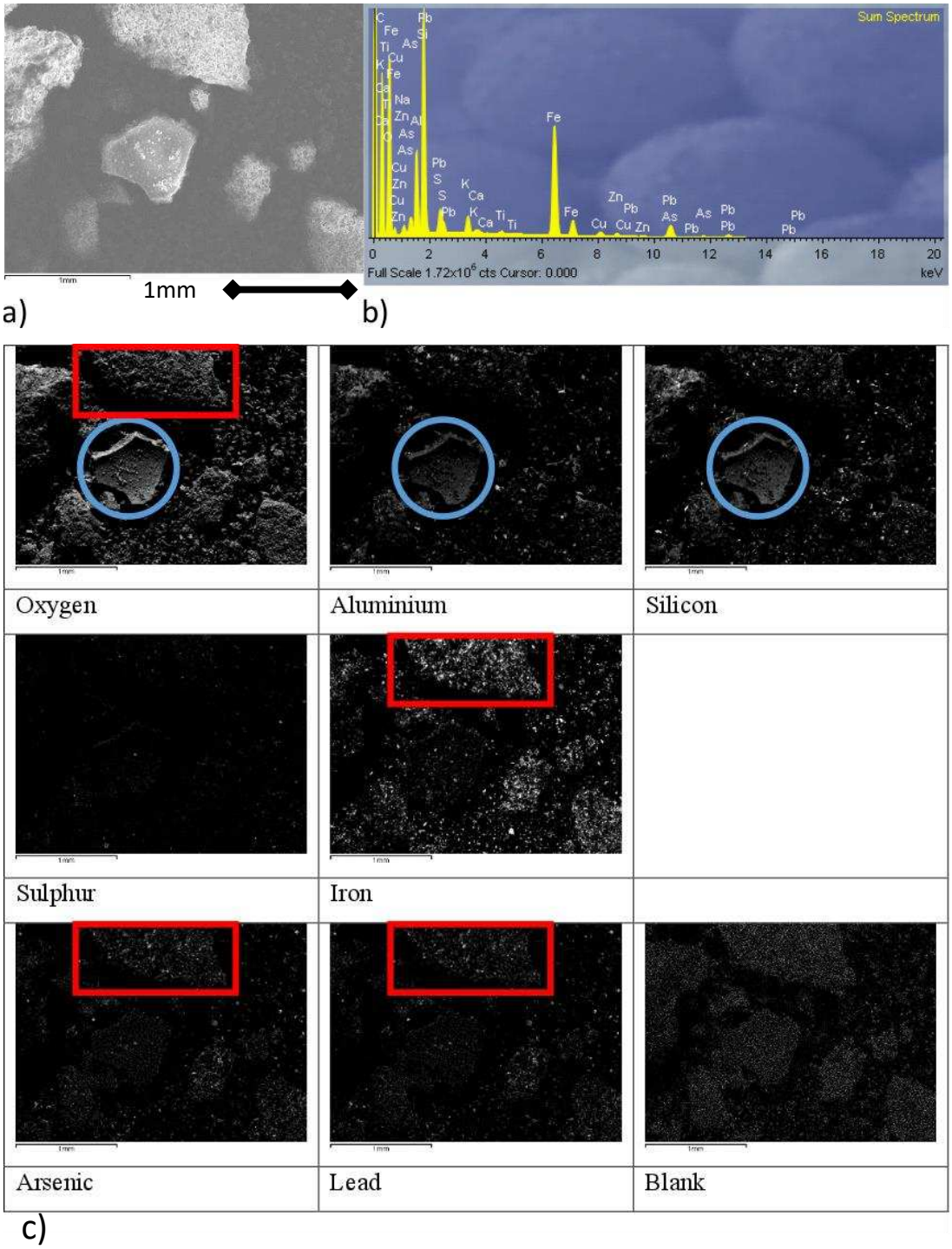

Figure 6.52 - a) SEM map area image showing S2aZA50, b) Corresponding EDX sum spectrum, and c) Corresponding EDX element map

An additional map was included due to disparities with the previous area analysed.

In the element map (Figure 6.53c), the amount of potassium is quite high due to illite. It can also be seen that lead and arsenic follow iron and oxygen in the areas shown by the orange circles, indicating an iron oxide interacting with the heavy metals. The area in the sulphur map, circled in blue, follows a bright area of oxygen,

lead and arsenic quite clearly. This could be due to lead sulphate. The amount of potassium detected is quite high due to illite and albite. The green circles show a connection between the heavy metals and a silicon oxide, possibly associated with gismondine.

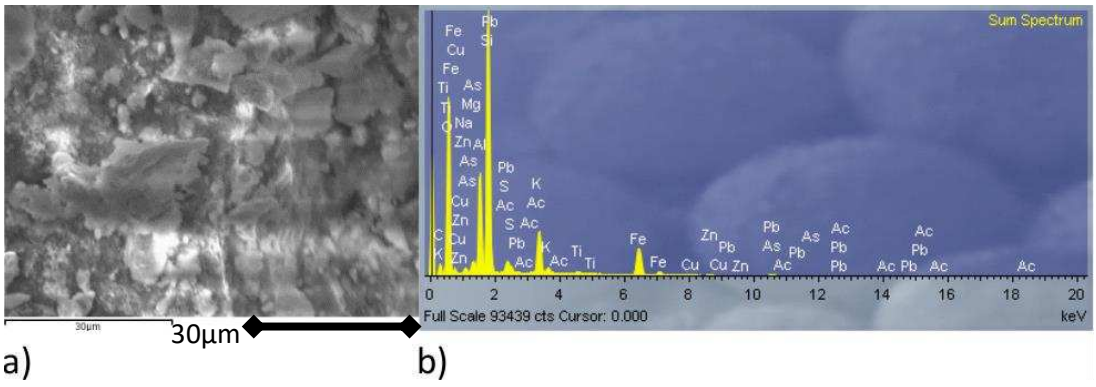

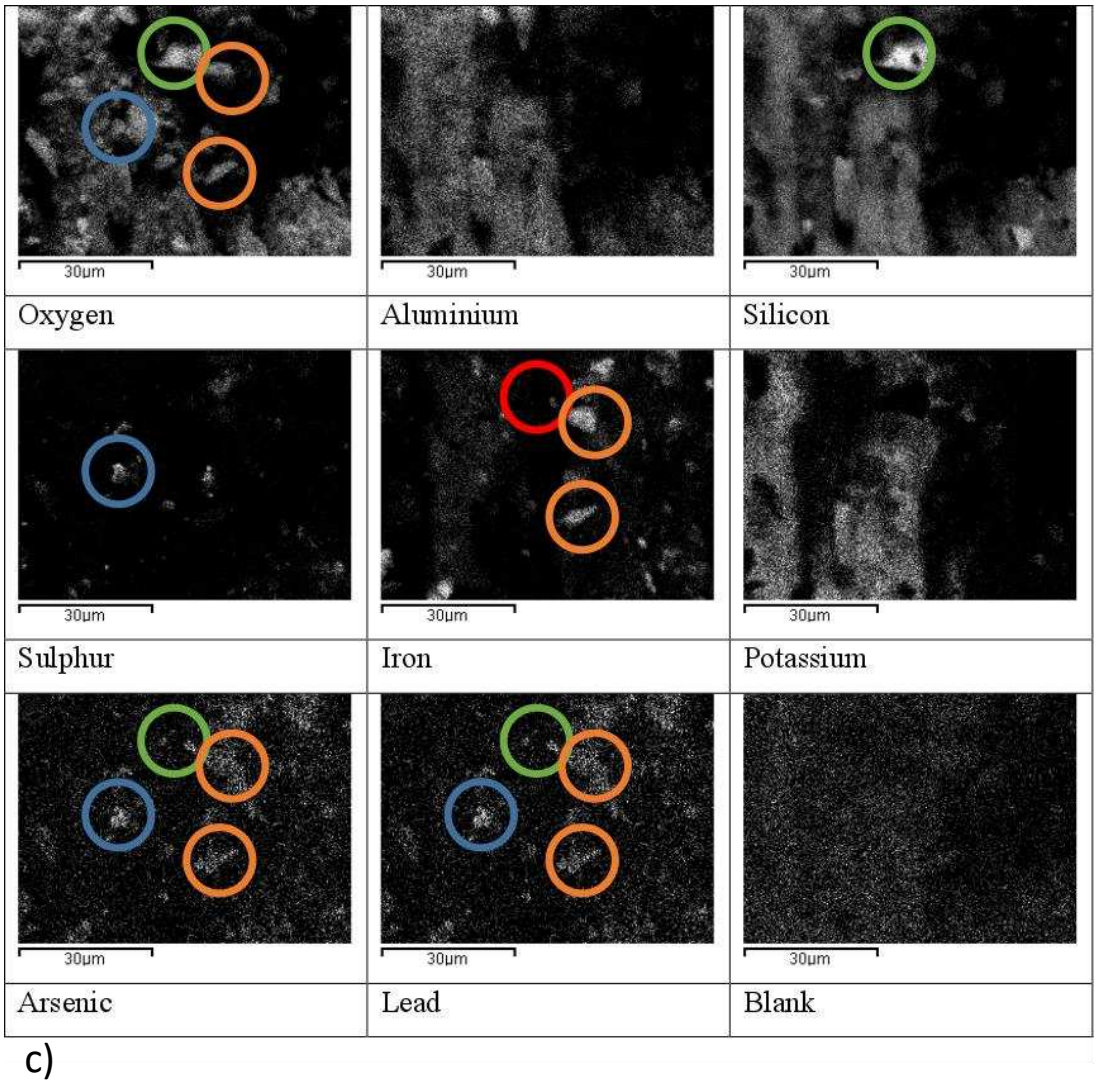

Figure 6.53 - a) SEM map area image 2 showing S2aZA50, b) Corresponding EDX sum spectrum 2, and c) Corresponding EDX element map 2

6.8.16 XRF of Soil 2 in Acid with Increasing Zeolite-A

The untreated soil shows a high concentration of lead as it has not been washed. The washed and treated soils show below 10% abundance and are within 4% of each other. As in the other soil residues, the low values make it difficult to detect an accurate trend, Figure 6.54.

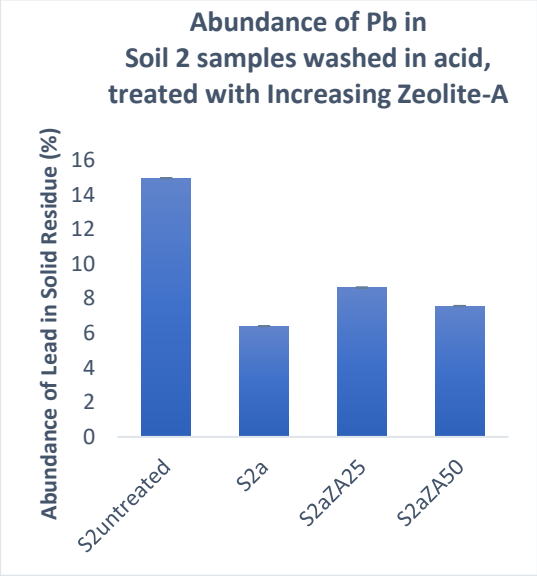

Figure 6.54 - XRF percentage composition of lead for Soil 2 (acid)

The data confirms that S2a, S2aZA25 and S2aZA50 have the same elements present, Table 6.16. The potassium detected in the EDX spectrum of the treated soils is explained by the presence of illite. XRF data confirms that potassium is detected above 0.9%.

Table 6.16 - XRF elemental composition above 0.9% for S2untreated, S2a, S2aZA25, and S2aZA50

S2untreated		S2a		S2aZA25		S2aZA50	
Element	Percentage (%)	Element	Percentage (%)	Element	Percentage (%)	Element	Percentage (%)
Fe	39.36	Fe	39.18	Fe	35.80	Fe	31.01
Pb	14.97	Si	23.88	Si	23.24	Si	24.74
Si	14.85	Pb	11.72	Pb	15.37	Pb	14.62
K	8.22	Al	6.60	Al	7.61	Al	13.41
As	6.07	As	6.04	As	7.42	As	6.03
Al	5.33	K	4.50	K	3.32	K	3.45
P	3.14	Zn	1.63	Zn	1.59	Ca	1.48
Zn	1.69	Ca	1.62	Ca	1.44	Zn	1.36
Ca	1.64	Cu	1.34	Cu	1.33	Cu	1.13
Cu	1.50						

6.9 XRF for Treated Soil 1 and 2 in Water

Soil 1 shows an increase in aluminium and silicon upon addition of zeolite in the solid residue, Figure 6.55. Conversely, there is a decrease in iron and sulphur. Arsenic and zinc are not detected in Soil 1. Copper and lead appear to stay present at a consistent amount. Potassium decreases, whilst sodium is increasing. This is probably due to the excess zeolite added, containing sodium ions. Partial ion exchange probably occurred with the sodium ions present in Zeolite-A.

Soil 2 follows a similar trend for the compounds. Aluminium and silicon increase upon addition of zeolite whilst iron decreases. Arsenic, calcium and potassium are present and appear to decrease slightly. Sulphur is detected in S2untreated only. There is a small amount of copper present and sodium is only detected in the soil treated with Zeolite-A. It increases significantly with further addition of zeolite, as expected.

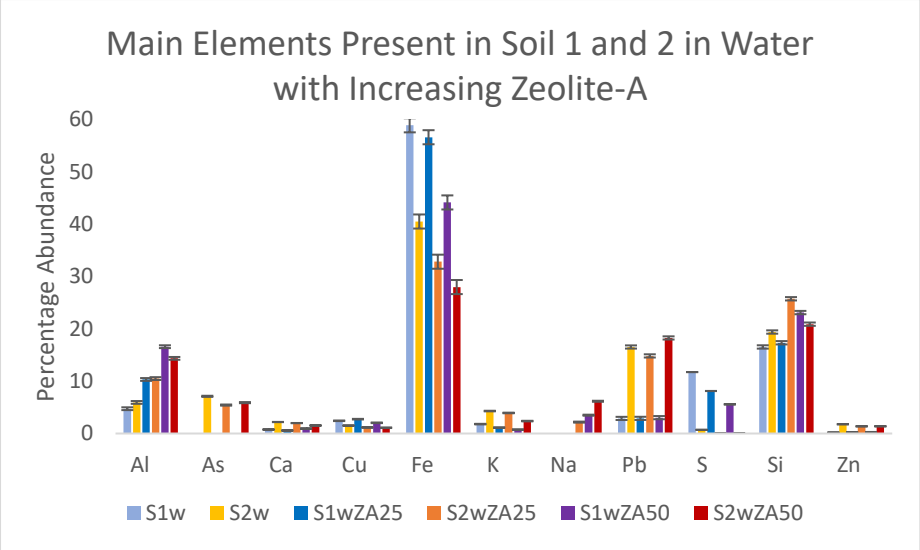

Figure 6.55 - XRF of Soil 1 and Soil 2 in water, normalised to 100%

6.10 XRF for Treated Soil 1 and 2 in Acid

The percentage of elements in the soil washed in acid is similar to the data from soil washed in water, Figure 6.56. The only differences are as follows; there is no sodium present in any of the soils. The acidic solutions could have caused any sodium present to be leached into solution. This would support the hypothesis that the Zeolite-A structure dissolves at a low pH and also that lead ions may exchange with sodium ions. As previously discussed in Section 6.3.3. It has been shown in other studies that sodium ions will exchange with cations including barium (Sherry & Walton, 1967).

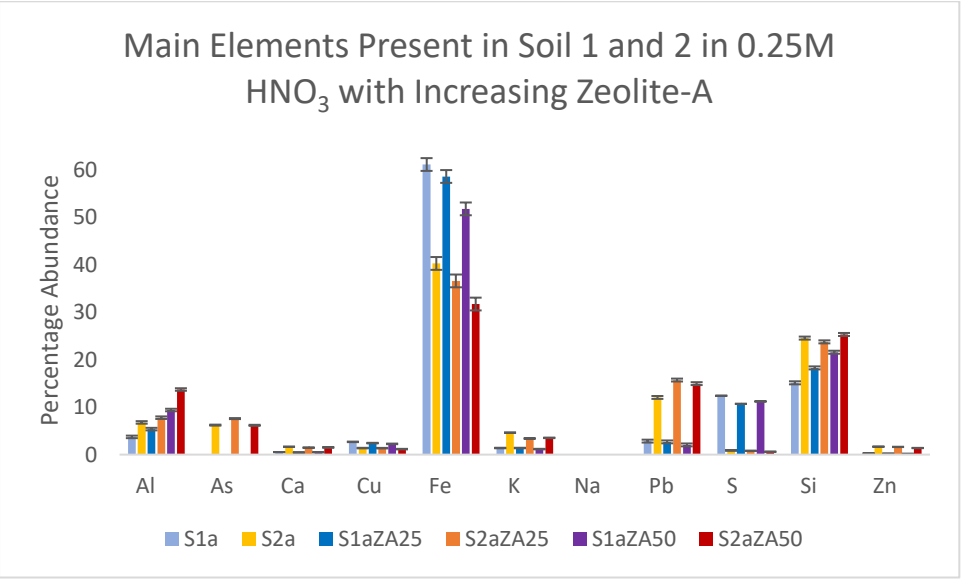

Figure 6.56 - XRF of Soil 1 and Soil 2 in dilute acid, normalised to 100%

6.11 Conclusions

- The untreated soil samples, taken from two different site locations, show qualitative and quantitative differences.
- S1untreated contains numerous sulphur, phosphate and zinc compounds, whilst S2untreated is composed of albite. The main compounds for both soils are hematite, pyrite and quartz.
- Washing both soils in water or dilute acid resulted in a new secondary mineral appearing. XRD patterns and matching software suggest that this phase may be due to gismondine as the pattern for lead silicate disappears.
- The secondary mineral appears in higher quantities after addition of Zeolite-A to the soil samples.
- According to Braithwaite et al, Gismondine can form via hydrothermal synthesis from fly ash, similarly to Zeolite-A.
- Gismondine has the capability to undergo ion exchange with the calcium ions inside its structure. As mentioned in Section 2.10.2, the calcium ions in gismondine are known to exchange with barium ions.
- Addition of Zeolite-A helps to raise the pH of the soil which decreases the leaching capability of the system. It can also be seen that addition of Zeolite-A has a direct link with the decrease of lead.
- Therefore, it is suggested that the addition of Zeolite-A works in several ways. It increases the pH, helps with the formation of the secondary mineral, undergoes ion exchange with lead ions and takes part in ion exchange, substituting its own sodium ions for lead ions.

Chapter 7 Leaching Experiments

7.1 Aim

The aim of this section is to detail the results of the leaching experiments conducted on the soils. As previously discussed, 0.00 g, 0.25 g and 0.50 g of synthesised Zeolite-A were added to soil that was then shaken in dilute nitric acid or purified water. The collection of the leachate was detailed in Section 5.9.1 and 5.9.2. The results will show that the addition of Zeolite-A does affect the recorded values of lead concentration in the liquid leachate, as determined by using Flame and Graphite Furnace Atomic Absorption Spectroscopy (FAAS/GFAAS). The amount of lead detected in the leachate decreases, which implies that the Zeolite-A must somehow be interacting with the soil and keeping the lead from escaping.

7.2 Introduction

Leachate experiments are used to determine the long-term impact of contaminating species on the groundwater pathway in soils (Kruger et al., 2012). They are often used for in-depth geochemical analysis and involve soil column experiments. The benefits of soil column experiments are that they provide a clearer representation of water flux. They allow for the consideration of the mobility between contaminants as well as the the movement of the contaminant within the soil (Katagi, 2013; Helling & Dragun, 1981; Lynch, 1995; OECD, 2004). What is covered in the current study, is a brief introduction to this method that includes analysis of the pH of the soil leachates. Future work could offer more in-depth analysis of the leachate experiments started in this chapter.

The detection limits of both the FAAS and the GFAAS were detailed in Section 3.1.3. Due to the limits being extremely low, they are not marked on any of the data graphs, as they would not show up above the lower axis due to the scale.

7.3 pH of Soil Leachate

The pH of the soil leachates provide insight regarding the effect of washing and adding Zeolite-A to the soils. The naming designations are described in detail in Section 5.9.3. The pH values are recorded in Figure 7.1.

It is clear that the addition of Zeolite-A causes an increase in the pH for both soils. For S1w, the addition of Zeolite-A increases the pH by 2.69. Doubling the amount of zeolite from 0.25 g to 0.50 g increases the pH by an additional 0.91, from 1.37 to 4.97. S2w produces a slightly greater change, addition of zeolite increases the pH by 2.99 and further addition increases it by another 0.96, totalling an increase of 3.95, from 4.94 to 8.89.

Washing the soil with acid reduces the pH of both Soil 1 and 2 to 0.17 and 0.30, respectively. S1a shows that an initial addition of zeolite results in an increase in pH by 2.12. Further addition increases the pH by an additional 0.3, totalling a 2.42 pH increase, from 0.17 to 2.59. Instead, S2a increases by 2.11 units and then a further 0.60 when 0.25 g and 0.50 g of Zeolite-A is added, respectively. This results in a total pH increase of 2.71, from 0.30 to 3.01.

These trends are particularly interesting as the initial addition of 0.25 g of Zeolite-A results in a pH increase of 2.11-2.99, independently of the original pH of the soil. This corresponds to a range of 60-1200% increase. Adding 0.50 g of zeolite increases the pH by a further 0.30-0.96 units. These samples, ending -ZA50, only resulted in a subsequent increase of 13-25% of the pH. This is only a 14-34% return of pH increase upon the additional increase of zeolite.

The data shows that Zeolite-A has the ability to increase pH but is bound by particular factors. These factors are based on a buffer system. At a low pH, Zeolite-A dissolves and raises the pH. After a rise in pH by 2 units, additional zeolite then acts as a buffer; the pH only increases further by a small amount. In the soils washed in water, Zeolite-A stays intact and increases the pH of both soil leachates by approximately 3 units. Further addition of zeolite then acts as a buffer as the further increases of pH is small. It is interesting to discover that regardless of initial pH, Zeolite-A affects the pH of soils in a regular and consistent manner.

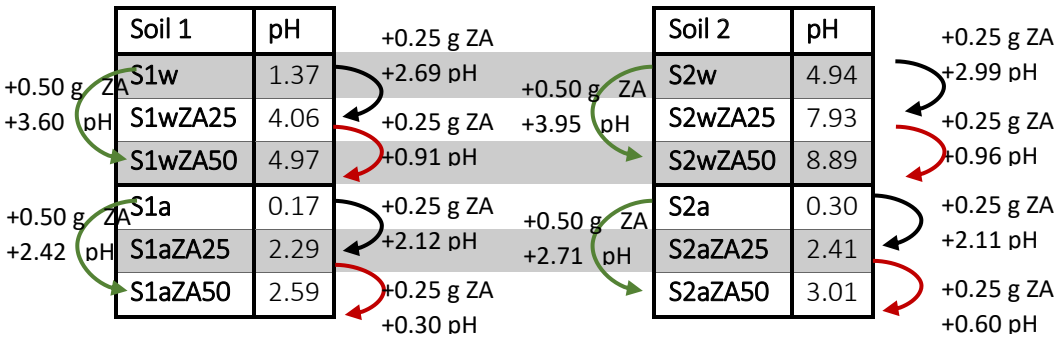

Figure 7.1 - pH of soil samples with noted changes in pH with the increase of Zeolite-A

7.4 Analysis of the Leachates for S1w, S1a, S2w and S2a

7.4.1 FAAS of the Leachates of S1w and S1a

To determine the total concentration of lead, the leachates of Soil 1 were obtained by washing the soil sample in purified water as well as 0.25M HNO_3. These leachates were initially analysed using FAAS. Figure 7.2 shows that S1w and S1a are both identifying lead as being present, however, at extremely low levels that fall well below the legal limits previously discussed.

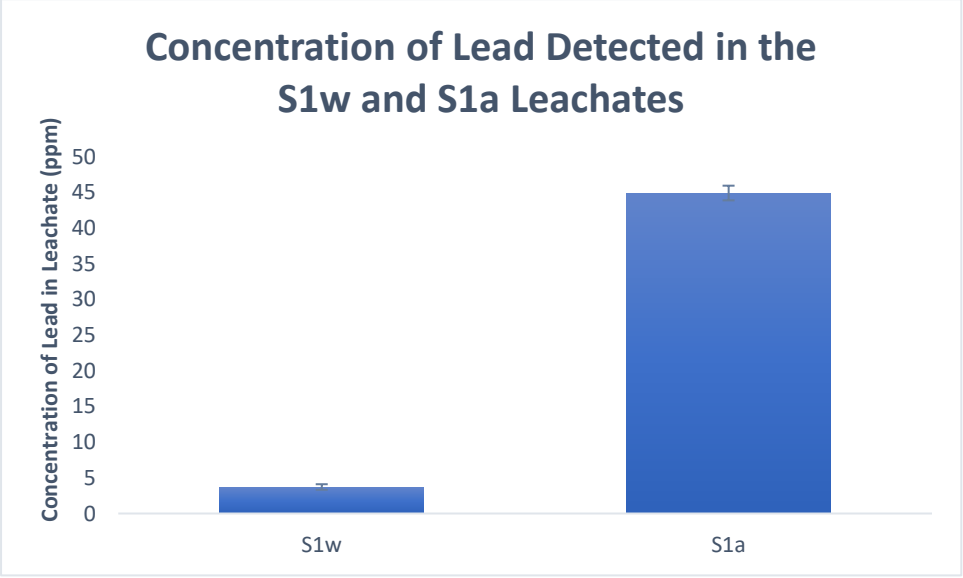

Figure 7.2 - FAAS results showing the concentration of lead in S1w and S1a leachates

7.4.2 GFAAS of the Leachates of S1w and S1a

The leachates from S1w and S1a were analysed using the graphite furnace, Figure 7.3. It was hypothesised that the flame, in FAAS, did not reach high enough temperatures, or have enough time to heat the samples to cause breaking down of the lead molecules. This would explain the lower concentration of lead being present,

i.e. not being within detection limits of the instrument. This is discussed, in detail, in Section 5.7.

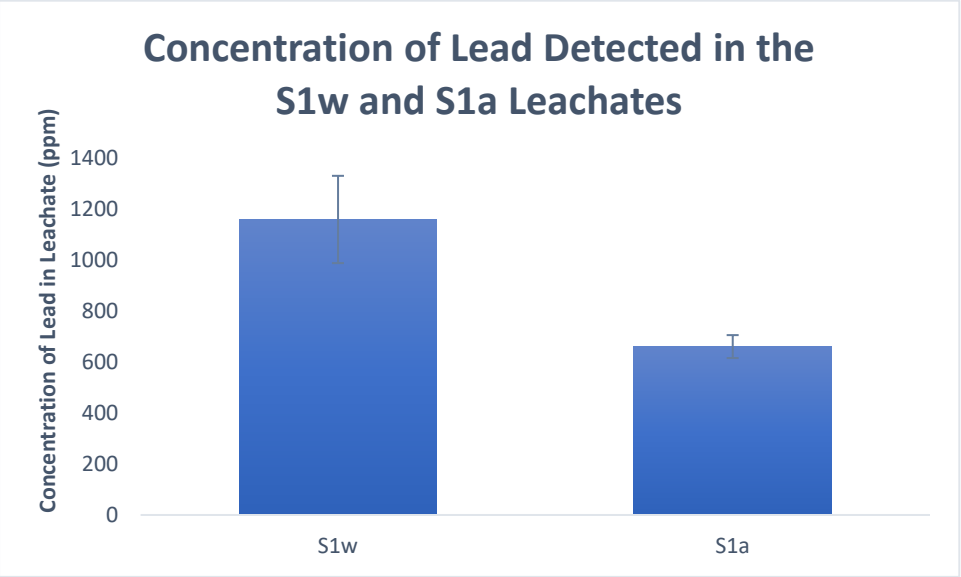

Figure 7.3 - GFAAS results showing the concentration of lead in S1w and S1a leachates

In addition, purified water was used instead of deionised water in order to produce results with more accuracy. The results indicate that the GFAAS detects significantly higher concentrations of lead present in both the acid and water leachates.

However, it appears that less lead is detected in the leachate when the soil is washed with acid. This is probably a secondary mineral effect. Lead ions could be staying in the soil due to the additional acid reacting to form another compound, such as a lead-substituted gismondine. S1w has a pH of 1.30, so the soil is already under acidic conditions. Adding additional acid via washing decreases the pH to 0.17. This is not a significant change in pH and therefore, including the error bars, there is only a difference of approximately 300 ppm. Overall, the results are still above the EPA recommendations for lead in residential soil.

7.4.3 FAAS of the Leachate of S2w and S2a

Figure 7.4 shows a concentration of S2a that is over the EPA recommended levels for lead in any area. This is especially significant because the FAAS detects less lead than actually present and as previously reported using ICP-MS analysis (Appendix 1). S2w does not show significant lead concentration because the flame did not

provide enough energy to disperse the ions sufficiently. The pH of S2w was recorded to be 4.94, and S2a was 0.30. The low pH of S2a caused Zeolite-A to dissolve, as discussed in Section 6.3.2, thus rendering its remediation capabilities less effective. In addition, it is possible that some of the soil components may not be acid-leachable.

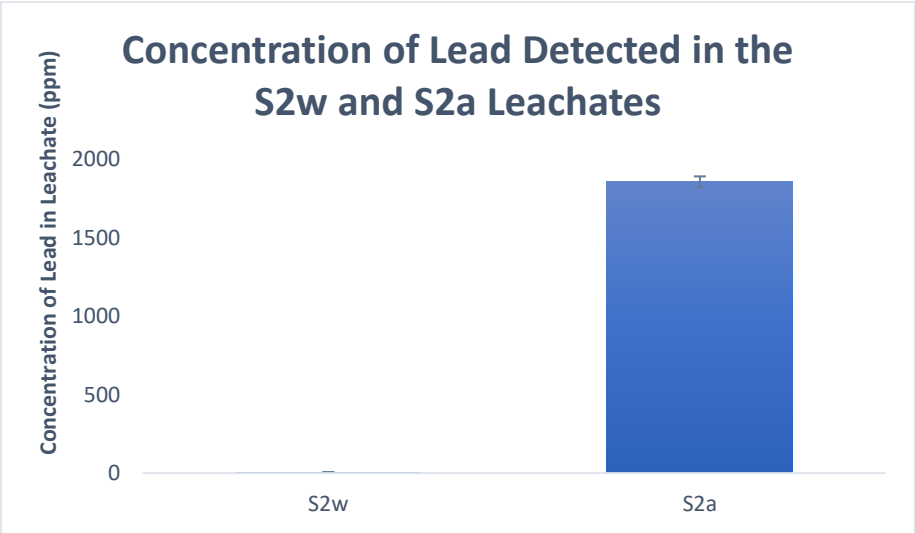

Figure 7.4 - FAAS results showing the concentration of lead in S2w and S2a leachates

7.4.4 GFAAS of the Leachate of S2w and S2a

Analysis of the leaching for S2w and S2a using GFAAS demonstrates high amounts of lead present in the leachate, Figure 7.5. Comparing rinsing with dilute acid and deionised water shows that there was more lead in the acidic leachate. This shows that the acid rain that Sweden experienced may have caused a large surge of heavy metals to leach into the nearby river, more than had been leaching due to rain alone.

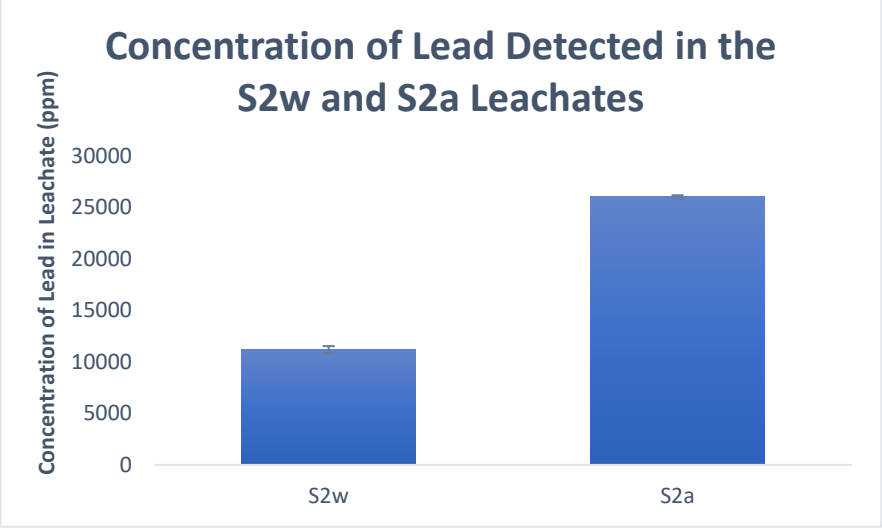

Figure 7.5 - GFAAS results showing the concentration of lead in S2w and S2a leachates

7.5 Analysis of the Leachate from Treated Soil 1 in Water or Acid with Increasing Zeolite-A

7.5.1 FAAS of the Leachate of Soil 1 in Water with Increasing Zeolite-A

Initial studies involved the use of FAAS. Figure 7.6 shows a successful trend of the remediation for Soil 1 in water, with an initial concentration of lead, in S1w, being high and then decreasing upon further addition of Zeolite-A. This implies that the amount of Zeolite-A added has an effect on the remediation of lead. However, it is important to note that the concentrations recorded are extremely low and, therefore, being used for trend purposes only.

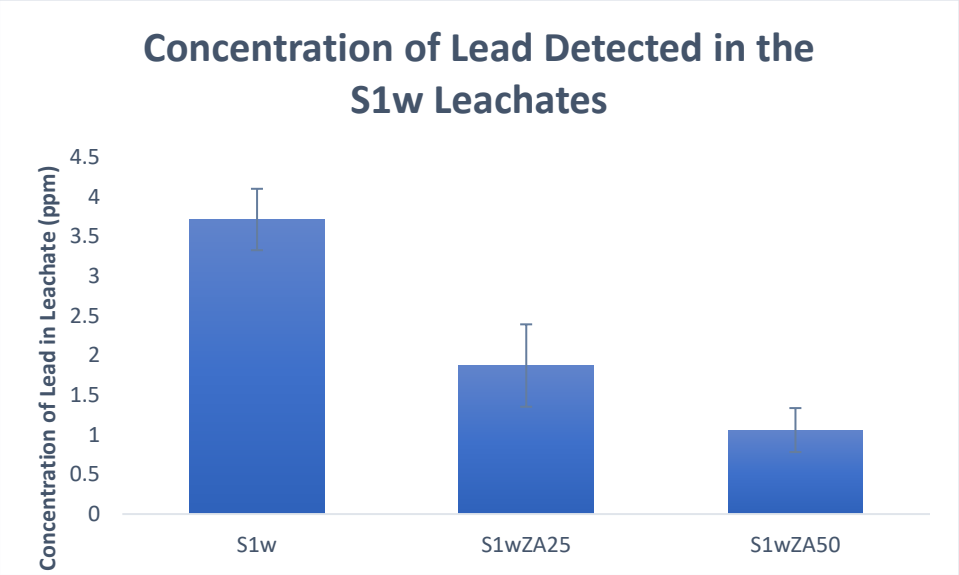

Figure 7.6- FAAS results showing the concentration of lead in S1w leachates with increasing Zeolite-A

7.5.2 GFAAS of the Leachate of Soil 1 in Water with Increasing Zeolite-A

As with the untreated soils discussed in Chapter 4, it was decided to use GFAAS instead of FAAS and Figure 7.7 shows that this method has a more a realistic concentration of lead. The concentration of lead in the S1w leachate is significantly higher than the EPA suggested limits for residential areas. However, it is less than 2000 ppm and, therefore, below the recommended safe levels for non-play areas.

Figure 7.7 indicates that the addition of Zeolite-A reduces the concentration of lead detected in the leachate to a negligible value. Further addition of Zeolite-A does not seem to have any measurable effect as the original addition was sufficient.

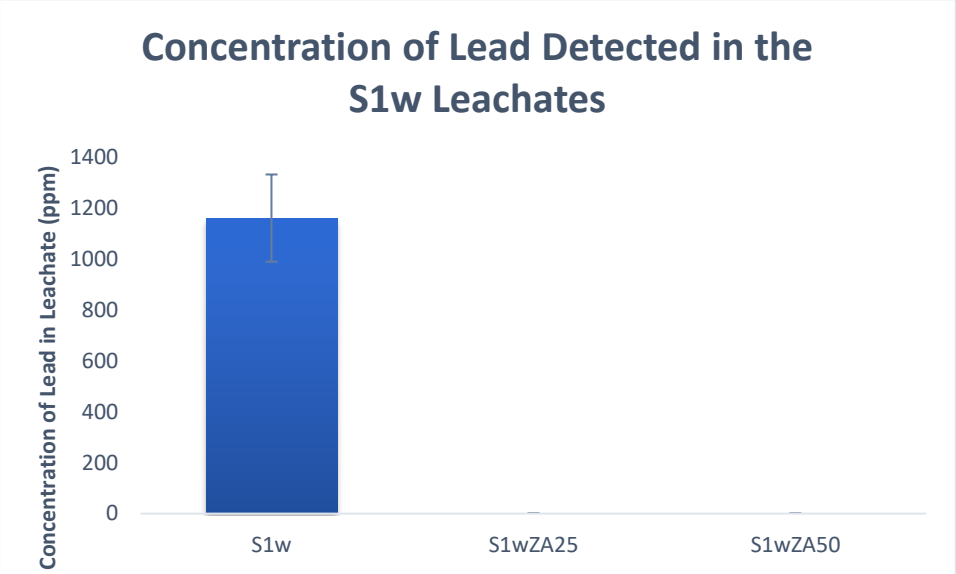

Figure 7.7 - GFAAS results showing the concentration of lead in S1w leachates with increasing Zeolite-A

7.5.3 FAAS of Leachate of Soil 1 in Acid with Increasing Zeolite-A

As with Soil 1 washed in water, the leachate of Soil 1 washed with dilute acid was analysed by FAAS. Figure 7.8 shows a decrease in the concentration of lead in Soil 1 upon initial addition of Zeolite-A when in acidic solution. There is a further decrease as more zeolite is added.

By washing a sample of Soil 1 with 0.50 g of Zeolite-A and 30 ml of acid, rather than the usual 15 ml, reported as sample S1aZA50A2, it can be seen that the concentration of lead is higher compared to S1aZA50. This is because Zeolite-A partially dissolves in acid and further addition of acid thereby dissolves more of the Zeolite-A, rendering the technique ineffective in an acidic environment. Hence, increasing the amount of acid encourages leaching of heavy metals from soil. However, the FAAS, again, shows low concentrations of lead, which are too low to be realistic, as discussed in Chapter 4.

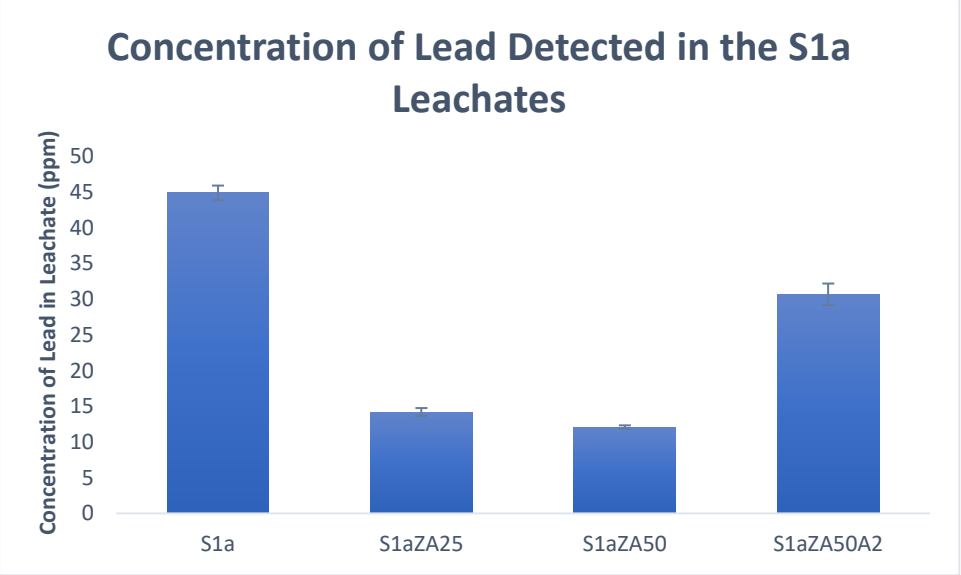

Figure 7.8 - FAAS results showing the concentration of lead in S1a leachates with increasing Zeolite-A

7.5.4 GFAAS of Leachate of Soil 1 in Acid with Increasing Zeolite-A

Analysis with the more suitable graphite furnace shows the same overall trend, as reported by the FAAS; adding zeolite decreases the concentration of lead, Figure 7.9. However, the initial decrease is only around 100 ppm. The values after addition of Zeolite-A are found to be high, and when potential experimental error, S1a and S1aZA25 have overlapping values within two standard deviations, corresponding to a 95% confidence interval. It is not possible to conclusively determine if the initial addition of Zeolite-A results in a decrease of the concentration of lead. It is possible that the initial addition of zeolite is completely dissolved and no reduction of lead concentration in the soil leachate has occurred. Further addition causes a substantial decrease in the concentration of lead, implying that not all of the Zeolite-A dissolves in S1aZA50 and that some of it is able to act as it did in the water-washed soil. Despite Zeolite-A being dissolved in the acid, it is still worth noticing that further addition of Zeolite-A is nevertheless successful in a highly acidic environment.

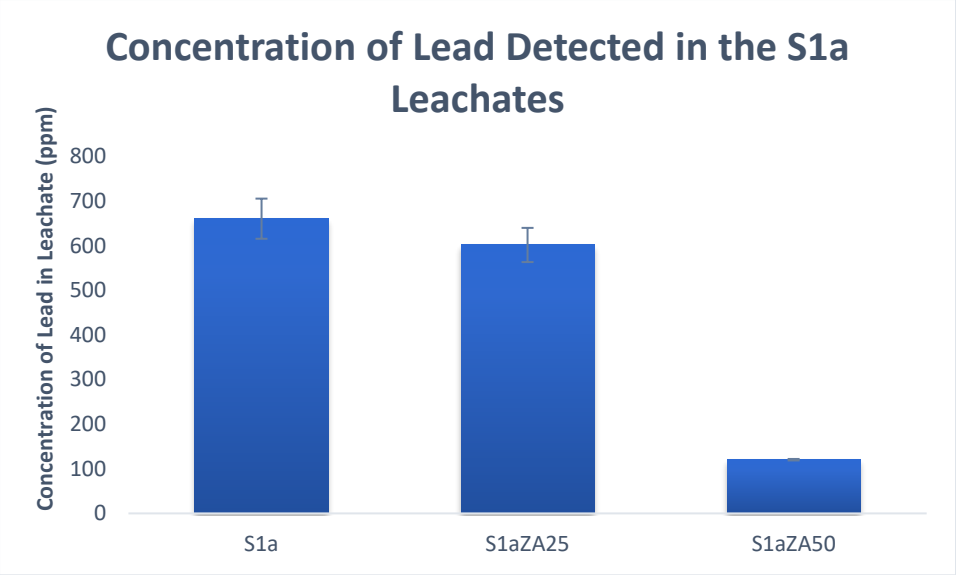

Figure 7.9 - GFAAS results showing the concentration of lead in S1a leachates with increasing Zeolite-A

7.6 Analysis of Leachate from Treated Soil 2 in Water with Increasing Zeolite-A

7.6.1 FAAS of Leachate of Soil 2 in Water with Increasing Zeolite-A

Figure 7.10 shows a different trend to the previous FAAS analyses of the soils. There is a low concentration of lead in the leachate for the soil without zeolite, and then a sharp increase upon addition of zeolite followed by a slight decrease with further zeolite addition.

The low lead concentration detected in the S2w leachate is due to the inability of the lead molecules to dissociate from the surrounding matrix. The flame failed to provide enough energy to obtain correct results, as detailed previously, and it is then corrected with GFAAS.

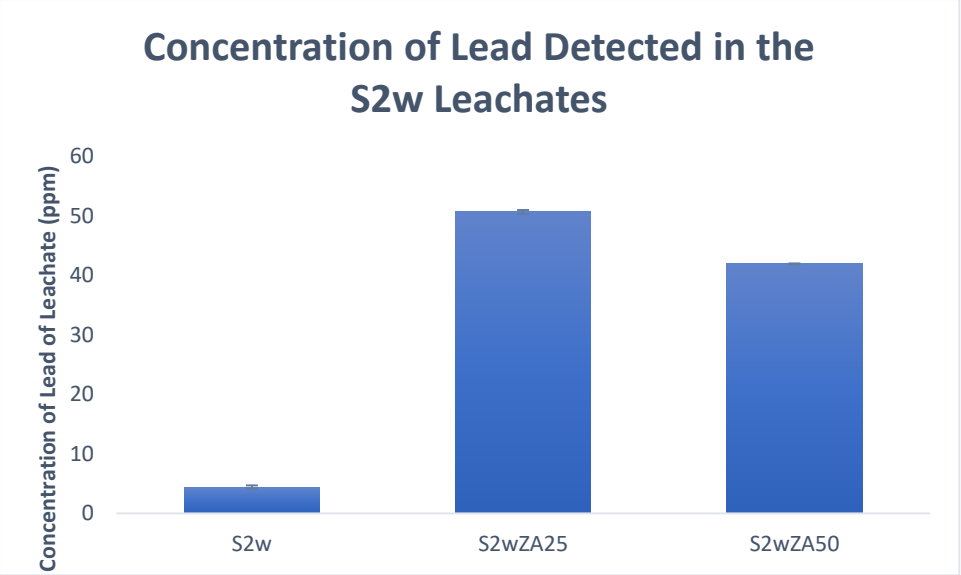

Figure 7.10 - FAAS results showing the concentration of lead in S2w leachates with increasing Zeolite-A

7.6.2 GFAAS of Leachate of Soil 2 in Water with Increasing Zeolite-A

GFAAS shows the expected results trend, Figure 7.11. A high concentration of lead before treatment, followed by a large decrease upon addition of Zeolite-A. This, again, shows that the graphite furnace supplied sufficient energy in the form of heat, to the samples allowing lead to be analysed.

The value for S2w is nearly 12,000 ppm. This is ten times over the EPA recommended value and in agreement with the ICP data collected previously (Appendix 1). This large concentration detected is probably due to the amount of purified water added to the sample. Considering how effective purified water seems to be in forming gismondine, Chapter 6, it might be possible to remediate the soil simply by removing soil, washing it through with a large amount of water, repeating, and then returning the soil. The water could be remediated with more ease and less cost.

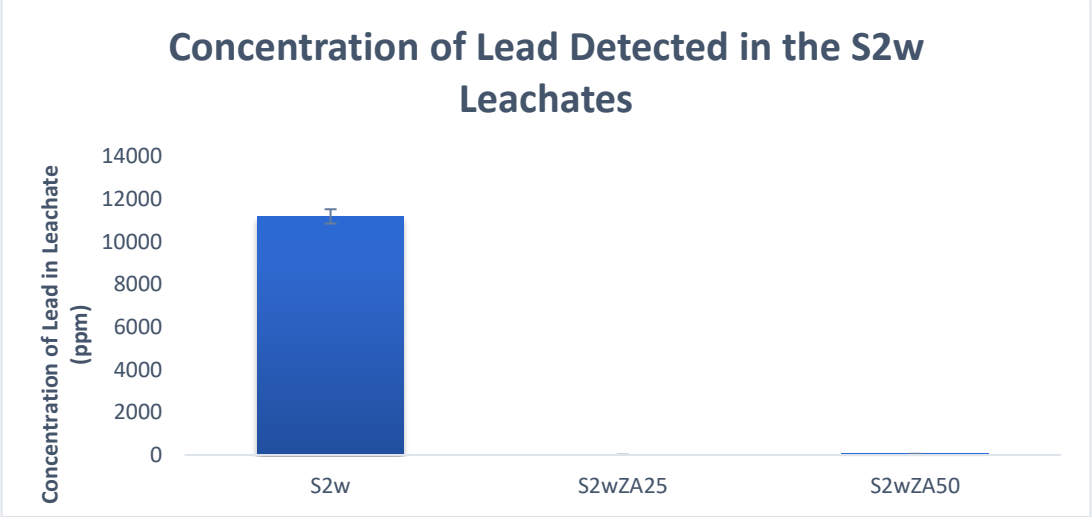

Figure 7.11 - GFAAS results showing the concentration of lead in S2w leachates with increasing Zeolite-A

7.6.3 FAAS of Leachate of Soil 2 in Acid with Increasing Zeolite-A

The addition of Zeolite-A decreases the concentration of lead in the leachate compared to the S2a, Figure 7.12. Further Zeolite-A decreases the concentration more, whilst addition of further acid (30 ml rather than 15 ml), S2aZA50A2, shows a slight increase in lead concentration. This will be due to more of the zeolite dissolving in the extra acid, cancelling out the added effect of increased zeolite. It is important to consider this when analysing Zeolite-A as an appropriate remediation technique.

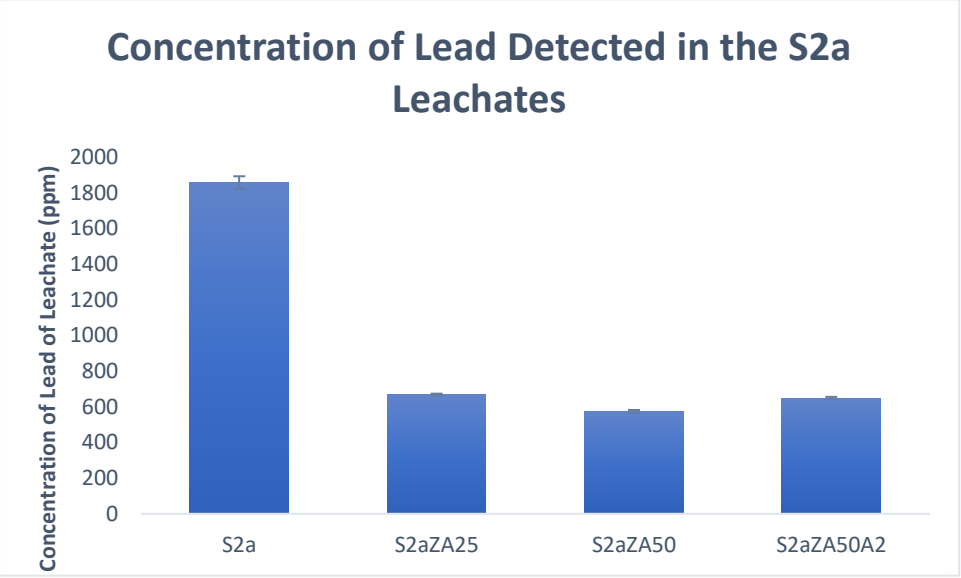

Figure 7.12 - FAAS results showing the concentration of lead in S2a leachates with increasing Zeolite-A

7.6.4 GFAAS of Leachate of Soil 2 in Acid with Increasing Zeolite-A

The GFAAS detected over 13 times more lead in the same sample than FAAS, Figure 7.13. The result is a staggering value that is over 20 times over the EPA higher limit value. It is also 10 times higher than the Swedish Environment Agency's definition of 'poisonous'.

Addition of Zeolite-A follows the trend of decreasing the concentration of lead and further addition of Zeolite-A results in less lead in the leachate. Initial addition of Zeolite-A lowers the concentration by around 5 times. This still results in a figure above the EPA recommended value. Further addition of zeolite lowers the concentration to less than 100 ppm, considered to be safe levels of lead.

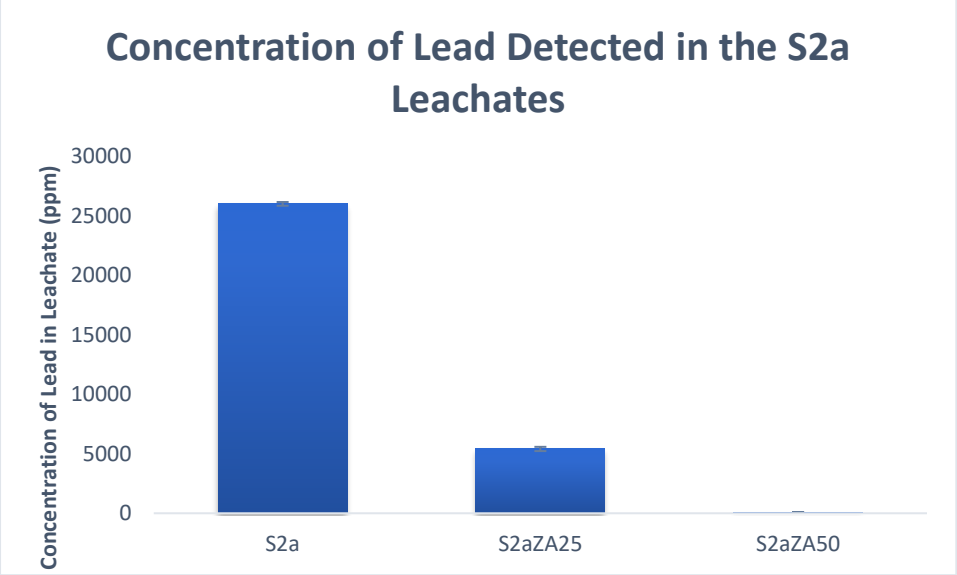

Figure 7.13 - GFAAS results showing the concentration of lead in S2a leachates with increasing Zeolite-A

7.7 Zeolite-A as a Remediation Technique

The results comparing the soils from the two different locations were compiled, in Table 7.1, to obtain a clear view of the suitability of Zeolite-A as a remediation technique. It is clear that the addition of Zeolite-A results in a high percentage decrease of lead in both purified water and dilute acid samples.

Table 7.1 - Remediation effects of Zeolite-A from GFAAS results

	Soil 1			Soil 2		
Mass of Zeolite-A (g)	Sample Name	Concentration of Lead (ppm)	Remediation Effect (Percentage Decrease of Lead Concentration (ppm))	Sample Name	Concentration of Lead (ppm)	Remediation Effect (Percentage Decrease of Lead Concentration (ppm))
0.00g	S1w	1159.58		S2w	11195.00	
0.25g	S1wZA25	0.08	99.99	S2wZA25	7.03	99.94
0.50g	S1wZA50	0.00	100.00	S2wZA50	51.03	99.54
0.00g	S1a	660.83		S2a	26014.58	
0.25g	S1aZA25	601.88	8.92	S2aZA25	5407.71	79.21
0.50g	S1aZA50	120.42	81.78	S2aZA50	76.25	99.71

7.7.1 Comparison of GFAAS Soil 1 and 2 in water

From previous ICP analysis (Appendix 1), it is known that the amount of lead is remarkably higher in S2untreated than S1untreated whilst it is found in the present study that the pH is much lower in S1untreated than S2untreated. Bearing this in mind, it is of interest to compare Zeolite-A's remediation ability by comparing the soils from the two sites.

These observations are summarised in Figure 7.14, confirming that Soil 2 has a significantly higher concentration of lead present than Soil 1. The pH values are also very different between the soils; Soil 2 has a higher pH than Soil 1. Upon addition of Zeolite-A, the concentration of lead in Soil 2 decreases whilst the pH increases. Further addition of zeolite causes a slight decrease in lead concentration as well as a small pH increase. Soil 1 follows the same trend but at an overall lower pH and lead concentration.

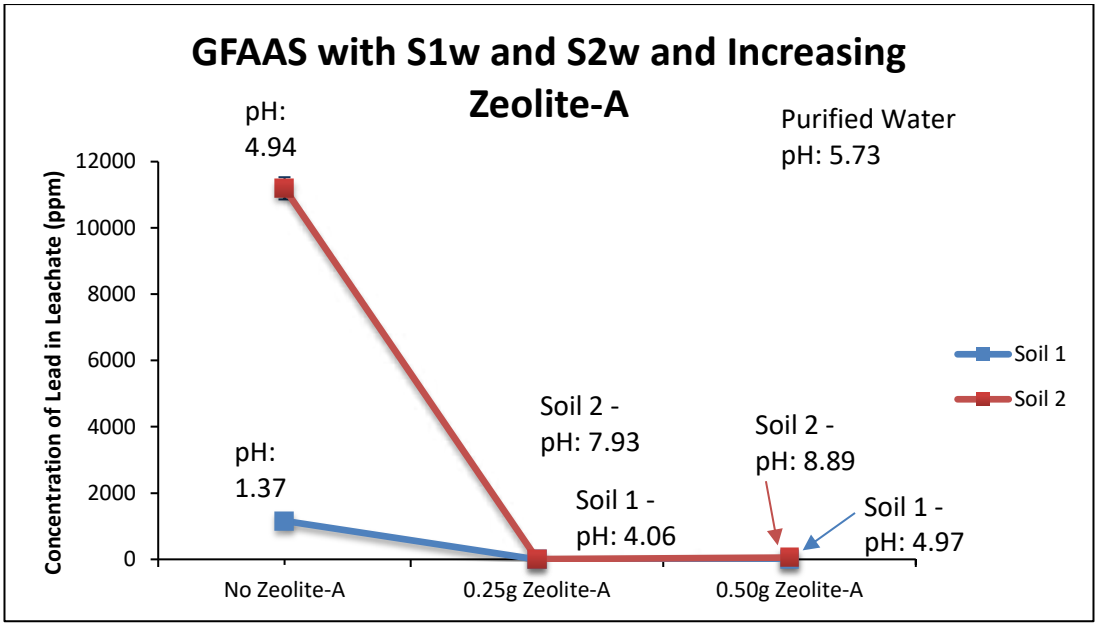

Figure 7.14 - GFAAS of S1w and S2w with increasing Zeolite-A

In Section 6.3.3, it was suggested that Zeolite-A dissolved at a pH of less than 4. It is clear that Soil 1 has a pH of less than 4, and Soil 2 is above a pH of 4. Washing the soils with water, the zeolite does not fully dissolve, even in Soil 1, as it causes the pH to rise over 4. Aside from gismondine, no further secondary minerals were formed, therefore lead must be interacting directly with Zeolite-A as well as the gismondine. Both minerals were detected in all treated water-washed samples whilst, as as discussed in the following section, only gismondine was detected in acid-washed water samples.

7.7.2 Comparison of GFAAS Soil 1 and 2 in acid

Upon washing with acid, Figure 7.15 shows that both Soil 1 and Soil 2 experience a decrease in pH and they both report similar acidic values. However, the 'success' of the remediation seemed to vary. Soil 2 shows that an increase in zeolite leads to a decrease in lead concentration in the leachate and an increase in pH. In Soil 1, only a small concentration of lead was detected, and, due to the statistical error bars, a trend is difficult to detect at this scale. The values decrease from approximately 660 ppm to 602 ppm and then to 120 ppm for Soil 1. When the amount of Zeolite-A added increases from 0.25 g to 0.50 g, a lower concentration of lead is detected in the leachate. The explanation for the improved remediation of lead associated with the higher zeolite addition is believed to be that the synthetic zeolite added dissolves in

the acid, increasing the pH of the leachate whilst also assisting in the formation of gismondine, which allows gismondine to act as a remediator. The XRD results in Chapter 6 confirmed this theory.

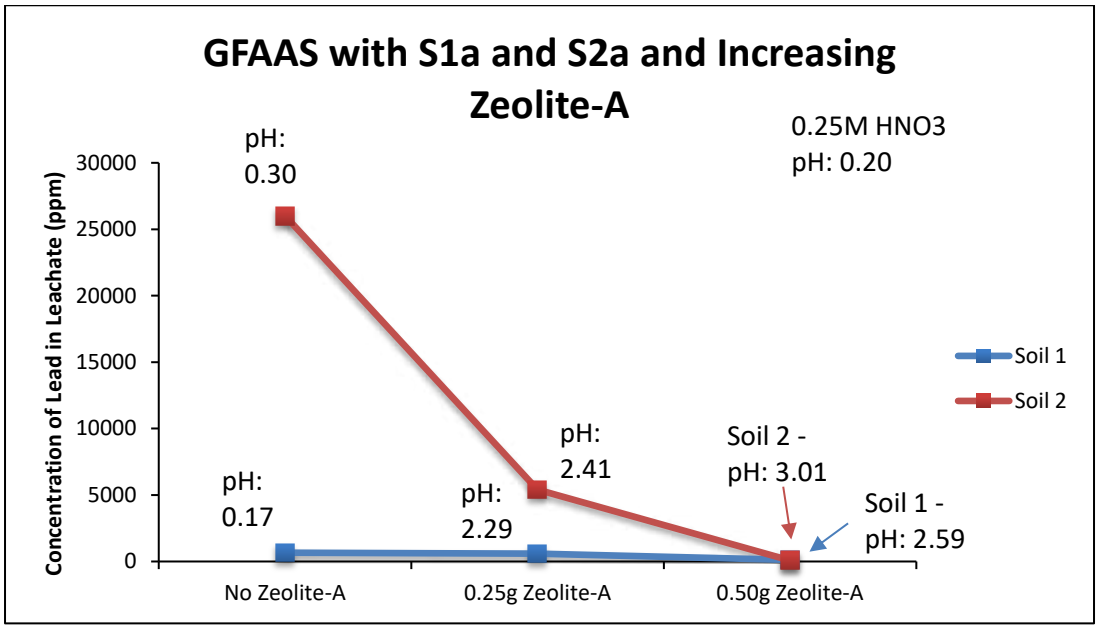

Figure 7.15 - GFAAS of S1a and S2a with increasing Zeolite-A

7.8 Conclusions

- FAAS was found to provide inaccurate readings of the concentration of lead, possibly due to not achieving high enough temperature or not heating the nebulised sample for a long enough period.
- GFAAS provided results that matched those previously recorded using ICP-MS.
- The recorded values showed that the concentration of lead was significantly above the legal limit for soil in any area (industrial or residential).
- The results show that adding Zeolite-A decreases the concentration of lead, even at a low pH where the Zeolite-A is thought to dissolve.
- Further work should be carried out involving soil column analysis.

Chapter 8 Results and Discussion: Computational Analysis

8.1 Aim

The aim of this section is to obtain a clearer idea of the mechanism by which the remediation of lead occurs. From the previous chapter, it is clear that Zeolite-A is reducing the concentration of lead detected in the leachate, as determined with Atomic Absorption Spectroscopy (AAS). The purpose of the computational analysis is to identify potential locations that the Pb^{2+} ion could sit within the zeolite structure, thus keeping it inside the solid residue and lowering the concentration of lead detected in the leachate.

8.2 Introduction

Computational modelling was undertaken as it was not clear from the experimental results how the lead ions were interacting with Zeolite-A. It was hoped that modelling the system would provide more information that could be useful to further experimental work with this particular synthetic zeolite mineral.

Computational Zeolite-A analyses have been reported in the literature. These studies consider interatomic potential (Higgins, et al., 2002; Higgins, et al., 1997; Jackson & Catlow, 1998; Bell, et al., 1992), first principles simulations (White, et al., 1997; Kolezynski, et al., 2016), and first principles molecular dynamics simulations (Yoshida, et al., 2013).

Computational studies have not been previously conducted on the comparison of Ba^{2+} and Pb^{2+}. Whilst barium and lead have very different chemistry in the environment, computationally they are very similar. Both ions are divalent cations with similar ionic radii; 1.35-1.61Å for Ba^{2+} and 0.98-1.49 Å for Pb^{2+} (Shannon, 1976). However, Pb^{2+} is known to be characterised by having an electron lone pair, which may alter the exchange behaviour and increase the ionic size.

The current project conducts a comparison between Ba^{2+} and Pb^{2+} ions to determine if both Ba^{2+} and Pb^{2+} are energetically favourable to exchange for Na^{+} ions in Zeolite-A and if the properties of the zeolite change as the loading of lead and barium ions increases. This provides insight regarding the stability of lead and barium

doped Zeolite-A structures and can be used to enhance the understanding of Zeolite-A as a remediator.

8.3 Method

All calculations were completed using the CRYSTAL09 program, which describes electron density from a set of Gaussian basis functions (see Section 4.8.4) (Dovesi, et al., 2009). As the computational cost increases exponentially with the number of particles present in the calculations, including electrons, the atoms were described using electron-core potentials (ECPs) together with Gaussian basis functions. This means that the core electrons were modelled by a mathematical potential optimised for the individual ion, whilst the valence electrons are defined by a set of Gaussian functions.

In this project, a minimal basis set, STO-3G (Hehre, et al., 1969), was considered and rejected due to poor SCF convergence. Hay-Wadt's large and small core ECPs were selected for Barium. The basis sets used were; O (3-1G), Si (3-1G), Al (3-1G), Na (3-1G) (Hay & Wadt, 1985), Ba (3-11G) (Habas, et al., 1998), and Pb (2-11G) (Piskunov, et al., 2004). The cut-offs used for the integrals were 6,6,6,6,12 (default values in CRYSTAL09), whilst the energy accuracy for the SCF calculations was 10^{-6}H. For geometry optimisation, all calculations were converged to at least 10^{-5}H per atom in the unit cell. The functional of choice was B3LYP as discussed in Section 4.8.3.

Two different metal ion concentrations were investigated: 25% and 50%. This was because at 50%, there were fewer atoms present and, therefore, allowing the calculations to be run with high symmetry, which requires fewer computer resources. 25% was the subsequent, more costly, setting. For 25%, the unit cells contained 672 atoms, and no symmetry was used in the calculations (space group P1), all calculations were conducted within the Γ-point (1x1x1 Brillouin zone). This cell was created by building a 2x2x2 supercell from the original high symmetry F*m-3C* primitive cell. The Na^+ ions were systematically substituted for Ba^{2+} and Pb^{2+} ions. The cell charge needed

to remain neutral so the number of sodium ion vacancies created needed to be equal to the number of sodium ions substituted. Equation 8.1 describes this statement.

$$2Na^{+} \rightarrow M^{2+} + V_{Na} \quad (8.1)$$

Three different distributions for lead and barium ions were considered for cation exchange: S6R, S6R-S8R and S8R, where S6R and S8R denotes the structural location, Figure 8.1. These sites were chosen as several research studies carried out analysis using the same locations and obtained results that did not involve destruction of the framework, thereby proving the locations to be valid and capable of loading Pb^{2+} (Kim, et al., 2006; Tang, et al., 1992; Togashi, et al., 2001; Heo, et al., 2004; Lim, et al., 2005).

The chemical formula for this substitution is: $MNa_3Al_{12}Si_{12}O_{48}$ (where M is Ba^{2+}, Pb^{2+}), and is referred to as 25% loading. Substitution energies were calculated based on Equation 8.2, where M corresponds to Pb^{2+} or Ba^{2+}.

$$E_{tot}(\text{Na-Zeolite-A}) + 16\ E_{tot}(M^{2+}) \rightarrow E_{tot}(\text{M-Zeolite-A}) + 32\ E_{tot}(Na^{+}) \quad (8.2)$$

For 50% loading, the formula is: $M_4Na_4Al_{12}Si_{12}O_{48}$ (where M is Ba^{2+}, Pb^{2+}). A smaller periodic cell was also investigated making use of the symmetry in the structure. This cell contained 160 atoms when the sodium ions have been exchanged for barium or lead ions and all settings in CRYSTAL09 were equivalent to those for the 25% loading.

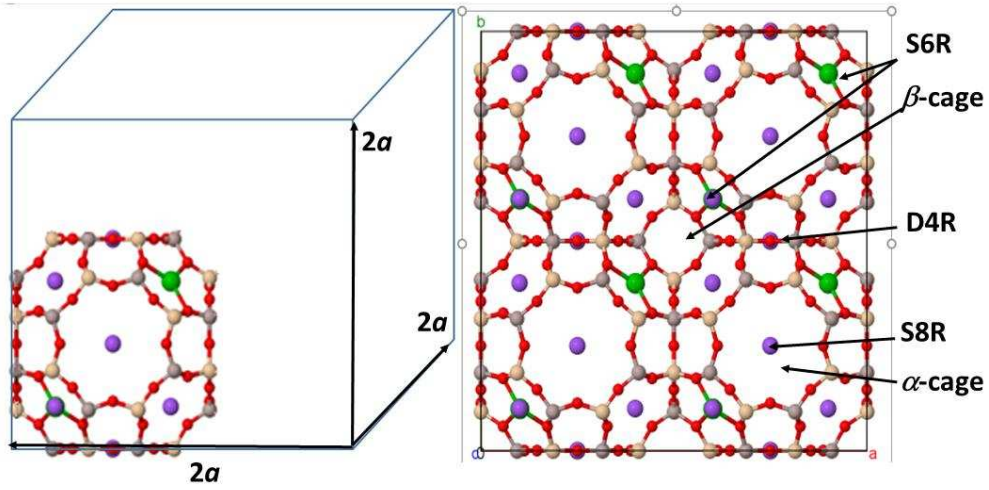

Figure 8.1 - Crystal structure of Zeolite-A showing a) a simplified cell containing 160 atoms (Fm-3c) and b) 2x2x2 supercell with 672 atoms (P1). The α-cage represents the super-cage and β-cage the sodalite cage. S6R, S8R and D4R represents the positions for which the cation substitutions have been analysed.

8.4 Results

8.4.1 Energies

As no computational study on lead substituted Zeolite-A structures had been previously presented in the literature, the first aim was to determine the location of the Pb^{2+} ions in the structure. Three different distributions are shown in Figure 8.2. These were described by Pb^{2+} ions replacing sodium ions in the sodalite cages (S6R position), removing sodium ions from the S8R, S6R and D4R positions. The distribution in which sodium ions are replaced by Pb^{2+} ions and vacancies created in at the S8R positions is named PB_S6R_S8R, Figure 8.2a.

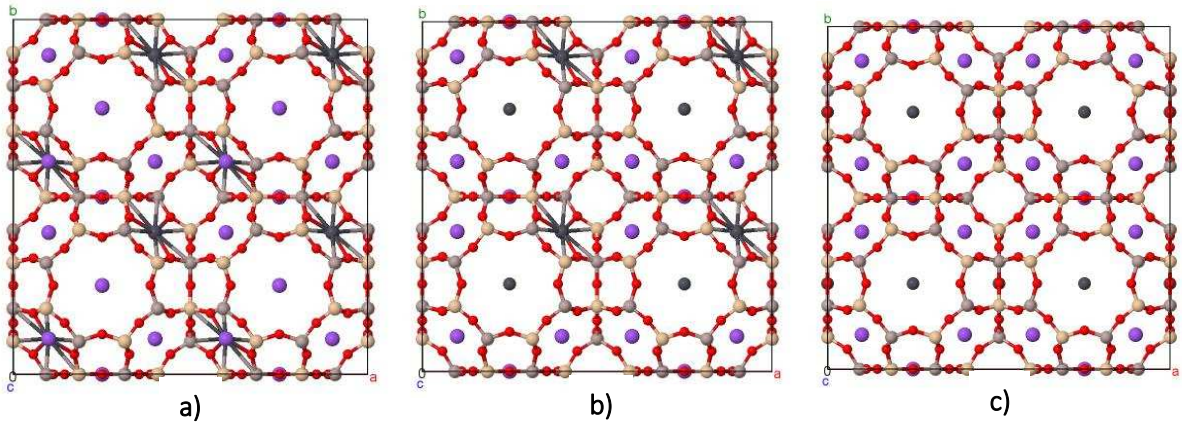

Figure 8.2 - 25% loading of lead in Zeolite-A corresponding to distributions; a) PB_S6R_S8R, b) PB_S6R/S8R_S8R, and c) PB_S8R_S8R

The most energetically stable distribution for the lead substituted structures is PB_S6R_S8R, Figure 8.2a, Table 8.1. In this structure, the sodium vacancies are created in the α-cages (S8R positions). The difference between the location of vacancies in the S8R and D4R positions is less than 1kJ mol^{-1} $atom^{-1}$. This small value shows that there is a preference for this vacancy location. For the other distributions, only sodium vacancies in the S8R positions were considered.

The calculations show a higher preference for Pb^{2+} ions located inside the sodalite cages, S6R, compared to the α-cages (S8R). The energy difference between these two distributions is more than 30 kJ mol^{-1} $atom^{-1}$.

Table 8.1 - Energy differences of the distributions of Pb^{2+} ions or Ba^{2+} ions in 25% loaded Zeolite-A. The first part of the name refers to the cation, the second part is the cation substitution site, and the third part of the name is associated with the sodium ion vacancy position.

Distribution	ΔE (kJ mol^{-1} $atom^{-1}$)
PB_S6R_S8R	0
PB_S6R_S6R	0.25
PB_S6R_D4R	0.89
PB_S6R/S8R_S8R	13.2
PB_S8R_S8R	31.2
BA_S6R_S8R	-225.8

The preferred location of Pb^{2+} ions in the sodalite cages agrees with an experimental study on Pb^{2+} substitution in Zeolite-A (Ronay & Seff, 1985). The research involved Pb^{2+} ions were introduced at two different pH values in order to determine the extent of exchange that occurred. The two pH values analysed were 4.3 and 6.0. The results concluded that the solution at a higher pH was capable of a higher extent of Pb^{2+} substitution, 50%. They also found that Pb^{2+} formed Pb^{4+} when bonding with the oxygen in the zeolite. This was proposed to be due to using a dehydrated zeolite structure. The placement of the lead ions in the zeolite structure at both pH values was determined to favour the smaller S6R cages. This concurs with the results found in the present study.

Conversely, experimental and theoretical studies on Ca-ion exchange in Zeolite-A are less conclusive. Most experimental work agrees that the Ca^{2+} ions are located close to the S6R position (Seff & Shoemaker, 1967; Adams & Haselden, 1984), however the distributions of Na^{+} ions vary. Seff and Shoemaker (1967) stated that the sodium ions are only located in the α-cages (S8R). Their work shows that it is energetically favourable to create sodium ion vacancies in S8R positions but the difference in energy is small. Instead, there is a larger energy gain when replacing all sodium ions inside the S6R rings before placing divalent cations in the S8R and D4R positions. This agrees with Adams and Haselden (1984) and could be due to the cation loading and water content in Zeolite-A (Higgins, et al., 2002). In the current computational study, only anhydrous Zeolite-A is considered. This is due to the large computer resource requirements for including water. It is common practice to analyse

a dehydrated system before accounting for the difficult hydration factors. In addition, there was no access to a computer that could manage such large calculations.

8.4.2 Structural Data

The structures in which 50% of the sodium ions have been substituted by barium or lead ions were analysed. It has been stated that the most stable structure is for the heavy metal cation to be located in the S6R position within the sodalite cage. The optimised lattice parameters (as previously discussed in Section 4.8.2 with regards to geometry optimisation) for the cations in this position are given in Table 8.2 (Pluth & Smith, 1980)[1], (Adams & Haselden, 1984)[2], (Higgins, et al., 1997)[3], (Ronay & Seff, 1985)[4].

Table 8.2 - Geometry optimised lattice parameters for Zeolite-A within the cubic structure Fm-3c. The structures correspond to 100% sodium ions as well as 50% of these ions replaced by calcium, barium, or lead ions.

Cation	Previous work (Å)		Optimised (Å)	
	Experiment (Å)	Calculations (Å)	50%	25%
Na-ion	24.56[1]		24.64	
Ca-ion	24.65[2]	24.72[3]		
Ba-ion			24.86	24.53
Pb-ion	24.32[4]		24.41	24.55

It can be seen in Table 8.2 that the lattice parameter in the geometry optimised sodium structure, 24.64 Å, is slightly increased compared to the experimental value, 24.56 Å (Pluth & Smith, 1980). Introducing 50% barium loading in the structure causes the lattice parameter to increase to 24.86 Å. This observation is in agreement with previous studies on calcium-containing Zeolite-A. Experimentally, the lattice parameter increases to 24.65 Å (Adams & Haselden, 1984). Interatomic potential calculations show a similar increase of approximately 14% compared to the sodium-rich structure (Higgins, et al., 1997).

The Pb^{2+}-substituted structure results in a decrease in the lattice parameter, 24.41 Å, despite that the ionic radius of the Pb^{2+} ion is larger than that of the Na^{+} ion. Vegard's law would suggest that an increase in size would result in an increase in lattice parameter, however, the law only accounts for a 1:1 substitution, and in this

case, two sodium ions must vacate for a single lead ion to substitute (Denton & Ashcroft, 1991). This uneven exchange causes the lattice parameter to decrease.

Another explanation for the decrease in lattice parameter could be the large reconstructions of the sodalite cages, Figure 8.3. The Ba^{2+}-substituted structure involves barium ions being located in a slightly more symmetrical position with Ba-O(2) and Ba-O(3) distances of 2.63 Å and 2.73 Å, respectively. The lead ions cause a distortion of the structure, resulting in Pb-O(2) and Pb-O(3) distances of 2.20 Å and 3.31 Å, respectively. It is also found that the lead ions are located further away from the S6R plane towards the centre of the sodalite cage.

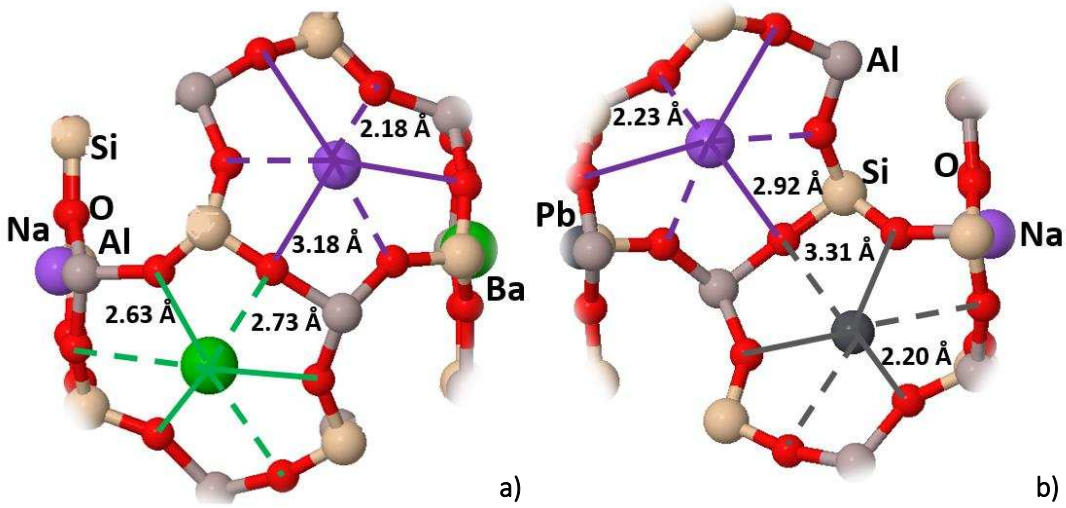

Figure 8.3 - 50% loading of a) barium and b) lead in Zeolite-A. Bond distances for the geometry optimised structures are given in Angstroms.

The bond distances are in good agreement with previous computational studies on barium ions in Zeolite-A, which report barium-oxygen distances of 2.57-3.14 Å (Higgins, et al., 1997) and experimental values of 2.51 Å (Kim, et al., 1980). In the previously mentioned study with PbI_2 loaded Zeolite-A, the experimental lead-oxygen distances were 2.52-3.47 Å (Ronay & Seff, 1985).

An interatomic potential study found that as the ionic radii of the cations increase, the cations have a tendency to diffuse from the S6R site towards the S8R cage. The S6R site is still preferred, as it has three stabilising cation-oxygen bonds that are possible, however, once there, the energy needed to move from the stable adsorption site to another was calculated (Higgins, et al., 1997). This was later supported by FTIR measurements and first principles simulations on Zeolite-A

exchanged with a number of different cations, including Ba^{2+} (Kolezynski, et al., 2016). This latter study used the equivalent of the previously defined 50% loading cell, considering only cations substituted in the S6R position. It was found that the larger ionic radii, the lower symmetry of the structure. This indicates that the cation is translated from the plane in the S6R position towards a lower symmetry position, within the sodalite cage. The results of this current study agree with this observation. However, it was found that the largest translation is for the Pb^{2+}, which has a slightly smaller ionic radius than the Ba^{2+} ion. This may be an indication that the electron lone-pair on the lead ion has a measurable effect but requires further investigation.

Decreasing the loading of heavy metals to 25%, the structures do not change significantly compared to the initial experimental structure containing only sodium ions. The lattice parameters were 4.53 Å and 4.55 Å for barium and lead, respectively. Also, M-O(2) and M-O(3) (where M = Ba^{2+}, Pb^{2+}) are similar to the initial sodium-oxygen distances of 2.32 Å and 2.9 1Å, respectively.

8.5 Conclusions

- Zeolite-A will substitute sodium ions for lead ions. This supports the experimental analysis carried out in this study.
- The calculations clearly favour the lead ions to sit inside in the sodalite cages.
- Depending on the cation loading, the reconstruction of the six-membered rings (S6R) will change. High loading shows large reconstructions.
- It is more favourable to create sodium vacancies in the eight-membered rings, but the dominating energy contribution is the replacement of sodium ions in the sodalite cages. This results in a high loaded structure described by empty α-cages with all heavy metals in the β-cages.
- It is energetically more favourable to replace sodium ions with barium ions, rather than lead ions, which suggests that Zeolite-A has a preference for barium when used for remediation.
- This is relevant for the current study and suggests that Zeolite-A is only a valid remediation tool in soil that does not contain any barium.

- It would be useful to undertake larger supercell calculations with different concentrations of barium and lead to understand if there is a concentration dependence.
- Further studies of mixed barium and lead distributions would help to understand if Zeolite-A prefers barium for lead. This would also be important to study experimentally.
- Substitution energies depend on the hydrolysis energy and not the ionic energies used as the reference state in this work. Hence, future work should include the effect of water in the calculations.

Chapter 9 Conclusions and Recommendations

9.1 Aims and Introduction

The aims of this study were to:

- Determine the suitability of Zeolite-A as a remediation technique for lead
- Characterise the mineral composition of the pyrite ash soil
- Perform leachate analysis
- Determine the influence of pH on the dissolution process
- Computationally analyse Zeolite-A for the ion exchange of lead ions

These aims were achieved through various experimental and computational experiments. The suitability of Zeolite-A was tested using GFAAS to analyse the soil leachate. Upon addition of zeolite, the concentration of lead decreased markedly. It is, therefore, possible to conclude that the addition of Zeolite-A to pyrite ash soil will help to decrease the concentration of lead that leaches into nearby water systems.

The pyrite ash soil was found to be mainly hematite-based. However, Soil 1 also demonstrated sulphur-based compounds not present in Soil 2. This is due to the nature of the industry based at the site, as detailed in Section 3.3. Site 1 (Soil 1) was located where the furnace was located for the roasting of iron sulphide minerals, forming oxides and pyrite ash, whilst Site 2 (Soil 2) was chosen to represent samples containing mainly pyrite ash waste. The minerals determined matched those expected to be present with the addition of lead sulphate and other lead-based compounds.

Leachate analysis was performed to determine if the levels of lead being leached at the site were above the legal guidelines stated by the EPA. It was found that at both locations where the soils were sampled, the concentration of lead detected was, indeed, well over the ‘safe levels’ and, therefore, needs to be remediated.

The dissolution of Zeolite-A is dependent on the pH. As determined in Section 6.3.2, at a pH of less than 4, Zeolite-A begins to dissolve and consequently its ability to remediate lead is negatively affected.

Computational analysis of Zeolite-A found that barium ions, which are less costly to run in simulations, act the same as lead ions. Whilst their chemistry in the environment is not similar, their results from the computational analysis allows them to be considered equal, which will benefit future analyses by allowing for less costly and shorter simulations. This will yield results more quickly. In addition, the locations for lead and barium ions to sit inside the zeolite structure coincide with previous studies, which adds credibility to the results.

9.2 Summary and Discussion

The two soils analysed in this study are different in several relevant ways. They have varying mineral composition and pH. Both of these attributes affect the type of remediation that would be most successful.

Soil 1 had a very low pH and was found to benefit from the addition of Zeolite-A. The zeolite caused an increase in the pH of the soil from 1.37 to 4.06 in water, and 0.17 to 2.29 in acid, with further zeolite acting as a buffer, maintaining the pH. This improves the quality of the soil and maintains safety for the surrounding environment by reducing the leaching of lead due to the less acidic environment.

Soil 2 has a higher pH value, of 4.94 in water and 0.30 in acid, but experiences a similar trend. Addition of 0.25 g of Zeolite-A to 1 g of soil sample raises the pH by 2-3 units, to a pH of 7.93 in water and 2.41 in acid. Further Zeolite-A will act as a buffer under these conditions and stabilise the pH.

Characterisation of the untreated soil samples showed that Soil 1 is formed of pyrite-based compounds, whilst Soil 2 is based on iron oxides being the by-product in the roasting procedure. Despite the two soils displaying such different properties, a secondary mineral, possibly gismondine, is formed in both. This is the principle cause of lead reduction detected in the leachate. A hypothesis is that gismondine is formed from the lead silicates originally detected in the untreated soil and it is further produced by the addition of Zeolite-A. Gismondine is stable at a low pH.

It is clear from the results table presented in Chapter 7, that Zeolite-A was a useful addition in all of the samples by increasing the pH of the system and, thereby, helping to keep the lead stable in the solid residue and prevent leaching.

9.3 Proposition of gismondine formation

Fly ash occurs naturally as a product from the process of coal-combustion (Headwaters Resources, 2013). It is similar to volcanic ash and classified into two broad types, Class F and Class C. These are differentiated by the amount of SiO_2+Al_2O_3+Fe_2O_3 present in the sample. The boundaries are having the specified minerals (SiO_2+Al_2O_3+Fe_2O_3) ≥70%, referred to as Class F, or between 50 and 70%, Class C (Vassilev & Vassileva, 2007; Zhang, et al., 2011). The soils under current study fell into the category of Class C fly ash, as Soil 1 contains approximately 68% of silicon, aluminium and iron oxide, and Soil 2 is 59% composed of these minerals determined from XRF, Appendix 3.

A study published in 2011 analysed low-calcium and high-calcium fly ash. They determined this composition by defining the former as CaO < 5%, and the latter as CaO > 15% (Zhang, et al., 2011). The study found that two types of zeolites were formed as secondary mineral depending on the calcium oxide content. Low calcium oxide content resulted in Faujasite (Zeolite-X) being the dominating zeolite phase. Conversely, high-calcium fly ash resulted in gismondine (Zeolite-P) being the favoured zeolite structure (Zhang, et al., 2011). A hypothesis for these observations was that the recognised chemical formula for faujasite is $Na_{20}[Al_{20}Si_{33}O_{106}]\cdot 70H_2O$, whilst the chemical formula for gismondine is $Ca[Al_2Si_2O_8]\cdot 4.5H_2O$. Hence, high-calcium fly ash would result in gismondine being formed, as the ionic radii of the compensating cation determines the zeolite crystallisation process.

Relating the study by Zhang et al. (2011) to the current study, S1untreated and S2untreated both had less than 5% of calcium ions detected whilst sodium was not detected in either of the untreated soils by XRF. Nevertheless, it was shown by the XRD analysis on Soil 2 that few of the compounds present contained sodium. Albite is only 8.3% composed of sodium (WebMineral, 2012) and, therefore, not showing in the XRF data. Consequently, the dominating zeolite forming cation is calcium and calcium-like cations, which include lead as they have a similar ionic radius and charge. Zhang et al. assumed in their conclusions that these low-calcium soils would have a higher concentration of sodium. However, in the current study, this is not the case.

In both soils, a secondary mineral is appearing, as shown by the XRD diffraction patterns. XRF data confirms that calcium is originally present and washing in water causes a slight increase in the percentage concentration of calcium detected by XRF. This could be due to the formation of gismondine and the subsequent substitution of calcium ions for lead ions. Calcium is also present in Soil 1, albeit below the 0.9% threshold used in the results. In addition, both samples contain a substantial amount of lead ions.

Gismondine has been found to exchange calcium ions with lead ions. Related studies using Zeolite-P have determined that lead will not fully exchange with sodium, as some sodium atoms were detected after Na^{+}/Pb^{2+} cation exchange (Nery, et al., 2003). Other studies, using Zeolite-X and Zeolite-A, have determined similarly, that lead will exchange into the structure, in varying percentage, including over-exchange (Yeom, et al., 1999; Yeom & Kim, 1997; Ronay & Seff, 1985). It was suggested that the extent of exchange is affected by the pH of the soil (Ronay & Seff, 1985).

It has been suggested that the more aluminium present in the soil, i.e. the larger the Al:Si ratio, the higher affinity there is for cations because the increased aluminium content creates a cage structure with a more negatively charged electron distribution, i.e. a negative charge is produced in the lattice, which is balanced by the cation being exchanged (Shaheen, et al., 2012).

It is well known that sodium ions in Zeolite-A may be exchanged by calcium ions. Zeolite-A also undergoes ion exchange for lead, and it has been found that lead has a higher affinity for Zeolite-A than cadmium, zinc, copper, or nickel ions (Ronay & Seff, 1985). Equation 9.1 was suggested as the Na^{+} - Pb^{2+} ion exchange reaction for lead and Zeolite-A, where (L) refers to the ions in solution and (Z) denotes ions in Zeolite-A.

$$Pb^{2+}(L) + 2Na^{+}(Z) \leftrightarrow Pb^{2+}(Z) + 2Na^{+}(L) \qquad (9.1)$$

The same study found that lead ions had a higher affinity than zinc ions and that the ion exchange is independent of temperature. This is unusual, as zinc and cadmium ions, for example, both have affinities that vary with temperature. It was

concluded that lead ions can be removed from solutions effectively at varying temperatures (Biskup & Subotic, 2000).

In this study, it was found that the addition of Zeolite-A to the samples did not hinder the formation of the secondary mineral. The hypothesis is that the secondary mineral, potentially gismondine, forms in both soils after washing whilst lead silicate seems to dissolve. This is confirmed in the XRD patterns, Figure 6.5 and 6.15. This may indicate that the lead silicate is a starting material for the formation of the secondary mineral.

The concentration of lead present in the leachate was found to decrease upon addition of Zeolite-A. This may be due to a combination of Zeolite-A and the secondary mineral both acting as remediators. This would explain why even when in acidic conditions, when the majority of Zeolite-A dissolves, there is still a marked decrease of lead detected in the leachate.

Computationally, the locations that lead ions sit within the Zeolite-A structure has been analysed by a previous study (Kim, et al., 2006) and confirmed in this investigation. Pb^{2+} prefers to sit inside the 6-ring sodalite cage, S6R, and the sodium ions are removed from the larger 8-ring sodalite cage, S8R.

Lead and barium have been shown to behave identically in the simulated ion exchange. This allows barium to be used for calculations in place of lead. Barium is easier to run as it does not have a lone pair. This will make future investigations cheaper in terms of computer time.

9.4 Future Work and Recommendations

Due to a secondary mineral forming and proving to take part in the remediation of lead, an in-depth study of gismondine as the principle remediator of lead in contaminated soils, containing pyrite ash as well as acid mine drainage, should be undertaken. This can confirm if gismondine is the secondary mineral formed and further analyse its properties.

Contrary to Zeolite-A, the secondary mineral does not dissolve at low pH. It would be valuable to attempt to synthesise gismondine from lead sillcate and to follow

the crystallisation process in an acidic environment. Braithwaite et al. (2001) studied lead-smelting slag from Yorkshire and reported the formation of barium-dominating gismondine (Ba-gismondine). It was proposed that barium sulphate ($BaSO_4$) is reduced during the smelting process to form barium sulphide (BaS). Under acidic conditions barium sulphide dissolves providing a source of barium ions which under certain conditions may interact with the silicate in the slag forming Ba-gismondine. Gismondine is known to form readily under mild hydrothermal conditions between 25^{o}C and 90^{o}C. Because it is easily formed, it is used as a water softener, e.g. washing powders with a gismondine content of up to 30% (Adams, et al., 1997). Furthermore, gismondine has a 'flexible' framework, which allows it to accommodate larger cations such as barium ion. Gismondine is known to crystallise in silicate-poor environments, such as pyrite ash waste, which contains large amounts of oxides. A future study would be to dissolve the lead silicates to determine if they assist gismondine formation as well as to determine if lead is incorporated into the structure forming Pb-gismondine. It would also be beneficial to run computational simulations using gismondine as the focus.

It would be interesting to conduct soil column and thorough plant analysis to determine if plants are able to uptake the lead that is held in the gismondine and Zeolite-A frameworks. Continuing to analyse the pH of the soils upon addition of gismondine and further Zeolite-A would be useful in analysing the buffer capabilities of both zeolites.

Finally, it would be ideal to test adding gismondine and Zeolite-A in situ, at the site studied in this project, particularly Site 2, where severe lead contamination has occurred. The results could be compared for adding each zeolite separately, or both together.

Chapter 10 References

Adams, C.J. et al., 1997. Zeolite MAP: the new detergent zeolite. *Studies in Surface Science and Catalysis*, 105B, pp.1667-74.

Adams, J.M. & Haselden, D.A., 1984. *Journal of Solid State Chemistry*, 51, p.83.

Adepoju-Bello, A.A. & Alabi, O.M., 2005. Heavy Metals: A Review. *The Nigerian Journal of Pharmaceutical Sciences*, 37, pp.41-45.

Adepoju-Bello, A.A., Ojomolade, O.O., Ayoola, G.A. & Coker, H.A.B., 2009. Quantitative Analysis of Some Toxic Metals in Domestic Water Obtained from Lagos Metropolis. *Nigerian Journal of Pharmaceutical Research*, 42(1), pp.57-60.

Agency for Toxic Substances and Disease Registry, 2012. *Lead Toxicity What are the Physiologic Effects of Lead Exposure*. [Online] Available at: www.atsdr.cdc.gov/csem/csem.asp?csem=7&po=10 [Accessed 12 May 2016].

Ahmed, I.A.M. et al., 2009. Coordination of Cd2+ ions in the internal pre system of zeolite-X: A combined EXAFS and isotopic exchange study. *Geochimica et Cosmochimica Acta*, 73, pp.1577-87.

Alfredsson, B., 1953-1965. *Private Communication with Analytical Chemist at Paper Mill Factory*.

Alfredsson, M.L., 2016. *Private Communication*. Canterbury.

Alloway, B.J., 1995. *Heavy Metals in Soils*. 2nd ed. London: Blackie Academic and Professional.

American Cancer Society, 2014. *Arsenic*. [Online] Available at: http://www.cancer.org/cancer/cancercauses/othercarcinogens/intheworkplace/arsenic [Accessed 4 May 2016].

Ames, L.L., January 16, 1962. Removal of cesium by sorption from aqueous solutions. *US Patent No. 30,017,242*.

Antosiewicz, D.M., 2005. Study of calcium-dependent lead-tolerance on plants differing in their level of Ca-deficiency tolerance. *Environmental Pollution*, 134, pp.23-34.

Araneo, A., 1987. Il pH di precipitazione degli idrossidi. In M. Piccin, ed. *Chimica Analitica Quantitativa*. Padova: Piccin Nuova Libraria, S.p.A. pp.62-69.

Armbruster, T., 2001. *Clinoptilolite - Heulandite: Applications and Basic Research in: A. Galarnau, F. Di Renzo, F. Faujula, J. Vedrine (Eds.), Studies in Surface Science and Catalysis 135, Zeolites and Mesoporous Materials at the Dawn of the 21st Century*. Amsterdam: Elsevier.

Atkins, P. & de Paula, J., 2010. *Atkins' Physical Chemistry*. 9th ed. Oxford, New York: Oxford University Press.

Atkins, P. et al., 2006. *Shriver & Atkins Inorganic Chemistry*. 4th ed. Oxford, New York: Oxford University Press.

Austrailian Microscopy and Microanalysis Research Facility, 2014. *Electron-matter interactions*. [Online] Available at: http://www.ammrf.org.au/myscope/sem/background/concepts/interactions.php [Accessed 19 July 2016].

Australian Microscopy and Microanalysis Research Facility, 2013. *Troubleshooting: edge effect, charging, sample damage*. [Online] Available at: http://www.ammrf.org.au/myscope/sem/practice/principles/troubleshooting.php [Accessed 1 June 2016].

Babel, S. & Kurniawan, T.A., 2003. Low-cost adsorbents for heavy metals uptake from contaminated water: a review. *Journal of Hazardous Materials* , 97(1-3), pp.219-43.

Baerlocher, C. & McCusker, L.B., 2016. *Database of Zeolite Structures*. [Online] Available at: http://www.iza-structure.org/databases/ [Accessed 15 February 2017].

Bailey, S.E., Olin, T.J., Bricka, R.M. & Adrian, D.D., 1999. A review of potentially low-cost sorbents for heavy metals. *Water Research*, 33(11), pp.2469-79.

Baker, B.J. & Banfield, J.F., 2003. Microbial communities in acid mine drainage. *FEMS Microbiology Ecology*, 44(2), pp.139-52.

Baltrenas, P. & Brannvall, E., 2006. Experimental investigation of a filter with natural sorbent charge for runoff cleaning from heavy metals and petroleum products. *Journal of Environmental Engineering and Landscape Management*, 14(1), pp.31-36.

Bao, W. et al., 2013. Adsorption of heavy metal ions from aqueous solutions by zeolite based on oil shale ash: kinetic and equilibrium studies. *Chemical Research in Chinese Universities*, 29(1), pp.126-31.

Barnett, V. & Buntine, M., 2008. *Atomic Absorption Spectroscopy*. [Online] Available at: https://usc.adelaide.edu.au/asistm/atomic/ [Accessed 1 June 2016].

Barrer, R.M. & Sand, L.B., 1978. *Natural Zeolites: Occurrence, Properties, Use*. Oxford: Pergamon Press Ltd.

Barthomeuf, D., 1991. Acidity and Basicity in Zeolites. *Studies in Surface Science and Catalysis*, 65, pp.157-69.

Barthomeuf, D., Coudurier, G. & Vedrine, J.C., 1988. Basicity and basic catalytic properties of zeolites. *Materials Chemistry and Physics*, 18(5-6), pp.553-75.

Bauer, T. & Baur, W.H., 1998. Structural changes in the natural zeolite gismondine (gis) induced by cation exchange with Ag, Cs, Ba, Li, Na, K, Rb. *European Journal of Mineralogy*, 10, pp.133-47.

Baur, W.H., 1992. Why the open framework of zeolite A does not collapse, while the dense framework of natrolite is collapsible. In Rozwadowski, M., ed. *Proceedings of the Polish-German zeolite colloquium*. Torun, 1992. Nicholas Copernicus University Press.

Baur, W.H., 1995. Framework mechanics: limits to the collapse of tetrahedral frameworks. In Rozwadowski, M., ed. *Proceedings of the 2nd Polish-German zeolite colloquium*. Torus, 1995. Nicholas Copernicus University Press.

BBC News, 2015. *COP21 climate change summit reaches deal in Paris*. [Online] Available at: http://www.bbc.co.uk/news/science-environment-35084374 [Accessed 11 May 2016].

Becke, A.D., 1988. Density-functional exchange-energy approximation with correct asymptotic behavior. *Physical Review A*, 38, p.3098.

Bell, R.G., Jackson, R.A. & Catlow, C.R.A., 1992. *Zeolites*, 12, pp.870-71.

Bergk, K.H., Porsch, M. & Drews, 1987. *Journal of Chemical Technologies (Leipzig)*, 39(7), p.308.

Berkgaut, V. & Singer, A., 1996. *Applied Clay Science*, 10, p.369.

Berzon, D.F.a.A., 2015. *Colorado Mine Spill Highlights Superfund Challenges*. [Online] Available at: www.wsj.com/articles/colorado-mine-spill-highlights-superfund-challenges-1442005828 [Accessed 11 May 2016].

Biskup, B. & Subotic, B., 2000. Removal of heavy-metal ions from solutions by means of zeolites. II. Thermodynamics of the exchange processes between zinc and lead ions from solutions and sodium ion from zeolite-a. *Separation Science and Technology*, 35(14), pp.2311-26.

Blanchard, G., Maunaye, M. & Martin, G., 1984. Removal of heavy metals from waters by means of natural zeolites. *Water Research*, 18(12), pp.1501-07.

Blaylock, M.J. & Huang, J.W., 2000. *Phytoextraction of metals. Phytoremediation of toxic metals: using plants to clean up the environment*. 1st ed. Toronto: John Wiley and Sons, inc.

Bowman, R.S., 2003. Applications of surfactant-modified zeolites to environmental remediation. *Microporous and Mesoporous Materials*, 61(1-3), pp.43-56.

Braithwaite, R.S.W., Dyer, A., Lamb, R.P.H. & Wilson, J.I., 2001. Gismondine-Ba, A Zeolite from the Weathering of Slags. *Journal of the Russell Society*, 7(2), pp.83-85.

Brock, T.D., 1994. *Biology of Microorganisms*. Englewood Cliffs, New Jersey: Prentice Hall.

Bruker Corporation, 2016. *Environmental Soil Analysis, Contaminated Soil Testing with Bruker's S1 TITAN Handheld XRF Analyzer*. [Online] Available at: https://www.bruker.com/products/x-ray-diffraction-and-elemental-analysis/handheld-xrf/applications/restricted-materials/contaminated-soil-analysis.html [Accessed 1 June 2016].

Buondonno, A., Coppola, E., de Nicola, E. & Colella, C., 2005. Zeolitized tuffs in restorative pedotechnical activities: evidence of soil toxicity abatement against biota through bio-test with sea urchin Paracentrotus lividus. *Studies in Surface Science and Catalysis*, 158, p.2057.

Burgot, J.L., 2012. *Ionic Equilibria in Analytical Chemistry*. New York, Dordrecht, Heidelberg, London: Springer.

Burns, R.G., 1976. The uptake of cobalt into ferromanganese nodules, soils, and synthetic manganese (IV) oxides. *Geochimica et Cosmochimica Acta*, 40, pp.95-102.

Campbell, L.S. & Davies, B.E., 1997. Experimental investigation of plant uptake of caesium from soils amended with clinoptilolite and calcium carbonate. *Plant and Soil*, 189, pp.65-74.

Canepa, P., 2011. *New insights on iron and lead-based materials beyond density functional theory*. Canterbury: University of Kent.

Casas, J.S. & Sordo, J., 2006. *Lead: Chemistry, analytical aspects, environmental impact and health effects*. 1st ed. Amsterdam, Boston: Elsevier.

Castaldi, P., Santona, L., Enzo, S. & Melis, P., 2008. Sorption processes and XRD analysis of a natural zeolite exchanged with Pb2+, Cd2+ and Zn2+ cations. *Journal of Hazardous Materials*, 156, pp.428-34.

Catalfamo, P. et al., 1994. *Materials Science and Engineering*, 5(2), p.159.

Centers for Disease Control and Prevention, 2007. *Lead Toxicity*. [Online] Available at: http://www.atsdr.cdc.gov/csem/csem.asp?csem=7&po=8 [Accessed 10 July 2016].

Central Facility for Advanced Microscopy and Microanalysis - U.C. Riverside, 2016. *Introduction to Energy Dispersive X-ray Spectrometry (EDS)*. [Online] Available at: cfamm.ucr.edu/documents/eds-intro [Accessed 19 July 2016].

Central Facility for Advanced Microscopy and Microanalysis, 2016. *Chapter 7 Guideline Sample Preparation*. [Online] Available at: http://cfamm.ucr.edu/documents/sample-prep.pdf [Accessed 16 February 2017].

Centre for Public Environmental Oversight (CPEO), 2010. *Electrochemical Remediation Technologies*. [Online] Available at: http://www.cpeo.org/techtree/ttdescript/ecrta.htm [Accessed 12 May 2016].

Chang, R., 2000. *Physical Chemistry for the chemical and biological sciences*. 3rd ed. Sausalito: University Science Books.

Chantiwas, R., Shiowatana, J., Nacapricha, D. & Edwards, R., 2000. Evaluation of metal stabilization ability of adsorbents for toxic metals in solid waste by sequential extraction. *Journal of Environmental Science and Health, Part A*, 35(6), pp.849-67.

Chao, T.T. & Theobald, P.K., 1976. The significance of secondary ion and manganese oxides in geochemical exploration. *Economic Geology*, 71, pp.1560-69.

Charlesworth, S.M. & Lees, J.A., 1999. The distribution of heavy metals in deposited urban dusts and sediments, Coventry, England. *Environmental Geochemistry and Health*, 21(2), pp.97-115.

Chelishchev, N.F., 1993. Use of natural zeolites at Chernobyl in: D.W., Mumpton, F.A., Ming (Eds.). *Natural Zeolites '93, International Committee on Natural Zeolites*, pp.525-32.

Chen, H.M., Zheng, C.R., Tu, C. & Shen, Z.G., 2000. Chemical methods and phytoremediation of soil contaminated with heavy metals. *Chemosphere*, 41(1), pp.229-34.

Christensen, J.B., Jensen, D.L. & Christensen, T.H., 1996. Effect of dissolved organic carbon on the mobility of cadmium, nickel and zinc in leachate polluted groundwater. *Water Research*, 30(12), pp.3037-49.

City Collegiate, 2014. *Sulphuric Acid (H2SO4)*. [Online] Available at: http://www.citycollegiate.com/sulphuric_acidIXa.htm [Accessed 22 July 2016].

Clark, J., 2013. *The Contact Process*. [Online] Available at: http://www.chemguide.co.uk/physical/equilibria/contact.html [Accessed 22 July 2016].

CLU-IN, US EPA Contaminated Site Clean-up Information, 2015. *X-Ray Fluorescence*. [Online] Available at: https://clu-in.org/characterization/technologies/xrf.cfm [Accessed 17 July 2016].

Colella, C., 1999. Environmental applications of natural zeolitic materials based on their ion-exchange properties in: P. Misaelides, F. Macasek, T.J. Pinnavaia, C. Colella (Eds.). *Application of Natural Microporous Materials in Environmental Technology - Kluwer, NATO Science Series*, E362 (Applied Sciences), pp.207-24.

Colella, C., 2007. Recent advances in natural zeolite applications based on external surface interaction with cations and molecules. *Studies in Surface Science and Catalysis*, 170, pp.2063-73.

Coles, D.G. et al., 1979. *Environmental Science and Technology*, 20, p.455.

College of Life Science - National Tsing Hua University, n.d. *Beer-Lambert Law*. [Online] Available at: http://life.nthu.edu.tw/~labcjw/BioPhyChem/Spectroscopy/beerslaw.htm [Accessed 18 July 2016].

Collins, E.D., 1982. *The three mile island accident and post-accident recovery - What did we learn?* Conference Report CONF-820559-1. Oak Ridge National Laboratory.

Collins, L.P., 2009. *Heavy Metal Contamination of the Environment Associated with Old Paper Mills, BSc Thesis*. Canterbury: University of Kent.

Cox, G.W., 1997. *Conservation Biology*. 2nd ed. William C. Brown Publishers.

CRYSTAL, 2016. *A Computational Tool for Solid State Chemistry and Physics*. [Online] Available at: www.crystal.unito.it/index.php [Accessed 19 July 2016].

Curkovic, L., Cerjan-Stefanovic, S. & Filipan, T., 1997. Metal ion exchange by natural and modified zeolites. *Water Research*, 31(6), pp.1379-82.

de Gree, A., 2015. *The History and Working Principle of the Scanning Electron Microscope (SEM)*. [Online] Available at: http://www.azonano.com/aarticle.aspx?ArticleID=3995 [Accessed 19 July 2016].

Dickson, H., 2012. *Atomic Absorption for Trace Element Analysis in the Food and Beverage Industry*. [Online] Available at: http://www.foodqualityandsafety.com/article/atomic-absorption-for-trace-element-analysis-in-the-food-and-beverage-industry/ [Accessed 1 June 2016].

Divjak, B., Franko, M. & Novic, M., 1998. Determination of iron in complex matrices by ion chromatography with UV–Vis, thermal lens and amperometric detection using post-column reagents. *Journal of Chromatography A*, 829(1-2), pp.167-74.

Dong, D. et al., 2007. Lead and cadmium adsorption onto iron oxides and manganese oxides in the natural surface coatings collected on natural substances in the Songhua River of China. *Chemical Research in Chinese Universities*, 23(6), pp.659-64.

Douglas, B., 2015. *Anger rises as Brazilian mine disaster threatens river and sea with toxic mud*. [Online] Available at: https://www.theguardian.com/business/2015/nov/22/anger-rises-as-brazilian-mine-disaster-threatens-river-and-sea-with-toxic-mud [Accessed 4 May 2016].

Dovesi, R. et al., 2009. CRYSTAL09 User's Manual. *University of Torino*.

Duke University, 2014. Acid mine drainage reduces radioactivity in fracking waste. *Science Daily*, 9 January. Available at: http://www.sciencedaily.com/releases/2014/01/140109132644.htm.

Dunlap, M. & Adaskaveg, J.E., 1997. *Introduction to the Scanning Electron Microscope*. U.C. Davis: Facility for Advanced Instrumentation.

Dunnivant & Ginsbach, 2009. Chapter 2 - Flame atomic absorption and emission spectroscopy. In *Flame Atomic Absorbance and Emission Spectroscopy and Inductively Coupled Spectrometry - Mass Spectrometry*. Whitman College.

Dyer, A., 1995. *Mineral Surfaces*. London: Chapman and Hall.

Ekpo, B.O. & Ibok, U.J., 1999. Temporal variation and distribution of trace metals in freshwater and fish from Calabar River, S.E. Nigeria. *Environmental Geochemistry and Health*, 21(1), pp.51-66.

EPA, U.E.P.A., 2016. *What is Acid Rain?* [Online] Available at: https://www.epa.gov/acidrain/what-acid-rain [Accessed 18 December 2016].

Esmaeili Bidhendi, M. et al., 2010. Potential of natural bed soil in adsorption of heavy metals in industrial waste landfill. *International Journal of Environmental Science & Technology*, 7(3), pp.545-52.

Evans Analytical Group Materials Characterization, 2016. *X-Ray Diffraction (XRD) Analysis*. [Online] Available at: http://www.eag.com/mc/x-ray-diffraction.html [Accessed 1 June 2016].

Fernandes-Machado, N.R.C. & Miotto, D.M.M., 2005. Synthesis of Na-A and -X zeolites from oil shale ash. *Fuel*, 84(18), pp.2289-94.

Finley, J.P., 2004. Using the local density approximation and the LYP, BLYP, and B3LYP functionals within Reference--State One--Particle Density--Matrix Theory. *Molecular Physics: An International Journal at the Interface Between Chemistry and Physics*, 102(7), pp.627-39.

First, E.L., Gounaris, C.E., Wei, J. & Floudas, C.A., 2011. Computational characterization of zeolite porous networks: an automated approach. *Physical Chemistry Chemical Physics*, 13(38), pp.17339-58.

Franklin, K.R. & Townsend, R.P., 1985. Multicomponent Ion Exchange in Zeolites - Part 1.- Equilibrium Properties of the Sodium/Calcium/Magnesium - Zeolite-A System.

Journal of the Chemical Society - Faraday Transactions 1: Physical Chemistry in Condensed Phases, 81(4), pp.1071-86.

Fraser Institute, 2012. *What is acid rock drainage?* [Online] Available at: http://www.miningfacts.org/Environment/What-is-acid-rock-drainage/ [Accessed 31 December 2016].

Gadepalle, V., Ouki, S., Van Herwijnen, R. & Hutchings, T., 2007. Immobilization of Heavy Metals in Soil Using Natural and Waste Materials for Vegetation Establishment on Contaminated Sites. *Soil and Sediment Contamination: An International Journal*, 16(2), pp.233-51.

Garcia, R. & Baez, A.P., 2012. *Atomic Absorption Spectrometry (AAS)*. Available at: http://www.intechopen.com/books/atomic-absorption-spectroscopy/atomic-absorption-spectrometry-aas.

Garcia-Sanchez, A., Alastuey, A. & Querol, X., 1999. Heavy metal adsorption by different minerals: application to the remediation of polluted soils. *The Science of the Total Environment*, 242, pp.179-88.

Garcia, R., Torres, M.C. & Baez, A., 2008. Determination of trace elements in total suspended particles at the Southwest of Mexico City from 2003 to 2004. *Chemistry and Ecology*, 24(2), pp.157-67.

Georgiev, D. et al., 2009. *Synthetic Zeolites - Structure, Clasification, Current Trends in Zeolite Synthesis Review*. Stara Zagora, Bulgaria: International Science Conference.

Glasel, J.A. & Deutscher, M., 1995. *Introduction to Biophysical Methods for Protein and Nucleic Acid Research*. San Diego, London: Academic Press, Inc.

Gonzalez-Nunez, R. et al., 2011. Remediation of metal-contaminated soils with the addition of materials - Part I: Characterization and viability studies for the selectio of non-hazardous waste materials and silicates. *Chemosphere*, 85, pp.1511-17.

Gonzalez-Nunez, R. et al., 2012. Remediation of metal-contaminated soils with the addition of materials - Part II: Leaching tests to evaluate the efficiency of materials in the remediation of contaminated soils. *Chemosphere*, 87, pp.829-37.

Google Maps Europe, 2011. *Google Maps Europe*. [Online] Available at: http://googlemapseurope.blogspot.co.uk/2011/05/map-of-sweden-cities-pictures.html [Accessed 15 February 2017].

Google Maps, 2014. *Oskarstrom Paper Mill Site*. [Online] Oskarstrom: Digital Globe (Oskarstrom) Available at: https://www.google.co.uk/maps/place/SVEAGATAN+5,+313+33+Oskarstr%C3%B6m,+Sweden/@56.7906781,12.9709437,389m/data=!3m2!1e3!4b1!4m5!3m4!1s0x4651af7c4e1e8f55:0xe95c2a1f5e1ef540!8m2!3d56.7906752!4d12.9731324.

Gounaris, V., Anderson, P.R. & Holsen, T.M., 1993. Characteristics and environmental significance of colloids in landfill leachate. *Environmental Science and Technology*, 27(7), pp.1381-87.

Greenwood, N.N. & Earnshaw, A., 1997. *Chemistry of the Elements*. 2nd ed. Oxford, Burlington: Butterworth-Heinemann.

Guiner, A., 1963. *X-ray Diffraction in Crystals, Imperfect Crystals and Amorphous Bodies*. New York: Dover Publications.

Guisnet, M. & Gilson, J.P., 2002. *Zeolites for Cleaner Technologies - Catalytic Science Series, Volume 3*. London: Imperial College Press.

Habas, M.P., Dovesi, R. & Lichanot, A., 1998. *Journal of Physics: Condensed Matter*, 10, pp.6897-909.

Hamon, R., McLaughlin, M. & Lombi, E., 2007. *Natural Attenuation of Trace Element Availability in Soils*. Florida: Society of Environmental Toxicology and Chemistry.

Hannaford, P.W.A., 2000. 19 December 1916 - 3 August 1998. *Biographical Memoirs of Fellows of the Royal Society*, 46, pp.533-64.

Hardinger, S., 2016. *Guide to Understanding X-ray Crystallography*. [Online] Available at: http://www.chem.ucla.edu/~harding/ec_tutorials/tutorial73.pdf [Accessed 19 July 2016].

Hartman, R.L. & Fogler, H.S., 2007. Understanding the Dissolution of Zeolites. *Langmuir*, 23(10), pp.5477-84.

Hart, M.R., Quin, B.F. & Nguyen, M.L., 2004. Phosphorus Runoff from Agricultural Land and Direct Fertilizer Effects. *Journal of Environmental Quality*, 33(6), pp.1954-72.

Hay, P.J. & Wadt, W.R., 1985. *Journal of Physical Chemistry*, 82, p.270.

Headwaters Resources, I., 2013. *About Fly Ash*. [Online] Available at: http://flyash.com/about-fly-ash/ [Accessed 22 July 2016].

Hehre, W.J., Stewart, R.F. & Pople, J.A., 1969. *Journal of Chemical Physics*, 51, pp.2657-64.

Henry, D., 2016. *Dem offers bill to present toxic mine spills*. [Online] Available at: thehil.com/policy/energy-environment/264986-democrat-pushes-bill-responding-to-summer-mine-waste-spill [Accessed 11 May 2016].

Heo, N., Kim, H.S., Lim, W.T. & Seff, K., 2004. Synthesis and Crystal Structure of Ag4I4 Nanoclusters in the Sodalite Cavities of Fully K+-Exchanged Zeolite A. *Journal of Physical Chemistry B*, 108(10), pp.3168-73.

Higgins, F.M., de Leeuw, N.H. & Parker, S.C., 2002. *Journal of Materials Chemistry*, 12, pp.124-31.

Higgins, F.M., Watson, G.W. & Parker, S.C., 1997. *Journal of Physical Chemistry B*, 101, pp.9964-72.

Hill, S.J., Bloxham, M.J. & Worsfold, P.J., 1993. Chromatography coupled with inductively coupled plasma atomic emission spectrometry and inductively coupled plasma mass spectrometry. A review. *Journal of Analytical Atomic Spectroscopy*, 8, pp.499-515.

Holler & Crouch, 2014. *Skoog and West's Fundamental Analytical Chemsitry*. 9th ed. Austrailia, Brazil, Japan, Korea, Mexico, Singapore, Spain, Uk, US: Brooks/Cole Cengage Learning.

Holler, H. & Wirsching, U., 1985. *Fortschr Mineral*, 63(1), p.21.

Huang, J.W.. & Cunningham, S.D., 1996. Lead phytoextraction: species variation in lead uptake and translocation. *New Phytologist*, 145, pp.75-84.

Huang, M.M., Kaliaguine, S., Muscas, M. & Auroux, A., 1995. Microcalorimetric Characterization of the Basicity in Alkali-Exchanged X Zeolites. *Journal of Catalysis*, 157, pp.266-69.

Inque, K., Tsunematsu, S. & Yamada, H., 1995. *Muk Materiaru*, 225(2), p.108.

International Zeolite Association, 2016. *Gismondine*. [Online] Available at: http://www.iza-online.org/natural/Datasheets/Gismondine/Gismondine.html [Accessed 18 July 2016].

Ivezic, V. et al., 2013. Comparison of Different Extraction Methods Representing Available and Total Concentrations of Cd, Cu, Fe, Mn, and Zn in Soil. *Poljoprivreda*, 19(1), pp.53-58.

Jackson, R.A. & Catlow, C.R.A., 1998. *Molecular Simulations*, 1, pp.207-24.

Jacobs, J., Hardison, R.L. & Rouse, J.V., 2001. In-Situ Remediation of Heavy Metals Using Sulfur-Based Treatement Technologies. *Hydrovisions*, 10(2), pp.1,4-5.

Jeffrey, K.L., 2011. *Analysis of Heavy Metal Contamination of Soil & Groundwater at a Former Industrial Stie in Oskarstrom, Sweden*. MSc Thesis. Kent: University of Kent, Canterbury.

Jenne, E.A., 1968. Controls on Mn, Fe, Co, Ni, Cu, and Zn concentrations in soils and water: The significant role of jydrous Mn and Fe oxides. *Trace Inorganics in Water*, pp.337-87.

Jennings, S.R., Neuman, D.R. & Blicker, P.S., 2008. *Acid Mine Drainage and Effects on Fish Health and Ecology: A Review*. Bozeman, MT: Reclamation Research Group Publication. Available at: http://reclamationresearch.net/publications/Final_Lit_Review_AMD.pdf.

Jensen, D.L., Ledin, A.L. & Christensen, T.H., 1999. Speciation of heavy metals in landfill-leachate polluted groundwater. *Water Research*, 33(11), pp.2642-50.

Kato, Y., Kakimoto, K., Ogawa, H. & Tomari, M., 1986. *Kogyo Yosui*, 338, p.37.

Katsou, E. et al., 2011. Regeneration of natural zeolite polluted by lead and zinc in wastewater. *Journal of Hazardous Materials*, 189, pp.773-86.

Kim, S.H. et al., 2006. Synthesis and crystal structure of lead iodide in the sodalite cavities of zeolite A (LTA). *Synthesis and crystal structure of lead iodide in the Zeolite-A*, 27(5), pp.679-86.

Kim, Y., Subramanian, V., Firor, R.L. & Seff, K., 1980. *Adsorption and Ion Exchange with Synthetic Zeolites*, Chapter 7, pp.137-53.

KK, S., 2012. *Manufacture of sulphuric acid (H2SO4) by Lead Chamber Process*. [Online] Available at: http://www.inclusive-science-engineering.com/manufacture-of-h2so4-by-chamber-process/ [Accessed 24 July 2016].

Klein, D.H. et al., 1975. Pathways of thirty-seven trace elements through coal-fired power plans. *Environmental Science and Technology*, 9, pp.937-39.

Kolezynski, A., Mikula, A. & Krol, M., 2016. *Spectrochimica Acta Part A: Molecular and Biomolecular Spectroscopy*, 157, pp.17-25.

Kolousek, D. et al., 1993. *Acta Universitatis Carolinae Geologica*, 37, p.167.

Kondash, A.J., Warner, N.R., Lahav, O. & Vengosh, A., 2014. Radium and barium removal through blending hydraulic fracturing fluids with acid mine drainage. *Environmental Science and Technology*, 48, pp.1334-42.

Kudra, T. & Mujumdar, A.S., 2009. *Advanced Drying Technologies*. 2nd ed. Boca Raton, London, New York: CRC Press - Taylor and Francis Group.

Larosa, J.L., Kwan, S. & Grutzeck, M.W., 1992. *Journal of American Ceramic Society*, 75(6), p.1574.

Laskowski, R. & Hopkin, S.P., 1996. Accumulation of Zn, Cu, Pb, and Cd in the garden snail (helix aspersa) implication for predators. *Environmental Pollution*, 91, pp.289-97.

Leach, A., 2001. *Molecular Modelling: Principles and Applications*. Pearson Education.

Lee, C., Yang, W. & Parr, R.G., 1988. Development of the Colle-Salvetti correlation-energy formula into a functional of the electron density. *Physical Review B*, 37, p.785.

Leggo, P.J., Ledesert, B. & Christie, G., 2006. The role of clinoptilolite in organo-zeolitic-soil systems used for phytoremediation. *Science of the Total Environment*, 363(1-3), pp.1-10.

Lewen, N., 2011. The use of atomic spectroscopy in the pharmaceutical industry for the determination of trace elements in pharmaceuticals. *Journal of Pharmaceutical and Biomedical Analysis*, 55(4), pp.653-61.

Liberti, L., Boghetich, G., Lopez, A. & Petruzelli, D., 1999. Application of microporous materials for the recovery of nutrients from wastewaters in: P. Misaelides, F. Macasek, T.J. Pinnavaia, C. Colella (Eds.). Application of Natural Microporous Materials in Environmental Technology, Kluwer, NATO Science Series. *University of Applied Sciences Dordrecht*, E362, pp.253-70.

Li, L.Y. et al., 2007. Remediation of Acid Rock Drainage by Regenerable Natural Clinoptilolite. *Water, Air, and Soil Pollution*, 180(1), pp.11-27.

Lichtfouse, E., Schwarzbauer, J. & Robert, D., 2013. *Pollutant Diseases, Remediation and Recycling*. Cham, Heidelberg, New York, Dordrecht, London: Springer.

Lim, W.T. et al., 2005. Synthesis and Crystal Structure of Ag4Br4 Nanoclusters in the Sodalite Cavities of Fully K+-Exchanged Zeolite A (LTA). *Bulletin of the Korean Chemical Society*, 26(7), p.1090.

Lin, C.F. & Hsi, H.C., 1995. *Environmental Science and Technology*, 29(4), p.1109.

Li, H., Shi, W., Shao, H. & Shao, M., 2009. The remediation of the lead-polluted garden soil by natural zeolite. *Journal of Hazardous Materials*, 169, pp.1106-11.

L, M.J., Mench, M. & Guckert, A., 1986. Measurement of Pb2+,Cu2+and Cd2+binding withmucilage exudates from maize (Zea mays L.) roots. *Biology and Fertility of Soils*, 2, pp.29-34.

Mader, S.S., 1996. *Biology*. 5th ed. William C. Brown Publishers.

Malliou, E., Loizidou, M. & Spyrellis, N., 1994. Uptake of lead and cadmium by clinoptilolite. *Science of the Total Environment*, 149(3), pp.139-44.

Massarani, L., 2015. *Brazilian mine disaster releases dangerous metals*. [Online] Available at: www.rsc.org/chemistryworld/2015/11/brazil-mine-disaster-dam-collapse [Accessed 11 May 2016].

Matthews, P., 1992. *Advanced Chemistry*. 3rd ed. Cambridge, New York: Cambridge University Press.

McBride, M.B., 1994. *Environmental Chemistry of Soils*. Oxford University Press.

McCann, C.M. et al., 2015. Remediation of a historically Pb contaminated soil using a model natural Mn oxide waste. *Chemosphere*, 138, pp.211-17.

McConnell, J.R. & Edwards, R., 2008. Coal burning leaves toxic heavy metal legacy in the Arctic. *Proceedings of the National Academy of Sciences of the United States of America*, 105(34), pp.12140-44.

McGraw-Hill, 2002. *McGraw-Hil Concise Encyclopedia of Physics*. The McGraw-Hill Companies, Inc.

McKenzie, R.M., 1980. The adsorption of lead and other heavy metals on oxides of manganese and iron. *Austrailian Journal of Soil Research*, 18(1), pp.61-73.

Mehta, A., 2012. *Ultraviolet-Visible (UV-Vis) Spectroscopy – Limitations and Deviations of Beer-Lambert Law*. [Online] Available at: http://pharmaxchange.info/press/2012/05/ultraviolet-visible-uv-vis-spectroscopy-%E2%80%93-limitations-and-deviations-of-beer-lambert-law/ [Accessed 24 June 2016].

Mellanby, K., 1988. *Air Pollution, Acid Rain and the Environment: Report Number 18*. London, New York: Elsevier Applied Science.

Michelic, S.K., Wieser, G. & Bernhard, C., 2011. On the representativeness of automated SEM/EDS analyses for inclusion characterisation with special regard to the measured sample area. *ISIJ International*, 51(5), pp.769-75.

Mills, C., 2012. *An Introduction to Acid Rock Drainage*. [Online] Available at: http://technology.infomine.com/enviromine/ard/Introduction/ARD.HTM [Accessed 31 December 2016].

mindat.org, 2016. *Cubanite*. [Online] Available at: http://www.mindat.org/min-1168.html [Accessed 17 July 2016].

mindat.org, 2016. *Illite*. [Online] Available at: http://www.mindat.org/min-2011.html [Accessed 17 July 2016].

Ming, D.W. & Mumpton, F.A., 1989. *Minerals in Soil Environments*. 2nd ed. Wisconsin: Soil Science of America.

Misaelides, P., 2011. Application of natural zeolites in environmental remediation: A short review. *Microporous and Mesoporous Materials*, 144, pp.15-18.

Mohapatra, J., Mitra, A., Bahadur, D. & Aslam, M., 2013. Controlled synthesis of MFe2O4 (M=Mn, Fe, Co, Ni, and Zn) Nanoparticles and their magnetic properties. *CrystEngComm*, 15(3), pp.524-32.

Moirou, A., Vaxevanidou, A., Christidis, G.E. & Paspaliaris, I., 2000. Ion Exchange of Zeolite Na-Pc WITH Pb 2+, Zn 2+, and Ni 2+ ions. *Clays and Clay Minerals*, 48(5), pp.563-71.

Moldan, F..C.B.J..W.R.F., 2013. Modeling Past and Future Acidification of Swedish Lakes. *Ambio*, 42(5), pp.577-86.

Momodu, M.A. & Anyakora, C.A., 2010. Heavy Metal Contamination of Ground Water: The Surulere Case Study. *Research Journal of Environmental and Earth Sciences*, 2(1), pp.39-43.

Mon, J., Deng, Y., Flury, M. & Harsh, J.B., 2005. Cesium incorporation and diffusion in cancrinite, sodalite, zeolite, and allophane. *Microporous Mesoporous Materials*, 86, pp.277-86.

Mondragon, F. et al., 1990. *Fuel*, 69(2), p.263.

Moreno, N. et al., 2001. Immobilization of heavy metals in polluted soils by the addition of zeolitic material synthesized from coal fly ash. In *International Ash Utilization Symposium, Centre for Applied Energy Research*. University of Kentucky, 2001.

Moseley, H.G.J., 1914. LXXX The High Frequency Spectra of the Elements. Part II. *Philosophical Magazine*, 27(160), p.703.

Munthali, M.W., Elsheikh, M.A., Johan, E. & Matsue, N., 2014. Proton Adsorption Selectivity of Zeolites in Aqueous Media: Effect of Si/Al Ratio of Zeolites. *Molecules*, pp.20468-81.

Nave, R., 2016. *Characteristic X-rays*. [Online] Available at: http://hyperphysics.phy-astr.gsu.edu/hbase/quantum/xrayc.html [Accessed 18 July 2016].

Nave, R., 2016. *Coloumb's Law*. [Online] Available at: http://hyperphysics.phy-astr.gsu.edu/hbase/electric/elefor.html [Accessed 19 July 2016].

Nery, J.G., Mascarenhas, Y.P. & Cheetham, A.K., 2003. A study of the highly crustalline, low-silica, fully hydrated zeolite P ion exchanged with (Mn2+, Cd2+, Pb2+, Sr2+, Ba2+) cations. *Microporous and Mesoporous Materials*, 57, pp.229-48.

Niemantsverdriet, J.W., 2007. *Spectroscopy in Catalysis. An introduction*. 3rd ed. Verlag: Wiley.

Nordback, e.a.., 2004. *Private Communication: Karaktariseing av kisaska, SGI-V550*.

Nordberg, G.F., Goyer, R.A. & Clarkson, T.W., 1985. Impact of effects of acid precipitation on toxicity of metals. *Environmental Health Persective*, 63, pp.169-80.

Norton Rose Fulbright, 2014. *Significant penalties imposed on shipowner involved in oil spill, but master escapes conviction*. [Online] Available at: http://www.nortonrosefulbright.com/knowledge/publications/118580/significant-penalties-imposed-on-shipowner-involved-in-oil-spill-but-master-escapes-conviction [Accessed 23 May 2016].

Nriagu, J.O., 1978. Lead in soils, sediments and major rock types. *The Biogeochemistry of Lead in the Environment: Ecological Cycles*, pp.16-72.

Nriagu, J.O. & Moore, P.B., 1984. *Phosphate Minerals*. Berlin, Heidelberg, New York, Tokyo: Springer-Verlag.

OHCHR, 2015. *Brazilian mine disaster: "This is not the time for defensive posturing" - UN rights experts*. [Online] Available at: www.ohchr.org/CH/NewsEvents/Pages/DisplayNews.aspx?NewsID=16803&LangID=E [Accessed 11 May 2016].

Ohmura, N., Kitamura, K. & Saiki, H., 1993. Selective adhesion of Thiobacillus ferrooxidans to Pyrite. *Applied and Environmental Microbiology*, 59(12), pp.4044-50.

O'Leary, D., 2000. *Sulphuric Acid*. [Online] Available at: http://www.ucc.ie/academic/chem/dolchem/html/comp/h2so4.html [Accessed 22 July 2016].

Oliveira, M.L.S. et al., 2012. Chemical composition and minerals in pyrite ash of an abandoned sulphuric acid production plant. *Science of the Total Environment*, 430, pp.34-47.

Olympus Corporation, n.d. *XRF Technology for Analysis of Arsenic and Lead in Soil*. [Online] Available at: http://www.olympus-ims.com/en/applications/xrf-technology-analysis-arsenic-lead-soil/ [Accessed 8 July 2016].

Open University, 1996. *PHYS 7.1: The atomic basis of matter*. [Online] Available at: http://www.physics.brocku.ca/PPLATO/h-flap/phys7_1.html [Accessed 22 December 2015].

Ording, E.T., 2009. *Heavy Metals and Coal: Carbon Footprint Aside, Coal is not Environmentally Friendly*. [Online] Available at: http://environmentalism.suite101.com/article.cfm/heavy_metals_and_coal [Accessed 19 December 2016].

O'Reilly, S.E. & Hochella Jr, M.F., 2003. Lead sorption efficiencies of matural and synthetic Mn and Fe-oxides. *Geochimica et Cosmochimica Acta*, 67, pp.4471-87.

Oste, L.A., Lexmond, T.M. & van Riemsdijk, W.H., 2002. Metal Immobilization in Soils Using Synthetic Zeolites. *Journal of Environmental Quality*, 31(3), pp.813-21.

Pansar, J., 2005. *Om försurning av sjöar och vattendrag*. Stockholm: Länsstyrelsens i Stockholms Lan.

Park, M. & Choi, 1995. *Journal of Clay Sciences*, 9(4), p.219.

Parr, R.G. & Yang, W., 1989. *Density Functional Theory of Atoms and Molecules*. New York: Oxford University Press.

Peppas, A., Komnitsas, K. & Halikia, I., 2000. Use of Organic Covers for Acid Mine Drainage Control. *Minerals Engineering*, 13(5), pp.563-74.

Perry, A. & Kleinmann, R.L.P., 1991. The use of constructed wetlands in the treatment of acid mine drainage. *Natural Resources Forum*, 15(3), pp.178-84.

Peskov, M., 2017. *Zeolites*. [Online] Available at: http://asdn.net/asdn/chemistry/zeolites.php [Accessed 15 January 2017].

Petersson, G., 2008. *Kemisk Miljövetenskap*. Chalmers.

Piskunov, S., Heifets, E., Eglitis, R.I. & Borstel, G., 2004. *Computational Materials Science*, 29, pp.165-78.

Pluth, J.J. & Smith, J.V., 1980. *Journal of the American Chemical Society*, 102, pp.4704-08.

Pyatt, F.B., 1987. Acid rain in scandinavia - some current data. *Environmentalist*, 7(3), pp.197-200.

Querol, X., Alastuey, A., Fernandez-Turiel, J.L. & Lopez-Soler, A., 1995. *Fuel*, 74(8), p.1226.

Querol, X., Alastuey, A., Lopez-Soler, A. & Plana, F., 1997. A fast method for recycling fly ash: microwave-assisted zeolite synthesis. *Environmental Science and Technology*, 31(9), pp.2527-33.

Querol, X. et al., 1997. *Environmental Science and Techology*, 31(9), p.2527.

Querol, X. et al., 2006. Immobilization of heavy metals in polluted soils by the addition of zeolite material synthesized from coal fly ash. *Chemosphere*, 62, pp.171-80.

Querol, X. et al., 1995. *International Journal of Coal Science and Technology*, 24, p.1979.

Querol, X., Plana, F., Alastuey, A. & Lopez-Soler, A., 1997. Synthesis of Na-zeolites from fly ash. *Fuel*, 76(8), pp.793-99.

Querol, X., Plana, F., Alastuey, A. & Lopez-Soler, A., 1997. Synthesis of Na-zeolites from fly ash. *Fuel*, 76(8), pp.793-99.

Querol, X. et al., 1998. Eighth Austrailian Coal Science Conference., 1998.

Querol, X. et al., 2001. Synthesis of zeolites from fly ash at pilot plant scale. Examples of potential applications. *Fuel*, 80(6), pp.857-65.

Radojevic, M. & Bashkin, V.N., 2009. *Practical Environmental Analysis*. 2nd ed. RSC Publishing.

Ravishankara, A.R., Daniel, J.S. & Portmann, R.W., 2009. Nitrous Oxide (N2O): The Dominant Ozone-Depleting Substance Emitted in the 21st Century. *Science*, 326(5949), pp.123-25.

Regionalt program, 2005. *Regionalt program for arbete med fororenade omraden i Vasternorrlands Ian 2005*. Regionalt program.

Ribeiro, F.R., 1984. *Zeolites: Science and Technology*. The Hague: Martinus Nijhoff Publishers.

Rickard, D.T. & Nriago, J.O., 1978. Aqueous environmental chemistry of lead. *The Biogeochemistry of Lead in the Environment: Ecological Cycles*, pp.219-84.

Rieuwerts, J.S., Thornton, I., Farago, M.E. & Ashmore, M.R., 1998. Factors influencing metal bioavailability in soils: preliminary investigations for the development of a critical loads approach for metals. *Chemical Speciation and Bioavailability*, 10(2), pp.61-75.

Roessle, M., 2009. *Basics of X-ray Scattering*. Hamburg: Luebeck University of Applied Science.

Ronay, C. & Seff, K., 1985. Crystal structures of Pb6-A and Pb9(OH)8(H2O)3-A. Zeolite A ion exchanged with Pb2+ at pH 4.3 and 6.0 and evacuated. *Journal of Physical Chemistry*, 89(10), pp.1965-70.

Rouessac, F. & Rouessac, A., 2007. *Chemical Analysis, Modern Instrumentation Methods and Techniques*. 2nd ed. Chichester, West Sussex: John Wiley & Sons, Ltd.

Royal Society of Chemistry, 2016. *Arsenic*. [Online] Available at: www.rsc.org/periodic-table/element/33/arsenic [Accessed 4 May 2016].

Russell, J., 2016. *Rainwater Quality and Filtration*. [Online] Available at: http://www.whollyh2o.org/rainwater-stormwater/item/122-rainwater-quality-and-filtration.html.

Russell, M.J. & Hall, A.J., 2006. The onset and early evolution of life. *Geological Society of America - Memoir 198*, pp.1-32.

Rylander, H., 2007. *Uppdaterade bedomningsgrunder for fororenade massor Rapport 2007:01*. Avfall Sverige utveckling.

Saether, O.M., Storroe, G., Segar, D. & Krog, R., 1997. Contamination of Soil and Groundwater at a Former Industrial Site in Trondheim, Norway. *Applied Geochemistry*, 12, pp.327-32.

Sahi, S.V., Bryant, N.L., N.C., S. & S.R., S., 2002. Characterization of a lead hyperaccumulator shrub, Sesbania drummondii. *Environmental Science and Technology*, 36, pp.4676-80.

Sandatlas, n.d. *Composition of the Crust*. [Online] Available at: http://www.sandatlas.org/composition-of-the-earths-crust/ [Accessed 17 July 2016].

Santoyo, E., Santoyo-Gutierrez, S. & Verma, S.P., 2000. Trace analysis of heavy metals in groundwater samples by ion chromatography with post-column reaction and ultraviolet–visible detection. *Journal of Chromatography A*, 884, pp.229-41.

Sartorius, 2016. *Minisart® NML Syringe Filters 16534*. [Online] Available at: https://www.sartorius.co.uk/en/product/product-detail/16534-guk/.

Sarzanini, C., 1999. Liquid chromatography: a tool for the analysis of metal species. *Journal of Chromatography*, 850(1-2), pp.213-28.

Schikorr, G., 1933. Eisen(II)-hydroxyd u. ein ferromagnetisches Eisen(III)-hydroxyd. *Zeitschrift fur anorganische und allgemeine Chemie*, 212(1), pp.33-39.

Schippers, A., Hallmann, R., Wentzien, S. & Sand, W., 1995. Microbial diversity in uranium mine waste heaps. *Applied Environmental Microbiology*, 61(8), pp.2930-35.

Schwertmann, U. & Taylor, R.M., 1989. Iron Oxides. *Minerals in Soil Environments*, pp.379-438.

Schwuger, M.J., 1997. *Surfactant Science Series*. New York: Marcel Dekker, Inc.

Schwuger, M.J. & Smolka, H.G., 1978. Sodium-Aluminium-Silicates in the washing process. *Colloid and Polymer Science*, 256(10), pp.1014-20.

Seff, K. & Shoemaker, D.P., 1967. *Acta Crystallographica*, 22, pp.162-70.

Semmens, M.J. & Martin, W.P., 1988. The influence of pretreatment on the capacity and selectivity of clinoptilolite for metal ions. *Water Research*, 22(5), pp.537-42.

Semmens, M.J. & Seyfarth, M., 1978. *Natural Zeolites: Occurrence, Properties, Use*. Oxford: Pergamon Press Ltd.

Shaheen, S.M., Derbalah, A.S. & Moghanm, F.S., 2012. Removal of Heavy Metals from Aqueous Solution by Zeolite in Competitive Sorption System. *International Journal of Environmental Science and Development*, 3(4), pp.362-67.

Shahzad, M.A., 2012. *Effect of temperature and time on acid sulfite cooking for dissolving pulp - MSc Thesis*. Karlstad: Karlstad University.

Shannon, R.D., 1976. Revised Effective Ionic Radii and Systematic Studies of Interactomic Distances in Halides and Chalcogenides. *Acta Crystallographica*, A32, pp.751-67.

Shannon, R.D., 1976. Revised effective ionic radii and systematic studies of interatomic distances in halides and chalcogenides. *Acta Crystallographica A*, 32, pp.751-67.

Sharma, B.K., 2007. *Environmental Chemistry*. 11th ed. Meerut: Goel Publishing House.

Sharma, P. & Dubey, R.S., 2005. Lead toxicity in plants. *Brazilian Journal of Plant Physiology*, 17, pp.35-52.

Sherrill, C.D., 2000. *An Introduction to Hartree-Fock Molecular Orbital Theory*. Georgia Institute of Technology.

Shigemoto, N., Shirakami, S., Hirano, S. & Hayashi, H., 1992. *Nippon Kagaku Kaishi*, 5, p.484.

Shih, W.H., Chang, H.L. & Shen, Z., 1995. Material Research Society Symposium Proceedings. In *Advances in Porous Materials*., 1995.

Simmons, W.B., 2016. *Encyclopedia Britannica - Amphibole*. [Online] Available at: http://www.britannica.com/science/amphibole#ref618197 [Accessed 18 May 2016].

Singer, A. & Berkgaut, V., 1995. *Environmental Science and Technology*, 29, p.1748.

Skolvision TM, 2016. *Försurning*. [Online] Available at: http://www.skolvision.se/DelEnergi/NkEnergi5Acidification.html.

Skousen, J., n.d. *Acid Mine Drainage*. [Online] Available at: http://aciddrainage.com/acid-mine-drainage/ [Accessed 30 December 2016].

Smart, L.E. & Moore, E.A., 2005. *Solid State Chemistry*. 2nd ed. Boca Raton: Taylor & Francis.

SMHI, 2016. *Dataserier med normalvarden for perioden 1961-1990.* [Online] Available at: http://www.smhi.se/klimatdata/meteorologi/temperatur/dataserier-med-normalvarden-1.7354.

Snoeyink, V.L. & Jenkins, D., 1980. *Water Chemistry*. New York: John Wiley and Sons.

Sout, W.L., Hern, J.L., Korcak, R.F. & Carlson, C.W., 1988. ARS-74 *Manual for Applyig Fuidized Bed Combustion Residue to Agricultural Lands*. Agricultural Research Service.

Stachel, D., Paulus, H., Guenter, C. & Fuess, H., 1992. Crystal structure of magnesium ultraphosphate, MgP4O11. *Zeitschrift fur Kristallographic*, 199, pp.275-76.

Statistiska Centralbyran , 2016. *Statistiska Centralbyran*. [Online] Available at: http://www.scb.se/statistik/MI/AA9999/2003M00/MI01S%C3%850001_14.pdf.

Stojilovic, N., 2012. Why Can't We See Hydrogen in X-ray Photoelectron Microscopy. *Journal of Chemical Education*, 89, pp.1331-32.

Sundin, C.E., 2016. *Proteins and Amino Acids, Isolation of Casein, Organic Chemistry 3510*. [Online] Available at: http://people.uwplatt.edu/~sundin/351/351h-pro.htm [Accessed 23 December 2016].

Suryanarayana, C. & Grant Norton, M., 1998. *X-ray Diffraction: A Practical Approach*. 1st ed. New York: Springer Science+Business Media.

Sutton, K., Sutton, R.M.C. & Caruso, J.A., 1997. Inductively coupled plasma mass spectrometric detection for chromatography and capillary electrophoresis. *Journal of Chromatography A*, 789(1-2), pp.85-126.

Szabo, A. & Ostlund, N.S., 1989. *Modern Quantum Chemistry Introduction to Advanced Electronic Structure Theory*. 1st ed. New York: McGraw-Hill Publishing Company.

Tang, Z.K., Nozue, Y. & Goto, T., 1992. Quantum Size Effect on the Excited State of HgI2,PbI2 and BiI3 Clusters and Molecules in Zeolite LTA. *Journal of the Physical Society of Japan*, 61(8), pp.2943-50.

Taylor, J., 1996. *The Microbiology of acid mine drainage*. [Online] Available at: http://www.taylorgeoservices.com/papers/acid%20mine%20paper.pdf [Accessed 30 December 2016].

Tchounwou, P.B., Yedjou, C.G., Patlolla, A.K. & Sutton, D.J., 2012. Heavy Metals Toxicity and the Environment. *Experientia Supplementum*, 101, pp.133-64.

Tessier, A., Campbell, P.G.C. & Bission, M., 1979. Sequential extraction procedure for the speciation of particulate trace metals. *Analytical Chemistry*, 51, pp.844-51.

Theng, B.K.G., 1979. *Formation and properties of clay-polymer complexes*. Amsterdam: Elsevier.

Theorin, G., 2015. Geochemistry of arsenic and heavy metals in pyrite ash - Speciation, solubility control mechanisms and geochemical modelling. *Swedish University of Agricultural Sciences, Upsala*. Master's thesis.

Thermo Elemental, 2001. *AAS, GFAAS, ICP or ICP-MS? Which should I use?* [Online] Available at: http://www.thermo.com/eThermo/CMA/PDFs/Articles/articlesFile_18407.pdf [Accessed November 2012].

Thornton, Z., 1981. Geochemical aspects of the distribution and forms of heavy metals in soils. In N.W. Lepp, ed. *Effect of Heavy Metals Pollution on Plants, Vol. 2, Metals in the Environment*. London: Applied Science Publishers. pp.1-33.

Togashi, N., Sakamoto, Y., Ohsuna, T. & Terasaki, O., 2001. Arrayed PbI2 clusters in the spaces of zeolite LTA. *Materials Science and Engineering A*, 312(1-2), pp.267-73.

Tokman, N., Akman, S. & Ozeroglu, C., 2004. Determination of Lead, Copper and Manganese by Graphite Furnace Atomic Absorption Spectrometry After Separation/Concentration Using a Water-soluble Polymer. *Talanta*, 63(3), pp.699-703.

Tokunaga, S. & Hakuta, T., 2002. Acid washing and stabilization of an artificial arsenic-contaminated soil. *Chemosphere*, 46(1), pp.31-38.

Tomlinson, M.J., Wang, J. & Caruso, J.A., 1994. Speciation of toxicologically important transition metals using ion chromatography with inductively coupled plasma mass spectrometric detection. *Journal of Analytical Absorption Spectroscopy*, 9, pp.957-64.

Tsymbal, E.Y., 2002. *Physics 927: Section 2: X-ray Diffraction and Reciprocal Lattice*. [Online] Available at: http://unlcms.unl.edu/cas/physics/tsymbal/teaching/SSP-927/Section%2002_X-ray_Diffraction.pdf [Accessed 18 July 2016].

Tugrul, N., Derun, E.M. & Piskin, M., 2007. Utilization of pyrite ash wastes by pelletization process. *Powder Technology*, 176, pp.72-76.

Tugrul, N., Derun, E.M., Piskin, M.B. & Ekerim, A., 2009. A study on the structural behavior of reduced pyrite ash pellets by XRD and XRF analysis. *Waste Management and Research*, 27, pp.281-87.

Turk, T., 2016. Optimization of arsenic removal from pyrite ash by NaOH leaching using central composite design. *Desalination and Water Treatment*, 57(18), pp.8575-82.

Tyler, G., 1991. *ICP Varian Report*.

Tyler, G. & Longjumeau, F., n.d. *ICP-OES, ICP-MS and AAS Techniques Compared, Technical Note 05, Jobin Yvon Horiba ICP Optical Emission Spectroscopy*. [Online] Available at: http://www.jobinyvon.com/usadivisions/Emission/applications/TN05.pdf [Accessed November 2012].

Tyler, L.D. & McBride, M.B., 1982. Mobility and Extractability of Cadmium, Copper, Nickel and Zinc in Organic and Mineral Soil Columns. *Soil Science*, 134(3), pp.198-205.

U.S. Environmental Protection Agency, 2016. *What is Acid Mind Drainage*. Save Our Sky Blue Waters.

Ulusoy, U. & Simsek, S., 2005. Lead removal by polyacrylamide-bentonite and zeolite composites: effect of phytic acid immobilization. *Journal of Hazardous Materials*, 127, pp.163-71.

United States Environmental Protection Agency (USEPA), 1986. Toxicity Characteristic Leaching Procedure (TCLP). *Proposed Rules*, U.S. Federal Register Vol 31 No. 9(Appendix 1), pp.1750-58.

United States Environmental Protection Agency (USEPA), 2000. EPA/600/R-99/107 *Introduction to Phytoremediation*.

University of Newcastle Upon Tyne, 2002. *Fluorescence*. [Online] Available at: http://www.oocities.org/edjmorris/text/fluorescence.htm [Accessed 17 July 2016].

Upmeier, M., 2006. Pollutant removal of stormwater from traffic areas using zeolite containing substrates, in: R.S. Bowman, S.E. Delap (Eds.). *Book of Abstracts of the 7th Intern. Conference on the Occurrence, Properties and Utilization of Natural Zeolites, Socorro, NM*, pp.234-35.

Van Hervijnen, R. et al., 2007. Remediation of metal contaminated soil with mineral-amended composts. *Environmental Pollution*, 150, pp.347-54.

Van Herwijnen, R. et al., 2006. How to remediate heavy metal contaminated sites with amended composts. London, 26 March 2006.

van Koningsveld, H. & Bennett, J.M., 1999. Zeolite Structure Determination rom X-Ray Diffraction. In *Molecular Sieves, Vol. 2*. Berlin, Heidelberg: Springer-Verlag. pp.1-29.

van Velzen, L., ed., 2015. *Woodhead Publishing Series in Energy - Environmental Remediation and Restoration of Contaminated Nuclear and Norm Sites*. Amsterdam: Woodhead Publishing.

Vassilev, S.V. & Vassileva, C.G., 2007. A new approach for the classification of coal fly ashes based on their origin, composition, properties, and behaviour. *Fuel*, 86(10-11), pp.1490-512.

Wang, Y.M., Chen, T.C., Yeh, K.J. & Shue, M.F., 2001. Stabilization of an elevated heavy metal contaminated site. *Journal of Hazardous Materials*, 88(1), pp.63-74.

Wang, C. et al., 2009. Evaluation of zeolites synthesized from fly ash as potential adsorbents for wastewater containing heavy metals. *Journal of Environmental Science*, 21, p.127.

Wang, Q.R., Liu, X.M., Cui, Y.S. & Dong, Y.P., 2003. Soil contamination and sources of heavy metal at inividual sites of industry and mining associate with waste water irrigation in China. *Journal of Environmental Science and Health, Part A: Toxic/Hazardous Substances and Environmental Engineering*, 38(5), pp.823-38.

Wang, S. & Peng, Y., 2010. Natural zeolites as effective adsorbents in water and wastewater treatment. *Chemical Engineering Journal*, 156, pp.11-24.

Wasag, H., 2007. Pretreatment of sewage by heavy metal sorption onto natural zeolite. In Pawlowski, L., Dudzinska, M.R. & Pawlowski, A., eds. *Preceedings of the Second National Congress of Environmental Engineering, Lublin, Poland, 4-8 September 2005*. London, 2007. Taylor & Francis Group.

WebMineral, 2012. *Albite Mineral Data*. [Online] Available at: http://webmineral.com/data/Albite.shtml#.V5DnL_mAOko [Accessed 21 July 2016].

Weitkamp, J., 2000. Zeolites and Catalysis. *Solid State Ionics*, 131(1-2), pp.175-88.

Weitkamp, J. & Puppe, L., 1999. *Catalysis and Zeolites: Fundamentals and Applications*. Berlin: Springer-Verlag.

Weller, P., 1982. Environment - The acid rain impact. *New Internationalist*, 114.

White, J.C., Nicholas, J.B. & Hess, A.C., 1997. *Journal of Physical Chemistry B*, 101, pp.590-95.

Winder, C. & Bonin, T., 1993. The genotoxicity of lead. *Mutation Research*, 285, pp.117-24.

Wingenfelder, U., Hansen, C., Furrer, G. & Schulin, R., 2005. Removal of Heavy Metals from Mine Waters by Natural Zeolites. *Environmental Science and Technology*, 39, pp.4606-13.

Wood, P., 1997. Remediation Methods for Contaminated Sites. In *R. Hester and R. Harrison, Contaminated Land and its Reclamation*. Cambridge: RSC Publishing. pp.47-71.

World Health Organisation, 2015. *Lead poisoning and health*. [Online] Available at: www.who.int/mediacentre/factsheets/fs379/en/ [Accessed 12 May 2016].

Yaffe, M.J. & Rowlands, J.A., 1997. X-ray detectors for digital radiography. *Physics in Medicine and Biology*, 42, pp.1-39.

Yeom, Y.H. & Kim, Y., 1997. Crystal Structure of Zeolite X Exchanged with Pb(II) at pH 6.0 and Dehydrated: (Pb4+)14(Pb2+)18(Pb4O4)8Si100Al92O384. *Journal of Physical Chemistry*, 101(27), pp.5314-18.

Yeom, Y.H., Kim, Y. & Seff, K., 1999. Crystal structure of Pb2+44Pb4+5Tl+18O2−17–Si100Al92O384, zeolite X exchanged with Pb2+ and Tl+ and dehydrated, containing Pb4O4(Pb2+,Pb4+mixed)4 clusters. *Microporous and Mesoporous Materials*, 28(1), pp.103-12.

Yeung, A.T. & Gu, Y., 2011. A review on techniques to enhance electrochemical remediation of contaminated soils. *Journal of Hazardous Materials*, 195, pp.11-29.

Yoshida, K., Toyoura, K. & Matsunaga, K., 2013. Atomic sites and stability of Cs+ captured within zeolitic nanocavities. *Scientific Reports*, 3, p.2457.

Yoshida, K. et al., 2013. *Scientific Reports*, 3, p.2457.

You, X.H., 2004. A Study on the effect of soil aggregate on organic matter in mixed forests of Chinese Fir and Phyllostachys heterocycla cv pubescen. *Acta Agriculturaes Universitatis of Jiangxiensis*, 26, pp.536-39.

Yuan, G. et al., 1999. Adsorption of some heavy metals by natural zeolites: XPS and batch studies. *Journal of Environmental Science and Health, Part A: Toxic/Hazardous Substances and Environmental Engineering*, A34(3), pp.625-48.

Zamzow, M.I., Eichbaum, B.R., Sangren, K.R. & Shanks, D.E., 1990. Removal of Heavy Metals and Other Cations from Wastewater Using Zeolites. *Separation and Science Technology*, 25(13-15), pp.1555-69.

Zeng-Yei, H. & Zueng-Sang, C., 2002. Digestion Methods for Total Heavy Metals in Sediments and Soils. *Water, Air, and Soil Pollution*, 141(1), pp.189-205.

Zhang, Z. et al., 2015. Screening and assessment of solidification/stabilization amendments suitable for soils of lead-acid battery contaminated site. *Journal of Hazardous Materials*, 288, pp.140-46.

Zhang, M. et al., 2011. Ammonium removal from aqueous solution by zeolites synthesised from low-calcium and high-calcium fly ashes. *Desalination*, 277, pp.46-53.

Zornoza, P. et al., 2002. Cadmium-stress innoculate white lupin: strategies to avoid toxicity. *Plant Physiology and Biochemistry*, 40, pp.1003-09.

Chapter 11 Appendices

Appendix 1 ICP-MS Report

Soil 1 and 2 were digested in aqua regia and analysed with ICP-MS after sieving and drying as described in Section 5.5. The soils were sent for analysis and the results are shown in Appendix Figure 1.1. These show that the soil from Site 1 (P1) showed the highest levels of lead at 26,000 ppm with the soil from Site 2 (P6) containing 3,000 ppm less. The Road analysis detected 2400 ppm of lead which can be treated as the baseline for the area.

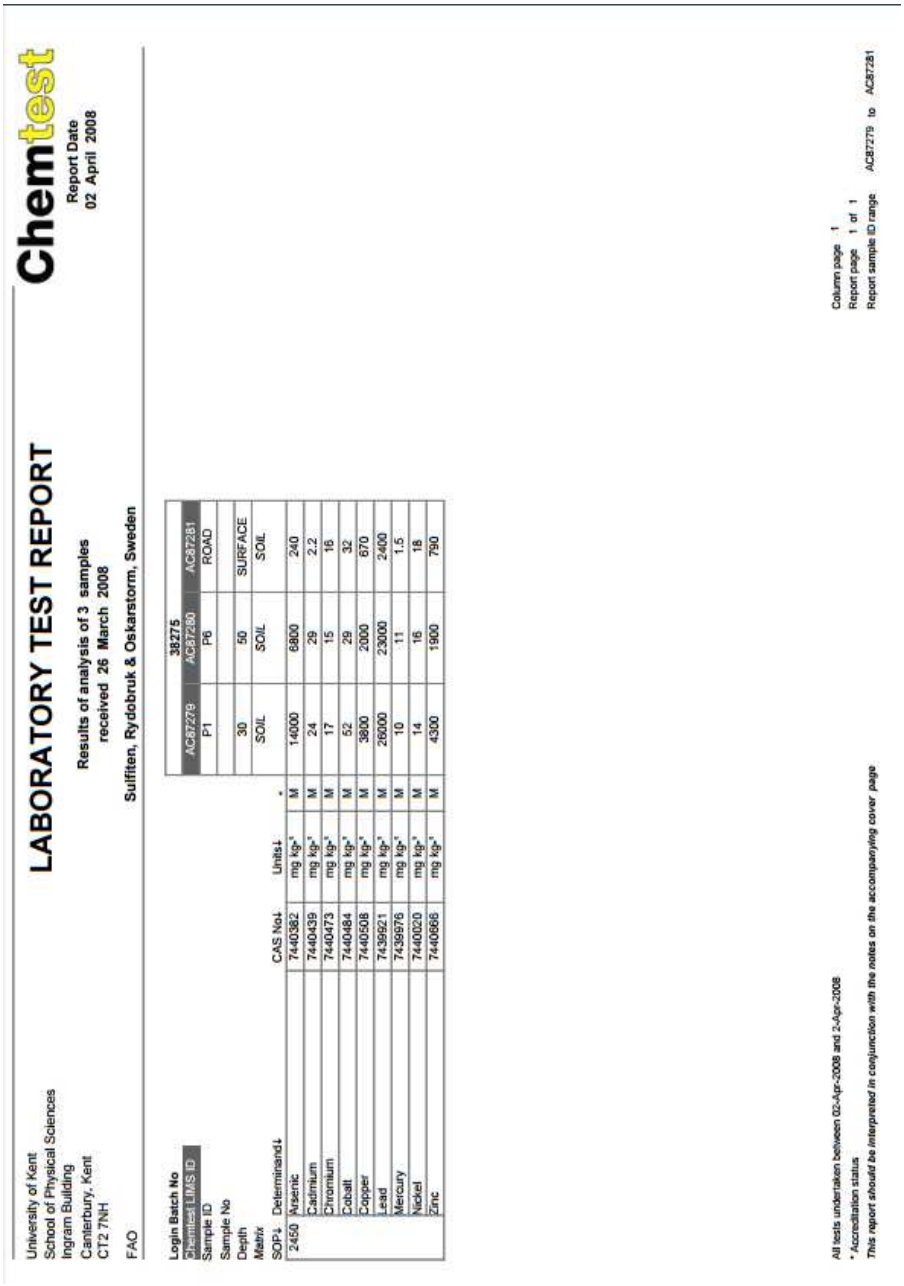

University of Kent
School of Physical Sciences
Ingram Building
Canterbury, Kent
CT2 7NH

FAO

LABORATORY TEST REPORT

Results of analysis of 3 samples
received 26 March 2008

Sulfiten, Rydobruk & Oskarstorm, Sweden

Chemtest

Report Date
02 April 2008

Login Batch No				38275		
Chemtest LIMS ID				AC87279	AC87280	AC87281
Sample ID				P1	P6	ROAD
Sample No						
Depth				30	50	SURFACE
Matrix				SOIL	SOIL	SOIL
SOP↓	Determinand↓	CAS No↓	Units↓	*		
2450	Arsenic	7440382	mg kg^{-1}	M	14000	6800	240
	Cadmium	7440439	mg kg^{-1}	M	24	29	2.2
	Chromium	7440473	mg kg^{-1}	M	17	15	16
	Cobalt	7440484	mg kg^{-1}	M	52	29	32
	Copper	7440508	mg kg^{-1}	M	3800	2000	670
	Lead	7439921	mg kg^{-1}	M	26000	23000	2400
	Mercury	7439976	mg kg^{-1}	M	10	11	1.5
	Nickel	7440020	mg kg^{-1}	M	14	16	18
	Zinc	7440666	mg kg^{-1}	M	4300	1900	790

Column page 1
Report page 1 of 1
Report sample ID range AC87279 to AC87281

All tests undertaken between 02-Apr-2008 and 2-Apr-2008
* Accreditation status
This report should be interpreted in conjunction with the notes on the accompanying cover page

Appendix Figure 1.1 - ICP-MS report for Soil 1 and Soil 2 (recorded as P1 and P6, respectively)

Appendix 2 GFAAS Results

The GFAAS data obtained was for the diluted soils. The dilution was factored in to the final concentrations as shown in Appendix Table 2.1.

Appendix Table 2.1 - Table of GFAAS results including dilution factors and final concentration of lead in ppm

Sample Name	Recorded Concentration of Lead in Diluted Sample (ppm)	Dilution Factor	Final Concentration of Lead in Undiluted Sample (ppm)
S1w	0.02783	41667	1160
S1wZA25	0.08487	1	0
S1wZA50	0.00490	1	0
S1a	0.01586	41667	661
S1aZA25	0.02889	20833	602
S1aZA50	0.00578	20833	120
S2w	0.26868	41667	11195
S2wZA25	0.16868	42	7
S2wZA50	0.12248	417	51
S2a	0.62435	41667	26015
S2aZA25	0.25957	20833	5408
S2aZA50	0.00366	20833	76

Appendix 3 XRF Results

The complete table of XRF results as well as raw data is given in Appendix Table 3.1. A sample spectrum for each untreated soil is shown in Appendix Figure 3.1 and Appendix Figure 3.2.

Appendix Table 3.1 - Complete XRF data for each soil sample as well as Zeolite-A

Element	Zeolite-A	S1untreated	S1w	S1wZA25	S1wZA50	S1a	S1aZA25	S1aZA50	S2untreated	S2w	S2wZA25	S2wZA50	S2a	S2aZA25	S2aZA50
Ag	0.13	0.61	0.54	0.56	0.53	0.56	0.54	0.53	0.56	0.49	0.43	0.43	0.48	0.39	0.37
Al	33.05	2.70	4.64	10.15	16.40	3.67	5.29	9.26	5.33	5.76	10.24	14.06	6.60	7.61	13.41
As	0.00	0.00							6.07	6.89	5.30	5.78	6.04	7.42	6.03
Ba		0.13	0.23	0.15	0.14	0.16	0.20	0.12	0.20	0.22	0.18	0.15	0.21	0.15	0.17
Ca	0.26	0.56	0.74	0.56	0.93	0.51	0.43	0.49	1.64	2.13	1.94	1.50	1.62	1.44	1.48
Ce		0.00	0.02						0.00						
Cl	0.02	0.00	0.00	0.06					0.29	0.30	0.20	0.39	0.14	0.19	0.20
Cr		0.00							0.02	0.03	0.02	0.03	0.02		0.02
Cu		2.86	2.38	2.69	2.02	2.64	2.39	2.23	1.50	1.47	1.13	1.08	1.34	1.33	1.13
Eu		0.00		0.11					0.00	0.15	0.12	0.09	0.12	0.12	
Fe	0.07	54.95	57.72	55.64	43.67	60.08	57.69	51.04	39.36	39.30	32.03	27.41	39.18	35.80	31.01
Ga		0.00	0.01	0.00	0.01	0.00	0.01	0.00	0.00	0.00	0.00	0.00	0.00	0.00	0.00
Ir		0.00	0.00	0.00	0.00	0.00	0.00	0.00	0.12	0.16	0.07	0.09	0.11	0.10	0.07
K	0.06	6.25	1.76	1.11	0.74	1.37	1.37	1.15	8.22	4.16	3.83	2.33	4.50	3.32	3.45
La		0.00	0.00	0.00	0.00	0.00	0.00	0.00	0.00			0.00			
Mg		0.55	0.65	0.39		0.40	0.37	0.30	0.48	0.55	0.55	0.27	0.60	0.34	0.34
Mn		0.08	0.09	0.05	0.06	0.08	0.08	0.07	0.11	0.09	0.07	0.06	0.07	0.07	0.10
Na	19.71	0.00			3.46				0.00		2.12	6.04			
Ni		0.03	0.02	0.01	0.02	0.03	0.01	0.01	0.00						
Os		0.02	0.02	0.03	0.03	0.02	0.01	0.02	0.03	0.04	0.04	0.03	0.03		0.02
P	0.49	5.97	0.08	0.09	0.13	0.07	0.00	0.03	3.14	0.21	0.11	0.09	0.13	0.06	0.15
Pb	0.00	1.85	2.83	2.84	2.99	2.80	2.64	2.02	14.97	16.04	14.47	17.89	11.72	15.37	14.62
Rb		0.01	0.01	0.01	0.01	0.01	0.01	0.01	0.01	0.01	0.01	0.00	0.01	0.01	0.01
Re		0.00	0.02				0.02	0.01	0.00						
S		12.77	11.50	7.98	5.51	12.19	10.53	11.05	0.75	0.68	0.00	0.00	0.86	0.79	0.60
Se		0.01	0.01		0.02	0.01		0.01	0.00						
Si	46.21	10.10	16.21	17.04	22.85	14.87	17.99	21.26	14.85	18.81	25.12	20.47	23.88	23.24	24.74
Sm		0.06		0.08					0.00						
Sr		0.01	0.06	0.02	0.03	0.02	0.02	0.02	0.05	0.07	0.03	0.03	0.05	0.03	0.05
Th		0.00							0.04	0.04	0.03	0.04	0.05	0.05	0.05
Ti	0.01	0.23	0.27	0.21	0.17	0.24	0.20	0.19	0.49	0.60	0.52	0.37	0.56	0.50	0.55
V		0.00		0.00	0.00	0.00	0.01	0.00	0.01	0.01	0.01	0.01	0.01	0.01	0.01
Zn		0.24	0.18	0.21	0.26	0.25	0.20	0.17	1.69	1.71	1.34	1.35	1.63	1.59	1.36
Zr		0.01	0.03	0.02	0.02	0.02	0.02	0.03	0.08	0.08	0.07	0.05	0.07	0.06	0.08

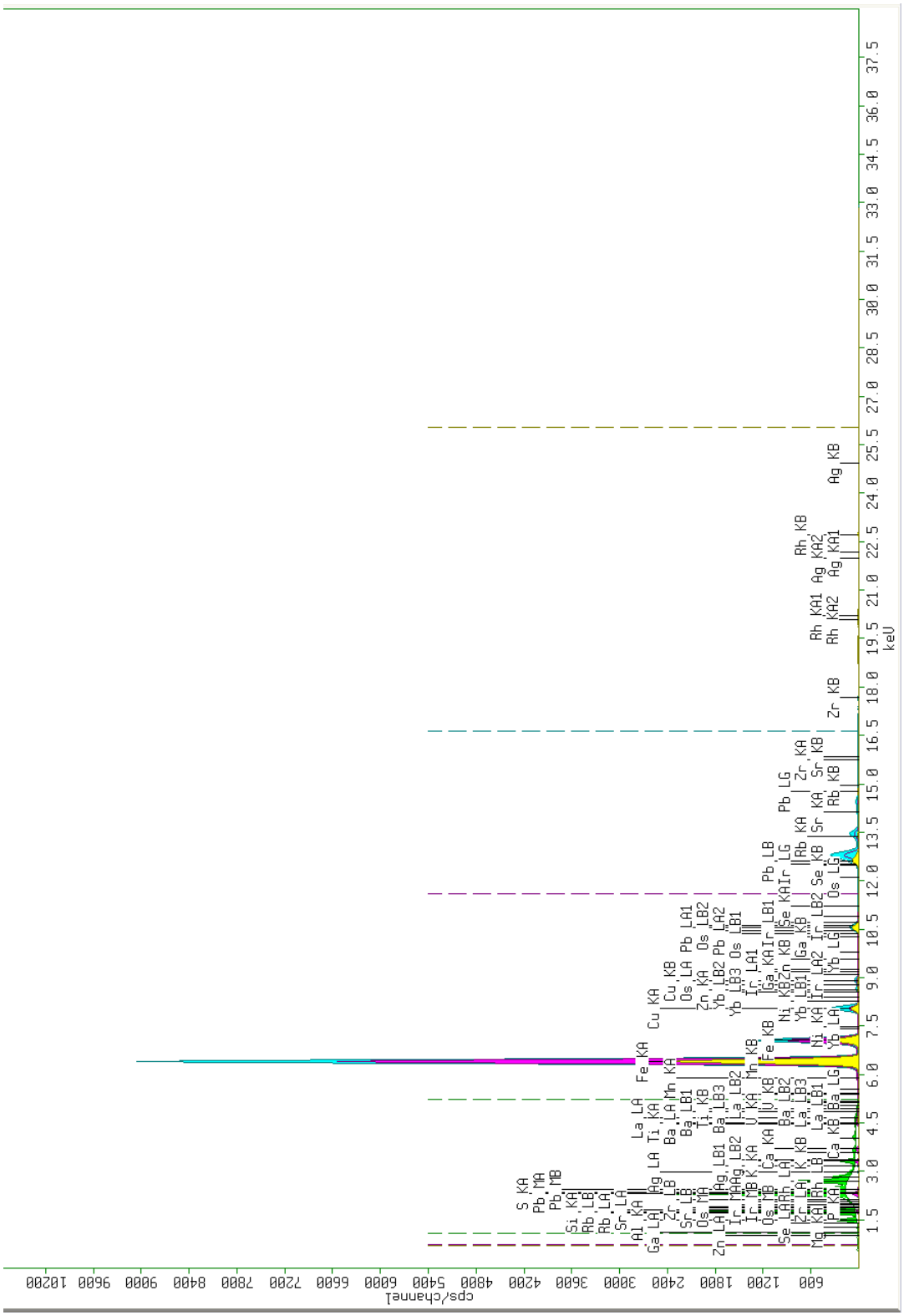

Appendix Figure 3.1 - XRF spectrum of S1untreated

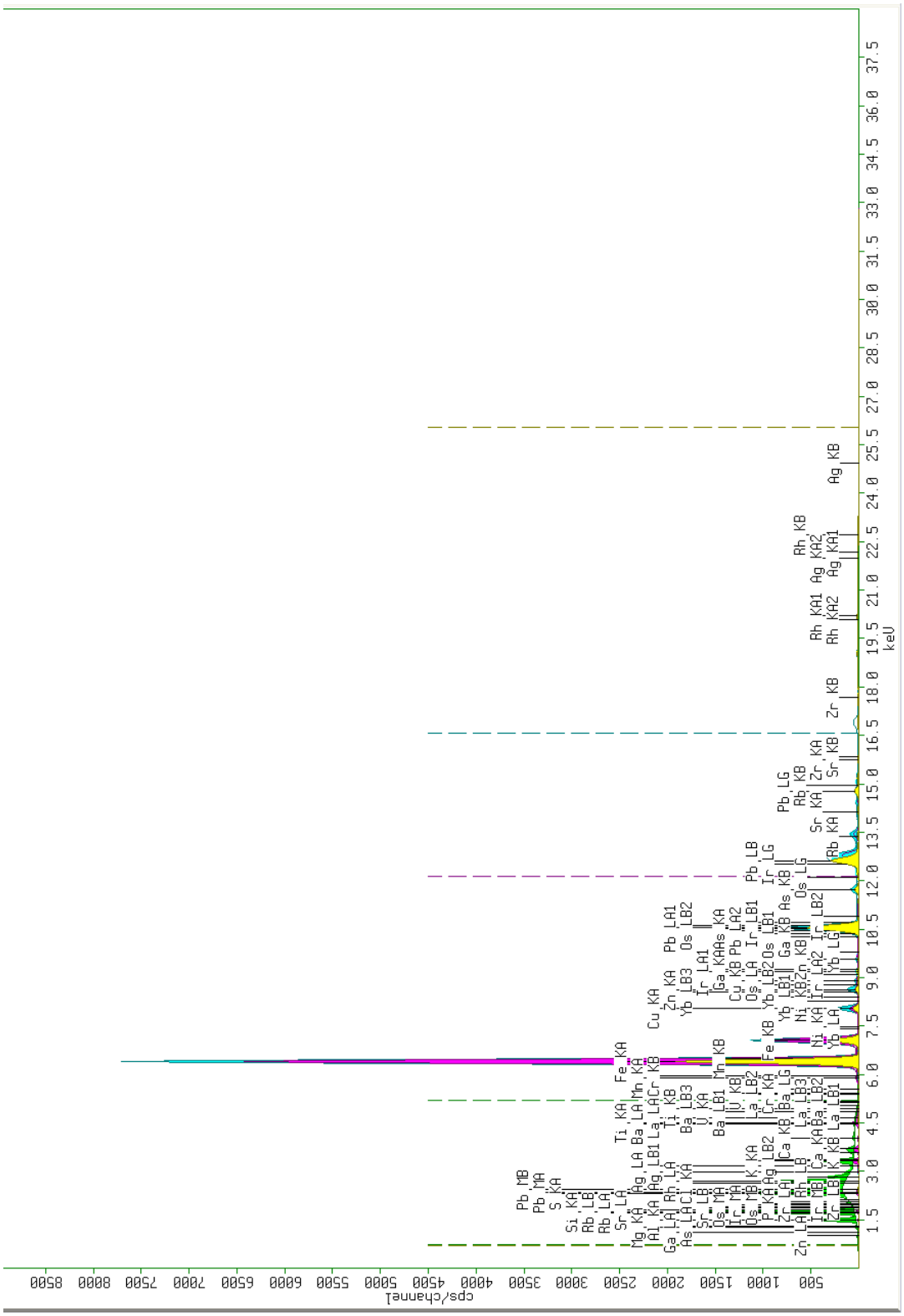

Appendix Figure 3.2 - XRF spectrum of S2untreated

Appendix 4 XRD Diffraction Patterns

The XRD diffraction patterns for the washed and treated soils that were omitted in Chapter 6 are shown Appendix Figure 4.1 to Appendix Figure 4.6. Appendix Figures 4.7 – 4.12 are the supplemental XRD patterns with the secondary mineral gismondine overlaid in red.

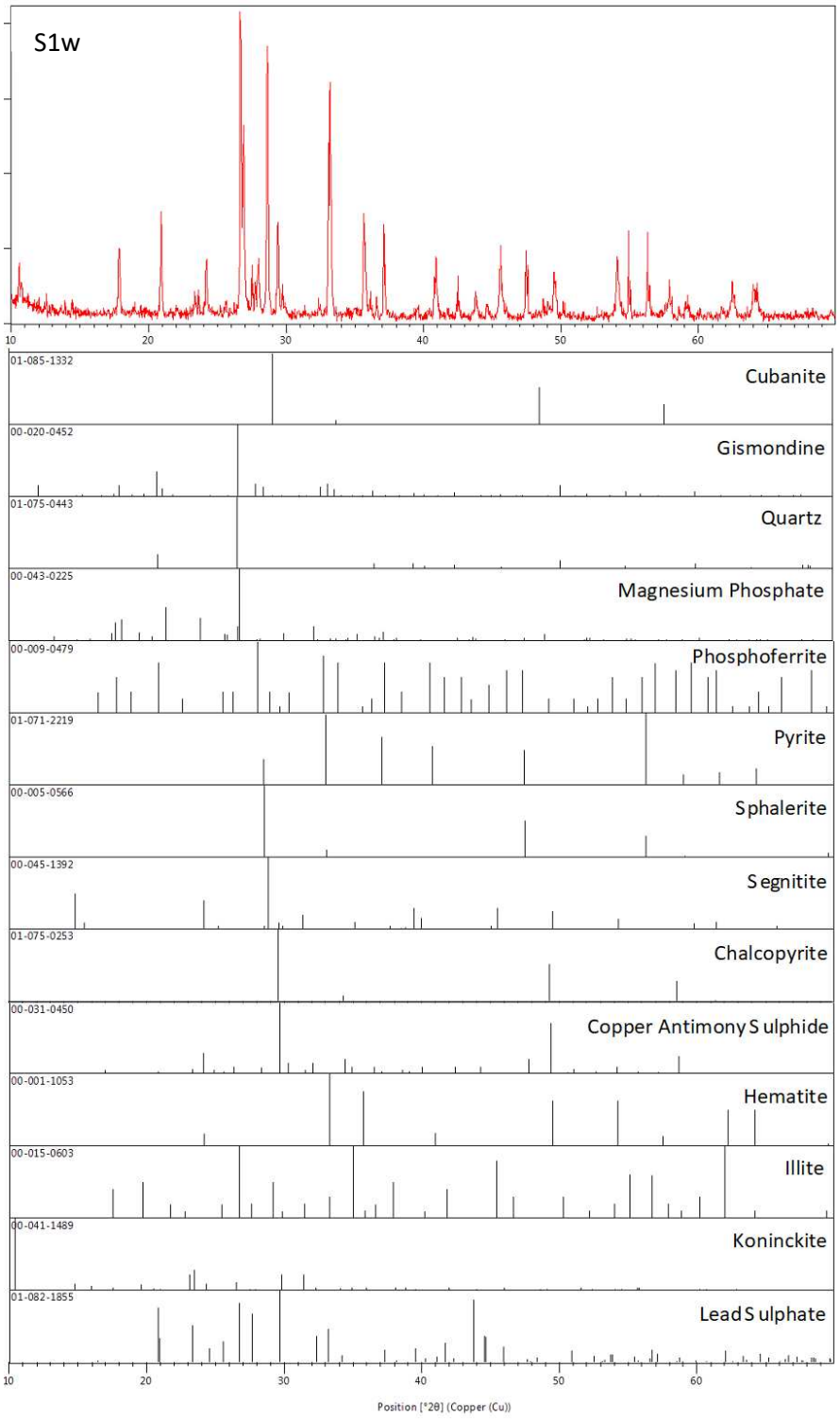

Appendix Figure 4.1 - XRD pattern of S1w

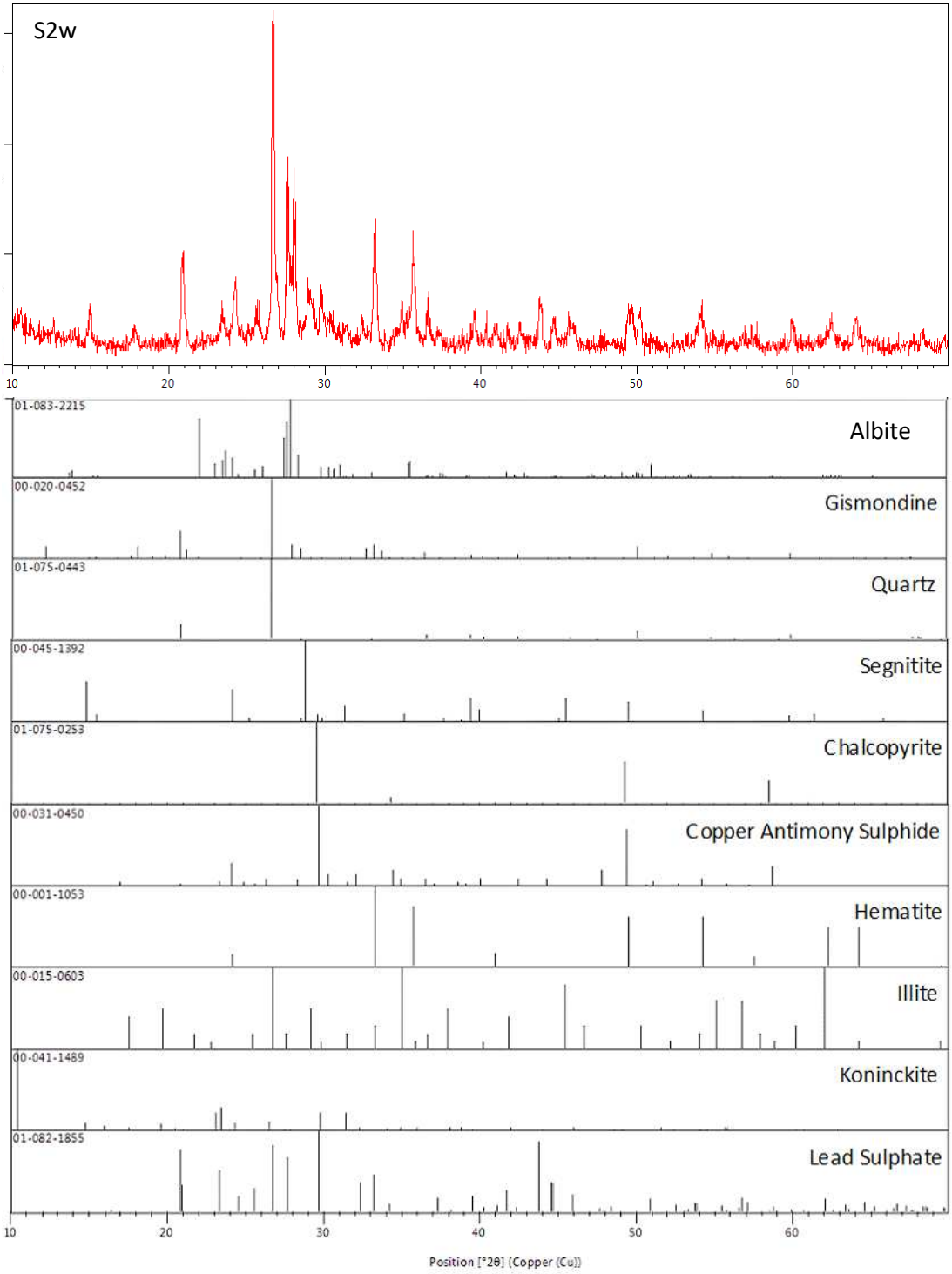

Appendix Figure 4.2 - XRD pattern of S2w

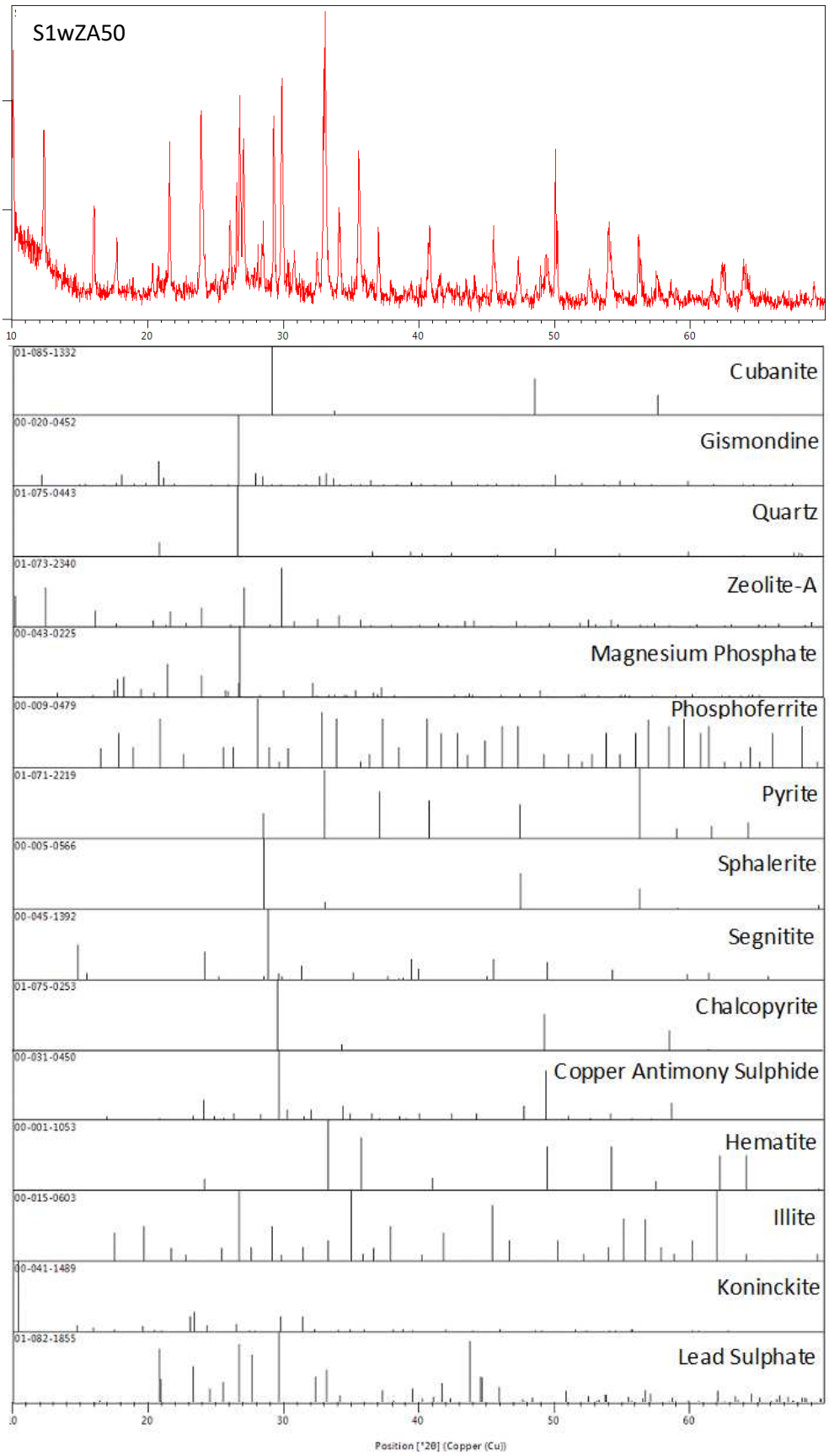

Appendix Figure 4.3 - XRD pattern of S1wZA50

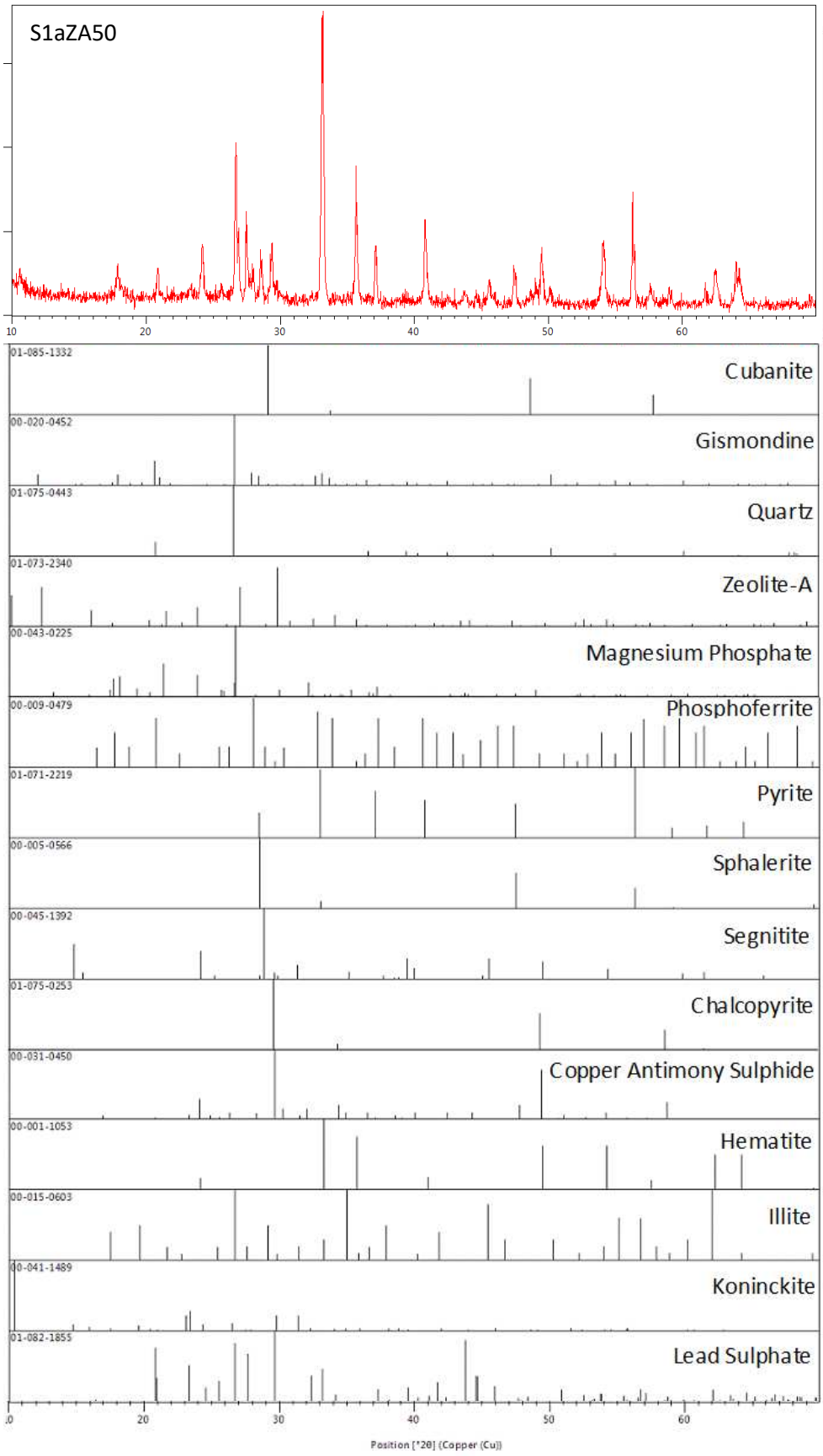

Appendix Figure 4.4 - XRD Pattern of S1aZA50

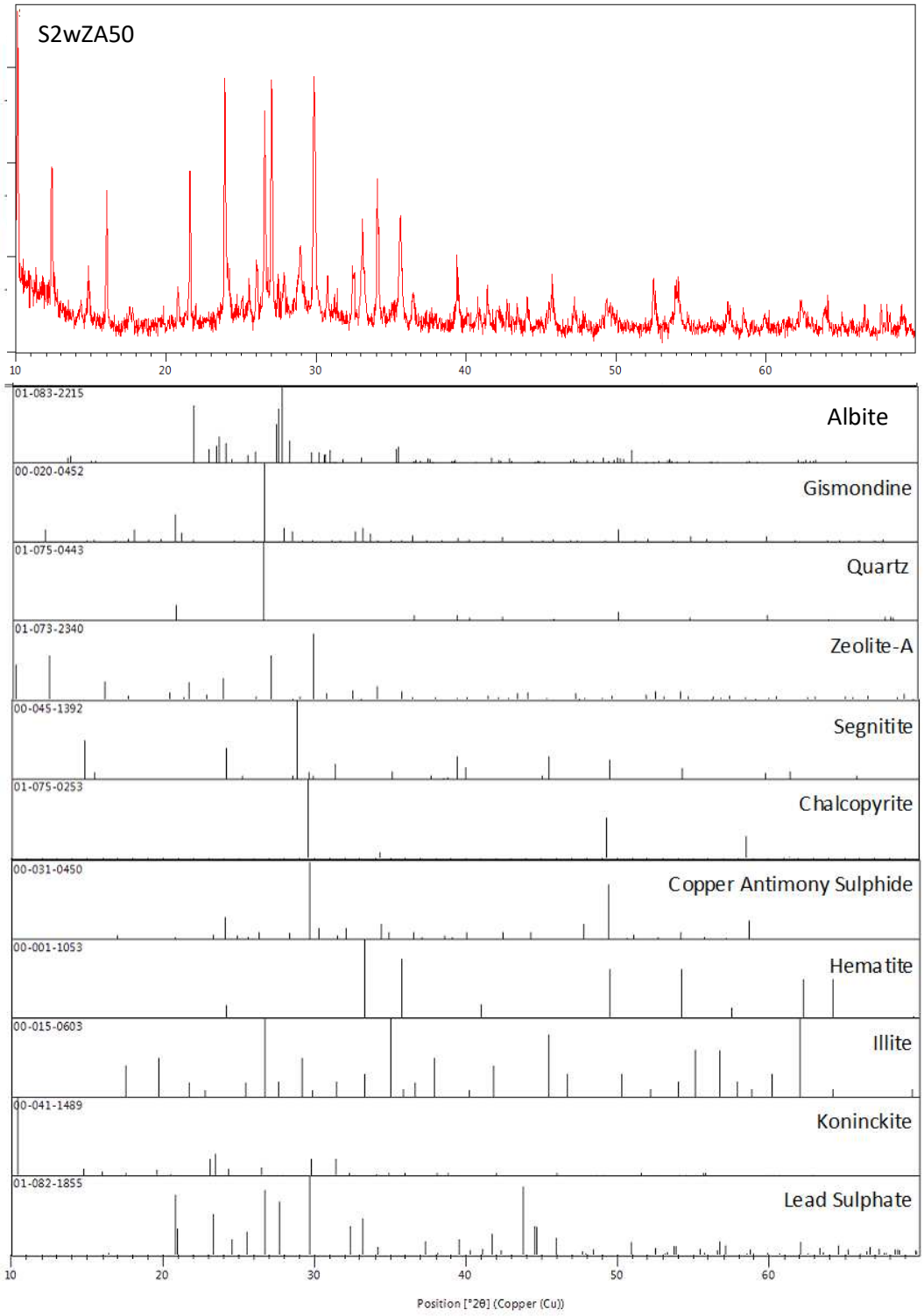

Appendix Figure 4.5 - XRD pattern of S2wZA50

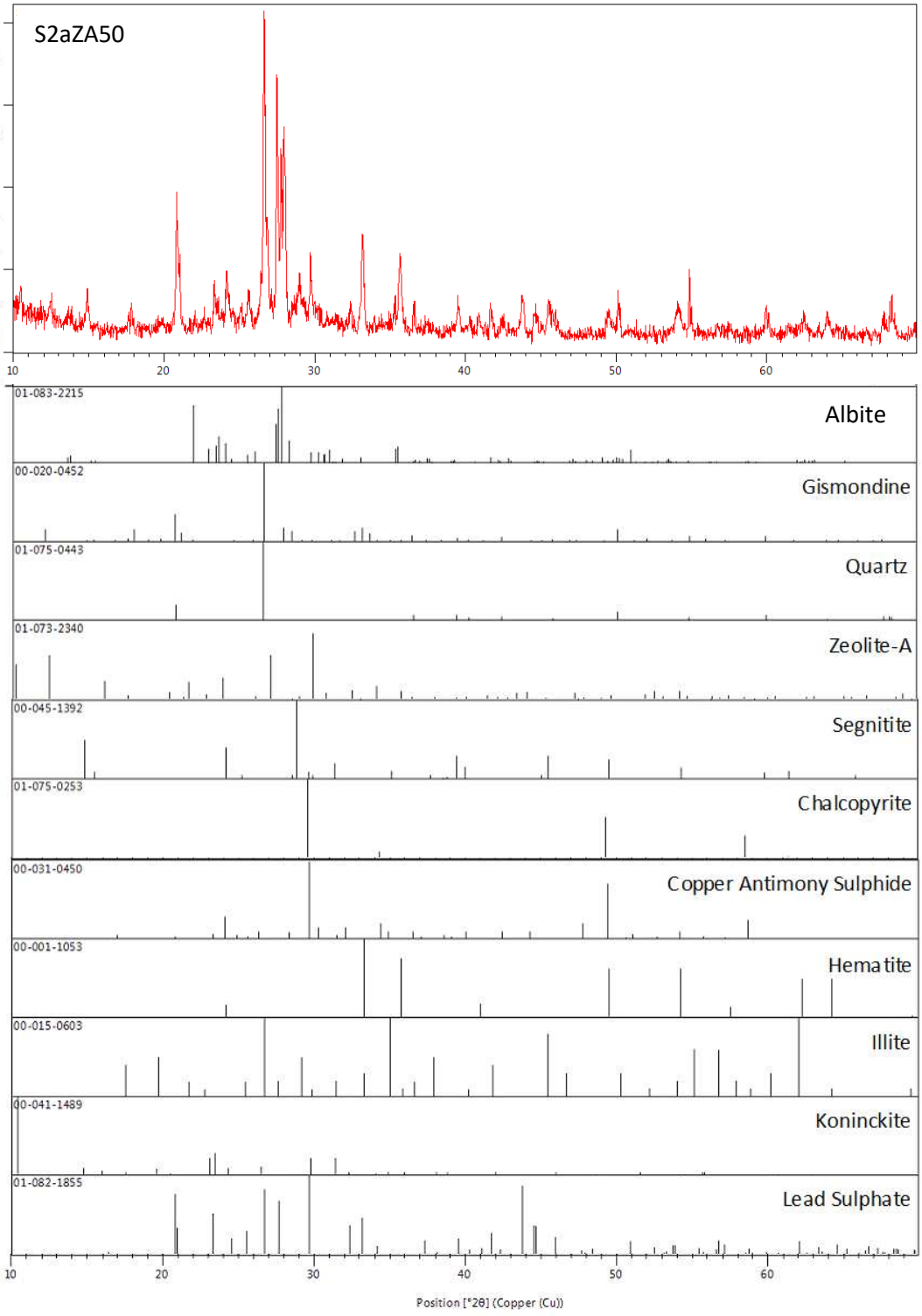

Appendix Figure 4.6 - XRD Pattern of S2aZA50

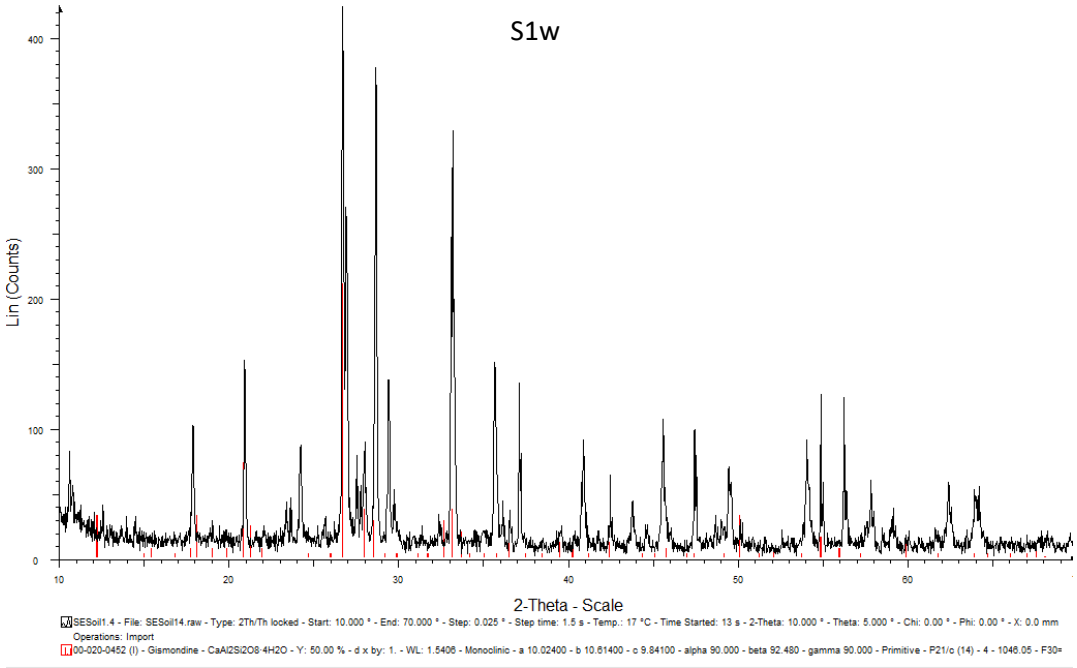

Appendix Figure 4.7 - XRD Pattern of S1w with gismondine peaks overlaid in red

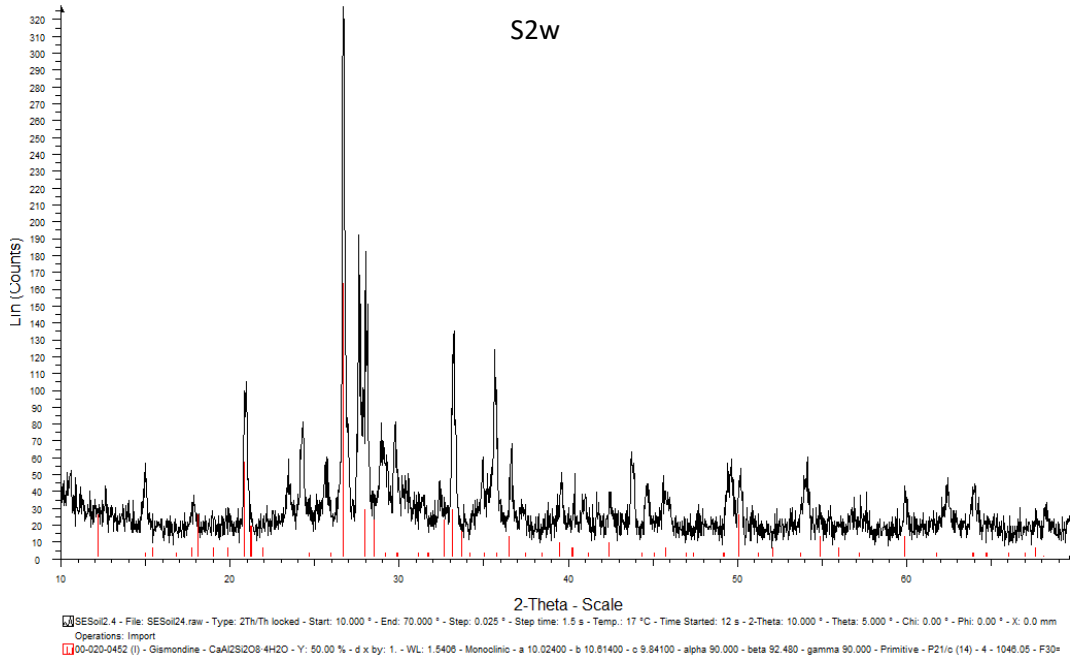

Appendix Figure 4.8 - XRD Pattern of S2w with gismondine peaks overlaid in red

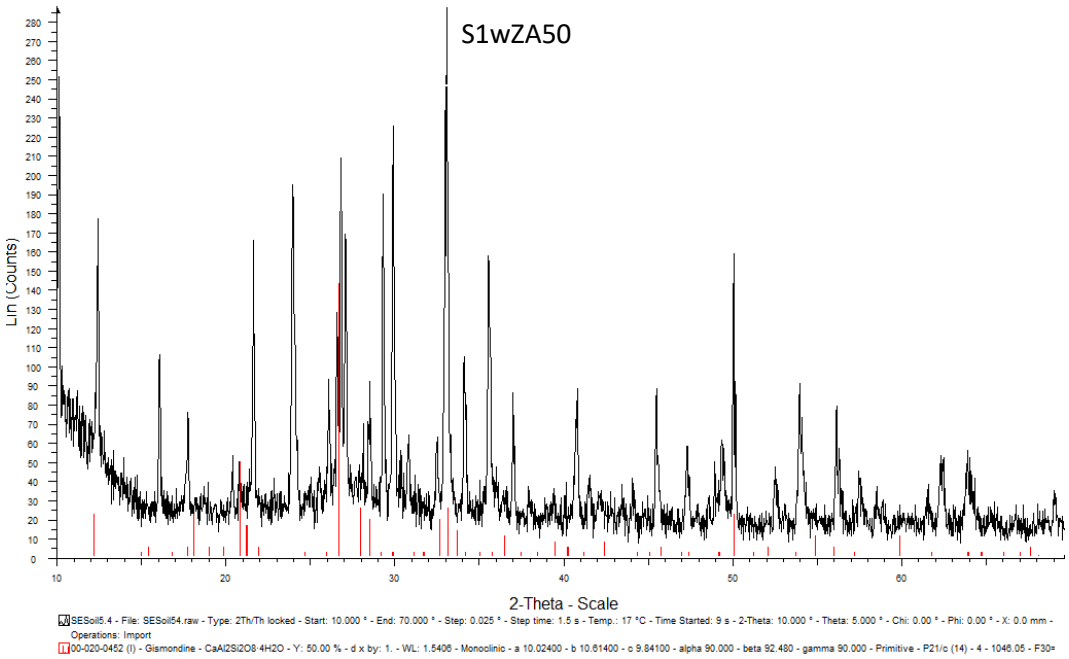

Appendix Figure 4.9 - XRD Pattern of S1wZA50 with gismondine peaks overlaid in red

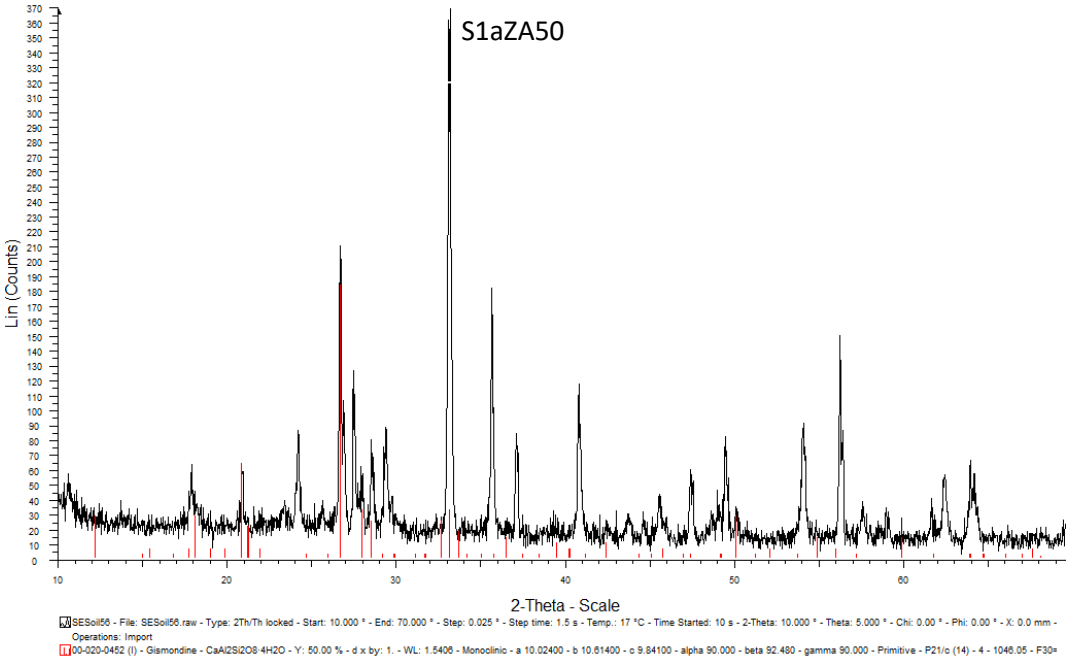

Appendix Figure 4.10 - XRD Pattern of S1aZA50 with gismondine peaks overlaid in red

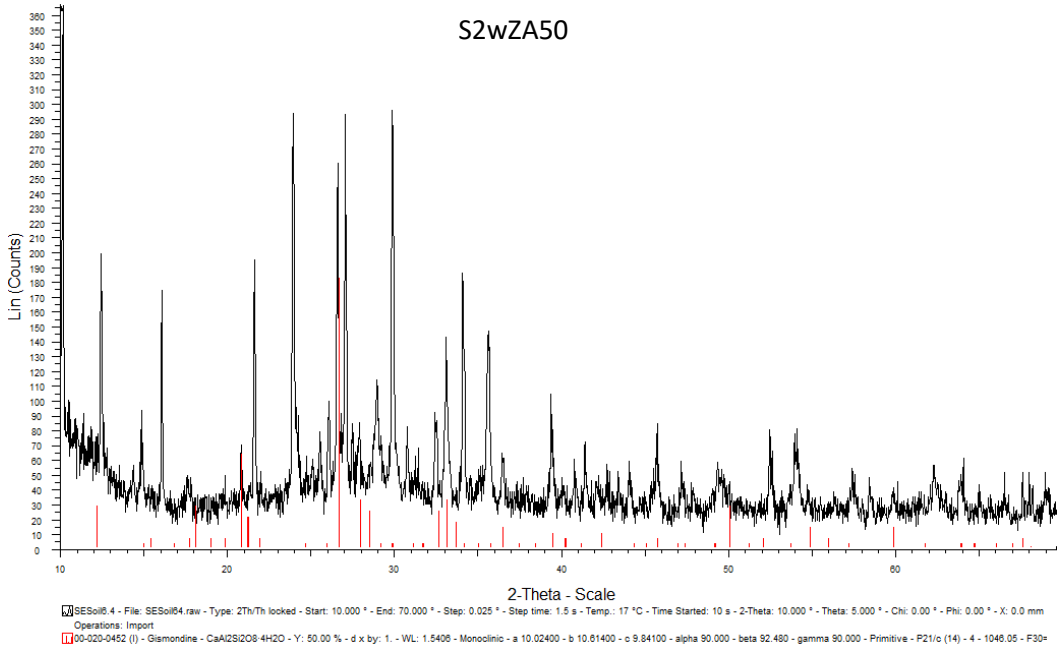

Appendix Figure 4.11 - XRD Pattern of S2wZA50 with gismondine peaks overlaid in red

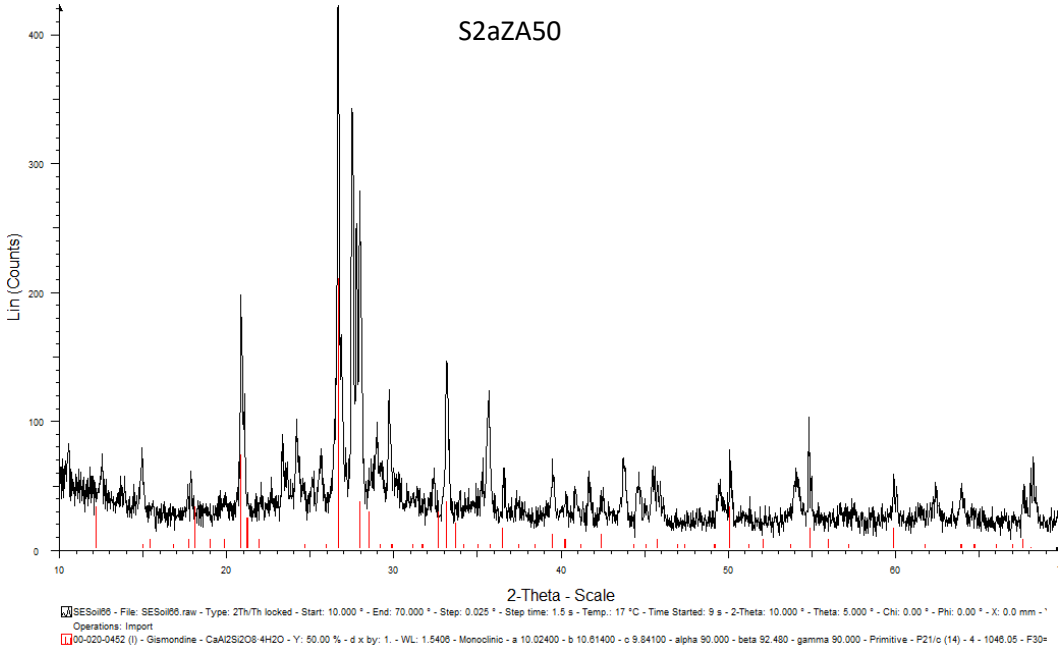

Appendix Figure 4.12 - XRD Pattern of S2aZA50 with gismondine peaks overlaid in red

Appendix 5 Computational Input File

Appendix Figure 5.1 is an example of the input files used to analyse a 25% substitution of lead or barium ions with the CRYSTAL09 software.

```
Example Input File of Anhydrous Zeolite A
Supercell with 16 Pb Inserted for Na and 16
Na Removed
CRYSTAL
0 0 0
001
24.52600000 24.52600000 24.52600000
90.000000 90.000000 90.000000
656
214 1.540744E-33 9.250000E-02 1.860000E-01
213 9.244464E-33 9.250000E-02 -3.140000E-01
213 1.540744E-33 -4.075000E-01 1.860000E-01
214 9.244464E-33 -4.075000E-01 -3.140000E-01
213 5.000000E-01 9.250000E-02 1.860000E-01
214 5.000000E-01 9.250000E-02 -3.140000E-01
214 5.000000E-01 -4.075000E-01 1.860000E-01
213 5.000000E-01 -4.075000E-01 -3.140000E-01
214 1.540744E-33 -9.250000E-02 1.860000E-01
213 9.244464E-33 -9.250000E-02 -3.140000E-01
213 1.540744E-33 4.075000E-01 1.860000E-01
214 9.244464E-33 4.075000E-01 -3.140000E-01
213 5.000000E-01 -9.250000E-02 1.860000E-01
214 5.000000E-01 -9.250000E-02 -3.140000E-01
214 5.000000E-01 4.075000E-01 1.860000E-01
213 5.000000E-01 4.075000E-01 -3.140000E-01
214 -1.540744E-33 -9.250000E-02 -1.860000E-
01
213 0.000000E+00 -9.250000E-02 3.140000E-01
213 -1.540744E-33 4.075000E-01 -1.860000E-01
214 0.000000E+00 4.075000E-01 3.140000E-01
213 5.000000E-01 -9.250000E-02 -1.860000E-01
214 5.000000E-01 -9.250000E-02 3.140000E-01
214 5.000000E-01 4.075000E-01 -1.860000E-01
213 5.000000E-01 4.075000E-01 3.140000E-01
214 -1.540744E-33 9.250000E-02 -1.860000E-01
213 0.000000E+00 9.250000E-02 3.140000E-01
213 -1.540744E-33 -4.075000E-01 -1.860000E-
01
214 0.000000E+00 -4.075000E-01 3.140000E-01
213 5.000000E-01 9.250000E-02 -1.860000E-01
214 5.000000E-01 9.250000E-02 3.140000E-01
214 5.000000E-01 -4.075000E-01 -1.860000E-01
213 5.000000E-01 -4.075000E-01 3.140000E-01
214 1.860000E-01 3.851860E-33 9.250000E-02
213 1.860000E-01 -3.081488E-33 -4.075000E-01
213 1.860000E-01 5.000000E-01 9.250000E-02
214 1.860000E-01 5.000000E-01 -4.075000E-01
213 -3.140000E-01 5.392604E-33 9.250000E-02
214 -3.140000E-01 1.848893E-32 -4.075000E-01
214 -3.140000E-01 5.000000E-01 9.250000E-02
213 -3.140000E-01 5.000000E-01 -4.075000E-01
214 9.250000E-02 1.860000E-01 0.000000E+00
213 9.250000E-02 1.860000E-01 5.000000E-01
213 9.250000E-02 -3.140000E-01 0.000000E+00
214 9.250000E-02 -3.140000E-01 5.000000E-01
213 -4.075000E-01 1.860000E-01 0.000000E+00
214 -4.075000E-01 1.860000E-01 5.000000E-01
214 -4.075000E-01 -3.140000E-01 0.000000E+00
213 -4.075000E-01 -3.140000E-01 5.000000E-01
214 -1.860000E-01 7.703720E-34 9.250000E-02
213 -1.860000E-01 0.000000E+00 -4.075000E-01
213 -1.860000E-01 5.000000E-01 9.250000E-02
214 -1.860000E-01 5.000000E-01 -4.075000E-01
213 3.140000E-01 7.703720E-34 9.250000E-02
214 3.140000E-01 -6.162976E-33 -4.075000E-01
214 3.140000E-01 5.000000E-01 9.250000E-02
213 3.140000E-01 5.000000E-01 -4.075000E-01
214 -9.250000E-02 1.860000E-01 0.000000E+00
213 -9.250000E-02 1.860000E-01 5.000000E-01
213 -9.250000E-02 -3.140000E-01 0.000000E+00
214 -9.250000E-02 -3.140000E-01 5.000000E-01
213 4.075000E-01 1.860000E-01 0.000000E+00
214 4.075000E-01 1.860000E-01 5.000000E-01
214 4.075000E-01 -3.140000E-01 0.000000E+00
213 4.075000E-01 -3.140000E-01 5.000000E-01
214 1.860000E-01 -7.703720E-34 -9.250000E-02
213 1.860000E-01 3.081488E-33 4.075000E-01
213 1.860000E-01 5.000000E-01 -9.250000E-02
214 1.860000E-01 5.000000E-01 4.075000E-01
213 -3.140000E-01 5.392604E-33 -9.250000E-02
214 -3.140000E-01 9.244464E-33 4.075000E-01
214 -3.140000E-01 5.000000E-01 -9.250000E-02
213 -3.140000E-01 5.000000E-01 4.075000E-01
214 -9.250000E-02 -1.860000E-01 0.000000E+00
213 -9.250000E-02 -1.860000E-01 5.000000E-01
213 -9.250000E-02 3.140000E-01 0.000000E+00
214 -9.250000E-02 3.140000E-01 5.000000E-01
213 4.075000E-01 -1.860000E-01 0.000000E+00
214 4.075000E-01 -1.860000E-01 5.000000E-01
214 4.075000E-01 3.140000E-01 0.000000E+00
213 4.075000E-01 3.140000E-01 5.000000E-01
214 -1.860000E-01 -3.851860E-33 -9.250000E-
02
213 -1.860000E-01 -3.081488E-33 4.075000E-01
213 -1.860000E-01 5.000000E-01 -9.250000E-02
214 -1.860000E-01 5.000000E-01 4.075000E-01
213 3.140000E-01 -3.851860E-33 -9.250000E-02
214 3.140000E-01 -9.244464E-33 4.075000E-01
214 3.140000E-01 5.000000E-01 -9.250000E-02
213 3.140000E-01 5.000000E-01 4.075000E-01
214 9.250000E-02 -1.860000E-01 0.000000E+00
213 9.250000E-02 -1.860000E-01 5.000000E-01
213 9.250000E-02 3.140000E-01 0.000000E+00
214 9.250000E-02 3.140000E-01 5.000000E-01
213 -4.075000E-01 -1.860000E-01 0.000000E+00
214 -4.075000E-01 -1.860000E-01 5.000000E-01
214 -4.075000E-01 3.140000E-01 0.000000E+00
213 -4.075000E-01 3.140000E-01 5.000000E-01
213 -9.250000E-02 -3.081488E-33 -1.860000E-
01
214 -9.250000E-02 -6.162976E-33 3.140000E-01
214 -9.250000E-02 5.000000E-01 -1.860000E-01
213 -9.250000E-02 5.000000E-01 3.140000E-01
214 4.075000E-01 3.081488E-33 -1.860000E-01
213 4.075000E-01 -3.081488E-33 3.140000E-01
213 4.075000E-01 5.000000E-01 -1.860000E-01
214 4.075000E-01 5.000000E-01 3.140000E-01
213 9.250000E-02 3.081488E-33 -1.860000E-01
214 9.250000E-02 0.000000E+00 3.140000E-01
214 9.250000E-02 5.000000E-01 -1.860000E-01
213 9.250000E-02 5.000000E-01 3.140000E-01
214 -4.075000E-01 9.244464E-33 -1.860000E-01
213 -4.075000E-01 3.081488E-33 3.140000E-01
213 -4.075000E-01 5.000000E-01 -1.860000E-01
214 -4.075000E-01 5.000000E-01 3.140000E-01
213 9.250000E-02 3.081488E-33 1.860000E-01
214 9.250000E-02 0.000000E+00 -3.140000E-01
214 9.250000E-02 5.000000E-01 1.860000E-01
213 9.250000E-02 5.000000E-01 -3.140000E-01
214 -4.075000E-01 -7.703720E-33 1.860000E-01
213 -4.075000E-01 1.540744E-32 -3.140000E-01
213 -4.075000E-01 5.000000E-01 1.860000E-01
214 -4.075000E-01 5.000000E-01 -3.140000E-01
213 -9.250000E-02 -3.081488E-33 1.860000E-01
214 -9.250000E-02 0.000000E+00 -3.140000E-01
214 -9.250000E-02 5.000000E-01 1.860000E-01
213 -9.250000E-02 5.000000E-01 -3.140000E-01
214 4.075000E-01 -1.232595E-32 1.860000E-01
213 4.075000E-01 0.000000E+00 -3.140000E-01
213 4.075000E-01 -5.000000E-01 1.860000E-01
214 4.075000E-01 5.000000E-01 -3.140000E-01
```

213 -1.540744E-33 -1.860000E-01 -9.250000E-02
214 6.162976E-33 -1.860000E-01 4.075000E-01
214 -1.540744E-33 3.140000E-01 -9.250000E-02
213 6.162976E-33 3.140000E-01 4.075000E-01
214 5.000000E-01 -1.860000E-01 -9.250000E-02
213 5.000000E-01 -1.860000E-01 4.075000E-01
213 5.000000E-01 3.140000E-01 -9.250000E-02
214 5.000000E-01 3.140000E-01 4.075000E-01
213 -1.860000E-01 -9.250000E-02 0.000000E+00
214 -1.860000E-01 -9.250000E-02 5.000000E-01
214 -1.860000E-01 4.075000E-01 0.000000E+00
213 -1.860000E-01 4.075000E-01 5.000000E-01
214 3.140000E-01 -9.250000E-02 0.000000E+00
213 3.140000E-01 -9.250000E-02 5.000000E-01
213 3.140000E-01 4.075000E-01 0.000000E+00
214 3.140000E-01 4.075000E-01 5.000000E-01
213 -1.540744E-33 1.860000E-01 -9.250000E-02
214 6.162976E-33 1.860000E-01 4.075000E-01
214 -1.540744E-33 -3.140000E-01 -9.250000E-02
213 6.162976E-33 -3.140000E-01 4.075000E-01
214 5.000000E-01 1.860000E-01 -9.250000E-02
213 5.000000E-01 1.860000E-01 4.075000E-01
213 5.000000E-01 -3.140000E-01 -9.250000E-02
214 5.000000E-01 -3.140000E-01 4.075000E-01
213 -1.860000E-01 9.250000E-02 0.000000E+00
214 -1.860000E-01 9.250000E-02 5.000000E-01
214 -1.860000E-01 -4.075000E-01 0.000000E+00
213 -1.860000E-01 -4.075000E-01 5.000000E-01
214 3.140000E-01 9.250000E-02 0.000000E+00
213 3.140000E-01 9.250000E-02 5.000000E-01
213 3.140000E-01 -4.075000E-01 0.000000E+00
214 3.140000E-01 -4.075000E-01 5.000000E-01
213 1.540744E-33 -1.860000E-01 9.250000E-02
214 -6.162976E-33 -1.860000E-01 -4.075000E-01
214 1.540744E-33 3.140000E-01 9.250000E-02
213 -6.162976E-33 3.140000E-01 -4.075000E-01
214 5.000000E-01 -1.860000E-01 9.250000E-02
213 5.000000E-01 -1.860000E-01 -4.075000E-01
213 5.000000E-01 3.140000E-01 9.250000E-02
214 5.000000E-01 3.140000E-01 -4.075000E-01
213 1.860000E-01 9.250000E-02 0.000000E+00
214 1.860000E-01 9.250000E-02 5.000000E-01
214 1.860000E-01 -4.075000E-01 0.000000E+00
213 1.860000E-01 -4.075000E-01 5.000000E-01
214 -3.140000E-01 9.250000E-02 0.000000E+00
213 -3.140000E-01 9.250000E-02 5.000000E-01
213 -3.140000E-01 -4.075000E-01 0.000000E+00
214 -3.140000E-01 -4.075000E-01 5.000000E-01
213 1.540744E-33 1.860000E-01 9.250000E-02
214 -6.162976E-33 1.860000E-01 -4.075000E-01
214 1.540744E-33 -3.140000E-01 9.250000E-02
213 -6.162976E-33 -3.140000E-01 -4.075000E-01
214 5.000000E-01 1.860000E-01 9.250000E-02
213 5.000000E-01 1.860000E-01 -4.075000E-01
213 5.000000E-01 -3.140000E-01 9.250000E-02
214 5.000000E-01 -3.140000E-01 -4.075000E-01
213 1.860000E-01 -9.250000E-02 0.000000E+00
214 1.860000E-01 -9.250000E-02 5.000000E-01
214 1.860000E-01 4.075000E-01 0.000000E+00
213 1.860000E-01 4.075000E-01 5.000000E-01
214 -3.140000E-01 -9.250000E-02 0.000000E+00
213 -3.140000E-01 -9.250000E-02 5.000000E-01
213 -3.140000E-01 4.075000E-01 0.000000E+00
214 -3.140000E-01 4.075000E-01 5.000000E-01
208 0.000000E+00 1.125000E-01 -2.500000E-01
208 0.000000E+00 1.125000E-01 2.500000E-01
208 0.000000E+00 -3.875000E-01 -2.500000E-01
208 0.000000E+00 -3.875000E-01 2.500000E-01
208 5.000000E-01 1.125000E-01 -2.500000E-01
208 5.000000E-01 1.125000E-01 2.500000E-01
208 5.000000E-01 -3.875000E-01 -2.500000E-01
208 5.000000E-01 -3.875000E-01 2.500000E-01
208 0.000000E+00 -1.125000E-01 -2.500000E-01
208 0.000000E+00 -1.125000E-01 2.500000E-01
208 0.000000E+00 3.875000E-01 -2.500000E-01
208 0.000000E+00 3.875000E-01 2.500000E-01
208 5.000000E-01 -1.125000E-01 -2.500000E-01
208 5.000000E-01 -1.125000E-01 2.500000E-01
208 5.000000E-01 3.875000E-01 -2.500000E-01
208 5.000000E-01 3.875000E-01 2.500000E-01
208 -2.500000E-01 0.000000E+00 1.125000E-01
208 -2.500000E-01 -6.162976E-33 -3.875000E-01
208 -2.500000E-01 5.000000E-01 1.125000E-01
208 -2.500000E-01 5.000000E-01 -3.875000E-01
208 2.500000E-01 4.622232E-33 1.125000E-01
208 2.500000E-01 -3.081488E-33 -3.875000E-01
208 2.500000E-01 5.000000E-01 1.125000E-01
208 2.500000E-01 5.000000E-01 -3.875000E-01
208 1.125000E-01 -2.500000E-01 0.000000E+00
208 1.125000E-01 -2.500000E-01 5.000000E-01
208 1.125000E-01 2.500000E-01 0.000000E+00
208 1.125000E-01 2.500000E-01 5.000000E-01
208 -3.875000E-01 -2.500000E-01 0.000000E+00
208 -3.875000E-01 -2.500000E-01 5.000000E-01
208 -3.875000E-01 2.500000E-01 0.000000E+00
208 -3.875000E-01 2.500000E-01 5.000000E-01
208 -1.125000E-01 -2.500000E-01 0.000000E+00
208 -1.125000E-01 -2.500000E-01 5.000000E-01
208 -1.125000E-01 2.500000E-01 0.000000E+00
208 -1.125000E-01 2.500000E-01 5.000000E-01
208 3.875000E-01 -2.500000E-01 0.000000E+00
208 3.875000E-01 -2.500000E-01 5.000000E-01
208 3.875000E-01 2.500000E-01 0.000000E+00
208 3.875000E-01 2.500000E-01 5.000000E-01
208 -2.500000E-01 -4.622232E-33 -1.125000E-01
208 -2.500000E-01 -3.081488E-33 3.875000E-01
208 -2.500000E-01 5.000000E-01 -1.125000E-01
208 -2.500000E-01 5.000000E-01 3.875000E-01
208 2.500000E-01 0.000000E+00 -1.125000E-01
208 2.500000E-01 6.162976E-33 3.875000E-01
208 2.500000E-01 5.000000E-01 -1.125000E-01
208 2.500000E-01 5.000000E-01 3.875000E-01
208 -1.125000E-01 -3.081488E-33 -2.500000E-01
208 -1.125000E-01 -3.081488E-33 2.500000E-01
208 -1.125000E-01 5.000000E-01 -2.500000E-01
208 -1.125000E-01 5.000000E-01 2.500000E-01
208 3.875000E-01 3.081488E-33 -2.500000E-01
208 3.875000E-01 9.244464E-33 2.500000E-01
208 3.875000E-01 5.000000E-01 -2.500000E-01
208 3.875000E-01 5.000000E-01 2.500000E-01
208 1.125000E-01 3.081488E-33 -2.500000E-01
208 1.125000E-01 3.081488E-33 2.500000E-01
208 1.125000E-01 5.000000E-01 -2.500000E-01
208 1.125000E-01 5.000000E-01 2.500000E-01
208 -3.875000E-01 -3.081488E-33 -2.500000E-01
208 -3.875000E-01 -6.162976E-33 2.500000E-01
208 -3.875000E-01 5.000000E-01 -2.500000E-01
208 -3.875000E-01 5.000000E-01 2.500000E-01
208 -7.703720E-34 -2.500000E-01 -1.125000E-01
208 3.081488E-33 -2.500000E-01 3.875000E-01
208 -7.703720E-34 2.500000E-01 -1.125000E-01
208 3.081488E-33 2.500000E-01 3.875000E-01
208 5.000000E-01 -2.500000E-01 -1.125000E-01

208 5.000000E-01 -2.500000E-01 3.875000E-01
208 5.000000E-01 2.500000E-01 -1.125000E-01
208 5.000000E-01 2.500000E-01 3.875000E-01
208 -2.500000E-01 -1.125000E-01 0.000000E+00
208 -2.500000E-01 -1.125000E-01 5.000000E-01
208 -2.500000E-01 3.875000E-01 0.000000E+00
208 -2.500000E-01 3.875000E-01 5.000000E-01
208 2.500000E-01 -1.125000E-01 0.000000E+00
208 2.500000E-01 -1.125000E-01 5.000000E-01
208 2.500000E-01 3.875000E-01 0.000000E+00
208 2.500000E-01 3.875000E-01 5.000000E-01
208 -2.500000E-01 1.125000E-01 0.000000E+00
208 -2.500000E-01 1.125000E-01 5.000000E-01
208 -2.500000E-01 -3.875000E-01 0.000000E+00
208 -2.500000E-01 -3.875000E-01 5.000000E-01
208 2.500000E-01 1.125000E-01 0.000000E+00
208 2.500000E-01 1.125000E-01 5.000000E-01
208 2.500000E-01 -3.875000E-01 0.000000E+00
208 2.500000E-01 -3.875000E-01 5.000000E-01
208 7.703720E-34 -2.500000E-01 1.125000E-01
208 0.000000E+00 -2.500000E-01 -3.875000E-01
208 7.703720E-34 2.500000E-01 1.125000E-01
208 0.000000E+00 2.500000E-01 -3.875000E-01
208 5.000000E-01 -2.500000E-01 1.125000E-01
208 5.000000E-01 -2.500000E-01 -3.875000E-01
208 5.000000E-01 2.500000E-01 1.125000E-01
208 5.000000E-01 2.500000E-01 -3.875000E-01
208 0.000000E+00 1.450000E-01 1.450000E-01
208 0.000000E+00 1.450000E-01 -3.550000E-01
208 0.000000E+00 -3.550000E-01 1.450000E-01
208 0.000000E+00 -3.550000E-01 -3.550000E-01
208 5.000000E-01 1.450000E-01 1.450000E-01
208 5.000000E-01 1.450000E-01 -3.550000E-01
208 5.000000E-01 -3.550000E-01 1.450000E-01
208 5.000000E-01 -3.550000E-01 -3.550000E-01
208 0.000000E+00 -1.450000E-01 1.450000E-01
208 0.000000E+00 -1.450000E-01 -3.550000E-01
208 0.000000E+00 3.550000E-01 1.450000E-01
208 0.000000E+00 3.550000E-01 -3.550000E-01
208 5.000000E-01 -1.450000E-01 1.450000E-01
208 5.000000E-01 -1.450000E-01 -3.550000E-01
208 5.000000E-01 3.550000E-01 1.450000E-01
208 5.000000E-01 3.550000E-01 -3.550000E-01
208 0.000000E+00 -1.450000E-01 -1.450000E-01
208 -3.081488E-33 -1.450000E-01 3.550000E-01
208 0.000000E+00 3.550000E-01 -1.450000E-01
208 -3.081488E-33 3.550000E-01 3.550000E-01
208 5.000000E-01 -1.450000E-01 -1.450000E-01
208 5.000000E-01 -1.450000E-01 3.550000E-01
208 5.000000E-01 3.550000E-01 -1.450000E-01
208 5.000000E-01 3.550000E-01 3.550000E-01
208 0.000000E+00 1.450000E-01 -1.450000E-01
208 -3.081488E-33 1.450000E-01 3.550000E-01
208 0.000000E+00 -3.550000E-01 -1.450000E-01
208 -3.081488E-33 -3.550000E-01 3.550000E-01
208 5.000000E-01 1.450000E-01 -1.450000E-01
208 5.000000E-01 1.450000E-01 3.550000E-01
208 5.000000E-01 -3.550000E-01 -1.450000E-01
208 5.000000E-01 -3.550000E-01 3.550000E-01
208 1.450000E-01 0.000000E+00 1.450000E-01
208 1.450000E-01 -6.162976E-33 -3.550000E-01
208 1.450000E-01 5.000000E-01 1.450000E-01
208 1.450000E-01 5.000000E-01 -3.550000E-01
208 -3.550000E-01 -1.540744E-33 1.450000E-01
208 -3.550000E-01 0.000000E+00 -3.550000E-01
208 -3.550000E-01 5.000000E-01 1.450000E-01
208 -3.550000E-01 5.000000E-01 -3.550000E-01
208 1.450000E-01 1.450000E-01 0.000000E+00
208 1.450000E-01 1.450000E-01 5.000000E-01
208 1.450000E-01 -3.550000E-01 0.000000E+00
208 1.450000E-01 -3.550000E-01 5.000000E-01
208 -3.550000E-01 1.450000E-01 0.000000E+00
208 -3.550000E-01 1.450000E-01 5.000000E-01
208 -3.550000E-01 -3.550000E-01 0.000000E+00
208 -3.550000E-01 -3.550000E-01 5.000000E-01
208 -1.450000E-01 0.000000E+00 1.450000E-01
208 -1.450000E-01 -3.081488E-33 -3.550000E-01
208 -1.450000E-01 5.000000E-01 1.450000E-01
208 -1.450000E-01 5.000000E-01 -3.550000E-01
208 3.550000E-01 -6.162976E-33 1.450000E-01
208 3.550000E-01 -6.162976E-33 -3.550000E-01
208 3.550000E-01 5.000000E-01 1.450000E-01
208 3.550000E-01 5.000000E-01 -3.550000E-01
208 -1.450000E-01 1.450000E-01 0.000000E+00
208 -1.450000E-01 1.450000E-01 5.000000E-01
208 -1.450000E-01 -3.550000E-01 0.000000E+00
208 -1.450000E-01 -3.550000E-01 5.000000E-01
208 3.550000E-01 1.450000E-01 0.000000E+00
208 3.550000E-01 1.450000E-01 5.000000E-01
208 3.550000E-01 -3.550000E-01 0.000000E+00
208 3.550000E-01 -3.550000E-01 5.000000E-01
208 1.450000E-01 0.000000E+00 -1.450000E-01
208 1.450000E-01 -6.162976E-33 3.550000E-01
208 1.450000E-01 5.000000E-01 -1.450000E-01
208 1.450000E-01 5.000000E-01 3.550000E-01
208 -3.550000E-01 -3.081488E-33 -1.450000E-01
208 -3.550000E-01 -6.162976E-33 3.550000E-01
208 -3.550000E-01 5.000000E-01 -1.450000E-01
208 -3.550000E-01 5.000000E-01 3.550000E-01
208 -1.450000E-01 -1.450000E-01 0.000000E+00
208 -1.450000E-01 -1.450000E-01 5.000000E-01
208 -1.450000E-01 3.550000E-01 0.000000E+00
208 -1.450000E-01 3.550000E-01 5.000000E-01
208 3.550000E-01 -1.450000E-01 0.000000E+00
208 3.550000E-01 -1.450000E-01 5.000000E-01
208 3.550000E-01 3.550000E-01 0.000000E+00
208 3.550000E-01 3.550000E-01 5.000000E-01
208 -1.450000E-01 0.000000E+00 -1.450000E-01
208 -1.450000E-01 -6.162976E-33 3.550000E-01
208 -1.450000E-01 5.000000E-01 -1.450000E-01
208 -1.450000E-01 5.000000E-01 3.550000E-01
208 3.550000E-01 -3.081488E-33 -1.450000E-01
208 3.550000E-01 -6.162976E-33 3.550000E-01
208 3.550000E-01 5.000000E-01 -1.450000E-01
208 3.550000E-01 5.000000E-01 3.550000E-01
208 1.450000E-01 -1.450000E-01 0.000000E+00
208 1.450000E-01 -1.450000E-01 5.000000E-01
208 1.450000E-01 3.550000E-01 0.000000E+00
208 1.450000E-01 3.550000E-01 5.000000E-01
208 -3.550000E-01 -1.450000E-01 0.000000E+00
208 -3.550000E-01 -1.450000E-01 5.000000E-01
208 -3.550000E-01 3.550000E-01 0.000000E+00
208 -3.550000E-01 3.550000E-01 5.000000E-01
208 5.700000E-02 5.700000E-02 1.725000E-01
208 5.700000E-02 5.700000E-02 -3.275000E-01
208 5.700000E-02 -4.430000E-01 1.725000E-01
208 5.700000E-02 -4.430000E-01 -3.275000E-01
208 -4.430000E-01 5.700000E-02 1.725000E-01
208 -4.430000E-01 5.700000E-02 -3.275000E-01
208 -4.430000E-01 -4.430000E-01 1.725000E-01
208 -4.430000E-01 -4.430000E-01 -3.275000E-01
208 -5.700000E-02 -5.700000E-02 1.725000E-01
208 -5.700000E-02 -5.700000E-02 -3.275000E-01
208 -5.700000E-02 4.430000E-01 1.725000E-01
208 -5.700000E-02 4.430000E-01 -3.275000E-01
208 4.430000E-01 -5.700000E-02 1.725000E-01
208 4.430000E-01 -5.700000E-02 -3.275000E-01
208 4.430000E-01 4.430000E-01 1.725000E-01

208 4.430000E-01 4.430000E-01 -3.275000E-01
208 5.700000E-02 -5.700000E-02 -1.725000E-01
208 5.700000E-02 -5.700000E-02 3.275000E-01
208 5.700000E-02 4.430000E-01 -1.725000E-01
208 5.700000E-02 4.430000E-01 3.275000E-01
208 -4.430000E-01 -5.700000E-02 -1.725000E-
01
208 -4.430000E-01 -5.700000E-02 3.275000E-01
208 -4.430000E-01 4.430000E-01 -1.725000E-01
208 -4.430000E-01 4.430000E-01 3.275000E-01
208 -5.700000E-02 5.700000E-02 -1.725000E-01
208 -5.700000E-02 5.700000E-02 3.275000E-01
208 -5.700000E-02 -4.430000E-01 -1.725000E-
01
208 -5.700000E-02 -4.430000E-01 3.275000E-01
208 4.430000E-01 5.700000E-02 -1.725000E-01
208 4.430000E-01 5.700000E-02 3.275000E-01
208 4.430000E-01 -4.430000E-01 -1.725000E-01
208 4.430000E-01 -4.430000E-01 3.275000E-01
208 1.725000E-01 5.700000E-02 5.700000E-02
208 1.725000E-01 5.700000E-02 -4.430000E-01
208 1.725000E-01 -4.430000E-01 5.700000E-02
208 1.725000E-01 -4.430000E-01 -4.430000E-01
208 -3.275000E-01 5.700000E-02 5.700000E-02
208 -3.275000E-01 5.700000E-02 -4.430000E-01
208 -3.275000E-01 -4.430000E-01 5.700000E-02
208 -3.275000E-01 -4.430000E-01 -4.430000E-
01
208 5.700000E-02 1.725000E-01 5.700000E-02
208 5.700000E-02 1.725000E-01 -4.430000E-01
208 5.700000E-02 -3.275000E-01 5.700000E-02
208 5.700000E-02 -3.275000E-01 -4.430000E-01
208 -4.430000E-01 1.725000E-01 5.700000E-02
208 -4.430000E-01 1.725000E-01 -4.430000E-01
208 -4.430000E-01 -3.275000E-01 5.700000E-02
208 -4.430000E-01 -3.275000E-01 -4.430000E-
01
208 -1.725000E-01 -5.700000E-02 5.700000E-02
208 -1.725000E-01 -5.700000E-02 -4.430000E-
01
208 -1.725000E-01 4.430000E-01 5.700000E-02
208 -1.725000E-01 4.430000E-01 -4.430000E-01
208 3.275000E-01 -5.700000E-02 5.700000E-02
208 3.275000E-01 -5.700000E-02 -4.430000E-01
208 3.275000E-01 4.430000E-01 5.700000E-02
208 3.275000E-01 4.430000E-01 -4.430000E-01
208 -5.700000E-02 1.725000E-01 -5.700000E-02
208 -5.700000E-02 1.725000E-01 4.430000E-01
208 -5.700000E-02 -3.275000E-01 -5.700000E-
02
208 -5.700000E-02 -3.275000E-01 4.430000E-01
208 4.430000E-01 1.725000E-01 -5.700000E-02
208 4.430000E-01 1.725000E-01 4.430000E-01
208 4.430000E-01 -3.275000E-01 -5.700000E-02
208 4.430000E-01 -3.275000E-01 4.430000E-01
208 1.725000E-01 -5.700000E-02 -5.700000E-02
208 1.725000E-01 -5.700000E-02 4.430000E-01
208 1.725000E-01 4.430000E-01 -5.700000E-02
208 1.725000E-01 4.430000E-01 4.430000E-01
208 -3.275000E-01 -5.700000E-02 -5.700000E-
02
208 -3.275000E-01 -5.700000E-02 4.430000E-01
208 -3.275000E-01 4.430000E-01 -5.700000E-02
208 -3.275000E-01 4.430000E-01 4.430000E-01
208 -5.700000E-02 -1.725000E-01 5.700000E-02
208 -5.700000E-02 -1.725000E-01 -4.430000E-
01
208 -5.700000E-02 3.275000E-01 5.700000E-02
208 -5.700000E-02 3.275000E-01 -4.430000E-01
208 4.430000E-01 -1.725000E-01 5.700000E-02
208 4.430000E-01 -1.725000E-01 -4.430000E-01
208 4.430000E-01 3.275000E-01 5.700000E-02
208 4.430000E-01 3.275000E-01 -4.430000E-01
208 -1.725000E-01 5.700000E-02 -5.700000E-02
208 -1.725000E-01 5.700000E-02 4.430000E-01
208 -1.725000E-01 -4.430000E-01 -5.700000E-
02
208 -1.725000E-01 -4.430000E-01 4.430000E-01
208 3.275000E-01 5.700000E-02 -5.700000E-02
208 3.275000E-01 5.700000E-02 4.430000E-01
208 3.275000E-01 -4.430000E-01 -5.700000E-02
208 3.275000E-01 -4.430000E-01 4.430000E-01
208 5.700000E-02 -1.725000E-01 -5.700000E-02
208 5.700000E-02 -1.725000E-01 4.430000E-01
208 5.700000E-02 3.275000E-01 -5.700000E-02
208 5.700000E-02 3.275000E-01 4.430000E-01
208 -4.430000E-01 -1.725000E-01 -5.700000E-
02
208 -4.430000E-01 -1.725000E-01 4.430000E-01
208 -4.430000E-01 3.275000E-01 -5.700000E-02
208 -4.430000E-01 3.275000E-01 4.430000E-01
208 -5.700000E-02 -5.700000E-02 -1.725000E-
01
208 -5.700000E-02 -5.700000E-02 3.275000E-01
208 -5.700000E-02 4.430000E-01 -1.725000E-01
208 -5.700000E-02 4.430000E-01 3.275000E-01
208 4.430000E-01 -5.700000E-02 -1.725000E-01
208 4.430000E-01 -5.700000E-02 3.275000E-01
208 4.430000E-01 4.430000E-01 -1.725000E-01
208 4.430000E-01 4.430000E-01 3.275000E-01
208 5.700000E-02 5.700000E-02 -1.725000E-01
208 5.700000E-02 5.700000E-02 3.275000E-01
208 5.700000E-02 -4.430000E-01 -1.725000E-01
208 5.700000E-02 -4.430000E-01 3.275000E-01
208 -4.430000E-01 5.700000E-02 -1.725000E-01
208 -4.430000E-01 5.700000E-02 3.275000E-01
208 -4.430000E-01 -4.430000E-01 -1.725000E-
01
208 -4.430000E-01 -4.430000E-01 3.275000E-01
208 5.700000E-02 -5.700000E-02 1.725000E-01
208 5.700000E-02 -5.700000E-02 -3.275000E-01
208 5.700000E-02 4.430000E-01 1.725000E-01
208 5.700000E-02 4.430000E-01 -3.275000E-01
208 -4.430000E-01 -5.700000E-02 1.725000E-01
208 -4.430000E-01 -5.700000E-02 -3.275000E-
01
208 -4.430000E-01 4.430000E-01 1.725000E-01
208 -4.430000E-01 4.430000E-01 -3.275000E-01
208 -5.700000E-02 5.700000E-02 1.725000E-01
208 -5.700000E-02 5.700000E-02 -3.275000E-01
208 -5.700000E-02 -4.430000E-01 1.725000E-01
208 -5.700000E-02 -4.430000E-01 -3.275000E-
01
208 4.430000E-01 5.700000E-02 1.725000E-01
208 4.430000E-01 5.700000E-02 -3.275000E-01
208 4.430000E-01 -4.430000E-01 1.725000E-01
208 4.430000E-01 -4.430000E-01 -3.275000E-01
208 -5.700000E-02 -1.725000E-01 -5.700000E-
02
208 -5.700000E-02 -1.725000E-01 4.430000E-01
208 -5.700000E-02 3.275000E-01 -5.700000E-02
208 -5.700000E-02 3.275000E-01 4.430000E-01
208 4.430000E-01 -1.725000E-01 -5.700000E-02
208 4.430000E-01 -1.725000E-01 4.430000E-01
208 4.430000E-01 3.275000E-01 -5.700000E-02
208 4.430000E-01 3.275000E-01 4.430000E-01
208 -1.725000E-01 -5.700000E-02 -5.700000E-
02
208 -1.725000E-01 -5.700000E-02 4.430000E-01
208 -1.725000E-01 4.430000E-01 -5.700000E-02
208 -1.725000E-01 4.430000E-01 4.430000E-01
208 3.275000E-01 -5.700000E-02 -5.700000E-02

```
208 3.275000E-01 -5.700000E-02 4.430000E-01
208 3.275000E-01 4.430000E-01 -5.700000E-02
208 3.275000E-01 4.430000E-01 4.430000E-01
208 5.700000E-02 1.725000E-01 -5.700000E-02
208 5.700000E-02 1.725000E-01 4.430000E-01
208 5.700000E-02 -3.275000E-01 -5.700000E-02
208 5.700000E-02 -3.275000E-01 4.430000E-01
208 -4.430000E-01 1.725000E-01 -5.700000E-02
208 -4.430000E-01 1.725000E-01 4.430000E-01
208 -4.430000E-01 -3.275000E-01 -5.700000E-
02
208 -4.430000E-01 -3.275000E-01 4.430000E-01
208 -1.725000E-01 5.700000E-02 5.700000E-02
208 -1.725000E-01 5.700000E-02 -4.430000E-01
208 -1.725000E-01 -4.430000E-01 5.700000E-02
208 -1.725000E-01 -4.430000E-01 -4.430000E-
01
208 3.275000E-01 5.700000E-02 5.700000E-02
208 3.275000E-01 5.700000E-02 -4.430000E-01
208 3.275000E-01 -4.430000E-01 5.700000E-02
208 3.275000E-01 -4.430000E-01 -4.430000E-01
208 5.700000E-02 -1.725000E-01 5.700000E-02
208 5.700000E-02 -1.725000E-01 -4.430000E-01
208 5.700000E-02 3.275000E-01 5.700000E-02
208 5.700000E-02 3.275000E-01 -4.430000E-01
208 -4.430000E-01 -1.725000E-01 5.700000E-02
208 -4.430000E-01 -1.725000E-01 -4.430000E-
01
208 -4.430000E-01 3.275000E-01 5.700000E-02
208 -4.430000E-01 3.275000E-01 -4.430000E-01
208 1.725000E-01 5.700000E-02 -5.700000E-02
208 1.725000E-01 5.700000E-02 4.430000E-01
208 1.725000E-01 -4.430000E-01 -5.700000E-02
208 1.725000E-01 -4.430000E-01 4.430000E-01
208 -3.275000E-01 5.700000E-02 -5.700000E-02
208 -3.275000E-01 5.700000E-02 4.430000E-01
208 -3.275000E-01 -4.430000E-01 -5.700000E-
02
208 -3.275000E-01 -4.430000E-01 4.430000E-01
208 -5.700000E-02 1.725000E-01 5.700000E-02
208 -5.700000E-02 1.725000E-01 -4.430000E-01
208 -5.700000E-02 -3.275000E-01 5.700000E-02
208 -5.700000E-02 -3.275000E-01 -4.430000E-
01
208 4.430000E-01 1.725000E-01 5.700000E-02
208 4.430000E-01 1.725000E-01 -4.430000E-01
208 4.430000E-01 -3.275000E-01 5.700000E-02
208 4.430000E-01 -3.275000E-01 -4.430000E-01
208 1.725000E-01 -5.700000E-02 5.700000E-02
208 1.725000E-01 -5.700000E-02 -4.430000E-01
208 1.725000E-01 4.430000E-01 5.700000E-02
208 1.725000E-01 4.430000E-01 -4.430000E-01
208 -3.275000E-01 -5.700000E-02 5.700000E-02
208 -3.275000E-01 -5.700000E-02 -4.430000E-
01
208 -3.275000E-01 4.430000E-01 5.700000E-02
208 -3.275000E-01 4.430000E-01 -4.430000E-01
211 1.000000E-01 1.000000E-01 1.000000E-01
211 1.000000E-01 1.000000E-01 -4.000000E-01
211 1.000000E-01 -4.000000E-01 1.000000E-01
211 1.000000E-01 -4.000000E-01 -4.000000E-01
211 -4.000000E-01 1.000000E-01 1.000000E-01
211 -4.000000E-01 1.000000E-01 -4.000000E-01
211 -4.000000E-01 -4.000000E-01 1.000000E-01
211 -4.000000E-01 -4.000000E-01 -4.000000E-
01
211 -1.000000E-01 -1.000000E-01 1.000000E-01
211 -1.000000E-01 -1.000000E-01 -4.000000E-
01
211 -1.000000E-01 4.000000E-01 1.000000E-01
211 -1.000000E-01 4.000000E-01 -4.000000E-01
211 4.000000E-01 -1.000000E-01 1.000000E-01
211 4.000000E-01 -1.000000E-01 -4.000000E-01
211 4.000000E-01 4.000000E-01 1.000000E-01
211 4.000000E-01 4.000000E-01 -4.000000E-01
211 1.000000E-01 -1.000000E-01 -1.000000E-01
211 1.000000E-01 -1.000000E-01 4.000000E-01
211 1.000000E-01 4.000000E-01 -1.000000E-01
211 1.000000E-01 4.000000E-01 4.000000E-01
211 -4.000000E-01 -1.000000E-01 -1.000000E-
01
211 -4.000000E-01 -1.000000E-01 4.000000E-01
211 -4.000000E-01 4.000000E-01 -1.000000E-01
211 -4.000000E-01 4.000000E-01 4.000000E-01
211 -1.000000E-01 1.000000E-01 -1.000000E-01
211 -1.000000E-01 1.000000E-01 4.000000E-01
211 -1.000000E-01 -4.000000E-01 -1.000000E-
01
211 -1.000000E-01 -4.000000E-01 4.000000E-01
211 4.000000E-01 1.000000E-01 -1.000000E-01
211 4.000000E-01 1.000000E-01 4.000000E-01
211 4.000000E-01 -4.000000E-01 -1.000000E-01
211 4.000000E-01 -4.000000E-01 4.000000E-01
282  0.0          0.75          0.75
282  0.5          0.75          0.25
282  0.0          0.25          0.75
282  0.5          0.75          0.75
282  0.0          0.75          0.25
282  0.5          0.25          0.25
282  0.0          0.25          0.25
282  0.5          0.25          0.75
211 1.000000E-01 1.000000E-01 -1.000000E-01
211 1.000000E-01 1.000000E-01 4.000000E-01
211 1.000000E-01 -4.000000E-01 -1.000000E-01
211 1.000000E-01 -4.000000E-01 4.000000E-01
211 -4.000000E-01 1.000000E-01 -1.000000E-01
211 -4.000000E-01 1.000000E-01 4.000000E-01
211 -4.000000E-01 -4.000000E-01 -1.000000E-
01
211 -4.000000E-01 -4.000000E-01 4.000000E-01
211 1.000000E-01 -1.000000E-01 1.000000E-01
211 1.000000E-01 -1.000000E-01 -4.000000E-01
211 1.000000E-01 4.000000E-01 1.000000E-01
211 1.000000E-01 4.000000E-01 -4.000000E-01
211 -4.000000E-01 -1.000000E-01 1.000000E-01
211 -4.000000E-01 -1.000000E-01 -4.000000E-
01
211 -4.000000E-01 4.000000E-01 1.000000E-01
211 -4.000000E-01 4.000000E-01 -4.000000E-01
211 -1.000000E-01 1.000000E-01 1.000000E-01
211 -1.000000E-01 1.000000E-01 -4.000000E-01
211 -1.000000E-01 -4.000000E-01 1.000000E-01
211 -1.000000E-01 -4.000000E-01 -4.000000E-
01
211 4.000000E-01 1.000000E-01 1.000000E-01
211 4.000000E-01 1.000000E-01 -4.000000E-01
211 4.000000E-01 -4.000000E-01 1.000000E-01
211 4.000000E-01 -4.000000E-01 -4.000000E-01
282 -2.500000E-01 -2.500000E-01 0.000000E+00
282 -2.500000E-01 -2.500000E-01 5.000000E-01
282 -2.500000E-01 2.500000E-01 0.000000E+00
282 -2.500000E-01 2.500000E-01 5.000000E-01
282 2.500000E-01 -2.500000E-01 0.000000E+00
282 2.500000E-01 -2.500000E-01 5.000000E-01
282 2.500000E-01 2.500000E-01 0.000000E+00
282 2.500000E-01 2.500000E-01 5.000000E-01
211 -2.500000E-01 0.000000E+00 -2.500000E-01
211 -2.500000E-01 -3.081488E-33 2.500000E-01
211 -2.500000E-01 5.000000E-01 -2.500000E-01
211 -2.500000E-01 5.000000E-01 2.500000E-01
211 2.500000E-01 0.000000E+00 -2.500000E-01
211 2.500000E-01 0.000000E+00 2.500000E-01
```

```
211 2.500000E-01 5.000000E-01 -2.500000E-01
211 2.500000E-01 5.000000E-01 2.500000E-01
END
214     2
INPUT
      4.                    1 2 2 0 0 0
      2.4627200             -2.9824000    -1
      9.4633800              6.0055800    -2
      2.4440800             23.7764200     0
      3.8258500              3.2034500    -2
      1.8302600              9.8643800     0
0 1 3 0. 1.
      1.1670000             -0.3240300
-0.0845000
      0.5268000              0.1843800
0.2378600
      0.1807000              0.7773700
0.5653200
0 1 1 0. 1.00
      0.13              1.              1.
213     2
INPUT
      3.                    1 2 2 0 0 0
      1.9555900             -3.0305500    -1
      7.7885800              6.0465000    -2
      1.9902500             18.8750900     0
      2.8314600              3.2946500    -2
      1.3847900              6.8702900     0
0 1 3 0. 1.
      0.9011000             -0.3037700
-0.0792900
      0.4495000              0.1338200
0.1654000
      0.1405000              0.7603700
0.5301500
0 1 1 0. 1.
      0.12            1.              1.
208     2
INPUT
      6.                    1 2 0 0 0 0
     16.1171800             -0.9255000    -1
      5.0534800              1.9606900    -2
     15.9533300             29.1344200     0
0 1 3 8. 1.
      8.5190000             -0.1455100
0.1100700
      2.0730000              0.0828600
0.3496900
      0.6471000              0.7432500
0.4809300
0 1 1 0.  1.
      0.2000000              0.2847200
0.3072700
211     2
INPUT
       1.                    1 2 2 0 0 0
      0.9000900             -2.3844600     -
1
      5.3723200              6.2341500     -
2
      1.1195900              9.0837400
0
      1.2915800              3.2397100     -
2
      0.6579100              2.5351400
0
0 1 3 0. 1.
      0.4299000             -0.2087400
-0.0257100
      0.0889700              0.3120600
0.2160800
      0.0355000              0.7030000
0.5419600
0 1 1 0. 1.
      0.27              1.              1.
282 4
HAYWLC
0 1 2 2. 1.
  1.335104   -0.1448789   -0.1070612
  0.7516086  1.0          1.0
0 1 1 0. 1.
  0.5536686  1.0          1.0
0 1 1 0. 1.
  0.1420315  1.0          1.0
0 3 1 0. 1.
  0.1933887  1.0
256 3
HAYWSC
0 1 3 8. 1.
   1.3144   -1.3797  -0.1776
   0.5144    1.1476   0.6089
   0.287     2.0729  -0.3133
0 1 1 0. 1.
   0.213     1.       1.
0 3 1 0. 1.
   0.330     1.
99 0
END
DFT
B3LYP
END
GUESSP
TOLDEE
7
SAVEWF
SCFDIR
LEVSHIFT
20 40
FMIXING
80
MAXCYCLE
20000
SHRINK
1 1
END
```

Appendix Figure 5.1 - Input file for Anhydrous Zeolite-A with basis sets for lead and barium both provided. Coordinates may be substituted as needed. This input file is for a 25% substitution of sodium.